

POLYMAT



eman ta zabal zazu



Universidad
del País Vasco

Euskal Herriko
Unibertsitatea

Blend membranes based on block copolymer/Ionic Liquids

Blend membranes based on block copolymer/ionic liquids

Ana Corres

PhD Thesis

ANA CORRES ORTEGA

International PhD Thesis
Donostia-San Sebastián - December 2016

POLYMAT

eman ta zabal zazu



Universidad
del País Vasco

Euskal Herriko
Unibertsitatea

BLEND MEMBRANES BASED ON BLOCK COPOLYMER/IONIC LIQUIDS

BY

ANA CORRES ORTEGA

A thesis submitted in partial fulfillment for the
degree of Doctor of Philosophy
in Applied Chemistry and Polymeric Materials

SUPERVISOR: Prof. DR. THOMAS SCHÄFER

POLYMAT, Institute for Polymer Materials

**Departamento de Ciencia y Tecnología de Polímeros-
Polimeroen Zientzia eta Teknologia Departamentua
Faculty of Chemistry, University of the Basque Country (UPV/EHU)**

DONOSTIA- SAN SEBASTIÁN Diciembre 2016

Pensé que sería imposible, pero parece que el fin de esta etapa, durante tanto tiempo soñado, llega a su fin. Quisiera comenzar agradeciendo al Dr. Thomas Schäfer, director de la tesis, por su apoyo, confianza y por la motivación que me ha ido transmitiendo durante todos estos años. Esta tesis no solo me ha hecho aprender a nivel científico, sino que también en muchos otros aspectos. Muchas gracias por todo lo que me has enseñado, con el enriquecimiento profesional y personal que ha supuesto.

Quería también agradecer el apoyo científico de Yanko, cuya amplia experiencia nos ha ayudado mucho durante la reflexión de los resultados. También a Onintza e Inés por su atención y eficiencia en solucionar todo tipo de trámites durante el doctorado.

I would like to express my gratitude to all people from Christian Albrechts-Universität, starting from Dr. Klaus Rätzke, who gave me the opportunity of going to Kiel to develop and go in depth in our studies. Thanks for being so patient teaching me all the new stuff and making me feel as being one more in the group. Thanks also to my colleges Dr. Christian Ohrt, Dr. Tönjes Koschine and Dr. Yuni Basuki. I will never forget this experience in Germany.

De Kiel también me llevo dos muy buenas amigas: Andrea y Lara quienes me hicieron la vida mucho más fácil y llevadera y que sin ellas no sé qué hubiera hecho por las tierras germanas.

A toda la gente con la que he coincidido a lo largo de la carrera y durante el doctorado, y con quienes hemos compartido todo tipo de “experiencias”. En especial a Robert e Izaskun, que con el paso del tiempo esos cafés con bailsys se han convertido en un extra de motivación.

Por supuesto al NanoBioSeparations group: Belén, Czengiz, Eli, Gabriela, Alessandro, Frank, Isabel y finalmente Ali. Muchas gracias por toda vuestra ayuda y sobretodo vuestro apoyo en los momentos más difíciles.

Agradecimientos

A mis Doctoras las Kortanas: Zaira, Laura y Ane Maite. Miles de gracias por esos buenos ratos en las comidas y cafés de los miércoles-jueves. Aun en los momentos más difíciles hemos sabido desconectar y acabar a carcajadas. ¡Habéis sido un gran apoyo! No me puedo olvidar tampoco de todos los Inasmetos... qué suerte tuvimos de encontrarnos y formar esa familia.

Agradecer también a mis amigas las Paisanas: Pobes, Méndez y Amelia, porque sin entender muy bien qué era esto de la tesis y viéndome desanimada en muchas ocasiones, nunca les han faltado palabras de ánimo y fe en mí. Gracias por todo chicas!

Gracias también a todos aquellos que forman parte de mi nueva vida laboral en Itasa. Aun con todo lo que tengo que aprender en el mundo del papel, reconozco que ir con ilusión cada mañana es de los mejores regalos que puedan existir.

Para terminar esta tesis no hubiera salido adelante sin la ayuda y el apoyo de mi familia. Aita, Ama y Marian. Gracias por estar siempre disponibles para todo. A pesar de que estos últimos años han sido complicados para compaginar trabajo y tesis, esto se ha convertido en un reto personal y aunque con mis altibajos, cada uno a su manera, habéis tenido una confianza plena y me habéis dado la fuerza y el ánimo necesario para terminar. No existen palabras para agradecer todo lo que habéis hecho por mí. Luján, Luka y ahora también Niko, no podría olvidarme de vosotros porque sin saberlo me habéis hecho aprender lo que es el amor incondicional. Gracias por ser vuestra "Aizeba Ana".

También dar las gracias a la familia Arsuaga-García, por tratarme como una hija más y valorar todo el esfuerzo que ha supuesto esta tesis.

A ti Javi te dejo el último... jamás podré agradecer la paciencia que has tenido y tienes conmigo. Tú eres quien más me sufres y siempre con una sonrisa en la cara. Ya sabes cuál es nuestro lema: SIEMPRE JUNTOS! Haces que la vida contigo no sea una vida cualquiera.

A todos y cada uno de los que estáis conmigo, MUCHAS GRACIAS, porque parte de este trabajo también es vuestro!!

CHAPTER 1

1.1	Ionic Liquids	3
1.2	Ionic liquids in separations	8
1.3	Ionic Liquid-Polymer blends	10
1.4	Thesis Scope and Outline	11
1.5	References	12

CHAPTER 2

2.1	Base Polymer	23
2.2	Ionic Liquids	23
2.3	Solvents	25
2.4	Membrane Preparation	25
2.4.1	Casting Procedure.....	25
2.4.2	Melting-Compression procedure.....	26
2.5	Membrane Material Characterization (analytical techniques)	28
2.5.1	Water Content.....	28
2.5.2	Melting-Compression procedure.....	29
2.5.3	Thermal Gravimetric Analysis (TGA)	30
2.5.4	Differential Scanning Calorimetry (DSC)	30
2.5.5	Polarized Optical Microscopy (POM)	31
2.5.6	Fourier Transform Infrared Spectroscopy (FTIR)	31
2.5.7	Solid State ¹³ C-Nuclear Magnetic Resonance.....	32
2.5.8	Positron Annihilation Lifetime Spectroscopy (PALS)	32
2.5.9	X-Ray Diffraction.....	33
2.6	Membrane Transport Studies	33
2.6.1	Saturated Vapour Permeability Measurements.....	33
2.6.2	Time-Lag gas Permeation Measurements.....	34
2.6.2.1	<i>Data Processing</i>	35
2.6.3	Cahn electrobalance.....	38

Index

2.6.3.1	Vapour Sorption Studies (dynamic sorption process)	41
2.6.3.2	Gas Sorption Studies (static process)	42
2.6.4	QCM-D.....	47
2.6.4.1	The QCM-D System.....	48
2.6.4.2	Quartz crystals.....	49
2.6.4.3	Sensor cleaning.....	49
2.6.4.4	Polymer deposition.....	50
2.6.5	Surface Plasmon Resonance (SPR)	52
2.6.6	Spin Coating.....	54
2.6.6.1	Spin Speed.....	55
2.6.6.2	Acceleration.....	56
2.7	References.....	58
 CHAPTER 3		
3.1	Introduction.....	67
3.2	Results and Discussion.....	72
3.2.1	Membrane Surface Analysis.....	75
3.2.2	Thermal Stability.....	77
3.2.3	Spectroscopic Characterization.....	96
3.2.4	Organic Vapour Permeation Tests.....	107
3.2.5	¹³ C NMR experiments with organic solvents.....	110
3.2.5.1	Pebax®2533-[BMIM][BF ₄] with organic solvents.....	114
3.3	Conclusions.....	117
3.4	References.....	119
 CHAPTER 4		
4.1	Introduction.....	135
4.2	Results and Discussion.....	135
4.2.1	Vapour Sorption Experiments.....	135
4.2.1.1	Solubility parameter of each vapour.....	135
4.2.1.2	Diffusivity of vapours.....	139

4.2.1.3	Permeability of vapours.....	148
4.2.2	Gas Permeation Studies.....	151
4.3	References.....	156

CHAPTER 5

5.1	Introduction.....	161
5.2	Sorption of CO₂ in [C₈MIM][Cl]- a case study.....	167
5.2.1	Gas Sorption Tests.....	169
5.2.2	Chemical Characterization.....	175
5.2.2.1	Fourier Transform Infrared Spectroscopy (FTIR)	175
5.2.2.2	¹³ C Nuclear Magnetic Resonance Spectroscopy (¹³ C-NMR)	177
5.2.2.3	Theoretical Calculations.....	181
5.3	References.....	187

CHAPTER 6

6.1	Introduction to the QCM-D technique.....	206
6.1.1	Fundamental principles.....	206
6.1.2	The dissipation factor.....	208
6.1.3	Data Interpretation.....	211
6.2	Results and Discussion.....	215
6.2.1	Morphological and Topographical characterization of Pebax [®] 2533 and Pebax2533-IL blended depositions on the quartz crystal.....	215
6.2.1.1	Atomic force microscopy.....	215
6.2.2	Reproducibility of the QCM-D technique.....	216
6.2.2.1	Pebax [®] 2533 layer depositions of different thickness.....	216
6.2.2.2	Reproducibility of vapour sorption in one and the same Pebax [®] 2533 layer depositions.....	219
6.3	References.....	223

CHAPTER 7

7.1	Introduction.....	231
7.2	Pebax®2533 vapour sorption coefficients.....	232
7.3	Pebax2533-ILs sorption coefficients.....	242
7.3.1	Ethanol.....	242
7.3.2	Water.....	245
7.3.3	Hexane.....	250
7.3.4	Ethyl Acetate.....	253
7.4	Conclusions.....	260
7.5	References.....	261

CHAPTER 8

8.1	Introduction.....	265
8.2	Results and Discussion.....	267
8.2.1	PALS measurements.....	267
8.2.2	X Ray Diffraction and DSC measurements.....	279
8.2.2.1	<i>PA phase.....</i>	<i>279</i>
8.2.2.2	<i>PE phase.....</i>	<i>283</i>
8.2.2.3	<i>Effect of membranes preparation method on crystallinity of the PA-phase.....</i>	<i>286</i>
8.3	Conclusions.....	287
8.4	References.....	289

CHAPTER 9

9.1	Introduction.....	297
9.2	Results and Discussion.....	297
9.3	References.....	308

CHAPTER 10

General Conclusions..... 309

APPENDIX

Abbreviations..... 315

El desarrollo de una captura selectiva de gases tales como el CO₂, H₂S o el SO₂ así como de vapores orgánicos se ha convertido en los últimos años en un difícil objetivo debido a los amplios requerimientos de reducir la emisión de gases contaminantes. Aun así ha quedado demostrado que el uso de membranas en separaciones [1]–[3] es una alternativa interesante ya que éstas pueden ser diseñadas dependiendo de los requerimientos y las necesidades de la aplicación final.

Es por este motivo que el uso de disolventes de baja volatilidad como es el caso de los líquidos iónicos (LIs) cumplimenta el principio de emisión de volátiles orgánicos debido a su baja o incluso despreciable presión de vapor. Además, la posibilidad de modular las propiedades de los líquidos iónicos variando el catión y anión constituyente del mismo permite el diseño del líquido iónico más adecuado para cada aplicación concreta, lo cual ha abierto todo un abanico de aplicaciones potenciales.

Una de las estrategias más reconocidas como método selectivo para la separación de compuestos combinando membranas y LIs, se basa en el empleo de membranas soportadas de líquidos iónicos (MSLIs) donde el LI queda inmovilizado en los poros de la membrana. Sin embargo, la literatura revela que su aplicación industrial tiene ciertas limitaciones, debido principalmente a lo que respecta su estabilidad operacional [4]. Como alternativa para superar los inconvenientes previamente citados con las membranas soportadas, esta tesis se basa en la incorporación de los LIs en matrices poliméricas no porosas. El concepto se centra en el empleo de una matriz polimérica no porosa en la cual los LIs se podrán incorporar como una segunda fase. De esa manera, además de intentar mejorar la permeabilidad y selectividad de la membrana compuesta por el hecho de incorporar una segunda fase líquida con cierta selectividad a determinados compuestos, el objetivo es además el de mantener las propiedades mecánicas globales de la matriz polimérica original.

En este caso, además de demostrar la viabilidad del concepto se ha estudiado no solo cómo se dispone el LI en la matriz polimérica sino además en determinar qué tipo de interacciones tienen lugar entre ambas fases.

Como matriz polimérica, se ha utilizado un copolímero de bloque Pebax®2533 debido a sus interesantes y diversas propiedades como: su gran flexibilidad, alta resistencia al impacto, resistencia térmica en un amplio rango de temperaturas así como sus resistencia química a gran número de disolventes orgánicos [5]. Su estructura química está formada por dos homopolímeros con características claramente distintas. Como la mayoría de los termoplásticos, uno de los bloques es altamente cristalino el cual co-cristaliza con el otro bloque en cadenas adyacentes. De este modo, uno de los homopolímeros consistirá en una fase de poliéter (PTMO) (en una proporción de un 80% en masa) cuya principal característica es la de proporcionar flexibilidad a la membrana, mientras que el segundo homopolímero consiste en una poliamida de 12 carbonos (PA12) altamente cristalizable (en una proporción de un 20% en masa), cuya función será principalmente la de dar estabilidad y cierta rigidez a la membrana. Puesto que ambas fases son incompatibles entre sí, la formación del copolímero de bloque da lugar a una separación de fases, algo muy habitual especialmente donde uno de los bloques es altamente cristalino.

Con el fin de analizar el sistema compuesto polímero-líquido iónico, la tesis se ha subdividido en 10 capítulos:

- El primer capítulo introductorio, detalla información general sobre líquidos iónicos y polímeros (principales características, aplicaciones y utilidades) además de un estudio bibliográfico general sobre las posibles interacciones que tienen lugar entre polímeros y líquidos iónicos.
- El segundo capítulo recoge una descripción exhaustiva de los materiales y métodos empleados a lo largo de toda la tesis. Se describe toda aquella información experimental desde la obtención de las membranas así como la descripción de las condiciones experimentales de caracterización de cada una de las técnicas empleadas.
- El tercer capítulo estudia de manera exhaustiva y mediante un gran número de técnicas experimentales la caracterización de las posibles interacciones que tienen

lugar entre los LIs seleccionados con el polímero base: Pebax®2533. Los LIs empleados, de distinta naturaleza física se han incorporado en una composición del 20% en peso a la matriz polimérica mediante un método de casting. De este modo, se ha verificado en primer lugar si es posible crear membranas estables con esa cantidad de fase líquida y por otra parte se ha estudiado el efecto y repercusión de incorporar dichos LIs al polímero base.

- Siguiendo con la posibilidad de determinar interacciones entre el copolímero y los LIs, en el capítulo cuarto se ha estudiado el efecto de la incorporación de un tercer componente como soluto. Como solutos se han empleado gases tales como CO₂ y N₂ así como vapores orgánicos que nos proporcionan una idea de la capacidad que tienen estas membranas compuestas en términos de separación. El comportamiento de las membranas compuestas se ha estudiado mediante diversas técnicas de permeación así como mediante distintas técnicas de caracterización analítica.
- En el capítulo quinto se ha estudiado el caso particular de la sorción del CO₂ en el LI: [C₈MIM][Cl]. En este caso se analiza la capacidad de sorción del mismo además de la importancia y el efecto inherente del agua en los LIs.
- Los capítulos sexto y séptimo, se han centrado en el estudio analítico mediante una conocida técnica como la microbalanza de cuarzo con disipación. En primer lugar, en el capítulo sexto, se ha evaluado, a pesar de que las condiciones experimentales no hayan sido completamente similares, si la técnica proporciona unos datos de sorción que se encuentren en un rango aceptable. Para ello, dichos resultados se han comparado con datos de sorción obtenidos de la bibliografía así como determinados en nuestro laboratorio a través de una electrobalanza Cahn, ampliamente conocida en el campo de las medidas de transporte. En vista de que la microbalanza de cuarzo puede considerarse una técnica válida para determinar la sorción de vapores orgánicos, el capítulo séptimo se ha focalizado en medir los coeficientes-de sorción de las membranas compuestas cuando son sometidas a un

gradiente de vapores orgánicos. En este apartado se ha evaluado también la importancia del factor de la disipación y el tipo de información que se puede obtener a través del mismo.

- El capítulo octavo, desarrollado completamente en la “Christian-Albrechts-Universität zu Kiel”, se ha enfocado en el estudio mediante las técnicas de espectroscopía de aniquilación de positrones (PALS) y de Rayos X, donde se ha determinado la disposición de los LIs en las membranas compuestas, verificando una de las principales hipótesis de este trabajo que los LIs ocuparían el volumen libre de entre las cadenas poliméricas viéndose un aumento del mismo.
- El capítulo noveno se ha centrado en el estudio de la estabilidad de las membranas compuestas en el tiempo, conocido como envejecimiento de las mismas. Para ello, se han analizado membranas compuestas por LI con una antigüedad de 5 años con idea de cuantificar hasta qué punto se podía observar una migración del LI de la fase polimérica.
- El capítulo décimo presenta las conclusiones generales más relevantes obtenidas en este trabajo.

References

- [1] K. Ghosal and B. D. Freeman, “Gas separation using polymer membranes: an overview,” *Polym. Adv. Technol.*, vol. 5, no. 11, pp. 673–697, **1994**.
- [2] R. W. Baker, *Membrane Technology and Applications*. John Wiley & Sons, Ltd, 2012.
- [3] A. Brunetti, F. Scura, G. Barbieri, and E. Drioli, “Membrane technologies for CO₂ separation,” *J. Memb. Sci.*, vol. 359, no. 1, pp. 115–125, **2010**.
- [4] L. J. Lozano, C. Godínez, A. P. de los Ríos, F. J. Hernández-Fernández, S. Sánchez-Segado, and F. J. Alguacil, “Recent advances in supported ionic liquid membrane technology,” *J. Memb. Sci.*, vol. 376, no. 1, pp. 1–14, **2011**.

- [5] Arkema, "Pebax2533 SA 01 Technical data sheet." [Online]. Available: <http://www.pebax.com/export/sites/pebax/.content/medias/downloads/literature/tds-pebax-2533sa01.pdf>.

Chapter 1

Introduction

1.1	Ionic Liquids.....	3
1.2	Ionic liquids in separations	8
1.3	Ionic Liquid-Polymer blends.....	10
1.4	Thesis Scope and Outline	11
1.5	References.....	12

1.1 Ionic liquids

Ionic liquids (ILs) are salts in the liquid state at or near room temperature. They are composed of a large size of asymmetric organic cations combined with anions (see Figure 1.1). In contrast to conventional ionic salts, their attractive forces are so weak that they do not achieve a high degree of packing which is why they remain in a liquid state at room temperature.

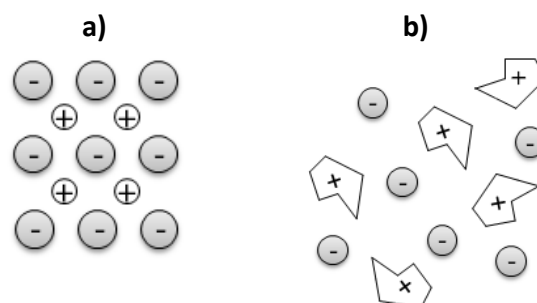


Figure 1.1 Schematic structure of the ion packaging in a) conventional ionic salts (symmetric anions and cations) and b) ionic liquids (non-symmetric large cations)

The physico-chemical properties of ILs can in principle be tailored for specific applications by selecting adequate anions and cations [1], [2]. The combination of a broad variety of cations and anions leads to a theoretically possible number of about 10^{18} ILs that can be synthesized [3], [4]. However, only about 1000 ILs are described in the literature, and approximately only 300 are commercially available [5], [6].

ILs are also denoted “designer solvents” [7] due to the fact that their physico-chemical properties such as viscosity, density, melting point, and/or affinity, depending on their final application, can to some extent be adjusted according to the anion/cation pair chosen. This tunability turned them into very attractive reaction or separation media since processes can in principle be easily optimized toward highest possible efficiency [8].

ILs have also been considered to be emerging green solvents and potential alternatives to classical volatile organic solvents owing to their relatively high thermal stability while remaining liquid up to their decomposition temperature (around 200-300°C), their lack of inflammability, low volatility, chemical stability and excellent miscibility with many organic compounds. However, it should be noted that not all ILs share these properties. In fact, there is a growing conscience that many ILs can indeed be non-green [9].

The first synthesis of an ionic liquid was reported by Paul Walden [10] in 1914, neutralizing ethylamine with concentrated nitric acid to yield ethylammonium nitrate [EtNH₃][NO₃]. Mixtures of 1-ethyl-3-methylimidazolium chloride with chloroaluminate (AlCl₃) yielded ILs that were molten at and below room temperature, however, these imidazolium ILs were extremely sensitive to moisture due to the high reactivity of chloroaluminate with even traces of water. In 1992, the first air and water stable imidazolium ILs were synthesized using nitrate [NO₃]⁻, tetrafluoroborate [BF₄]⁻, and acetate [CH₃COO]⁻ anions[11], respectively. Synthesis of moisture stable ILs is nowadays more usual, many with fluorinated anions such as hexafluorophosphate [PF₆]⁻ and bis(trifluoromethylsulfonyl)imide [N(CF₃SO₂)₂]⁻ or [TFSI], which considerably reduces the water solubility of these ILs. However, it must be noted that even these fluorinated ILs will absorb moisture from the atmosphere owing to the electrostatic nature of ILs.

The unique properties of ILs have generated an exponential growth in publications since late 1990s [12]–[16]. Recently, R.K.Seddon reported that papers related to ILs appear at a rate of over 120 per week [17]. At the same time recent literature presents evidences of several unfounded assumptions concerning the nature of ILs. As an example, while ILs were initially considered non-volatile, vapour pressure can in fact be measured (often with values between 10⁻¹¹ and 10⁻¹⁰ mbar) [18], [19] and ILs can also be distilled [20]. Moreover, toxicity tests of commonly used ILs in bioassays prove that they are not benign at all in general and can be considerably toxic [21].

As an example of interest, commonly used fluoro-based anions such as $[\text{PF}_6]^-$ are hydrolytically unstable, especially at elevated temperature. The instability of the hexafluorophosphate anion in protic media is caused by the protonation of fluorine atoms, followed by HF elimination and reaction with water. This mechanism of the hydrolysis has been intensively discussed in literature [22], [23]. As evidence, Rogers et al. [9] crystallographically identified 1-butyl-3-methylimidazolium fluoride hydrate as a decomposition product obtained from the hydrolytic degradation of $[\text{BMIM}][\text{PF}_6]$. During this purification process, they observed the evolution of acidic HF white fumes which are colorless, highly toxic and corrosive. On the other hand, it is worth mentioning that several 'uncatalyzed' reactions reported in ILs using $[\text{PF}_6]^-$, are catalyzed by adventitious HF [1].

Hence, the toxicity and/or stability of ILs need to be evaluated on a case-to-case basis. In this context, the belief of ILs being "green solvents" which is largely related to their low vapour pressure [24] should not be applied to all ILs in all situations, since there is much to learn about these heterogeneous compounds, their structural possibilities and environmental hazards.

Understandably, the properties of an IL will depend on the functional groups of its "core" structure, the anion, and the substituents as represented in Figure 1.2.

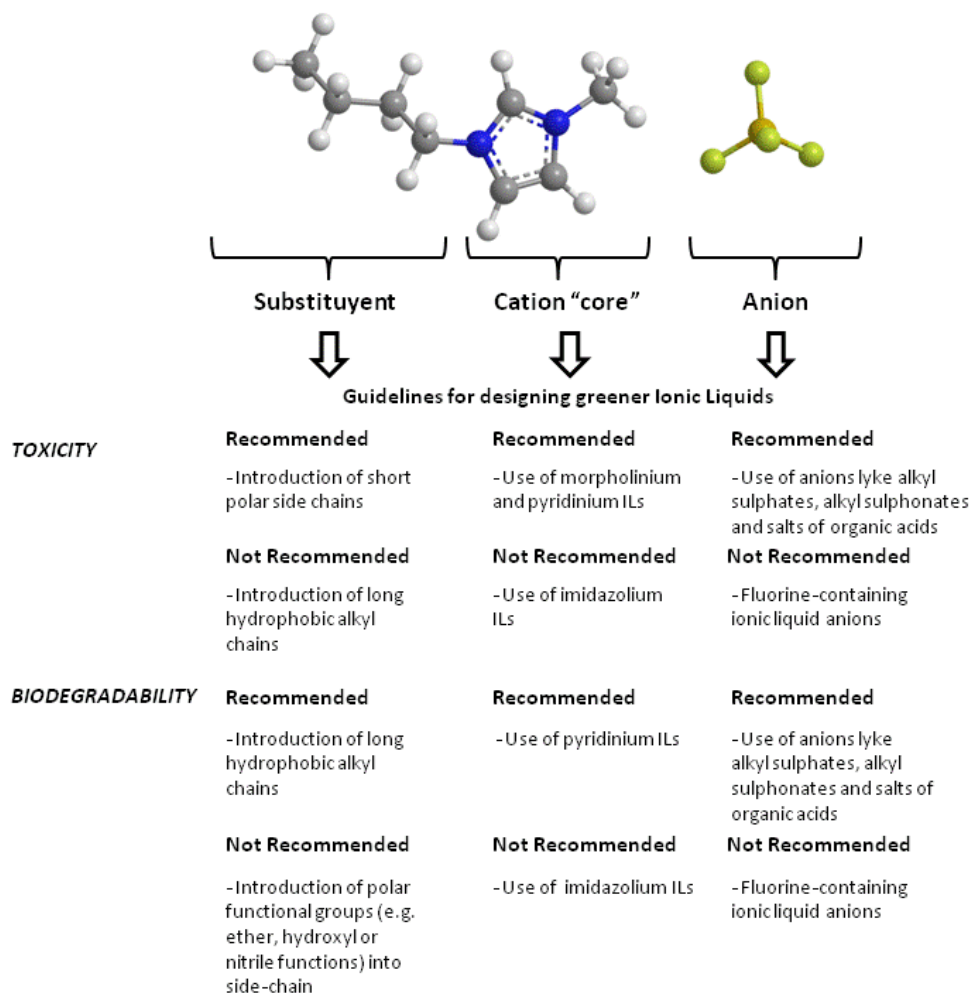


Figure 1.2 Several guidelines for the design of greener ILs (adapted from [18])

Although possibly not benign, ILs can provide either better yields or lower toxicities than conventional solvents [25], [26] while ensuring the safety of employees during handling of these solvents is required at all times [18].

The potential fields of applications of ILs can be extremely varied [27] as indicated in Figure 1.3., comprising synthesis [28], separations [29], [30], electrochemistry [31], [32],

nanotechnology [33], [34] biotechnology [35] and catalytic processes [36], [37] enabling in some cases better performances than employing conventional solvents [38].

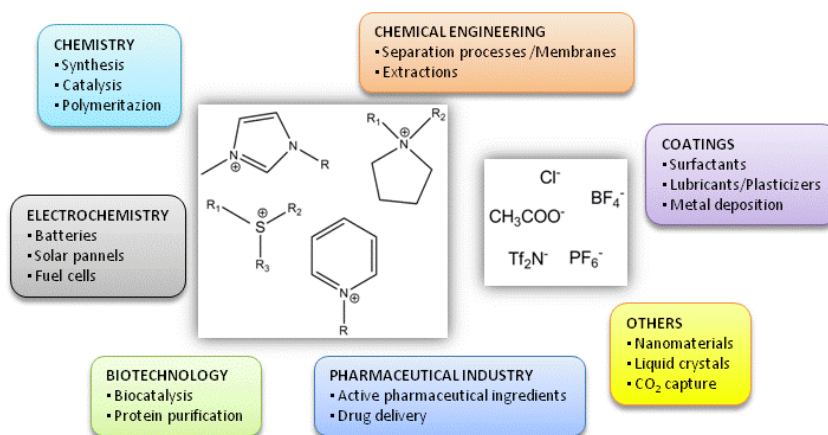


Figure 1.3 Potential applications of ILs (Adapted from [18] and [39])

Despite of the many advantages and unique properties of ILs as well as the multiple combinations of cations and anions that can be conceived, the use of ILs in the chemical industry is still limited due to their rather high price and their relatively reduced commercial availability. Nowadays, the costs of ILs per kilogram amount to tens of thousands euros more compared to common organic solvents such as acetone. However, this cost can be significantly reduced by adequate recycling strategies [40], [41]. As an example, in the case of imidazolium ILs, Wagner et al. [42] anticipated a price around 50-100 € per kilogram for large quantities of production in industry.

The first industrial process involving ILs was announced in March, 2003, by BASF, called BASIL (Biphasic Acid Scavenging Using Ionic Liquids). It was anticipated by Wagner et al [43] that in the case of imidazolium ILs, the price would be around 50-100€ per kilogram if the industries produced large quantities. Besides, ILs are not intrinsically expensive (their typical price range is about 25-250€/kg) [44]. Owing to the possibility of choosing between

a myriad of cations and anions composing the ionic liquid, they may cover a wide range of costs [45]

Another hurdle for the more wide-spread use of ILs relates to their synthesis, as it involves the use of conventional organic solvents such as acetonitrile, toluene, or THF, although in the future it is expected that the emergence of new synthesis methods may eliminate the need of using conventional solvents, as could be achieved by supercritical fluids and microwave synthesis [46]. Eventually, also mass transport limitations may be encountered in ILs owing to their viscosity being significantly higher than that of organic solvents. This problem may be partially overcome by changing the nature of the anions or increasing temperature but it needs to be evaluated on a case-to-case basis.

1.2 Ionic liquids in separations

Ionic liquids have been employed in several analytical separations [47] such as mobile phase additives and surface-bonded stationary phases in chromatography separations [48], [49] and as the extraction solvent in sample preparations [50] amongst others. However, probably, the highest impact of ILs on separations has been as “promising materials for CO₂ separations” due to the fact that ILs exhibit a higher solubility to CO₂ than to other gases such as N₂, CH₄, O₂ and H₂ [51].

Continuous attempts are being made to create CO₂-selective membranes that are capable of overcoming the so-called “Robeson upper bound” [52], a limit beyond which so far no experimental data exist when plotting selectivity versus permeability for a defined separation of two gases. Approaches include mixed-matrix membranes (MMMs) [53], inorganic membranes, e.g. carbon membranes, [54] metal-organic framework (MOF) membranes [53], [55] zeolite membranes [56] and facilitated transport membranes [57]. Nevertheless, despite the numerous new materials synthesized and developed, few of them eventually have been patented for commercial application in the gas separation market [58].

The concept of combining ILs and membranes for CO₂ separations was developed less than 15 years ago [59], [60]. Literature has revealed several alternatives of membranes and membranes processes involving ILs. The most attractive technique and widely investigated so far due to energy efficiency and operational simplicity are supported ionic liquid membranes (SILMs) [61]–[64] where the separation performance is generally attributed to the intrinsic IL characteristics, rather than to the membrane substrate. However, other membrane alternatives containing ILs can also be found in literature such as poly(ionic liquid) membranes (PILMs), poly(ionic liquid)–ionic liquid (PIL–IL) composite membranes, polymer-ionic liquid composite membranes, ion-gel membranes, and membrane absorption processes based on ILs [63].

The use of ILs for CO₂ physisorption processes has been widely reported in literature to be a great “success” [65]. This statement is not always supported by all studies and becomes somehow controversial once analyzing and comparing the literature data of ILs with other commercially available materials. However, why is the reason of the big interest CO₂ and ILs promote?

CO₂ is a linear molecule with a quadrupole moment of negative sign, indicating that the electron density of the oxygen atoms is much higher than that of the carbon atom. Buckingham was the first to determine the quadrupoles of molecules and its role on interactions [66]. This quadrupole results in CO₂ interacting with surrounding charges and explains its interaction with a charged solvent such as an ionic liquid. However, it should be emphasized that even an omnipresent gas such as N₂ possesses a quadrupole moment, and equally of negative sign. Hence, the fact that CO₂ possesses a quadrupole is not an explanation in itself for its supposed favourable interaction with ILs, such as can be stated in literature [67]. It is certainly true, however, that the quadrupole of CO₂ ($-14,3 \cdot 10^{-40}$ C) [68], explaining a somewhat stronger interaction with surrounding charges. Several studies furthermore reveal [69], that a molecule of CO₂ can strongly interact with the anion of the ionic liquid due to an induced dipole formed in CO₂ during collisions of both species [70], [71].

On a critical note, the question arises to what extent the use of ILs is a viable alternative to existing separation technologies taking into consideration their costs as well as the most relevant drawbacks they present, such as little physical stability, a certain reactivity or their variability in viscosity and surface tension during solute uptake [72], [73].

1.3 Ionic liquid-polymer blends

In the field of polymer materials, ILs have often been employed as functional additives for a wide variety of applications. Some examples include ILs as compatibilizers [74], functional additives into polymer electrolytes [75], [76] or as lubricants [77] and plasticizers [78]–[82], also for building blocks in polymer matrixes [83], [84] or as surfactants in layered silicates in nanocomposites [85] representing a new route to the design of high-performance materials.

When being incorporated into a polymer matrix as mere plasticizers, ILs have shown to outperform conventional plasticizers that suffer from limited compatibility, poor stability at high temperatures or when exposed to UV rays, diminished lubricity at low temperatures, and flammability [79], [81], [82], [86].

What makes ILs so different compared to conventional plasticizers? The main reason seems to be the interactions taking place between the polymer matrix and the ILs. As shown by Sebastian Livi et al. [87], ILs as additives in the polymer matrix produce a variation in the polymer morphology and, hence, their physical and thermo-mechanical properties. Coulombic and hydrogen-bond interactions have been reported to be dominating between ILs and the polymer matrix [88], but the complexity and extent of the underlying interactions is difficult to decipher on a molecular scale. As regards the latter, little has been reported in literature and speculations about how ILs interact with polymers on the molecular scale mainly rely on indirect observations. Hereafter, to date there is a need to elucidate further interactions of ILs with polymers and how the fact that

introducing ILs into the polymer induces changes in morphology, thermal properties, crystallinity, as well as mechanical properties, all of which indicate possible interactions as well as material modifications.

1.4 Thesis scope and outline

The overall objective of this thesis is the generation of a deeper knowledge on the development of composite materials based on non-porous polymeric membranes containing ILs. The accomplishment of such objective will be complemented by the setup of the respective apparatus and adequate experimental methods.

The work will focus first of all on demonstrating the possibility of using a commercial block copolymer as a base material when incorporating different ILs. Secondly, in view of the modular morphology of the base material, the behavior, effect and evolution of these composite membranes will be studied when blended with ILs.

1.5 References

- [1] J. G. Huddleston, A. E. Visser, W. M. Reichert, H. D. Willauer, G. a. Broker, and R. D. Rogers, "Characterization and comparison of hydrophilic and hydrophobic room temperature ionic liquids incorporating the imidazolium cation," *Green Chem.*, vol. 3, no. 4, pp. 156–164, **2001**.
- [2] P. Navia, J. Troncoso, and L. Romani, "Viscosities for ionic liquid binary mixtures with a common ion," *J. Solution Chem.*, vol. 37, no. 5, pp. 677–688, **2008**.
- [3] R. D. Rogers, "CHEMISTRY: Ionic Liquids--Solvents of the Future?," *Science (80-.)*, vol. 302, no. 5646, pp. 792–793, **2003**.
- [4] M. Ramdin, T. Z. Olasagasti, T. J. H. Vlugt, and T. W. De Loos, "High pressure solubility of CO₂ in non-fluorinated phosphonium-based ionic liquids," *J. Supercrit. Fluids*, vol. 82, pp. 41–49, **2013**.
- [5] N. Galonde, K. Nott, A. Debuigne, M. Deleu, C. Jérôme, M. Paquot, and J. P. Wathélet, "Use of ionic liquids for biocatalytic synthesis of sugar derivatives," *J. Chem. Technol. Biotechnol.*, vol. 87, no. 4, pp. 451–471, **2012**.
- [6] M. Kambic, R. Kalb, T. Tasner, and D. Lovrec, "High Bulk Modulus of Ionic Liquid and Effects on Performance of Hydraulic System," **2014**.
- [7] C. Chiappe and D. Pieraccini, "Ionic liquids: Solvent properties and organic reactivity," *J. Phys. Org. Chem.*, vol. 18, no. 4, pp. 275–297, **2005**.
- [8] R. D. Noble and D. L. Gin, "Perspective on ionic liquids and ionic liquid membranes," *J. Memb. Sci.*, vol. 369, no. 1–2, pp. 1–4, **2011**.
- [9] R. P. Swatloski, J. D. Holbrey, and R. D. Rogers, "Ionic liquids are not always green: hydrolysis of 1-butyl-3-methylimidazolium hexafluorophosphate," *Green Chem.*, vol. 5, no. 4, p. 361, **2003**.
- [10] P. Walden, "Molecular Weights and electrical conductivity of several fused salts," *Bull. Russ. Acad. Sci.*, vol. 8, pp. 405–422, **1914**.
- [11] J. S. Wikes, "Air and Water stable emim-based ionic liquids," *J. Chem. Soc. Commun.*, vol. 04, pp. 965–967, **1992**.
- [12] J. F. Brennecke, R. D. Rogers, and K. R. Seddon, "Ionic Liquids IV," *ACS Symp. Ser.*, vol. 975, pp. xi–xv, **2007**.
- [13] D. R. MacFarlane and K. R. Seddon, "Ionic liquids-progress on the fundamental

issues," *Aust. J. Chem.*, vol. 60, no. 1, pp. 3–5, **2007**.

- [14] N. V. Plechkova and K. R. Seddon, "Applications of ionic liquids in the chemical industry.," *Chem. Soc. Rev.*, vol. 37, pp. 123–150, **2008**.
- [15] A. García, S. Eceolaza, M. Iriarte, C. Uriarte, and A. Etxeberria, "Barrier character improvement of an amorphous polyamide (Trogamid) by the addition of a nanoclay," *J. Memb. Sci.*, vol. 301, no. 1–2, pp. 190–199, **2007**.
- [16] F. Atefi, M. T. Garcia, R. D. Singer, and P. J. Scammells, "Phosphonium ionic liquids: design, synthesis and evaluation of biodegradability," *Green Chem.*, vol. 11, no. 10, pp. 1595–1604, **2009**.
- [17] M. Deetlefs, M. Faselow, and K. R. Seddon, "Ionic liquids: the view from Mount Improbable," *RSC Adv.*, vol. 6, pp. 4280–4288, **2016**.
- [18] M. C. Bubalo, K. Radošević, I. R. Redovniković, J. Halambek, and V. G. Srček, "A brief overview of the potential environmental hazards of ionic liquids.," *Ecotoxicol. Environ. Saf.*, vol. 99, pp. 1–12, **2014**.
- [19] O. Aschenbrenner, S. Supasitmongkol, M. Taylor, and P. Styring, "Measurement of vapour pressures of ionic liquids and other low vapour pressure solvents," *Green Chem.*, vol. 11, no. 8, pp. 1217–1221, **2009**.
- [20] M. J. Earle, J. M. S. S. Esperança, M. A. Gilea, J. N. Canongia Lopes, L. P. N. Rebelo, J. W. Magee, K. R. Seddon, and J. A. Widegren, "The distillation and volatility of ionic liquids," *Nature*, vol. 439, no. 7078, pp. 831–834, **2006**.
- [21] B. Clare, A. Sirwardana, and D. R. Macfarlane, "Synthesis, purification and characterization of ionic liquids.," *Top. Curr. Chem.*, vol. 290, pp. 1–40, **2010**.
- [22] M. Ponikvar, B. Zemva, and J. F. Liebman, "The analytical and descriptive inorganic chemistry of the hydrolysis of hexafluoropnictate ions, PnF₆⁻ (Pn = P, As, Sb, Bi)," *J. Fluor. Chem.*, vol. 123, no. 2, pp. 217–220, **2003**.
- [23] N. V. Ignat'ev and U. Welz-Biermann, "New Hydrophobic Ionic Liquids (Molten Salts) with Highly Fluorinated Anions. Synthesis and Properties.," *Electrochem. Soc. Proc.*, **2004**.
- [24] G. Cevasco and C. Chiappe, "Are ionic liquids a proper solution to current environmental challenges?," *Green Chem.*, vol. 16, p. 2375, **2014**.
- [25] M. Petkovic, K. R. Seddon, L. P. N. Rebelo, and C. S. Pereira, "Ionic liquids: a pathway to environmental acceptability," *Chem. Soc. Rev.*, vol. 40, no. 3, pp. 1383–1403, **2011**.

- [26] A. B. Pereiro, J. M. M. Araújo, J. M. S. S. Esperança, I. M. Marrucho, and L. P. N. Rebelo, "Ionic liquids in separations of azeotropic systems - A review," *J. Chem. Thermodyn.*, vol. 46, pp. 2–28, **2012**.
- [27] K. Ghandi, "A Review of Ionic Liquids , Their Limits and Applications," *Green Sustain. Chem.*, vol. 4, no. February, pp. 44–53, **2014**.
- [28] T. W. Peter Wasserscheid, "Ionic Liquids in Synthesis, 2 Volume Set, 2nd Edition," **2007**.
- [29] B. Tang, W. Bi, M. Tian, and K. H. Row, "Application of ionic liquid for extraction and separation of bioactive compounds from plants," *J. Chromatogr. B Anal. Technol. Biomed. Life Sci.*, vol. 904, pp. 1–21, **2012**.
- [30] X. Lin, Y. Wang, Q. Zeng, X. Ding, and J. Chen, "Extraction and separation of proteins by ionic liquid aqueous two-phase system," *Analyst*, vol. 138, no. 21, pp. 6445–6453, **2013**.
- [31] Y. M. Liu, W. Tian, Y. X. Jia, and H. Y. Yue, "Electrochemical Applications of Room-Temperature Ionic Liquids," *Electrophoresis*, vol. 30, no. 8, pp. 1406–1411, **2009**.
- [32] D. Wei and A. Ivaska, "Applications of ionic liquids in electrochemical sensors," *Anal. Chim. Acta*, vol. 607, no. 2, pp. 126–135, **2008**.
- [33] T. Ichikawa, M. Yoshio, A. Hamasaki, T. Mukai, H. Ohno, and T. Kato, "Self-organization of room-temperature ionic liquids exhibiting liquid-crystalline bicontinuous cubic phases: Formation of nano-ion channel networks," *J. Am. Chem. Soc.*, vol. 129, no. 35, pp. 10662–10663, **2007**.
- [34] Y. Wang and H. Yang, "Synthesis of CoPt nanorods in ionic liquids," *J. Am. Chem. Soc.*, vol. 127, no. 15, pp. 5316–5317, **2005**.
- [35] C. Roosen, P. Müller, and L. Greiner, "Ionic liquids in biotechnology: Applications and perspectives for biotransformations," *Appl. Microbiol. Biotechnol.*, vol. 81, no. 4, pp. 607–614, **2008**.
- [36] N. V. P. and K. R. Seddon, "Ionic Liquids Completely UnCOILed: Critical Expert Overviews," *Wiley*, **2015**.
- [37] S. Werner, M. Haumann, and P. Wasserscheid, "Ionic liquids in chemical engineering," *Annu. Rev. Chem. Biomol. Eng.*, vol. 1, pp. 203–30, **2010**.
- [38] H. Rodríguez, "Ionic Liquids for Better Separation Processes," p. 233, **2015**.
- [39] T. P. T. Pham, C.-W. Cho, and Y.-S. Yun, "Environmental fate and toxicity of ionic

liquids: a review.," *Water Res.*, vol. 44, no. 2, pp. 352–72, **2010**.

- [40] K. Haerens, S. Van Deuren, E. Matthijs, and B. Van der Bruggen, "Challenges for recycling ionic liquids by using pressure driven membrane processes," *Green Chem.*, vol. 12, no. 12, p. 2182, **2010**.
- [41] S. I. Abu-Eishah, "Ionic Liquids Recycling for Reuse," *Ion. Liq. – Classes Prop. (Edited by Scott T. Handy)*, no. 2003, pp. 239–272, **2011**.
- [42] M. Wagner, Markus and Uerdingen, "Industrial Aspects of Ionic Liquids," *Multiph. Homog. Catal.*, pp. 566–568, **2005**.
- [43] B. Cornils, W. A. Herrmann, I. T. Horváth, W. Leitner, S. Mecking, H. Olivier-Bourbigou, and D. Vogt, "Multiphase Homogeneous Catalysis," *Wiley*, p. 905, **Aug. 2005**.
- [44] C. Meyer, S. Werner, M. Haumann, and P. Wasserscheid, "Ionic Liquids Completely UnCOILed: Critical Expert Overviews," *Wiley*, p. 592, **2015**.
- [45] L. Andreani and J. D. Rocha, "Use of Ionic Liquids in Biodiesel Production: a Review," *Brazilian J. Chem. Eng.*, vol. 29, no. 01, pp. 1–13, **2012**.
- [46] M. Messali and S. A. Ahmed, "A Green Microwave-Assisted Synthesis of New Pyridazinium-Based Ionic Liquids as an Environmentally Friendly Alternative," *Green Sustain. Chem.*, vol. 1, no. August, pp. 70–75, **2011**.
- [47] X. Han and D. W. Armstrong, "Ionic liquids in separations," *Acc. Chem. Res.*, vol. 40, no. 11, pp. 1079–1086, **2007**.
- [48] V. Pino and A. M. Afonso, "Surface-bonded ionic liquid stationary phases in high-performance liquid chromatography-A review," *Anal. Chim. Acta*, vol. 714, pp. 20–37, **2012**.
- [49] M. C. García-Alvarez-Coque, M. J. Ruiz-Angel, A. Berthod, and S. Carda-Broch, "On the use of ionic liquids as mobile phase additives in high-performance liquid chromatography. A review," *Anal. Chim. Acta*, vol. 883, pp. 1–21, **2015**.
- [50] L. Vidal, M. L. Riekkola, and A. Canals, "Ionic liquid-modified materials for solid-phase extraction and separation: A review," *Anal. Chim. Acta*, vol. 715, pp. 19–41, **2012**.
- [51] S. D. Hojniak, A. L. Khan, O. Hollóczki, B. Kirchner, I. F. J. Vankelecom, W. Dehaen, and K. Binnemans, "Separation of Carbon Dioxide from Nitrogen or Methane by Supported Ionic Liquid Membranes (SILMs): Influence of the Cation Charge of the Ionic Liquid," *J. Phys. Chem. B*, vol. 117, pp. 15131–15140, **2013**.

- [52] L. C. Tomé and I. M. Marrucho, "Ionic liquid-based materials: a platform to design engineered CO₂ separation membranes," *Chem. Soc. Rev.*, **2016**.
- [53] B. Seoane, J. Coronas, I. Gascon, M. E. Benavides, O. Karvan, J. Caro, F. Kapteijn, and J. Gascon, "Metal-organic framework based mixed matrix membranes: a solution for highly efficient CO₂ capture?," *Chem. Soc. Rev.*, vol. 44, no. 8, pp. 2421-2454, **2015**.
- [54] S. M. Saufi and A. F. Ismail, "Fabrication of carbon membranes for gas separation - A review," *Carbon N. Y.*, vol. 42, no. 2, pp. 241-259, **2004**.
- [55] H. B. Tanh Jeazet, C. Staudt, and C. Janiak, "Metal-organic frameworks in mixed-matrix membranes for gas separation," *Dalt. Trans.*, vol. 41, no. 46, pp. 14003-14027, **2012**.
- [56] B. Wang, W. S. W. Ho, J. D. Figueroa, and P. K. Dutta, "Bendable Zeolite Membranes: Synthesis and Improved Gas Separation Performance," *Langmuir*, vol. 31, no. 24, pp. 6894-6901, **2015**.
- [57] J. Liao, Z. Wang, C. Gao, S. Li, Z. Qiao, M. Wang, S. Zhao, X. Xie, J. Wang, and S. Wang, "Fabrication of high-performance facilitated transport membranes for CO₂ separation," *Chem. Sci.*, vol. 5, no. 7, pp. 2843-2849, **2014**.
- [58] D. Campos, A. Edward Feiring, S. Majumdar, and S. Nemser, "Membrane separation of ionic liquid solutions," *US9120834*, **2015**.
- [59] P. Scovazzo, A. E. Visser, J. H. Davis, R. D. Rogers, C. A. Koval, D. L. DuBois, and R. D. Noble, "Supported Ionic Liquid Membranes and Facilitated Ionic Liquid Membranes," *ACS Symp. Ser.*, vol. 818, pp. 69-87, **2002**.
- [60] P. Scovazzo, J. Kieft, D. A. Finan, C. Koval, D. DuBois, and R. Noble, "Gas separations using non-hexafluorophosphate [PF₆]⁻ anion supported ionic liquid membranes," *J. Memb. Sci.*, vol. 238, no. 1-2, pp. 57-63, **2004**.
- [61] P. Luis, T. Van Gerven, and B. Van Der Bruggen, "Recent developments in membrane-based technologies for CO₂ capture," *Prog. Energy Combust. Sci.*, vol. 38, no. 3, pp. 419-448, **2012**.
- [62] P. Bernardo, E. Drioli, and G. Golemme, "Membrane Gas Separation: A Review/State of the Art," *Ind. Eng. Chem. Res.*, vol. 48, no. 10, pp. 4638-4663, **2009**.
- [63] D. Zhongde, R. D. Noble, D. L. Gin, X. Zhang, and D. Liyuan, "Combination of ionic liquids with membrane technology: A new approach for CO₂ separation," *J. Memb. Sci.*, vol. 497, pp. 1-20, **2016**.

- [64] R. Couto, L. Neves, P. Simões, and I. Coelho, "Supported Ionic Liquid Membranes and Ion-Jelly® Membranes with [BMIM][DCA]: Comparison of Its Performance for CO₂ Separation.," *Membranes (Basel)*, vol. 5, no. 1, pp. 13–21, **2015**.
- [65] J. L. Anthony, E. J. Maginn, and J. F. Brennecke, "Solubilities and Thermodynamic Properties of Gases in the Ionic Liquid 1- n -Butyl-3-methylimidazolium Hexafluorophosphate," *J. Phys. Chem. B*, vol. 106, no. 29, pp. 7315–7320, **2002**.
- [66] A. D. B. and R. L. Disch, "The Quadrupole Moment of the Carbon Dioxide Molecule on JSTOR," *Proc. R. Soc. Lond. A. Math. Phys. Sci.*, vol. 273, no. 1353, pp. 275–289, **1963**.
- [67] Eleanor D. Bates, Rebecca D. Mayton, A. Ioanna Ntai, and J. . James H. Davis, "CO₂ Capture by a Task-Specific Ionic Liquid," **2002**.
- [68] C. Graham, D. A. Imrie, and R. E. Raab, "Measurement of the electric quadrupole moments of CO₂, CO, N₂, Cl₂ and BF₃," *Mol. Phys. An Int. J. Interface Between Chem. Phys.*, vol. 93, no. 1, pp. 49–56, **1998**.
- [69] X. Li, G. C. Schatz, and D. J. Nesbitt, "Anion Effects in the Scattering of CO₂ from the Room-Temperature Ionic Liquids [bmim][BF₄] and [bmim][Tf₂N]: Insights from Quantum Mechanics / Molecular Mechanics Trajectories," *J. Phys. Chem. B*, vol. 116, pp. 3587–3602, **2012**.
- [70] B. L. Bhargava and S. Balasubramanian, "Probing anion-carbon dioxide interactions in room temperature ionic liquids: Gas phase cluster calculations," *Chem. Phys. Lett.*, vol. 444, no. 4–6, pp. 242–246, **2007**.
- [71] B. L. Bhargava and S. Balasubramanian, "Insights into the structure and dynamics of a room-temperature ionic liquid: ab initio molecular dynamics simulation studies of 1-n-butyl-3-methylimidazolium hexafluorophosphate ([bmim][PF₆]) and the [bmim][PF₆]-CO₂ mixture," *J. Phys. Chem. B*, vol. 111, no. 17, pp. 4477–87, **2007**.
- [72] P. Cserjésii, N. Nemestóthy, and K. Bélafi-Bakó, "Gas separation properties of supported liquid membranes prepared with unconventional ionic liquids," *J. Memb. Sci.*, vol. 349, no. 1–2, pp. 6–11, **2010**.
- [73] S. M. Mahurin, P. C. Hillesheim, J. S. Yeary, D. Jiang, and S. Dai, "High CO₂ solubility, permeability and selectivity in ionic liquids with the tetracyanoborate anion," *RSC Adv.*, vol. 2, pp. 11813–11819, **2012**.
- [74] A. A. Shamsuri and R. Daik, "Applications of ionic liquids and their mixtures for preparation of advanced polymer blends and composites: A short review," *Rev. Adv. Mater. Sci.*, vol. 40, no. 1, pp. 45–59, **2015**.

- [75] M. Armand, F. Endres, D. R. MacFarlane, H. Ohno, and B. Scrosati, "Ionic-liquid materials for the electrochemical challenges of the future.," *Nat. Mater.*, vol. 8, no. 8, pp. 621–9, **2009**.
- [76] A. E. Somers, B. Khemchandani, P. C. Howlett, J. Sun, D. R. MacFarlane, and M. Forsyth, "Ionic liquids as antiwear additives in base oils: influence of structure on miscibility and antiwear performance for steel on aluminum.," *ACS Appl. Mater. Interfaces*, vol. 5, no. 22, pp. 11544–53, **2013**.
- [77] J. Sanes, F. J. Carrión, A. E. Jiménez, and M. D. Bermúdez, "Influence of temperature on PA 6–steel contacts in the presence of an ionic liquid lubricant," *Wear*, vol. 263, no. 1–6, pp. 658–662, **2007**.
- [78] M. P. Scott, C. S. Brazel, M. G. Benton, J. W. Mays, J. D. Holbrey, and R. D. Rogers, "Application of ionic liquids as plasticizers for poly(methyl methacrylate)," *Chem. Commun.*, no. 13, pp. 1370–1371, **2002**.
- [79] M. P. Scott, M. Rahman, and C. S. Brazel, "Application of ionic liquids as low-volatility plasticizers for PMMA," *Eur. Polym. J.*, vol. 39, no. 10, pp. 1947–1953, **2003**.
- [80] L. X. Hou and S. Wang, "Study on ionic liquid [bmim]PF₆ and [hmim]PF₆ as plasticizer for PVC paste resin," *Polym. Bull.*, vol. 67, no. 7, pp. 1273–1283, **2011**.
- [81] M. Rahman and C. S. Brazel, "Ionic liquids: New generation stable plasticizers for poly(vinyl chloride)," *Polym. Degrad. Stab.*, vol. 91, no. 12, pp. 3371–3382, **2006**.
- [82] P. Zhang, L. Peng, and W. Li, "Application of ionic liquid [bmim]PF₆ as green plasticizer for poly(L-lactide)," *e-Polymers*, vol. 8, no. 1, pp. 1970–1975, **2008**.
- [83] M. Xanthos, "Functional Fillers for Plastics," *Wiley*, **2005**.
- [84] K. Hanke, M. Kaufmann, G. Schwaab, M. Havenith, C. T. Wolke, O. Gorlova, M. A. Johnson, B. P. Kar, W. Sander, and E. Sanchez-Garcia, "Understanding the ionic liquid [NC4111][NTf₂] from individual building blocks: an IR-spectroscopic study.," *Phys. Chem. Chem. Phys.*, vol. 17, no. 13, pp. 8518–29, **2015**.
- [85] D. Mecerreyes, "Applications of Ionic Liquids in Polymer Science and Technology," *Springer*, **2015**.
- [86] F. J. Carrión, J. Sanes, and M. D. Bermúdez, "Effect of ionic liquid on the structure and tribological properties of polycarbonate–zinc oxide nanodispersion," *Mater. Lett.*, vol. 61, no. 23–24, pp. 4531–4535, **2007**.
- [87] S. Livi, J.-F. Gérard, and J. Duchet-Rumeau, "Ionic liquids: structuration agents in a

fluorinated matrix,” *Chem. Commun. (Camb)*, vol. 47, no. 12, pp. 3589–91, **2011**.

- [88] P. Madhavan, R. Sougrat, A. R. Behzad, K.-V. Peinemann, and S. P. Nunes, “Ionic liquids as self-assembly guide for the formation of nanostructured block copolymer membranes,” *J. Memb. Sci.*, vol. 492, pp. 568–577, **2015**.

Chapter 2

Materials and Methods

2.1	Base Polymer.....	23
2.2	Ionic Liquids	23
2.3	Solvents.....	25
2.4	Membrane Preparation	25
2.5	Membrane Material Characterization (analytical techniques)	28
2.6	Membrane Transport Studies	33
2.7	References.....	58

2.1 Base Polymer

Pebax® copolymers consist of two dissimilar homopolymers along the polymer chain backbone. The material used in this study was Pebax®2533 SA 01. The designation "SA 01" indicates that the polymer is free of additives and especially designed for food applications. In our case, the interest was to have a polymer free of additives such as to better elucidate pure polymer-ionic liquid interactions. This polymer will be further referred to as "Pebax®2533". Its chemical structure is shown in Figure 2.1 where the first segment contains a 20 wt% of a regular linear chains of rigid polyamide (PA 12), covalently linked to a second segment of 80 wt% of soft, flexible polyether (PTMO) [1]. The molecular weight of polyether is between 600 and 2000 Da while the one of polyamide is between 600 and 4000 Da. The soft and hard segments are relatively short blocks which alternate "n" times to give a polymer of high molecular weight [2], [3].

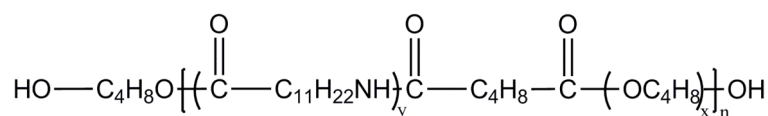


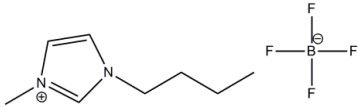
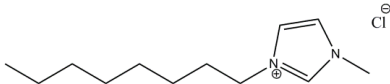
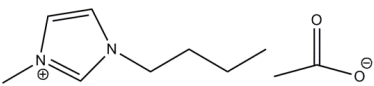
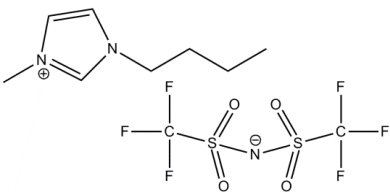
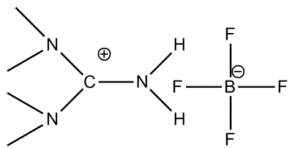
Figure 2.1 Chemical structure of poly(ether-block-amide) Pebax®2533 [amide y= 0.2, ether x= 0.8].

2.2 Ionic Liquids

The ILs used in this study: [BMIM][BF₄]; [C₈MIM][Cl]; [BMIM][Ac]; [BMIM][Tf₂N]; and [TMG][BF₄]; (>98% pure) are commercially available (Solvionic, France).

Table 2. 1 lists the ILs and their respective chemical structures:

Table 2. 1 Molecular structures of the ILs used in this study

Compound	Chemical Structure	Abbreviation	CAS Number
1-butyl-3-methylimidazolium tetrafluoroborate		[BMIM][BF ₄]	174501-65-6
1-methyl-3-octylimidazolium chloride		[C ₈ MIM][Cl]	64697-40-1
1-butyl-3-methylimidazolium acetate		[BMIM][Ac]	284049-75-8
1-butyl-3-methylimidazolium bis(trifluoromethane sulfonyl)imide		[BMIM][Tf ₂ N]	174899-83-3
1,1,3,3-Tetramethylguanidinium tetrafluoroborate		[TMG][BF ₄]	Not Determined

2.3 Solvents

Ethanol, ethyl acetate, hexane, toluene and water were used as solvents for the characterization of polymer/IL/solvent interactions and permeation tests. They were reagent grade purchased from Aldrich and used as received. Water was of ultra-pure quality (18 M Ω , LaboStar, Siemens, Germany)

2.4 Membrane Preparation

2.4.1 Casting Procedure

Pebax[®]2533 (Arkema Inc.) in the form of melt-processed pellets (2–3 mm in diameter), isopropanol and n-butanol (from Sigma Aldrich) were used without further purification. Pebax[®]2533 was dissolved in a mixture of isopropanol/n-butanol, (mass ratio 3:1) at 80°C with reflux for 2h under stirring to form a homogeneous solution containing 3 wt% of the polymer [4]–[7]. Membranes containing ILs were prepared following the same procedure by adding ILs at a ratio of 20 wt% to the polymer solution [8], [9].

The resulting solution was then cast on hot petri-dishes at 50°C and maintained at this same temperature until the solvent had entirely evaporated. Finally, dense membranes were peeled off from the glass petri-dishes, followed by complete drying at 60°C under vacuum in an oven for 7 days so as to remove any residual solvent. The thickness of each membrane was measured with an electromagnetic device MEGACHECK 5F-ST from Neurtek Instruments that fulfills the ISO 2178. It works with a resolution of 0.1 μm and a precision of 1 μm . The thickness of dry membranes was at the order of around 50 μm . Until just before carrying out any characterization of the membrane material, it was maintained in an oven at 60°C with vacuum so as to remove as much as possible any possible contaminants, including water.

2.4.2 Melting-compression procedure

Pebax®2533 and Pebax2533-[C₈MIM][Cl] blend membranes were also produced based on a thermal compression technique. The aim was to understand in how far thermal compression provides advantages and/or drawbacks compared to the solvent casting method. A potential advantage could be the absence of any solvent as a third interacting phase during the membrane formation. On the other hand, reaching the polymer melting temperature must not cause any degradation of the IL being used.

For membrane formation, and following the recommendations of the manufacturer, Pebax®2533 was dried in an oven at 60°C overnight prior to processing. In the case of pristine Pebax®2533 membranes, first an injection moulded sample was obtained by means of an extruder (Rheocord 90) under the following experimental conditions: spindle temperature: 150°C; nozzle temperature: 165°C; spin speed of the spindle: 20-22 rpm; speed of material collection: 1.2 Ohm (potentiometer). The extruded Pebax®2533 specimen was then placed between the two metallic plates (scheme in Figure 2. 2) of the hot-press (Santec), followed by heating up to 150°C maintaining the temperature constant for 2 min. After this period the specimen was in a molten state and a pressure of 220 bar was applied while maintaining the temperature at 150°C for another 3 minutes. Finally, the specimen was cooled down to room temperature in the hot press and a flat membrane was obtained.

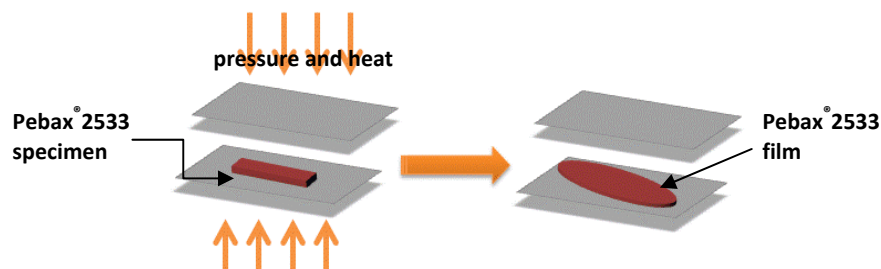


Figure 2. 2 Compression of a specimen obtained from an injection mould

For the thermal compression of blend membranes containing $[C_8MIM][Cl]$, the experimental procedure differed slightly. Instead of producing an injection moulded specimen in a first step, we compressed the mixed material Pebax2533- $[C_8MIM][Cl]$ directly from the composite pellets impregnated with the IL (see scheme in Figure 2. 3).

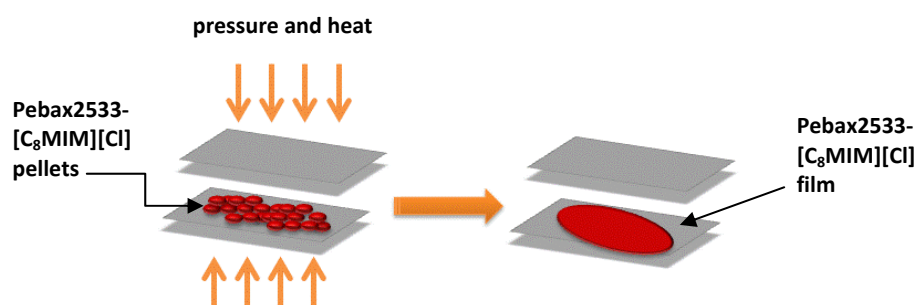


Figure 2. 3 Compression of the co-polymer blend from pellets

This variation of the experimental procedure was due to the presence of the IL. When impregnating the polymer pellets with IL, they become lubricated making their processing in an extruder impossible as they will not move along the screw. Thus, in order to obtain Pebax2533- $[C_8MIM][Cl]$ pellets, once Pebax®2533 was already into the extruder, spinning around the screw, the IL was added in a last step with a digital gauge with a piston (to control the quantity added) (see Figure 2. 4).

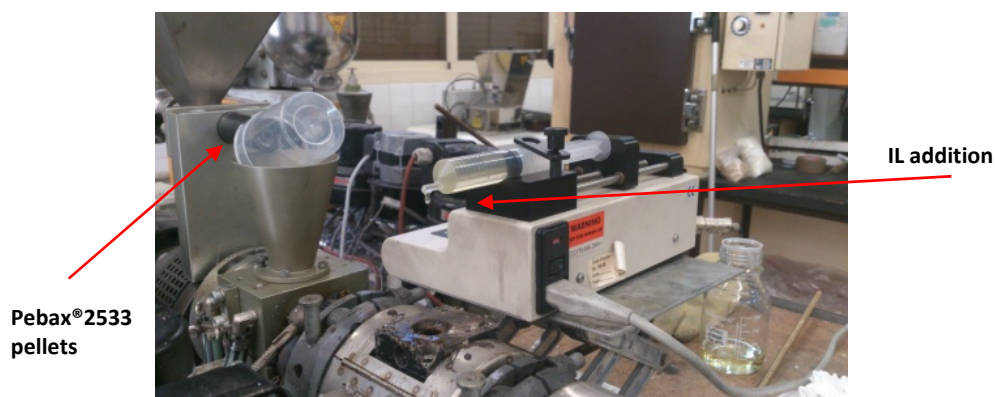


Figure 2. 4 Image of extrusion procedure followed by the addition of the IL

Then, a Pebax2533-[C8MIM][Cl] “extruded tube” was obtained containing a 20 wt% of [C₈MIM][Cl] and 80 wt% of Pebax®2533. Afterwards, in order to have a rigid material to be able to get chopped, this extruded tube was firstly passed through liquid nitrogen, to get cooled, and then it was cut.

In the last step, the procedure in the hot pressing machine was done in the same conditions as for the obtention of Pebax®2533 membranes. The membranes obtained were of about 300µm thickness.

2.5 Membrane Material Characterization (analytical techniques)

2.5.1 Water Content

A complete removal of water from room-temperature ILs is nearly impossible [10], [11] and their contamination by water is one of the biggest issues when working with ILs. Due to their charge, ILs are hygroscopic and even those featuring hydrophobic domains can absorb a significant amount of water from the atmosphere [12]. Due to this fact, extensive

studies have been focused on the investigation of water-RTIL mixtures, especially for imidazolium-based RTILs [13]–[18].

Water can modify both the structure and dynamics of ILs. For example, high water content in ILs can lead to a disruption of polar networks [17] an accelerated self-diffusion of ions, [19] and reduced viscosity [20]. Systematic studies have revealed that the extent of the modification of the ILs' structure and dynamics by water depends strongest on factors such as: the water content, the nature of the IL anion, and the length of the alkyl chain [21]–[23].

In our studies, water content of the ILs was determined by Karl Fischer using a Metrohm 831 coulometer. Prior to determining the water content, ILs were kept in an oven under vacuum at 60°C. Once they were taken from the oven, they were immediately sealed in a recipient and let reach room temperature. Once opening again the recipient, Karl Fischer measurements using a syringe of 1 ml were carried out rapidly in order to avoid as much as possible absorption of humidity from the atmosphere. Triplicate measurements were performed on each sample. Data provided represent therefore an average of the three measurements with its standard deviation.

2.5.2 Atomic Force Microscopy (AFM)

AFM images were obtained operating in tapping mode (TM–AFM) with a scanning probe microscope (NanoScope IIIa, MultimodeTM from Digital Instruments, Veeco) equipped with silicon tips of an average diameter of 10 nm having a resonance frequency of about 300 kHz (same manufacturer). In order to obtain representative results, all AFM imaging was carried out with scan sizes of $10 \times 10 \mu\text{m}^2$ under ambient conditions with a scan velocity of $1 \mu\text{m} \cdot \text{s}^{-1}$. The images from AFM were processed with NanoScope v720. AFM measurements were performed in the Escuela Politécnica Donostia, by the Unit of Materials and Surfaces (Macroconducta-Mesoconducta-Nanotecnología) from the General Services SG-Iker (UPV/EHU).

2.5.3 Thermal Gravimetric Analysis (TGA)

Thermogravimetric data were collected by a thermobalance TA instrument TGA-Q500. About 10 mg of sample (previously taken from an oven at 60°C with vacuum) were placed in a pan inside the tube furnace. Measurements were performed by heating from room temperature to 600°C at a heating rate of 10°C/min under nitrogen atmosphere. The TG and DTG curves were obtained using a standard procedure provided by “Universal Analysis 2000” software from TA Instruments

2.5.4 Differential Scanning Calorimetry DSC)

DSC analysis of Pebax®2533 and mixed membranes of Pebax®2533/IL were performed using a differential scanning calorimeter DSC Q2000 containing a refrigerator cooling system. Samples (~10 mg) were placed in hermetically sealed aluminum pans and heated from room temperature to 200°C with a heating rate of 10°C/min (the hermetically sealed pans were found necessary to avoid any spillage of the IL from the blended membranes and possible contamination of the equipment). All DSC runs were carried out under nitrogen atmosphere to minimize possible oxidative degradation. During the second scan, samples were cooled from 200°C to -90°C. Melting and crystallization peaks, as well as glass transition temperature values were obtained from second scan thermograms. The glass transition temperature was determined as the temperature where a baseline inflection occurred, and the melting temperature was determined as the peak temperature of the endothermic event of the DSC curves. All the results (heat of fusion, glass transition, melting point and crystallization temperatures) were calculated using the TA Universal analysis 2000 software.

DSC analysis of Pebax®2533 and mixed membranes of Pebax®2533/IL were also characterized in Christian Albrechts Universität zu Kiel in the temperature range from T = -120 to 250°C by using a Perkin Elmer DSC 204 calorimeter. Measurements were performed at the scan rate of 10°C/min, and the experiments were conducted by using a

nitrogen purge gas stream. Melting and glass-transition temperature values were obtained from first scan thermogrammes, while the crystallization peaks were obtained during the cooling step.

2.5.5 Polarized Optical Microscopy (POM)

Polarized optical microscopy was used to observe the thermal effects on the morphology of pristine Pebax®2533 and a blend membrane containing C₈MIMCl. A Leitz Aristomet optical microscope equipped with a Mettler FP80 central processor and FP82 hot stage was used (temperature control precision of ±4°C). Images were captured employing a Leica DC420 with software of IM-100 during heating or cooling rates of 2°C/min. For the measurements, samples were placed onto a glass slide covered with a coverslip. Once introduced in the heating device, they were heated at maximum velocity up to 190°C to obtain the molten material. Samples were then maintained at this temperature for 10 min with the aim of eliminating their thermal history. Subsequently, they were cooled down to 30°C at 2°C/min. During this latter process, photographs were periodically taken in order to optically evaluate the creation of spherulites.

2.5.6 Fourier Transform Infrared Spectroscopy (FTIR)

Transmission infrared spectra of all films were recorded at room temperature by means of a FTIR Nicolet 6700 Thermo scientific spectrophotometer. Measurements were obtained at room temperature in the scanning range of 4000 to 400cm⁻¹ during 32 scans to yield a high signal-to-noise ratio, and with a 2cm⁻¹ nominal resolution. In order to increase the analytical resolution, films of a thickness under 50µm were obtained by casting the pristine Pebax®2533 or Pebax®/IL films onto a glass slide. Once the solvent had evaporated, the film was mounted into the sample holder and data were collected after scanning the background. For the measurement involving ILs only, a couple of droplets of IL were placed onto a KBr pellet. The resulting spectra were processed using the OMNIC 7.1a (Thermo

Electron, Inc., Lafayette, CO) Raw spectra were subtracted from relative the background and an automatic baseline correction was employed to flatten the baseline.

2.5.7 Solid State ^{13}C Nuclear Magnetic Resonance

NMR spectra were obtained using a Bruker 400 WB Plus spectrometer. Spectra of the pristine polymers and polymer/IL blends were collected by using a 4mm CP-MAS probe at a spinning rate of 10000Hz. ^{13}C CPMAS spectra of solid samples were recorded for 12h using the standard pulse sequence at 100.6 MHz, a time domain of 2 K, a spectral width of 29 kHz, a contact time of 1.5ms and an interpulse delay of 5s. For the analysis of polymer that had been previously in contact with vapours, samples were in contact with the respective organic solvents for 30h prior to analysis. Subsequently, they were superficially wiped with tissue paper to remove excess liquid. NMR spectra were processed using the software of MNova by Mestrelab Research (www.mestrec.com), Spain. Measurements were performed by the Unit of Materials and Surfaces (Resonancia Magnética Nuclear) from the General Services SG-Iker (UPV/EHU).

2.5.8 Positron Annihilation Lifetime Spectroscopy (PALS)

Positron annihilation lifetime experiments were conducted with a setup consisting of a fast-fast coincidence setup with a home-made temperature controllable sample holder under high vacuum conditions described in more detail elsewhere [24], [25]. Polymeric films were cut into 9mm×9mm pieces and stacked with a Na^{-22} source (1 MBq) in a sandwich-like manner such as to obtain a total sample thickness of about 1.2mm in order to ensure complete absorption of the positrons in the sample. The sandwich was wrapped in aluminium-foil and placed into the sample holder. Positron annihilation spectra were recorded typically with 10^7 counts within 12h. The evaluation was performed with the LT 9.2 routine program [26] by using the common background subtraction and the final resolution function, which was determined as a sum of two Gaussians with FWHMs (full

width at half maximum) of approximately 247 and 390 ps and weight of 80% and 20%; three lifetime components were assumed where the first was kept fixed at 125ps (lifetime of p-Ps in vacuum).

2.5.9 X-Ray Diffraction

X-Ray diffraction was used as a complementary technique to DSC in order to determine the crystallinity of the membrane samples at room temperature. The X-ray diffractometer used in this study was a Seifert XRD 3000, theta theta goniometer, Cu K alpha wavelength. The diffractometer was operated in the step-scan mode with a step width of 0.02° of 2θ and counting of 10s per step. The angles measured ranged from 10° to 28° of 2θ. The measurements were performed at room temperature.

2.6 Membrane Transport Studies

2.6.1 Saturated Vapour Permeability Measurements

A gravimetric permeation set-up was employed as described in detail elsewhere [27], [28]. The home-made permeation cell (Figure 2. 5) consisted of two pieces: a base compartment partially filled with the corresponding solvent, above which the membrane is placed without being in contact with the solvent. Sealing and fixation of the membrane was achieved by screwing the upper ring onto the base. In the base compartment, a saturated vapour would then form according to the vapour-liquid equilibrium at the experimental temperature. This solvent vapour permeated the polymeric membrane from where it was supposed to freely desorb and evaporate into the air. The latter was recorded as a reduction in overall weight loss by a Sartorius BP 210D balance with a resolution of 10⁻⁵ g. The balance was interfaced with a computer for data acquisition. The entire permeation cell consisted of PTFE (polytetrafluoroethylene) due to its high chemical resistance. The whole experimental set-up was placed in a cabinet thermostatted at 25°C.

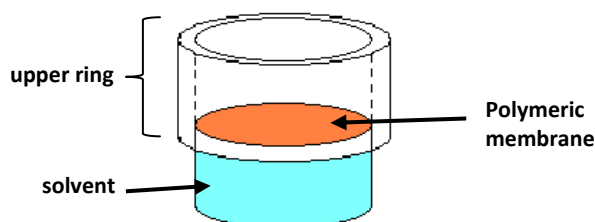


Figure 2. 5 Device made of PTFE for permeation tests

2.6.2 Time-lag gas Permeation Measurements

Permeation of CO₂ and N₂, respectively, through the polymer/IL blend membranes was measured using the “time-lag” method [29] which in principle allows the simultaneous determination of permeability and diffusivity. For this purpose, a custom-made permeation device was employed in which the upstream (feed) and downstream (permeate) compartment can be independently evacuated, monitored each with a capacitive pressure gauge (model 627B from Baratron, MKS Instruments, USA). The pressure gauges covered the range of 0.001-1000 mbar with a precision of 0.15%. Details on the construction and operation of this experimental setup can be found described in detail elsewhere [30].

For the measurement, the sample membrane was placed onto a highly porous sintered disk with a diameter of 2.85 cm providing mechanical stability. Prior to measurements, the experimental set-up was degassed under vacuum during 12 hours. Gas permeation experiments were performed at 23°C (temperature controller Conartec 4400) and an upstream (feed) pressure of 1 bar while the initial downstream pressure (permeate) was ~0.01 mbar. Once the experiment started (pressurization of the feed chamber), gas permeated the membrane and desorbed into the permeate chamber of constant volume resulting in a progressive increase of the permeate pressure registered by the pressure transducer. As long as the downstream pressure is small compared to the upstream pressure, the increase in permeate pressure is constant over time.

All permeation experiments were conducted at least in quadruplicates with one and the same membrane being used for each measurement of the permeability of CO₂ and N₂, respectively. Between experiments, the permeation cell and lines were evacuated on both upstream and downstream sides as described above. When using polymer/IL blend membranes, no residual IL was found inside the permeation cell at the end of the experiments.

2.6.2.1 Data Processing

The gas transport through a dense membrane can be modelled according to the solution-diffusion mass transfer model where the permeability P_i of a solute is the product of its solubility S_i and diffusivity D_i in the membrane polymer [29], [31]–[33].

$$\text{Equation 2. 1} \quad P_i = S_i \cdot D_i$$

Although not a SI unit, the gas permeability is usually expressed in in Barrer:

$$\text{Equation 2. 2} \quad 1\text{Barrer} = 10^{-10} \frac{\text{cm}^3(\text{STP}) \cdot \text{cm}}{\text{cm}^2 \cdot \text{s} \cdot \text{cmHg}}$$

The solution-diffusion model is the most widely used for the permeation of gases in polymer membranes [31]. The fundamental mechanism of gas transport across a polymer membrane was not developed until 1866 by Thomas Graham [34] where he postulated that the permeation process involves three steps: solution of the permeant molecules into the membrane surface, followed by the diffusion of these molecules through the membrane material, and then desorption of the permeant on the downstream side of the membrane [35]. Graham made several important observations at the time: (1) Permeability was independent of pressure; (2) The increase of temperature led to decrease in penetrant solubility but made the membrane more permeable, (3) A prolonged

exposure to elevated temperature affected the retention capacity of the membrane and (4) A variation in the membrane thickness alters the permeation rate but not the separation characteristics of the polymer. More recent work done by Glicksman [36] provides a comprehensive review of recent developments in the field of modelling of diffusion in solids.

The separation between different permeants ("permselectivity") is then achieved due to a difference in sorption ("sorption selectivity") and the rate at which the material diffuses through the membrane ("diffusion selectivity"). In this model, sorption and desorption are assumed to be very fast relative to the diffusion through the polymer, such that the latter becomes the rate-limiting step in mass transport across the membrane. Permselectivity is hence expressed as the product of the diffusion selectivity and the sorption selectivity as follows in Equation 2. 3:

$$\text{Equation 2. 3} \quad \alpha_{i/j} = \frac{P_i}{P_j} = \left(\frac{D_i}{D_j} \right) \cdot \left(\frac{S_i}{S_j} \right)$$

The steady-state flux J_i of a solute across a membrane under a transmembrane pressure drop Δp_i and for a certain membrane thickness l_m follows then as:

$$\text{Equation 2. 4} \quad J_i = \frac{D_i \cdot S_i}{l} \cdot \Delta p_i$$

Assuming that the experimental conditions warrant solute transport across the membrane according to Equation 2. 4 the flux can then experimentally be determined measuring the variation of permeate (downstream) pressure ΔP_p and using Equation 2. 5, where V_p is the permeate (downstream) volume, A_m is the effective membrane surface area, Δt is the experimental time, R is the universal gas constant and T is the temperature:

$$\text{Equation 2.5} \quad J_i = \frac{V_p \Delta P_p}{A_m \cdot \Delta t \cdot R \cdot T}$$

The rate of flow and the concentration of a diffusant at any point of the thickness of a membrane vary with time. Assuming the diffusion coefficient to be constant, the membrane at first will be completely free of diffusant and diffusant will continually be removed from the low concentration side ($C_2=0$) and the amount of diffusant, Q_t , which passes through the membrane in time, t , is given by Equation 2.6:

$$\text{Equation 2.6} \quad \frac{Q_t}{lC_1} = \frac{D \cdot t}{l^2} - \frac{1}{6} - \frac{2}{\pi^2} \sum_1^{\infty} \frac{(-1)^n}{n^2} \exp\left(\frac{-Dn^2\pi^2t}{l^2}\right)$$

As steady state is approached, $t \rightarrow \infty$, the exponential terms become negligibly small, allowing for plotting Q_t versus t as in Equation 2.7:

$$\text{Equation 2.7} \quad Q_t = \frac{DC_1}{l} \left(t - \frac{l^2}{6D} \right)$$

The time-lag parameter θ indicates the time which passes before achieving steady-state flux. It is determined in a permeate pressure versus time plot as the x-axis intercept that results from extrapolating the slope of the linear increase of the permeate pressure down to the intercept time axis as described in Equation 2.8 (see Figure 2.6)

$$\text{Equation 2.8} \quad \theta = \frac{l^2}{6D}$$

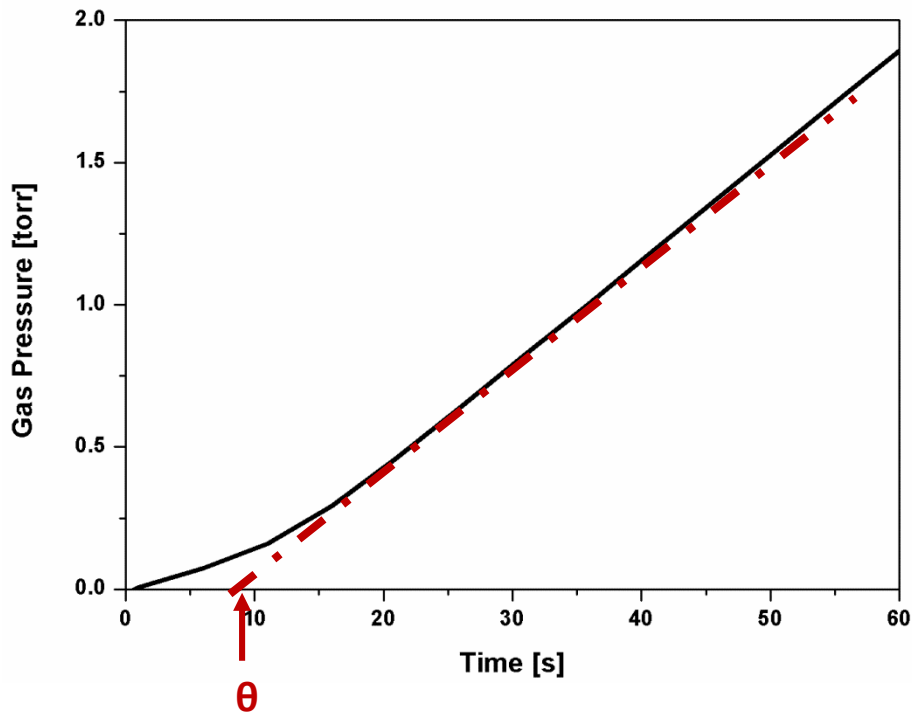


Figure 2. 6 Representation of how the time lag (θ) is determined

The determination of θ is not always precise and even less so for systems where the diffusion coefficient is very high, since the resulting time lag is usually very short, consequently prone to a big error and thus resulting in results of little confidence.

2.6.3 Cahn electrobalance

Sorption measurements were performed employing a Cahn D-200 electrobalance placed in a thermostatic chamber with temperature control [37]. Two different sample holders were used (see Figure 2. 7) depending on the material of study.



Figure 2. 7 Sample holder for a) film and b) liquids

Polymer films (solid samples) were placed in an aluminum sample holder as a grid. On the other hand, for ILs (liquid samples), the sample holder consisted of a concave reservoir where a small quantity of the liquid (max. 100 mg) can be placed. In both cases, according to the equipment manufacturer, the material of the sample holder was totally inert and thus will in principle not adsorb any significant amount of solvents or gases. In any case, blank measurements were conducted before a series of experiments as is described below. The main difference between both sample holders is that in the case of liquids, only the upper part is directly in contact with the penetrant being studied, while in solid samples, the gases/vapour molecules will be able to pass through the sample holder and thus contact with the solid film from both sides.

During sorption, the mass gain of the samples measured is continuously recorded. However, these measured data still require correction for (1) the buoyancy force and (2) possible adsorption phenomena in absence of the sample. The hydrodynamic buoyancy effect takes into account the hydrodynamic force the gas applies against the sample due to Archimedes' Principle stating that a body immersed in a fluid, whether fully or partially submerged, displaces a volume equal to the weight of the fluid that the body displaces. This correction is necessary as during zeroing of the balance the gas/vapour has not yet

been introduced into the chamber. Omitting this correction would, hence, result in a subestimation of the real mass sorbed. If solute sorption is very low, it can therefore even happen that negative sorption values are obtained if the hydrodynamic buoyancy is not taken into account [38].

For the determination of the hydrodynamic buoyancy effect (m_{buoyancy}) using Equation 2. 9, it is assumed that the gas introduced behaves as an ideal gas and that the pressure at working conditions is lower than 1bar [39].

$$\text{Equation 2. 9} \quad m_{\text{buoyancy}} = \frac{P_{\text{gas/vapour}} \cdot \frac{m_{\text{polymer}}}{\rho_{\text{polymer}}} \cdot MW_{\text{gas}}}{R \cdot T}$$

$P_{\text{gas/vapour}}$ refers to the gas pressure in the balance during sorption, m_{polymer} corresponds to the mass of the polymer sample, ρ_{polymer} is the density of the polymer sample, the MW is the molecular weight of the gas, R corresponds to the ideal gas constant and T is the temperature at which the experiment has been carried out. Equation 2. 9 was used for both gas and vapour samples, assuming that the latter behaves like an ideal gas.

The second correction which needs to be applied to the originally measured mass sorption data corresponds to the possible unspecific sorption of gas or vapour by the balance itself, denoted the "sorption of the blank". This occurs when the components of the balance are in contact with the gas/vapour could adsorb traces of the latter. A blank run is therefore done at the same pressure and temperature conditions as the actual measurement, but without any sample. Depending on the sorption capacity of the sample, this value may be negligible in comparison with the gas/vapour sorbed by the sample. As an example for a relevant case for this correction, Chapter 5 illustrates how this blank measurement affects the vapour absorption in the sample being tested.

Employing both corrections, the buoyancy effect and the sorption of the blank, the real mass absorbed by the sample of interest is calculated using Equation 2. 10.

$$\text{Equation 2. 10} \quad m_{\text{real}} = m_{\text{absorbed}} + m_{\text{buoyancy}} - m_{\text{blank}}$$

In this work, sorption studies were conducted for both gases and vapours with the respective experimental procedure being slightly different in either case. For measuring the sorption of vapours, the set-up consisted in a dynamic sorption process which would minimize possible condensation effects that could interfere with the measurement. For gases, the conventional static set-up was employed. Both set-ups are described in detail in the following.

2.6.3.1 Vapour Sorption Studies (dynamic sorption process)

The experimental procedure was the same for all vapours. Prior to the experiment, polymer or polymer/IL samples were stored in an oven at 60°C under vacuum. Due to the small thickness of solid membranes, 4-6 rectangles of the membrane (25X10 mm) were cut and stacked such as to obtain samples with enough thickness and weight to be sensible to the equipment procedure. In the case of ILs, some droplets of each IL were placed as received from the manufacturer into the sample holder without any further treatment. After placing the sample in its respective sample holder and into the balance sorption chamber, the system was purged at 24 ±1°C with N₂ (purity 99.998%) under a flux of 50 mL/min for 24-30h until the weight of the sample showed a mass variation of less than 0.2%/h. The temperature was controlled with an automatic controller Conatec 4400 connected to a resistance of 1000W, regulated with a fan. Subsequently, the saturated organic vapour was introduced into the thermostatted chamber by passing N₂ gas with a constant flow rate of 50 mL/min through the organic solvent which was placed in a bubbler (see Figure 2. 8).

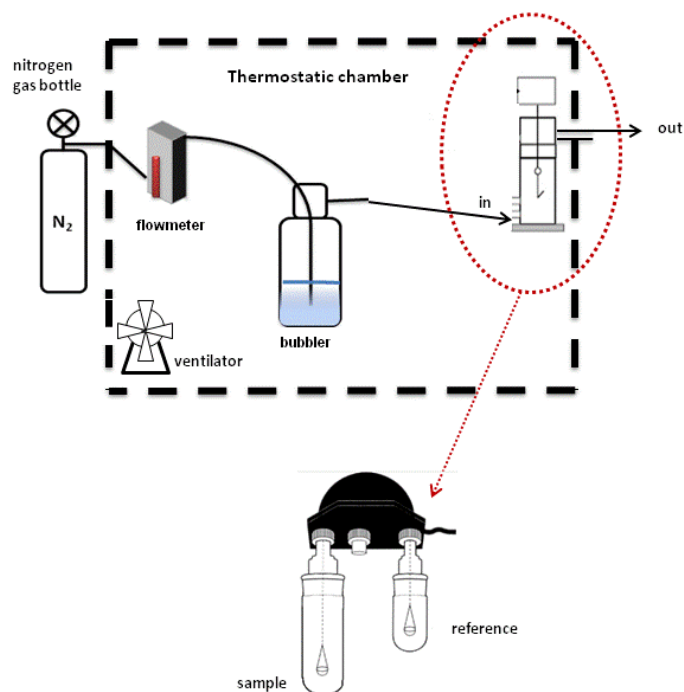


Figure 2. 8 Scheme of a Cahn electrobalance in dynamic mode (vapour system)

Experiments were conducted until a steady state was reached which generally took about 2 days. Steady-state was considered to have been achieved when the mass change was below 0.5 wt%/h. Each experiment was repeated 2-3 times, each time using a new sample. Such measurement therefore yields both transient and steady-state sorption data.

2.6.3.2 Gas Sorption Studies (static process)

Gas sorption studies were carried out in a static set-up as shown in Figure 2. 9. The main difference with regard to vapour sorption experiments consisted in the fact that in this case the overall system was evacuated removing the air and any other possible volatiles inside the chamber and the sample (desorption). Once the sample weight was stable, the

sorption was measured by introducing the sample gas under static conditions as will be described in more detail below.

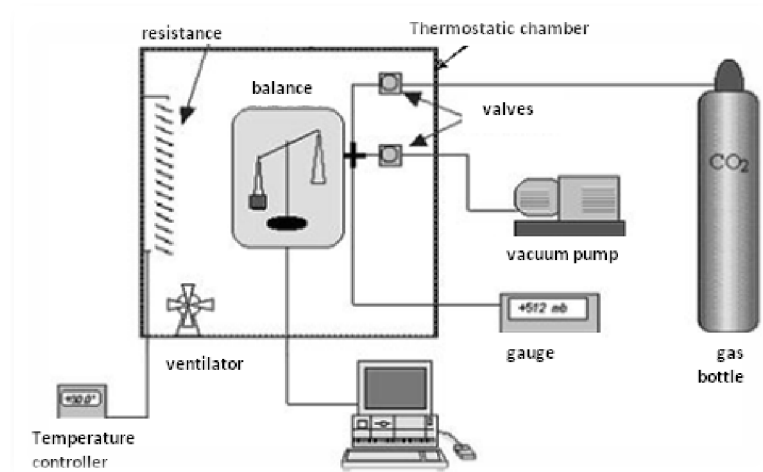


Figure 2. 9 Schematic part of a Cahn electrobalance in static mode (gas system)

Prior to any measurement, the sample preparation procedure was similar to the dynamic sorption. The sample, in this case an IL, was stored in an oven at 60°C under vacuum prior to placing it into the sample holder of the Cahn electrobalance. An average sample mass was about 100 mg. The sample then underwent desorption until stabilization using a vacuum pump (Varian DS102). A "stable" steady-state mass was considered when the variation in the sample mass was less than 0.2%/h which commonly was achieved after 28 days of experiment. Subsequently, the gas was introduced at a pressure of 1bar. Once the gas pressure was indicated as being stable by the pressure gauge, the latter was closed and the sample let reach the sorption equilibrium. The gas pressure in the chamber was measured with a capacitance manometer Leybold Inficon CM3, with a precision of 10^{-3} bar.

Each experiment was repeated twice, each time using a new sample. Real sorption data were corrected by taking into consideration buoyancy effects and by subtracting a blank run, as described previously.

- Cahn Data Processing

Once all the corrections were considered, the real mass of solute sorbed until reaching the equilibrium (m_∞) is obtained as represented schematically in Figure 2. 10.

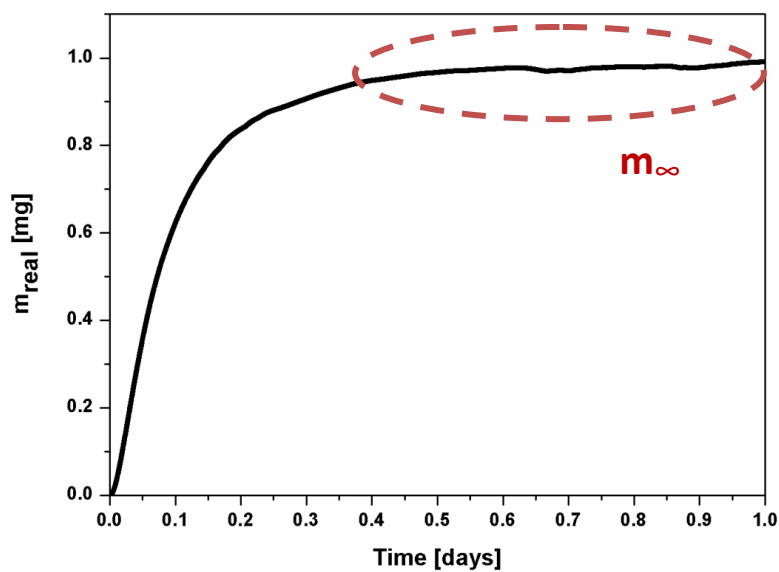


Figure 2. 10 Plot of m_{real} [mg] as a function of time [days] during a typical sorption experiment

The mass fraction [w_i] of the gas sorbed by the sample at equilibrium is calculated by dividing the equilibrium mass (m_∞) by the sample mass initially placed in the sample holder, m_{initial} + the mass gained after the vapour absorption.

$$\text{Equation 2. 11} \quad w_i = \frac{m_\infty}{m_{\text{initial}} + m_\infty}$$

From the transient in Figure 2. 10 the diffusivity D can be derived. The higher the diffusivity, the faster the gas or vapour permeates through the membrane. In this work,

diffusivity values were obtained in two different ways, namely by (1) applying analytical solutions of Fick's second law for parts of the sorption curve or by (2) fitting the whole sorption curve with Fick's second law.

In the case of dynamic sorption process, when working with thin films, it will be considered that the diffusion will only take place in the perpendicular axis of the plane, supposing negligible diffusion from the thin planes of the film. In this case the system can be modeled as a semi-infinite slab with one-dimensional diffusion across the film thickness. It also will be assumed that the diffusion coefficient is constant, i.e., independent of the solute concentration in the sample. This is strictly only the case for very dilute systems and deviations from ideality can be expected when high affinity solute concentrations are employed such as is the case in saturated vapour experiments. For one-dimensional diffusion with a constant coefficient, Crank in 1986 (Polymer additive analysis industrial plastic and case studies) derived an analytical solution to Fick's second law Equation 2. 12 yielding Equation 2. 13 or Equation 2. 14 [40]–[42].

$$\text{Equation 2. 12} \quad \frac{\partial c}{\partial t} = D\nabla^2 c$$

$$\text{Equation 2. 13} \quad \frac{m_t}{m_\infty} = 1 - \frac{8}{\pi^2} \sum_{n=0}^{\infty} \frac{1}{(2n+1)^2} \exp\left[-\frac{(2n+1)^2 \pi^2 D t}{l^2}\right]$$

Equation 2. 13 can be reorganized in:

$$\text{Equation 2. 14} \quad \frac{m_t}{m_\infty} = 2 \left(\frac{Dt}{l^2} \right)^{1/2} \left(\frac{1}{\pi^{1/2}} + 2 \sum_{n=1}^{\infty} (-1)^n \operatorname{ierfc} \frac{nl}{\sqrt{Dt}} \right)$$

“ m_t ” is the mass of penetrant (vapour or gas) sorbed by the film at any time t , “ m_∞ ” is the final equilibrium mass of penetrant in the film, “ D ” is the diffusion coefficient of penetrant in the film, and “ l ” is the film thickness.

The initial mass change during Fickian diffusion ideally shows a linear dependence between m_t/m_∞ and $t^{1/2}$. This linear region provides a way to obtain D directly from the initial slope of a plot of m_t/m_∞ versus $t^{1/2}$ by using Equation 2. 15, obtained from Equation 2. 14 at the limit of short experimental times (the error is in the range of 0.1% when the ratio of m_t/m_∞ is lower than 0.5 as discussed in detail by Vergnaud 1991 [43]).

$$\text{Equation 2. 15} \quad \frac{m_t}{m_\infty} = \frac{2}{l} \left(\frac{Dt}{\pi} \right)^{1/2}$$

On the other hand, in the case of **long-time diffusion** and for the data range of $m_t/m_\infty > 0.5$, Equation 2. 13 can be written as follows:

$$\text{Equation 2. 16} \quad \frac{m_t}{m_\infty} = 1 - \frac{8}{\pi^2} \exp \left[\frac{-D\pi^2 t}{4l^2} \right]$$

But Equation 2. 16 is usually used in the form of Equation 2. 17 given as follows:

$$\text{Equation 2. 17} \quad \ln\left(1 - \frac{m_t}{m_\infty}\right) = \ln\left(\frac{8}{\pi^2}\right) - \frac{D\pi^2 t}{4l^2}$$

While the complete mass uptake curve can, in principle, be fit using Equation 2. 15 or Equation 2. 17 to obtain D, it should be said that they act as analytical solutions to lineal parts of the total mass uptake curve.

These estimations show in principle similarly negligible error on the order of 0.1% as determined by Vergnaud [43]. It can happen that the Fickian model with a constant diffusion coefficient does not appear to adequately describe the complete sorption transient of the polymer. This is not unexpected since polymers are well known to exhibit non-Fickian behavior, owing to, for example, swelling effects [44]. In the case of such non-ideal effect to occur, diffusion coefficients determined during "short" (Equation 2. 15) and "long" (Equation 2. 17) will be found to differ accordingly.

While the abovementioned "shortcuts" to obtaining analytical solutions for the diffusion coefficients are convenient, they still are based on approximations that might not be all valid. We therefore have also determined the diffusion coefficient by fitting the whole sorption transient according to Fick's Second Law using the discretization method by Crank-Nicholson [45].

2.6.4 Quartz Crystal Electrobalance with Dissipation Monitoring (QCM-D)

The QCM-D used for this work was the E1 System from Biolin Scientific/ Q-Sense AB, Västra Frölunda, Sweden. All experiments were conducted at $23 \pm 0.1^\circ\text{C}$. Sensors used (Q-Sense sensor QSX 301) were quartz crystals of 14mm in diameter with the area of the gold electrode being 1 cm^2 .

2.6.4.1 The QCM-D System

The equipment consists of several parts (Figure 2. 11):

- a. The sensor crystal.
- b. The flow module (QFM 401), in which the sensor crystal is mounted.
- c. An accessory chamber into which the flow module placed allowing a temperature-controlled environment for the crystal during the measurement.
- d. The electronics unit that controls the QCM-D measurements.
- e. The data acquisition software, Q-Soft 401 (Q-Sense, Sweden), and data analysis software, Q-Tools (Q-Sense, Sweden).
- f. A vapour-mixing unit with a bubbler for creating different vapour activities
- g. the nitrogen carrier gas supply

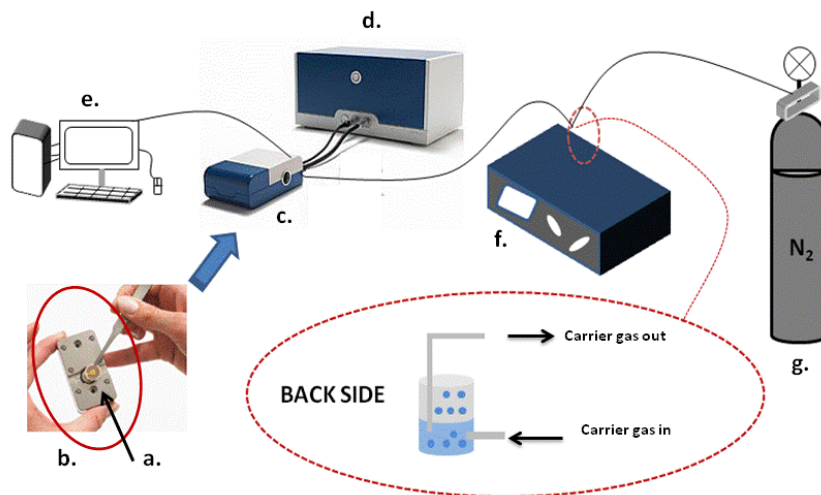


Figure 2. 11 Schematic setup of the vapour sorption measurement system using QCM-D

The computer-controlled vapour mixer (IB-32 GasMIXer, Iberfluid, Spain) could be programmed in terms of exposure time and the vapour activity to be reached.

2.6.4.2 Quartz Crystals

The quartz crystal employed consist in a thin piezoelectric quartz disc sandwiched between gold electrodes. Figure 2. 12 a) depicts the sensing side onto which the polymer is deposited. Figure 2. 12 b) depicts the counter electrode which is not in contact with any vapour and must be kept absolutely clean, also after the polymer deposition.

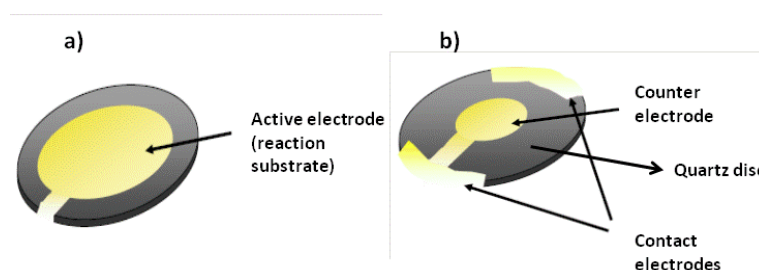


Figure 2. 12 Image of the two sides of the QCM-D quartz crystal: a): the sensing side and, b), the contact side.

Sensors with gold coating on the sensing side were chosen as in our case the polymers attached relatively easy to this surface. However, alternative materials can be sputtered or adsorbed onto the gold surface such as SiO_2 , Al_2O_3 , TiO_2 , and monolayers with functional groups such as thiol or amine groups which may allow better adhesion of the polymer material onto the surface.

2.6.4.3 Sensor cleaning

This procedure is applicable to both QCM-D sensors as well as SPR's.

Before starting the experiments with new sensors, these were sonicated for 10min in ethanol and then dried with N_2 (purity 99.998%). During the cleaning process the crystals

where held in a teflon sensor holder (Biolin, Sweden). For the cases with re-used quartz crystals, the cleaning process was the following:

- (1) 15min sonication with the solvent of the copolymer (3:1 solution isopropanol:n-butanol);
- (2) 10 min sonication with ultrapure water (electrical resistivity of 18M Ω -cm);
- (3) 10 min UV/ozone cleaner (Bioforce Nanosciences, USA); (4) drying process with N₂ (purity 99.998%).

For those cases where used sensors visually showed a significant deposit on their surface, they were immersed in base piranha solution. Base piranha solution is a strong oxidizing mixture of deionized water, NH₄OH (25%) and H₂O₂ (30%) of a ratio of 5:1:1 suitable for removing organic matter. When required, the sensors were placed at 75°C during 5 minutes in this solution prior to the earlier described standard protocol of cleaning.

2.6.4.4 Polymer deposition

Spin coating is the preferred method for application of thin, uniform films to flat substrates because it is a relatively simple to use. The spin coating technique is described in detail under 2.6.6 section in this chapter.

For creating the thin polymer films on the sensor surface, Pebax®2533 grains were dissolved in a mixture of isopropanol/n-butanol, (mass ratio 3:1) described in this chapter, in section 2.4 yielding a stock solution from which dilutions were made as required.

Throughout this work, one and the same spin coating procedure was used and is described as follows. A droplet of 6 μ L of the polymer solution was deposited with a micropipette onto the sensor surface and the spin coating initiated with the program conditions being:

1st step: 10 seconds to reach a velocity of 20rps followed by 20 seconds at 20 rps.

2nd step : 10 seconds to reach a velocity of 25rps followed by 20 seconds at 25 rps.

The thickness of the polymer layer deposited was determined as the change in frequency measured between the pristine sensor and once the sample layer was deposited, using the "stich file" option of the acquisition programme (see Figure 2. 13 as an example).

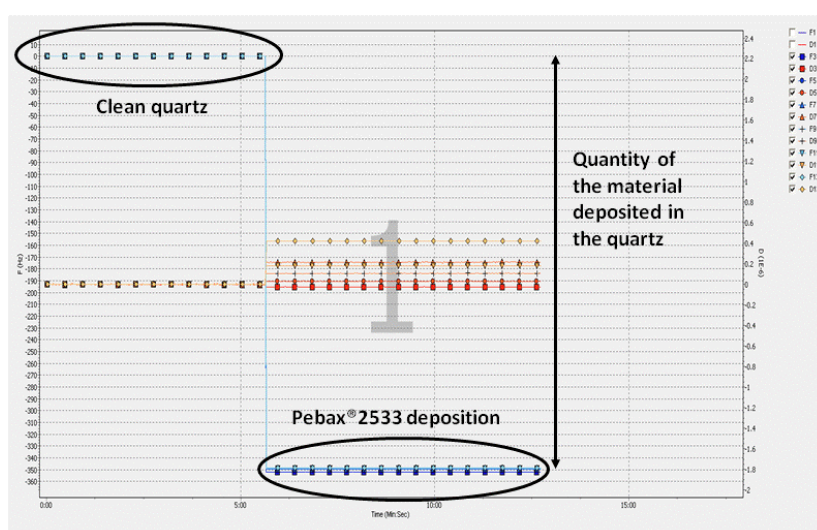


Figure 2. 13 Change in frequency as a consequence of the Pebax®2533 layer deposition

Measurements were made under nitrogen-flow of 50 ml/min to ensure a steady flow regime over the sensor surface during thickness determination. The thickness was then calculated using the Sauerbrey equation [46] and assuming the density of the polymer to be 1g/cm^3 [47]

2.6.4.5 Vapour sorption measurements

Vapour sorption measurements in QCM-D were carried out using a gas mixer (IB-32 Gas mixer-Iberfluid) at different vapour activities and a total vapour flow of $50\mu\text{l/min}$. The total flow was kept constant at all times as slight variations in the flow rate would result in a

response of the quartz sensor. This system is composed of a reservoir where the solvent to be studied is placed at a volume of 30 ml aprox., and subsequently bubbled with N₂ in order to generate a saturated vapour. Using mass flow controllers, this saturated vapour is diluted with N₂ to reach the desired vapour activity and maintaining the overall flow rate constant. More details on the experimental procedure are provided in Chapter 6.

For data analysis, as a first attempt the Sauerbrey model was applied in order to transform frequency changes measured into masses. In general, the fundamental overtone (n=1) should be disregarded, since it is affected by the mechanical stress imposed by the o-ring which fixes the quartz sensor in the chamber (information provided by the manufacturer). In our case, after a thorough study to determine the most representative overtones, the fifth and the eleventh have been selected (for details, please see Chapter 6) as the most reliable ones. Viscoelastic modelling is suggested when there are significant differences between overtones [48] as for viscoelastic or soft films the Sauerbrey relation, based on the frequency alone, will underestimate the mass since the film is not fully coupled to the motion of the sensor surface. More details about the data processing are provided in the validation section (Chapter 6).

2.6.5 Surface Plasmon Resonance (SPR)

A multi-parameter surface plasmon resonance (MP-SPR) system from Bionavis, Finland, was used to repeat some of the measurements conducted with QCM-D. SPR is based on a change of the refractive index as opposed to QCM-D which relies on a piezoelectric effect. As a consequence, artifacts may occur in QCM-D when the deposited material swells strongly, requiring viscoelastic modelling. The objective of using SPR was therefore to understand in how far SPR and QCM-D yield similar results on vapour sorption data, where they differ, and if so, why.

Sensor cleaning and preparation as well as vapour generation was as described for the QCM-D, with the only difference that the total vapour flow was set to 40 ml/min.

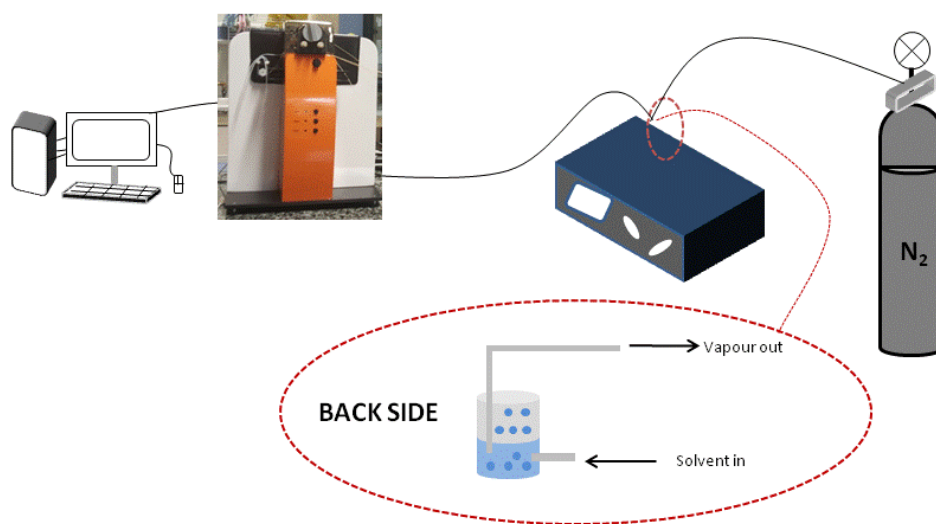


Figure 2. 14 Schematic part of the vapour measurement setup using SPR

Data obtained from these last two experiments (QCM-D and SPR) were also compared and evaluated with data obtained from an additional technique such as Cahn electrobalance. The experimental conditions are already described previously in this chapter (section 2.6.3.1 Vapour sorption studies-dynamic sorption process). It will be demonstrated that although not the same experimental conditions, some of the values registered fit considerably between techniques as well as with data from literature.

2.6.6 Spin Coating

For the polymer sample deposition onto the QCM-D and SPR sensors, spin coating (LOT Oriel Group Europa, Darmstadt, Germany) was employed as being one of the most used methods for depositing thin films. The advantage of spin coating is its ability to quickly and easily produce relatively uniform films from a few nanometres to a few microns in thickness. This widespread process involves a deposition of a small quantity of a polymer (dissolved in an adequate solvent) onto the center of a substrate, followed by a spin process at high speed. The rotation of the substrate at high speed means that the centrifugal force combined with the surface tension of the solution pulls the liquid coating into an even covering of the electrode. During this time the solvent then evaporates, leaving the desired material on the substrate in form of an even deposition.

The final film thickness and its homogeneity/distribution will depend on several factors such as: the nature of the polymer (viscosity, solvent evaporation rate, surface tension) and the parameters chosen for the spin process. For example, the rotational speed or the acceleration will contribute to the final properties of the coated film. For a better understanding, Figure 2. 15 shows a scheme of each step during the spin coating process:

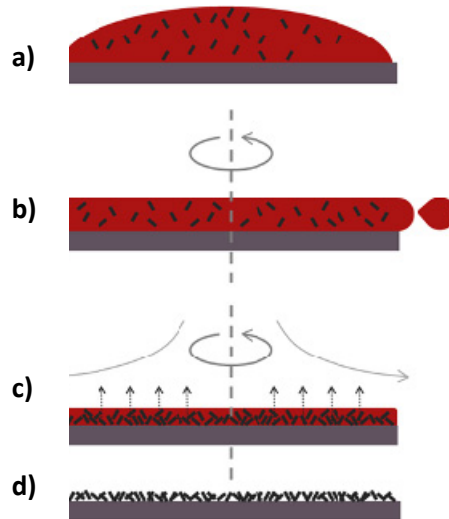


Figure 2. 15 Scheme of the spin coating process (Retrieved from [49])

- a) First, the substrate is coated with the polymer solution.
- b) Then, the substrate is rotated at high speed and the excess of the material deposited is flung off the side.
- c) Airflow then dries the majority of the solvent in the solution.
- d) Before the film fully dries, the polymer chains supposedly adapt across the whole substrate.

2.6.6.1 Spin Speed

The rotation speed of the substrate affects the degree of radial (centrifugal) force applied to the liquid solution as well as the velocity and characteristic turbulence of the air immediately above it. In particular, the high speed spin step generally defines the final film thickness. Film thickness is largely a balance between the force applied to shear the fluid resin towards the edge of the substrate and the drying rate which affects the viscosity of the polymer solution. As the polymer solution dries, the viscosity increases until the radial

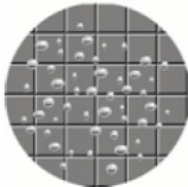
force of the spin process can no longer appreciably move the polymer over the surface. At this point, the film thickness will not decrease significantly with increased spin time.

2.6.6.2 Acceleration

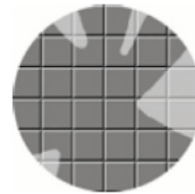
The acceleration of the substrate towards the final spin speed can also affect the coated film properties. Since the polymer solution begins to dry during the first part of the spin cycle, it is important to accurately control acceleration. In some processes, 50% of the solvents in the polymer solution will be lost due to evaporation in the first few seconds of the process.

Repeatability is highly important during spin coating. Slight variations in the parameters that define the spin coating process can result in drastic variations in the coated film. Even variations in the ambient conditions can alter the final result and therefore need to be maintained constant. Possible problems occurring during the spin-coating process are listed in Table 2. 2.

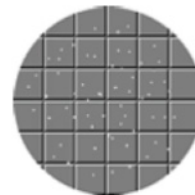
Table 2. 2 Examples of process troubleshooting process (Retrieved from [49])

Description	Image
Film too thin/thick	
Air bubbles on the substrate surface	

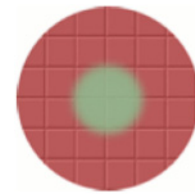
Uncoated Areas



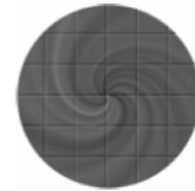
Pinholes



Center circle (Chuck Mark)



Swirl pattern



In case any of the above mentioned problems occurred, the deposition procedure was repeated until yielding a satisfactory deposition. The parameters for the spin coating process vary greatly for different materials and substrates so that there are no fixed rules for spin coat processing, only general guidelines.

2.7 References

- [1] J. P. Sheth, J. Xu, and G. L. Wilkes, "Solid state structure-property behavior of semicrystalline poly(ether-block-amide) PEBAX[®] thermoplastic elastomers," *Polymer (Guildf.)*, vol. 44, no. 3, pp. 743–756, **2002**.
- [2] H. N. Ng, A. E. Allegrezza, R. W. Seymour, and S. L. Cooper, "Effect of segment size and polydispersity on the properties of polyurethane block polymers," *Polymer (Guildf.)*, vol. 14, no. 6, pp. 255–261, **1973**.
- [3] L. De Physique and D. Narbonne, "A thermally stimulated current technique for measuring the molecular parameters of Pebax, a polyether-block amide copolymer," *J. Mater. Sci.*, vol. 22, pp. 675–678, **1987**.
- [4] W. Liu, L. Cheng, Y. Zhang, H. Wang, and M. Yu, "The physical properties of aqueous solution of room-temperature ionic liquids based on imidazolium: Database and evaluation," *J. Mol. Liq.*, vol. 140, no. 1–3, pp. 68–72, **2008**.
- [5] L. L. C. A, F. XS, and L. D, "Separation of VOCs from N2 using Poly(ether block amide) membranes," *Can. J. Chem. Eng.*, vol. 87, no. 3, pp. 456–465, **2009**.
- [6] A. Car, C. Stropnik, W. Yave, and K. V. Peinemann, "Pebax??/polyethylene glycol blend thin film composite membranes for CO2 separation: Performance with mixed gases," *Sep. Purif. Technol.*, vol. 62, no. 1, pp. 110–117, **2008**.
- [7] I. Pinnau, J. G. Wijmans, I. Blume, T. Kuroda, and K. V. Peinemann, "Gas permeation through composite membranes," *J. Memb. Sci.*, vol. 37, no. 1, pp. 81–88, **1988**.
- [8] A. Car, C. Stropnik, W. Yave, and K. V. Peinemann, "PEG modified poly(amide-b-ethylene oxide) membranes for CO2 separation," *J. Memb. Sci.*, vol. 307, no. 1, pp. 88–95, **2008**.

- [9] J. Shi, P. Wu, and F. Yan, "Further investigation of the intermolecular interactions and component distributions in a [Bmim][BF₄]-based polystyrene composite membranes using two-dimensional correlation infrared spectroscopy," *Langmuir*, vol. 26, no. 13, pp. 11427–11434, **2010**.
- [10] G. Feng, X. Jiang, R. Qiao, and A. a Kornyshev, "Water in Ionic Liquids at Electric Interfaces: The Anatomy of," *ACS Nano*, vol. 8, no. 11, pp. 11685–11694, **2014**.
- [11] Y. Kohno and H. Ohno, "Ionic liquid/water mixtures: from hostility to conciliation," *Chem. Commun.*, vol. 48, no. 57, pp. 7119–7130, **2012**.
- [12] T. W. Peter Wasserscheid, "Ionic Liquids in Synthesis, 2 Volume Set, 2nd Edition," **2007**.
- [13] J. L. Anthony, E. J. Maginn, and J. F. Brennecke, "Solubilities and Thermodynamic Properties of Gases in the Ionic Liquid 1- n -Butyl-3-methylimidazolium Hexafluorophosphate," *J. Phys. Chem. B*, vol. 106, no. 29, pp. 7315–7320, **2002**.
- [14] S. Rivera-Rubero and S. Baldelli, "Influence of water on the surface of hydrophilic and hydrophobic room-temperature ionic liquids," *J. Am. Chem. Soc.*, vol. 126, no. 38, pp. 11788–11789, **2004**.
- [15] R. M. Lynden-Bell, J. Kohanoff, and M. G. Del Popolo, "Simulation of interfaces between room temperature ionic liquids and other liquids.," *Faraday Discuss.*, vol. 129, pp. 57–67; discussion 89–109, **2005**.
- [16] Y. Wang, T. Kakiuchi, Y. Yasui, and M. V Mirkin, "Kinetics of ion transfer at the ionic liquid/water nanointerface.," *J. Am. Chem. Soc.*, vol. 132, no. 47, pp. 16945–52, **2010**.
- [17] R. Hayes, S. Imberti, G. G. Warr, and R. Atkin, "How water dissolves in protic ionic liquids.," *Angew. Chem. Int. Ed. Engl.*, vol. 51, no. 30, pp. 7468–71, **2012**.

- [18] I. Khan, M. Taha, P. Ribeiro-Claro, S. P. Pinho, and J. A. P. Coutinho, "Effect of the cation on the interactions between alkyl methyl imidazolium chloride ionic liquids and water.," *J. Phys. Chem. B*, vol. 118, no. 35, pp. 10503–14, **2014**.
- [19] A. Menjoge, J. Dixon, J. F. Brennecke, E. J. Maginn, and S. Vasenkov, "Influence of water on diffusion in imidazolium-based ionic liquids: a pulsed field gradient NMR study.," *J. Phys. Chem. B*, vol. 113, no. 18, pp. 6353–9, **2009**.
- [20] M. S. Kelkar and E. J. Maginn, "Effect of temperature and water content on the shear viscosity of the ionic liquid 1-ethyl-3-methylimidazolium bis(trifluoromethanesulfonyl)imide as studied by atomistic simulations.," *J. Phys. Chem. B*, vol. 111, no. 18, pp. 4867–76, **2007**.
- [21] L. Cammarata, S. G. Kazarian, P. A. Salter, and T. Welton, "Molecular states of water in room temperature ionic liquids," *Phys. Chem. Chem. Phys.*, vol. 3, no. 23, pp. 5192–5200, **2001**.
- [22] B. L. Bhargava, Y. Yasaka, and M. L. Klein, "Computational studies of room temperature ionic liquid-water mixtures.," *Chem. Commun. (Camb)*, vol. 47, no. 22, pp. 6228–41, **2011**.
- [23] S. Feng and G. A. Voth, "Molecular dynamics simulations of imidazolium-based ionic liquid/water mixtures: Alkyl side chain length and anion effects," *Fluid Phase Equilib.*, vol. 294, no. 1–2, pp. 148–156, **2010**.
- [24] M. Q. Shaikh, K. Rätzke, J. C. Gaukler, W. Possart, and F. Faupel, "Reactive epoxies with functional zeolite fillers: IR spectroscopy and PALS studies," *J. Mater. Res.*, vol. 26, no. 22, pp. 2877–2886, **2011**.
- [25] J. Kruse, K. Rätzke, F. Faupel, D. M. Sterescu, D. F. Stamatialis, and M. Wessling, "Free volume in C60 modified PPO polymer membranes by positron annihilation lifetime spectroscopy.," *J. Phys. Chem. B*, vol. 111, no. 50, pp. 13914–8, **2007**.

- [26] J. Kansy, "Microcomputer program for analysis of positron annihilation lifetime spectra," *Nucl. Instruments Methods Phys. Res. Sect. A Accel. Spectrometers, Detect. Assoc. Equip.*, vol. 374, no. 2, pp. 235–244, **1996**.
- [27] C. J. Guo, D. De Kee, and B. Harrison, "Diffusion of organic solvents in rubber membranes measured via a new permeation cell," *J. Appl. Polym. Sci.*, vol. 56, no. 7, pp. 823–829, **1995**.
- [28] O. Miguel, M. J. Fernandez-Berridi, and J. J. Iruin, "Survey on transport properties of liquids, vapors, and gases in biodegradable poly(3-hydroxybutyrate) (PHB)," *J. Appl. Polym. Sci.*, vol. 64, no. 9, pp. 1849–1859, **1997**.
- [29] J. Mulder, *Basic Principles of Membrane Technology*. Springer Netherlands, 1996.
- [30] M. S. Eceolaza Soraluze, "Diversos ámbitos de aplicación de las propiedades de transporte de gases en materiales poliméricos," *PhD Thesis*, **2006**.
- [31] J. G. Wijmans and R. W. Baker, "The solution-diffusion model: a review," *J. Memb. Sci.*, vol. 107, no. 1–2, pp. 1–21, **1995**.
- [32] W. J. Koros and G. K. Fleming, "Membrane-based gas separation," *J. Memb. Sci.*, vol. 83, no. 1, pp. 1–80, **1993**.
- [33] R. W. Baker, *Membrane Technology and Applications*. John Wiley & Sons, Ltd, 2012.
- [34] T. Graham, "On the absorption and dialytic separation of gases by colloid septa," *J. Chem. Soc.*, vol. 20, pp. 235–288, **1867**.
- [35] H. A. Daynes, "The process of Diffusion through a Rubber Membrane," *Proc. R. Soc. London*, pp. 286–307, **1920**.
- [36] M. E. Glicksman, *Diffusion in Solids: Field Theory, Solid-State Principles, and*

Applications. Wiley, 1999.

- [37] C. Etxabarren, M. Iriarte, A. Etxeberria, C. Uriarte, and J. J. Iruin, "Determination of the diffusion coefficients of organic solvents in polyepichlorohydrin: A comparative study of inverse gas chromatography and sorption methods," *J. Appl. Polym. Sci.*, vol. 89, no. 8, pp. 2216–2223, **2003**.
- [38] N. W. Burningham, "Thermal decomposition of high-temperature resistant polymers," p. PhD Thesis, **1970**.
- [39] "The Behavior of Real Gases." [Online]. Available: <http://2012books.lardbucket.org/books/principles-of-general-chemistry-v1.0/s14-08-the-behavior-of-real-gases.html>. [Accessed: 11-Mar-2016].
- [40] A. Hines and R. N. Maddox, "Mass Transfer: Fundamentals and Applications," *Mc Graw Hill Educ.*, **1985**.
- [41] J. Crank, "The Mathematics of Diffusion," *CLARENDON Press OXFORD*, **1979**.
- [42] M. Karimi, "Diffusion in Polymer Solids and Solutions," *Mass Transf. Chem. Eng. Process.*, vol. InTech, **2011**.
- [43] J. M. Vergnaud, "Liquid transport process in polymeric materials. Application with plasticized PVC with low matter transfer," *Macromol. Symp.*, vol. 84, no. 1, pp. 377–391, **1994**.
- [44] D. A. Edwards, "Non-fickian diffusion in thin polymer films," *J. Polym. Sci. Part B Polym. Phys.*, vol. 34, no. 5, pp. 981–997, **1996**.
- [45] J. Crank and P. Nicolson, "A practical method for numerical evaluation of solutions of partial differential equations of the heat-conduction type," *Adv. Comput. Math.*, vol. 6, no. 1, pp. 207–226, **1996**.

- [46] G. Sauerbrey, "Verwendung von Schwingquarzen zur Wägung dünner Schichten und zur Mikrowägung," *Zeitschrift für Phys.*, vol. 155, no. 2, pp. 206–222, **1959**.
- [47] Arkema, "Pebax2533 SA 01 Technical data sheet." [Online]. Available: <http://www.pebax.com/export/sites/pebax/.content/medias/downloads/literature/tds-pebax-2533sa01.pdf>.
- [48] Q-Sense, "Study of viscoelastic films – a comparison between the voigt viscoelastic model and the sauerbrey relation," *Online*, 2007. [Online]. Available: <http://www.biolinscientific.com/>. [Accessed: 11-Mar-2016].
- [49] "Spin Coating: A Guide to Theory and Techniques – Ossila." [Online]. Available: <http://www.ossila.com/pages/spin-coating>. [Accessed: 11-Mar-2016].

Chapter 3

Interactions of Pebax®2533 with ionic liquids

3.1	Introduction	67
3.2	Results and Discussion.....	72
3.3	Conclusions	117
3.4	References.....	119

This chapter reports on creating non-porous polymeric membranes containing room-temperature ionic liquids (RTILs) as additives. It investigates the fundamental interactions taking place between selected ionic liquids (ILs) and polyether block amide polymer as well as the separation performance of the resulting blend membranes when exposed to organic vapours. The permeability of the membranes was determined to be significantly modified by the addition of the IL when compared to the pristine polymer, but without sacrificing the selectivity between solutes. In this way, the common trade-off between selectivity (α) and permeability (P) was overcome and even partially improved.

3.1 Introduction

The use of ILs for sensors and separations, including membrane separations technology, has been widely studied [1]–[3]. As regards membrane processes involving ILs, mainly supported liquid membranes (SILMs) have been investigated. SILMs are produced by immobilizing ILs in a porous support structure as schematically depicted in Figure 3. 1.

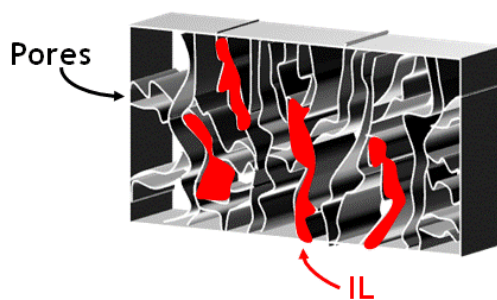


Figure 3. 1 Scheme of a SILM

Although of facile preparation, SILMs show several practical drawbacks such as their limited operational stability and lacking reproducibility. For instance, during operation conditions upon solute uptake, changes in the IL's viscosity and surface tension commonly occur which result in a lack of the membrane stability [4]–[6]. Besides, concerning the heterogeneity of porous supports, the distribution of the IL across the porous membrane

cannot be controlled and hence is not always reproducible [7]. Finally, possible migration of the IL from the support has also been widely reported in literature as a potential problem when working with this type of membranes [8]–[11]. In principle, these limitations should be overcome by incorporating ILs into a dense polymer matrix obtaining thermoplastic dense membranes [12]. It was shown by D. Miranda [13], S. Livi [14] and M. Kárászová [15], that when there is an affinity between the IL and the polymer matrix, the physico-chemical properties of both IL and polymer can be taken advantage of. For example, an improved permeability to gases or better mechanical properties can be obtained [16], [17].

On the other hand, several authors such as Scott, Rahman, or Hou, have been using ILs as mere plasticizers in their composite materials [18]–[22]. Plasticizers are low-molecular-weight molecules that when added to polymeric materials modify the tridimensional organization of the polymeric matrix, decreasing the intermolecular attraction forces between polymer chains and consequently increasing the flexibility, workability and mobility of the bulk material [23], [24]. As a consequence, the addition of plasticizers to polymers reduces the melting viscosity, decreases the temperature of the second order transition and reduce the elastic modulus of the overall material [25]. Using ILs as plasticizers yielded improvements in terms of mixing of otherwise partially immiscible polymer phases with the IL serving as a mediator between both, as well as an increased thermal stability, improved mechanical processability and higher mechanical flexibility. Hereby, apparently the main drawback of common plasticizers such as the migration or evaporation from the polymer's surface were apparently avoided [26].

The permeability of polymer/ionic liquid blends has been widely studied mainly for gases [27]–[29] and more particularly in Pebax® polymer [30]–[34] showing in many cases a change or even improvement of the transport properties, such as increased permeabilities. However, it has remained widely unclear why exactly permeabilities were found increased

and what kind of interactions between the base material and the functional groups of the ILs were hereby taking place within the blend.

The aim of this study is therefore focused on the preparation of stable mixed matrix membranes based on polymer matrix such as Pebax®2533 and elucidate the effect ILs have on the base polymer into which they are incorporated. For this purpose, the goal consists on determining possible interactions taking place between the ILs and the base polymer chosen for our study, Pebax®2533 by using various characterization techniques.

Pebax® is a widely used polymer family known for its good processability, notable mechanical strength, thermal and chemical resistance and/or serving in form of membranes as a semi-permeable barrier for the separation of gases and vapours [35]. This family of elastomeric multiblock copolymers has a molecular structure combining linear chains of rigid polyamide segments (PA) interspaced with flexible polyether segments (PE). It is produced by polycondensation of a dicarboxylic polyamide and a polyetherdiol under vacuum and in the presence of heat and a catalyst [36].

The general structure of the PEBAX® repeating unit is:

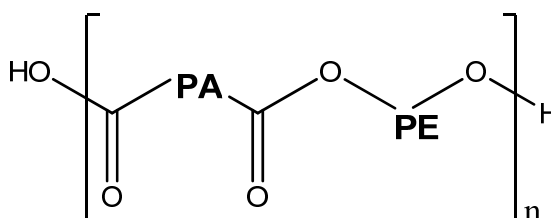


Figure 3. 2 General structure of poly(ether–block–amide) (Pebax®)

Whilst PA is an aliphatic polyamide "hard segment", i.e., Nylon-6 [PA6], or Nylon-12 [PA12], PE is an amorphous polyether "soft segment" consisting of either poly(ethylene oxide), or poly(tetramethylene oxide). This mixed crystalline/amorphous structure creates a blend of properties of thermoplastics and rubbers which can be highly beneficial for

separations: the hard amide block provides the mechanical strength, while gas transport occurs primarily in the soft ether segments [37]. As other segmented copolymers, Pebax®2533 is reported to show a microphase separation morphology in the solid state because of the high polarity [38] difference between its hard and soft segments [39]–[41].

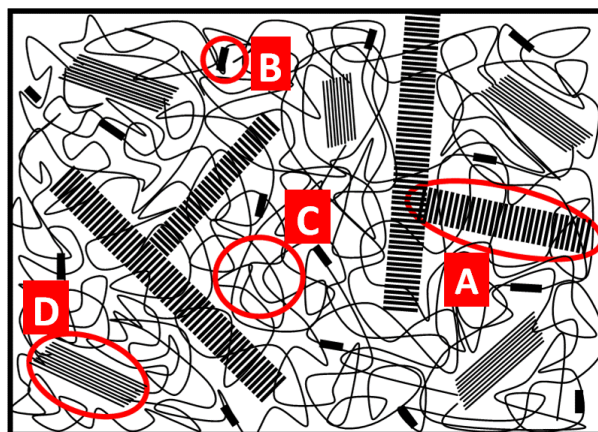


Figure 3. 3 General structure of poly(ether–block–amide) (Pebax®). Chemical structure of poly(ether–block–amide). The circled areas represent (A) crystalline hard segments, (B) non crystallized rigid hard segments, (C) continuous amorphous soft phase and (D) crystalline soft phase.

The amide blocks in which the less permeable phase resides provide the main contribution to crystallinity of the copolymer, whereas the ether blocks act as the permeable phase due to their high chain mobility [42]–[44]. The extent of hard/soft segment mixing depends on the overall content of both segment lengths and the affinity between both segments. Sheth et al [45] have reported that hard domains are reasonably pure but soft domains consist of flexible segments with some hard segments entrapped. This stems from the possibility of -NH_2 groups of the hard segment forming hydrogen bonds with oxygen of the ether linkage of the soft segment. The polyether and polyamide blocks can be furthermore interconnected with adipic acid (as shown in Figure 3. 4) to allow creating ester-type linkage between hard and soft segments [46].

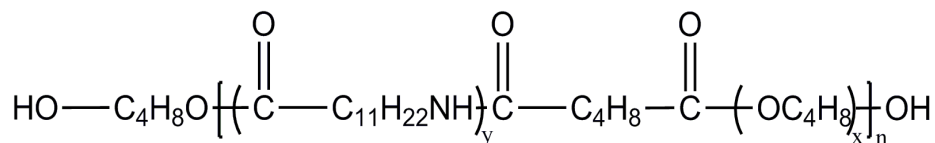


Figure 3. 4 Chemical structure of poly(ether–block–amide) (Pebax®2533) [Amide y= 0.2, Ether x= 0.8].

Therefore, Pebax®2533 has been chosen as a base polymer for being, on one hand, the one with the highest content of PE segments resulting in a relatively high hydrophobicity and affinity for organic compounds; on the other hand, it has also taken advantage of the presence of the hydrophilic, hard PA domains in order to understand whether an IL would establish preferential interactions with either hydrophobic or hydrophilic domains, or whether the hydrophilicity/hydrophobicity of the polymer would be widely irrelevant for how the IL accommodated within the polymer matrix.

Due to the hydrophobic polyether soft chains combined with the hydrophilic polyamide rigid chains, Pebax® has been reported in literature to be hydrophobic or hydrophilic, depending on the author [17], [47]–[49]. In this work, with Pebax®2533 yielding a water contact angle between 85-90° and accounting for both the polyamide phase representing a hydrophilic block [50] while the polyether phase represents the hydrophobic one [51], the overall polymer is considered as being at the border between an hydrophobic and hydrophilic material [52], [53].

ILs used to create the polymer/IL blends were chosen either due to having been widely reported in literature or based on a systematic variation of the cation and/or anion in order: for the cases of [BMIM][BF₄], [BMIM][Tf₂N] and [BMIM][Ac], they share the same imidazolium cation, however, varying the anion. On the other hand, [TMG][BF₄] shares the same anion with [BMIM][BF₄], while the cation differs entirely. Finally, [C₈MIM][Cl] also contains an imidazolium cation but with a longer alkyl chain of 8 carbons which could in principle interact favourably with the PE block in Pebax®2533.

Vapour transport through dense Pebax®2533 films is commonly described as obeying the solution-diffusion mechanism [49], [54]. The solution–diffusion model involves three successive steps: (1) sorption of components from the feed into the surface layer of a selective polymeric membrane; (2) diffusion of the solute across the membrane polymer according to the concentration gradient or, more generally, the chemical potential gradient; and (3) desorption of the solute at the permeate (downstream) side of the membrane. The solubility of a solute in a polymer matrix depends, as a first approximation, on favorable chemical interactions between respective functional groups of the polymer and the solute, while the diffusivity correlates with the mobility of the solute within the polymer, its packing density and hence the free volume available to allow movement of the solute molecules. Upon incorporating an IL into the copolymer structure, the question therefore arises in how far both parameters, solubility and diffusivity, are affected and whether IL and polymer will act in synergy or whether they will rather remain as a two independent phases.

3.2 Results and Discussion

IL-polymer blends can range from IL-doped polymers to polymer gels depending on the quantity of IL added. In the former, the IL is supposed to serve as a kind of plasticizer in a mechanically stable membrane; in the latter, the membrane can lose its mechanical stability to a degree of possessing a limited practical utility as a separation membrane. P. Bernardo *et al.* found that IL-polymer blends between 0.5 to 80 wt% of IL in Pebax®2533 yielded mechanically stable membranes [17]. Our attempts of casting IL-blend membranes using Pebax®XX33 grade base material with a higher content in PA were dismissed as the resulting membranes became extremely fragile (see Figure 3. 5)

a)



b)



c)



Figure 3. 5 Samples of cast membranes obtained with different Pebax®XX33 grades. a) Pebax®2533, b) Pebax®5533 and c) Pebax®7033

We therefore chose Pebax®2533 as base material and the concentration of IL in each membrane was selected to be 20 wt% as this is a commonly accepted concentration of

additives such as plasticizers in polymers [55], [56]. Some examples of respective blend membranes are depicted in Figure 3. 6.

a)



b)



c)



Figure 3. 6 Examples of IL-Pebax[®]2533 blended membranes. a) Pebax2533-[C₈MIM][Cl], b) Pebax2533-[BMIM][Ac] and c) Pebax2533-[TMG][BF₄]

3.2.1 Membrane surface analysis

With the aim of studying the effect of incorporating an IL into the base block-copolymer, the surface morphology of an IL- Pebax®2533 composite film was characterized by AFM. As an example, Figure 3. 7 depicts topographic images of membranes consisting of pristine Pebax®2533 (Figure 3. 7a and c) and Pebax®2533 doped with [C₈MIM][Cl] (Figure 3. 7b and d). As already observed by Sheth et al [45] both phases of the copolymer (PE and PA) can be seen well defined in AFM phase images. Differences are observed when comparing images from Pebax®2533 with the [C₈MIM][Cl]-blended membrane. Topography images (Figure 3. 7a and Figure 3. 7b) illustrate that upon adding [C₈MIM][Cl] to the polymer the surface roughness seems increased compared to the pristine Pebax®2533 membrane. Accounting for the mobility/flexibility of the IL within the polymer matrix, a surface organization of the polymer may have occurred due to the presence of the ILs resulting in the surface roughness. The displacement of the cantilever in the tapping mode gets doubled from 73.5 to 134.7nm. Additionally, the phase image of the [C₈MIM][Cl] doped membrane (Figure 3. 7d), shows evident differences when compared to pristine Pebax®2533 (Figure 3. 7c). In the blend membrane, the borders between PA and PE phases seem less defined suggesting that the IL is homogeneously distributed along both blocks of the copolymer, apparently diminishing in this way the formation of microphases which can otherwise be detected.

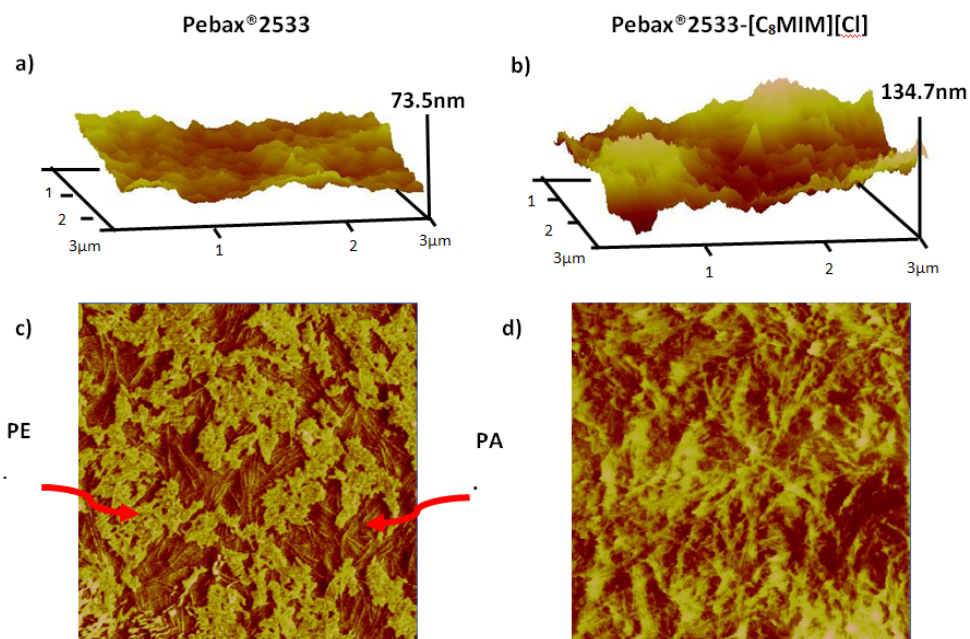


Figure 3. 7 TM-AFM topography images a) Pebax®2533 and b) Pebax2533-[C₈MIM][Cl]. Phase images of c) Pebax®2533 and d) Pebax®2533-[C₈MIM][Cl].

Based on this surface analysis, it seems that the [C₈MIM][Cl] distributes homogeneously within the polymer regardless the phase of the copolymer. As a note of caution, however, it should be stressed that as a consequence of the liquid nature of the IL, the tapping mode image of the blend membrane could also be misleading: traces of the IL could possibly attach to the cantilever tip resulting in an apparently IL-impregnated surface structure while this is in fact not the case. This proves that AFM is a tool of limited utility to determine the effect of incorporation of ILs into polymers.

3.2.2 Thermal stability

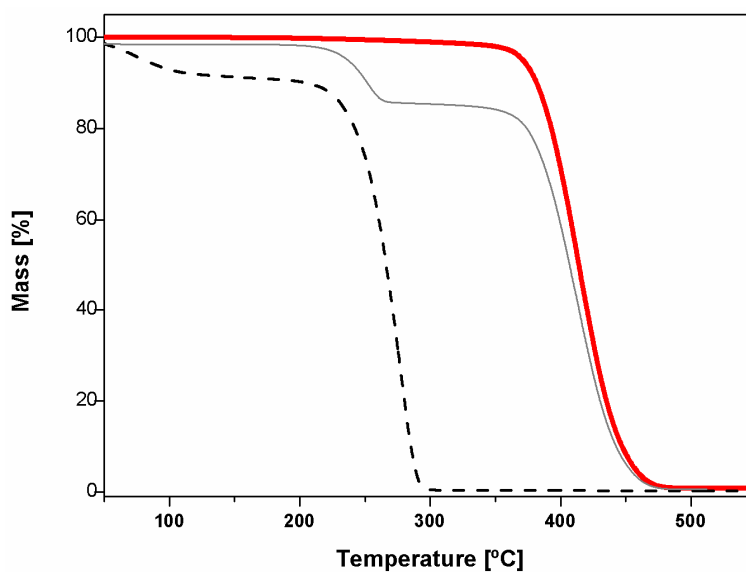
Thermal decomposition of materials is a consequence of overcoming specific interactions (dipole-dipole interaction, van der Waals forces (London dispersion forces), and hydrogen bonding) between the different macromolecules or molecules present in the polymer [57]. Chain scission or bond dissociation takes place when the supplied thermal energy exceeds the bond dissociation energy of the respective bond or group. The decomposition temperature is defined as a temperature at which the weight loss exceeds 1 wt% [58] and a high thermal stability of a polymer blend can be understood as a higher stability between the chemical bonds existing in the respective material, and vice versa. Therefore, it was expected that TGA could provide some evidence on how an IL interacts with the pristine matrix polymer in case the overall blend yields a different thermal stability compared to the pristine polymer.

ILs are usually defined to be thermally stable because of their relatively high decomposition temperature [59]. Two possible effects on the onset of the decomposition temperature can therefore be conceived when incorporation of ILs into Pebax®2533. First, if the interactions between the polymer and the IL are weak, then lower overall decomposition values would be expected because less energy would be needed to break the chemical bonds as they have been weakened by the incorporation of the IL. On the contrary, if the IL stabilizes the system (for example, as mediators between phases), the decomposition temperature onset would be increased because this stabilization would require more energy to overcome the overall more favorable interactions.

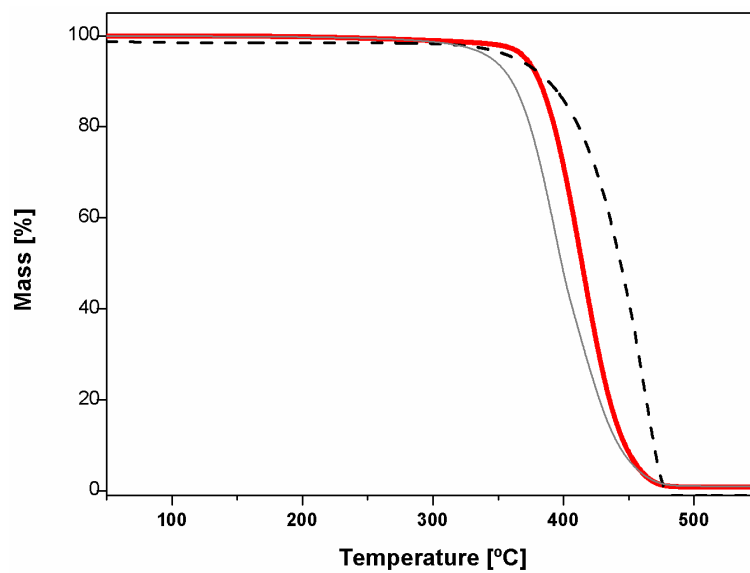
The exact onset of thermal decomposition of ILs can be difficult to be determined due to their hydrophilic nature and, hence, water content. After having been stored in an oven (see Chapter 2), according to Karl Fischer (KF) measurements the ILs employed contained the following amount of water: 0.4, 0.5, 1.5, 5.2, 9.1 wt% for [BMIM][Tf₂N], [BMIM][BF₄], [TMG][BF₄], [C₈MIM][Cl], and [BMIM][Ac], respectively. As can be seen in Figure 3. 8, this tendency is reflected in the step decrease in mass clearly observed when heating all ILs (dashed lines), except for [BMIM][BF₄] and [BMIM][Tf₂N], which according to KF

measurements as expected. [BMIM][Tf₂N] is the most hydrophobic IL amongst those tested [60], [61] while [BMIM][BF₄] is clearly the thermally most stable IL of all tested. In general, imidazolium based ILs suffer an endothermic breakdown mechanism where the nucleophilic anion causes a decomposition via dealkylation or proton transfer [62]. However, in the case of non-nucleophilic anions such as [Tf₂N], an exothermic breakdown occurs as a consequence of the degradation of the anion by sulfur dioxide release while the cation remains intact [59], [62]. Still, this thermal breakdown of pristine ILs is not observable in these TGA measurements where the degradation occurs in only one step.

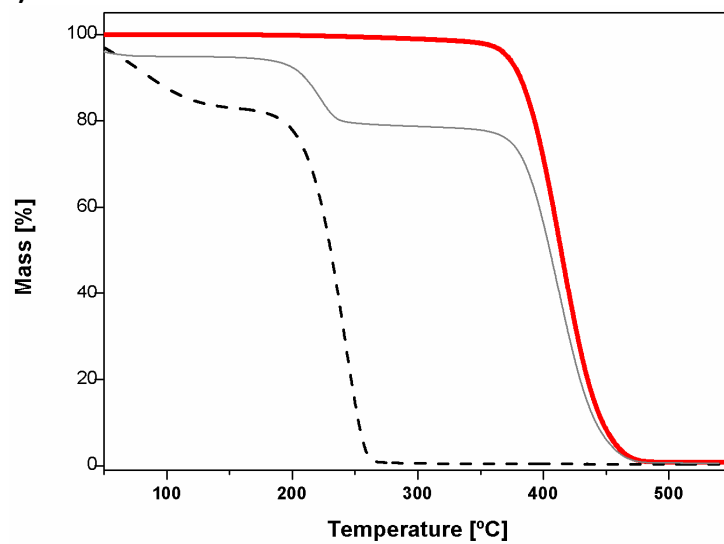
a)



b)



c)



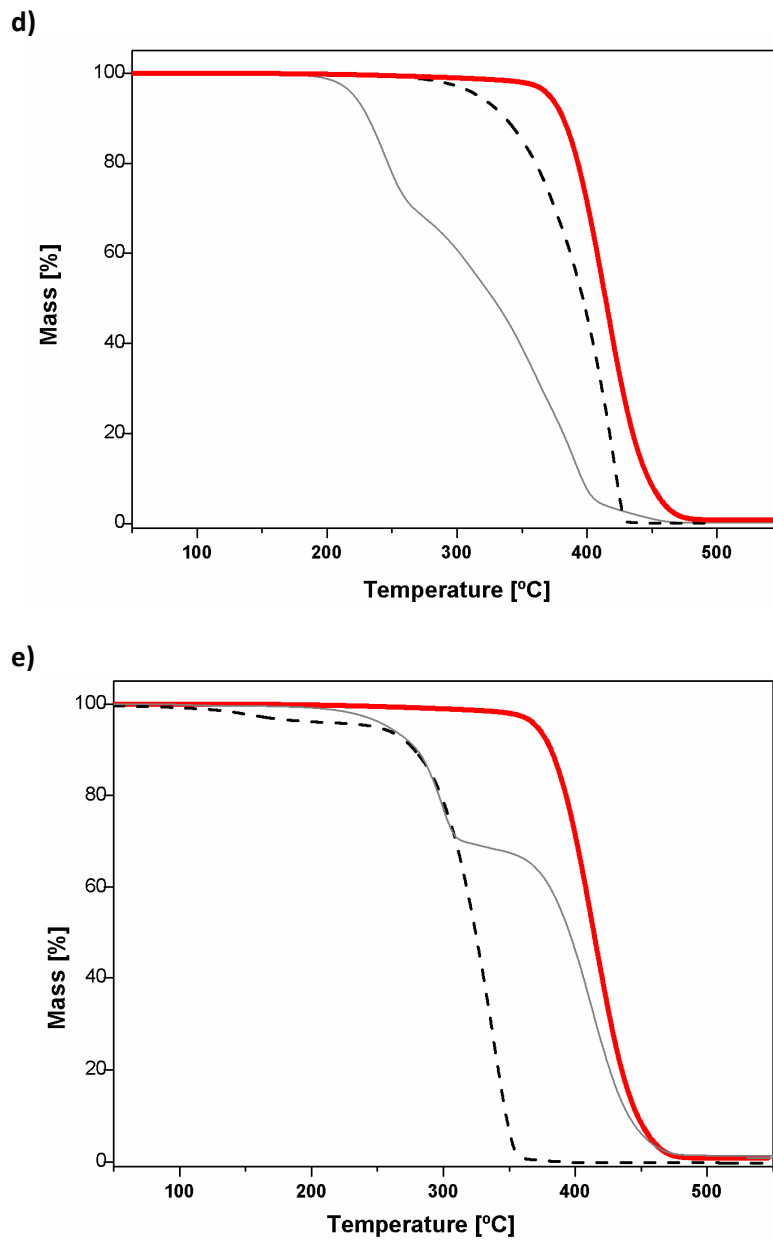


Figure 3. 8 TGA of each mixed-matrix-membrane compared with its respective IL and the pristine polymer. Thick red solid line: pristine Pebax[®]2533; dashed line: pristine IL; thin solid line: blend membrane. Mixed-matrix-membranes with a) $[C_8MIM][Cl]$, b) $[BMIM][BF_4]$, c) $[BMIM][Ac]$, d) $[BMIM][Tf_2N]$ and e) $[TMG][BF_4]$, respectively.

The blend membrane containing [BMIM][BF₄] as the most thermally stable IL shows a decomposition thermogram located at a little lower temperature than both pristine Pebax®2533 and pure [BMIM][BF₄]. According to literature, the thermal stability of the imidazolium salts increases by alkyl substitution [63], and also by decreasing the number of carbon atoms in the alkyl chains [64] as well as fluorination. An example for the latter are [BMIM][BF₄] and [BMIM][Tf₂N] that contain fluorinated groups and whose pristine decomposition temperature takes place at a higher temperature (above 400°C). On the other hand, [BMIM][BF₄] and [TMG][BF₄] sharing the same anion exhibit a very different thermal behavior owing to the cation. Following what literature reviews [65] that the anion plays an important role in the thermal effect demonstrating that the type of associated anion has the primary effect on the thermal stability of ILs [66].

Figure 3. 8 shows that the blend membranes containing [C₈MIM][Cl], [BMIM][Ac] and [TMG][BF₄] show a thermal stability which is, at the first glance, intermediate between the one of the respective pristine materials with the first degradation step corresponding to the decomposition of the IL and the second one to the block copolymer. At a second glance, it can be observed that only Pebax2533-[TMG][BF₄] depicts a degradation curve which perfectly follows that of the pristine materials, indicating therefore that apparently no interaction between both phases occurred and they rather co-exist in the blend. The degradation curves of Pebax2533-[C₈MIM][Cl] and Pebax2533-[BMIM][Ac] coincide with the ones of the pristine polymer at higher temperature but exhibit a slightly retarded degradation onset for the IL in the respective blend. As a consequence, it may be assumed that these two ILs interact favourably with the polymer matrix becoming more stabilized, but without interfering with the polymer itself.

In contrast, Pebax2533-[BMIM][Tf₂N] suffered a very evident decrease in its decomposition temperature (T_d) compared to the pristine materials. In this case, its T_d is lowered about 85°C. Incorporation of the IL therefore seems to destabilize the bulk polymer significantly. This could on one hand be due to repulsive interactions between the IL and the polymer matrix which significantly destabilize both phases. This is interesting as much as

[BMIM][Tf₂N] is the only hydrophobic IL tested while all others are hydrophilic. On the other hand, this observed phenomenon can also be as a consequence of the exothermic breakdown of [BMIM][Tf₂N]. Also Pebax2533-[BMIM][BF₄] suffered an overall lower onset of T_d indicating destabilizing interactions between IL and polymer although to a lesser extent, and with the particularity that the latest IL possessed a slightly higher thermal stability than the polymer.

These observations are further confirmed by the respective DTG curves as displayed in Figure 3. 9.

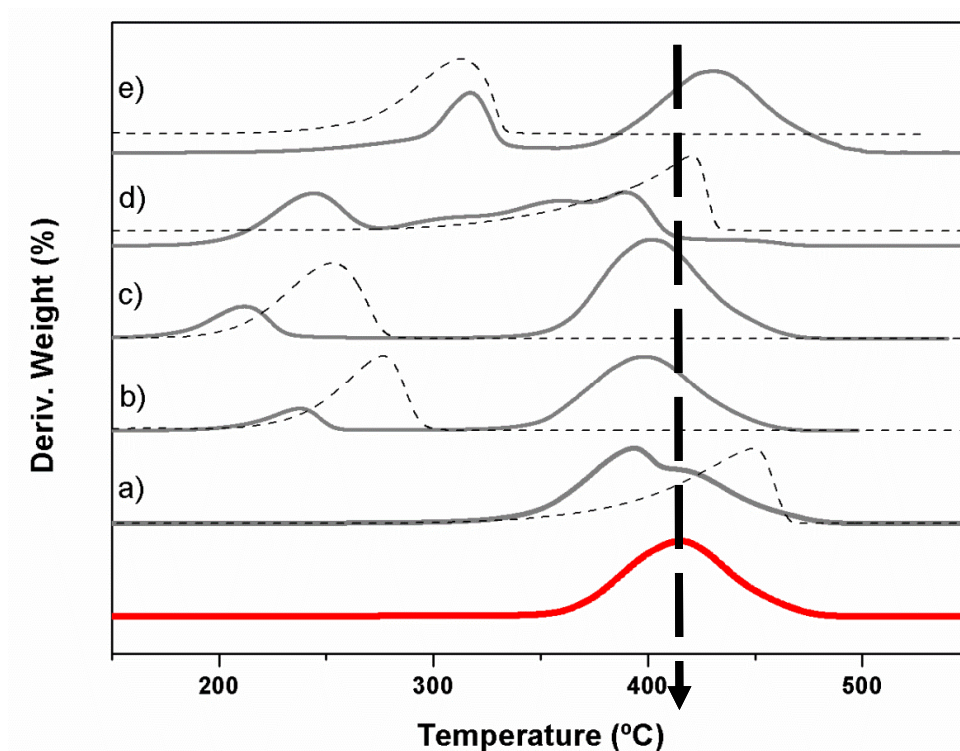


Figure 3. 9 DTG curves (vertically shifted for clarity) under an inert atmosphere. Thick red solid line for pristine Pebax[®]2533. Dotted line for each IL and continuous line for the mixed matrix membranes. a) Pebax2533-[BMIM][BF₄], b) Pebax2533-[C₈MIM][Cl], c) Pebax2533-[BMIM][Ac], d) Pebax2533-[BMIM][Tf₂N] and e) Pebax2533-[TMG][BF₄]

As can be seen, Pebax®2533 starts degrading between 350-400°C while [C₈MIM][Cl], [BMIM][Ac] and [TMG][BF₄] show a notable earlier degradation onset temperature that lies between 250 and 350°C. On the contrary, [BMIM][BF₄] and [BMIM][Tf₂N] exhibit a higher thermal stability showing their maximum peak at a temperature near to the one of Pebax®2533 or even slightly above.

It can clearly be seen that in the case of the blend membranes containing [C₈MIM][Cl], [BMIM][Ac] and [TMG][BF₄], each component in the blend membrane (IL and copolymer) degrade at a temperature widely independent from the other component with [C₈MIM][Cl] and [BMIM][Ac] showing a slightly retarded degradation temperature as mentioned above. On the other hand, [BMIM][BF₄] and [BMIM][Tf₂N], although both ILs are based on fluorinated anions, behave completely different when incorporated in Pebax®2533. While [BMIM][BF₄] yields a thermally stable blend material, [BMIM][Tf₂N] seems to strongly destabilize the block copolymer.

As a result, Pebax®2533 appears to be a good base polymer for incorporating ILs since its thermal properties in terms of degradation seem to suffer little indicating at least no unfavourable interactions for the hydrophilic ILs tested. The only hydrophobic IL tested destabilized the polymer; it would require further experiments with other hydrophobic ILs to confirm whether this is a trend. It would prove that while Pebax®2533 has both hydrophilic and hydrophobic segments, interactions with the former are more predominant when possible.

Continuing with the study of the thermal properties of the blend membranes, DSC analysis was employed [67] since it can provide further information about any possible interaction taking place between the block-copolymer and the ILs.

Theoretically, when a polymer and a miscible small molecule diluents are mixed, the chemical potential for the molten state is lowered, decreasing the melting temperature and reducing the fraction of polymer that crystallizes [68]. Consequently, the stronger the

interaction between the polymer and the diluents, the greater the decrease of the melting point and reduction of crystallinity

Figure 3. 10 collects the DSC thermograms of Pebax2533 pristine membrane as well as IL-blended membranes. For neat Pebax[®]2533, two dominant endothermic peaks are present whose maxima occur approximately between 10-13°C and 139-141°C. These endotherms are attributed to the fusion of the crystalline fraction of the blocks of polytetramethylene oxide (PTMO) and polyamide 12 (PA12), respectively, corroborating the phenomena of a microphase separation between both phases. The glass transition temperature (T_g) of both segments in Pebax[®]2533 is difficult to identify in DSC thermograms. As reported by Sheth et al [45], the T_g of PE takes place at a temperature around -80°C, while the relatively short PA segments possibly mix with some of the PE segments involving a broad and unpredictable transition.

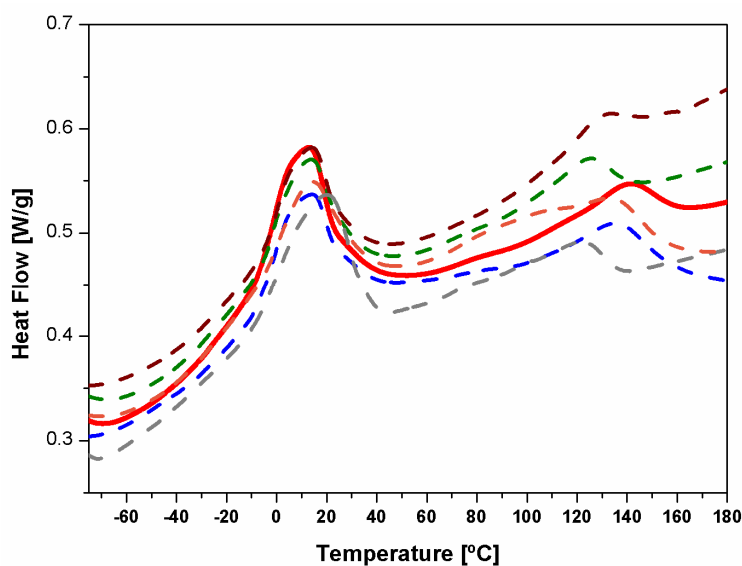


Figure 3. 10 DSC thermogram of mixed-matrix-membrane compared to pristine Pebax[®]2533 membrane. First peak corresponds to the melting of PE phase and the second to the PA one. Thick red solid line for pristine Pebax[®]2533 and dashed lines for IL-Polymer blends. Green line: Pebax2533-[C₈MIM][Cl], blue: Pebax2533-[BMIM][BF₄], brown: Pebax2533-[BMIM][Ac], grey: Pebax2533-[BMIM][Tf₂N] and orange: Pebax2533-[TMG][BF₄].

As can be seen in Figure 3. 10, upon introducing ILs into the polymer, the PA-phase was mostly affected in contrast to the widely unaltered melting peaks in of the PE segments which did not suffer any relevant decrease in the melting temperature, therefore suggesting no change in the order or stability of the PE phase. The PA peaks, however, suffered a decrease of the melting temperature depending on the IL. A possible explanation could be a decrease in the perfection of the PA crystalline phase and/or the lamellar thickness when the ILs are added, lowering, hence, the proportion of the hard segments. [BMIM][Tf₂N], the only hydrophobic IL employed, caused the largest decrease of the melting temperature of the PA phase of almost 20°C, an observation in line with results from TGA measurements. This indicates that [BMIM][Tf₂N] interacts with the PA-phase but owing to its hydrophobic nature destabilizes it by apparently decreasing the degree of order in the lamellar structure.

Similar evidences have been reported in literature by B. Lotz et al [69] and C. Robitaille [70] in terms of the thermal and mechanical properties of block copolymers once complexed with a second component. In this study, all hydrophilic ILs employed maintain the melting temperature of the hydrophobic PE phase, while the largest decrease of about 5-15°C of the PA melting temperature is observed for [BMIM][Ac] and [C₈MIM][Cl]. Blends containing the [BF₄] anion appear to be the ones which find the melting temperature of their respective phases almost unaltered, which particularly for [TMG][BF₄] is entirely in line with the results from TGA.

With the aim of validating these results with those obtained from literature, Table 3. 1 lists the enthalpy of fusion for the polyether phase (PE) as well as polyamide (PA) in Pebax®2533 studies taken from literature along with those obtained in our study.

Table 3. 1 Comparison between literature data and data from our work on the melting enthalpy ΔH_f and melting temperature of each of the blocks in Pebax[®]2533

Polyether phase (PE)		Polyamide phase (PA)		Ref.
ΔH_f (J/g)	T_m (°C)	ΔH_f (J/g)	T_m (°C)	
22.7	7	6.2	135	[17]
	6		138	[67]
	7-10			[45]
20.2	11	4.0	140	This work

It can be noted that all T_m values of the PE segments are distinctly lower in Pebax[®]2533 than those reported in literature for homogeneous PTMO where the data range from 35° to 60°C [71]. This lower T_m peak of the PE segments in Pebax[®]2533 can arise from the inability to develop thicker, more perfect lamellae crystals that are promoted in the respective homopolymer due to the absence of the PA phase [72], [73]. Apparently, also the lamellae of the PA phase are less perfect in the copolymer Pebax[®]2533 compared to the homopolymer, as the theoretic value of a T_m in the homopolymer of PA12 is situated at 178-187°C while in Pebax[®]2533 we are observing a T_m value of around 40°C less [74].

From the DSC data measured, the degree of semi-crystallinity of the IL-blended materials can be estimated. One would expect to be based on the aforementioned that the ILs modified to some extent the semi-crystallinity but it should also be noted that crystallinity values highly vary depending on the experimental technique used for the measurement of the underlying data.

In this particular case the polymer is presumed to be composed of distinct, non-interacting amorphous and crystalline regions where the reordering of the polymer structure only occurs at the melting temperature of the crystalline component. Despite the obvious

limitations of this model, it is widely used in industry to determine the crystallinity of polymers [75].

On this basis, an approximation of the degree of crystallinity of each segment can be calculated following Equation 3. 1 [76], [77].

$$\text{Equation 3. 1} \quad X_c = \frac{\Delta H_f}{w_{\text{phase}} \cdot \Delta H_f^\circ}$$

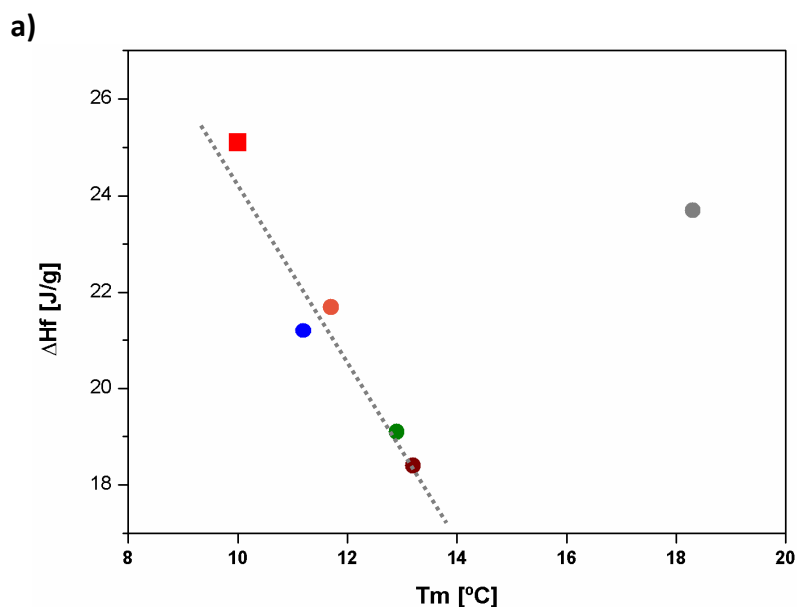
where ΔH_f and ΔH_f° are the measured melting enthalpy of the copolymer phase and the melting enthalpy of a 100% pure crystalline homopolymer respectively. w_{phase} is the mass fraction of each phase in the copolymer, i.e. 0.8 for PE and 0.2 for PA. ΔH_f° is 167J/g for PTMO and 246J/g for PA, respectively [78].

Table 3. 2 ΔH_f (heat of fusion) and T_m (maximum value of melting enthalpy) of each copolymer phase and the crystallinity of each phase

MATERIALS	PE melting peak (J/g)		PA melting peak (J/g)		PE	PA
	ΔH_f [J/g]	T_m [°C]	ΔH_f [J/g]	T_m [°C]	X_c [%]	X_c [%]
Pebax®2533	25.1	10	6.3	140.0	19	12
Pebax2533-[C₈MIM][Cl]	19.1	12.9	5.1	124.3	14	11
Pebax2533-[BMIM][BF₄]	21.2	11.2	5.3	135.3	16	10
Pebax2533-[BMIM][Ac]	18.4	13.2	4.8	129.0	14	10
Pebax2533-[BMIM][Tf₂N]	23.7	18.3	5.7	121.6	18	12
Pebax2533-[TMG][BF₄]	21.7	11.7	3.8	138.7	16	8

Table 3. 2 shows the most relevant thermal peaks in each of the phases of the block-co-polymer. The ΔH_f value provides an insight into the variation on the semi-crystallinity in the PE and PA phase, respectively. It is observed that in the PE phase ΔH_f shifts to lower values upon incorporation of the IL meaning a slight decrease in semi-crystallinity. On the other hand, T_m increases for all ILs in comparison to the pristine Pebax[®]2533 with Pebax2533-[BMIM][Tf₂N] suffering the biggest shift in the PE melting temperature of about 8 °C .

This may be interpreted as a stabilization of the PE-phase in presence of the ILs as compared to the pristine polymer. It is interesting to note that there is a linear correlation between the heat of fusion of the PE segment and its melting temperature (Figure 3. 11a) for all hydrophilic ILs. This means that the more those ILs stabilize the PE-phase, the respective heat of fusion is actually lowered, although the respective changes occur in a narrow data range. Pebax2533-[BMIM][Tf₂N] is a clear outlier as it exhibits the highest melting temperature while almost maintaining the heat of fusion of the pristine polymer.



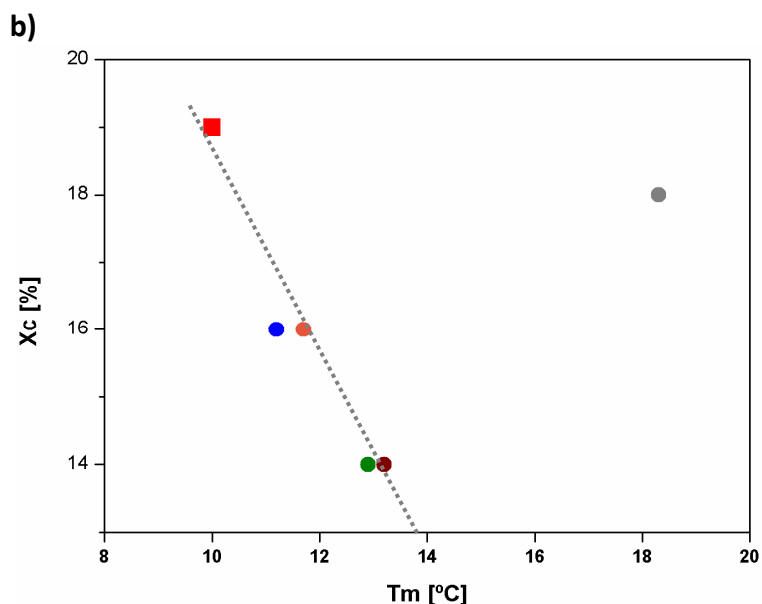


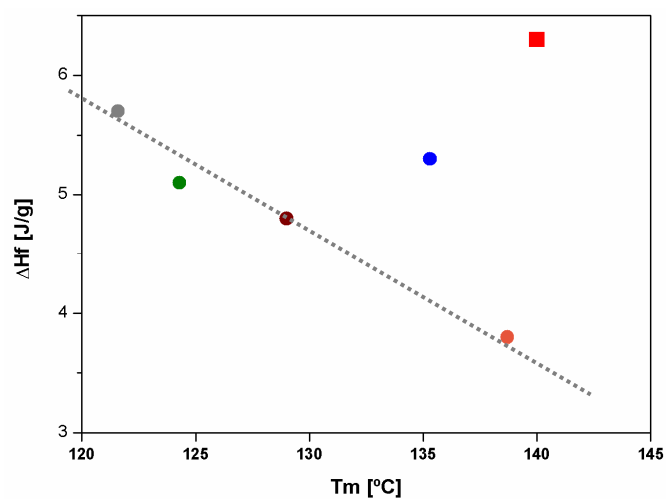
Figure 3. 11 Linear correlation between in PE phase a) heat of fusion and melting temperature; b) semi-crystallinity and melting temperature. Red square: Pebax®2533 pristine membrane, circles for IL-Polymer blends. Green: Pebax-[C₈MIM][Cl], blue: Pebax-[BMIM][BF₄], brown: Pebax-[BMIM][Ac], grey: Pebax-[BMIM][Tf₂N] and orange: Pebax-TMG[BF₄].

This indicates that [BMIM][Tf₂N] interacts most the PE-segment creating interactions that result in a relatively high heat of fusion in view of the high melting temperature, an observation which is in line with the hydrophobicity of [BMIM][Tf₂N]. It should be noted that Equation 3. 1 calculates semi-crystallinity based on the measured heat of fusion without taking such interactions between IL and the PE-segment into account. The high semi-crystallinity of Pebax2533-[BMIM][Tf₂N] depicted Figure 3. 11b might therefore be misleading.

PA segments, on the other hand, show a decrease in both T_m as well as ΔH_f upon addition of ILs . The respective melting temperature of the PA segments is lowered between 2 and 20°C depending on the IL incorporated which could be the consequence of a decrease in the perfection of the semi-crystalline phase or a decrease in the lamellar thickness. Also for

the PA phase a linear correlation between T_m and ΔH_f can be established for some ILs, Figure 3. 12 with the same tendency as observed for the PE-phase.

a)



b)

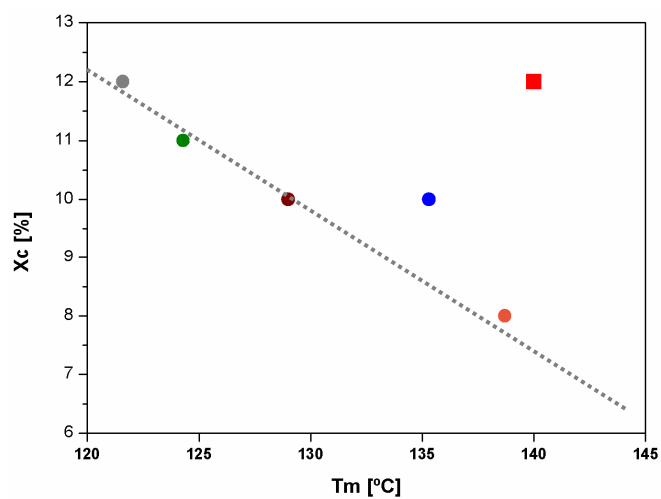


Figure 3. 12 Linear correlation between in PA phase a) heat of fusion and melting temperature; b) semi-crystallinity and melting temperature. Red square: Pebax®2533 pristine membrane, circles for IL-Polymer blends. Green: Pebax-[C₈MIM][Cl], blue: Pebax-[BMIM][BF₄], brown: Pebax-[BMIM][Ac], grey: Pebax-[BMIM][Tf₂N] and orange: Pebax-[TMG][BF₄].

As can be seen (also see Table 3. 2), the two ILs with the [BF₄] anion destabilize least the PA segments while [BMIM][BF₄] seems to establish additional favourable interactions which result in a relatively high heat of fusion. It should be recalled that Pebax2533-[BMIM][BF₄] was found thermally more stable than pristine Pebax®2533 during TGA-experiments. This effect appears negligible when calculating the semi-crystallinity based on Equation 3. 1 (Figure 3. 12b).

The abovementioned observations were confirmed when conducting the cooling step after the melting scan in order to determine the temperature of crystallization (T_c). Figure 3. 13 depicts that also in this case the PA phase suffers a biggest variations while changes in the crystallization peak of the PE phase are negligible.

In the melting scan, it is observed and confirmed that for each polymer/IL blended membrane melting temperatures are smaller compared to pristine Pebax®2533. This indicates that the heat of fusion for crystallization decreases as the crystalline fraction of PA12 decreases [79]. These melting temperatures also decrease depending on the IL used in each blend, likely due to the formation of PA12 crystals with different numbers of integer folds [80]–[84]. This indicates that the chain ends could not be located within the crystalline lamellae but are rejected into the amorphous layers separating the crystals. Hence, ILs would behave as anti-nucleants agents preventing the polymeric chains to organize when they are trying to form the crystalline structure.

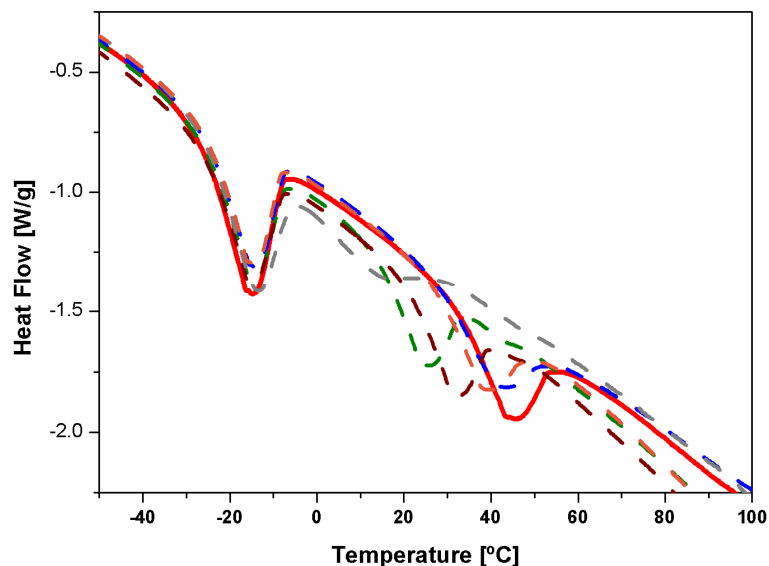


Figure 3. 13 Comparison of crystallization peaks of Pebax®2533 and those of the mixed membrane's. Thick red solid line for pristine Pebax®2533 and dashed lines for IL-Polymer blends. Green line: Pebax-[C₈MIM][Cl], blue: Pebax-[BMIM][BF₄], brown: Pebax-[BMIM][Ac], grey: Pebax-[BMIM][Tf₂N] and orange: Pebax-[TMG][BF₄].

Table 3. 3 lists the differences in the crystallization temperature of the PA peak in each membrane.

Table 3. 3 Temperature position of the crystallization peak of PA phase and its respective shift with relation to pristine Pebax®2533 PA peak

	Pebax®2533	Pebax-[C ₈ MIM][Cl]	Pebax-[BMIM][BF ₄]	Pebax-[BMIM][Ac]	Pebax-[BMIM][Tf ₂ N]	Pebax-[TMG][BF ₄]
T_c (°C)	44.6	24.8	42.6	32.2	14.27	38.9
ΔT (°C)	0	~20	~2	~12.5	~30	~6

[BMIM][Tf₂N] is the IL that most modifies the PA phase in the blended membrane (also bigger variation in the T_m in the melting scan) possibly due to its hydrophobic nature [85] which results in a low affinity for the polyamide. [C₈MIM][Cl] and [BMIM][Ac] also lower the T_c in the PA phase during crystallization. Here, it is assumed that both ILs show a

high water content that could interact with amide groups in the copolymer disturbing in this way the crystal formation. In general, the tendency observed for T_c is similar to that observed for T_m of the PA-phase, although both are not strictly linearly correlated (Figure 3. 14)

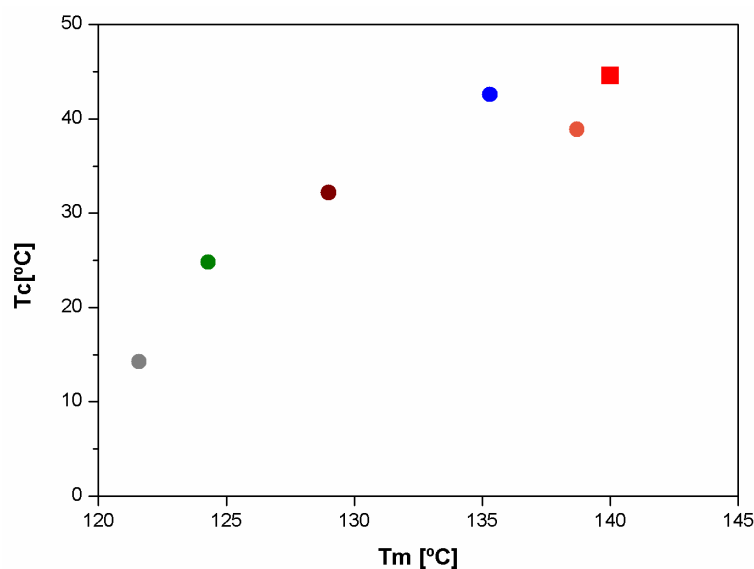


Figure 3. 14 Non-linear correlation between T_c and T_m in the PA phase. Green: Pebax-[C₈MIM][Cl], blue: Pebax-[BMIM][BF₄], brown: Pebax-[BMIM][Ac], grey: Pebax-[BMIM][Tf₂N] and orange: Pebax-[TMG][BF₄].

As a result, both TGA and DSC experiments point out that when ILs are incorporated in the matrix structure, they indeed produce an important modification in the semi-crystalline structure of the membrane. Since crystallinity is lowered when ILs are incorporated in the membrane, we could establish the hypothesis that this might affect the transport properties of these membranes. Considering that gas/vapours are thought to permeate better through amorphous phases [86] we would expect that a less perfect crystalline structure will cause an enhanced permeability of the solutes.

As observed in DSC and TGA, [BMIM][Tf₂N] is the IL that most has changed the thermal properties of the copolymer and most remarkably in both the hydrophilic and the

hydrophobic segments of the polymer. Being the only hydrophobic IL, this suggests that the physico-chemical nature of ILs is relevant upon incorporation into a base material such as Pebax[®]2533. This is to a certain extent remarkable given that ILs are all charged which would suggest that interactions with the non-charged polymer are minimal. Indeed, all ILs showed perfect miscibility with the base polymer and yielded mechanically stable membranes. Amongst the hydrophilic ILs, [BMIM][BF₄] and [TMG][BF₄] are the ILs that least modified the thermal polymer properties which seems to indicate that here the anion plays an important role. This role might, however, be an indirect one as the other two ILs, [C₈MIM][Cl] and [BMIM][Ac], intrinsically absorb more water which might have indirectly contributed to how these ILs affect the polymer structure.

This confirms the statement of Flory [68] indicating that the stronger the interaction between the polymer and the diluents, the greater the melting point suppression and reduction of crystallinity.

With one of the principal findings of the thermal analysis being that the semi-crystalline structure of Pebax[®]2533 changed upon incorporation of ILs, crystallization behaviour was also studied by polarized optical microscopy (POM).

The aim was to evaluate whether the addition of ILs to the base copolymer matrix would interfere with the spherulite formation during the cooling step [87]. For this purpose (see section 2.2.5 in Chapter 2-Materials and Methods for the description of the setup), samples of Pebax[®]2533 and Pebax2533-[C₈MIM][Cl] were heated until melting and then gradually cooled down. During this controlled cooling step photographs were taken every 30 seconds in order to monitor the spherulite formation.

As can be observed in Figure 3. 15 and Figure 3. 16 for Pebax[®]2533 and Pebax2533-[C₈MIM][Cl], respectively, the addition of [C₈MIM][Cl] delays the crystallization. The spherulite appearance not only take place at 40°C, about 40°C below the one that

corresponds to pristine Pebax®2533 (80°C), but also the size of the spherulites is visibly much smaller. This is in very good agreement with DSC measurements from which it was concluded that the perfection and degree of crystallinity of the PA phase in the block copolymer was decreased upon addition of ILs to the block copolymer.

Pebax®2533

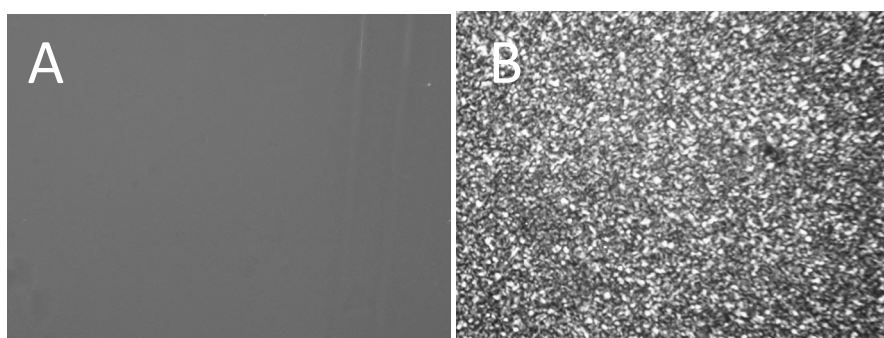
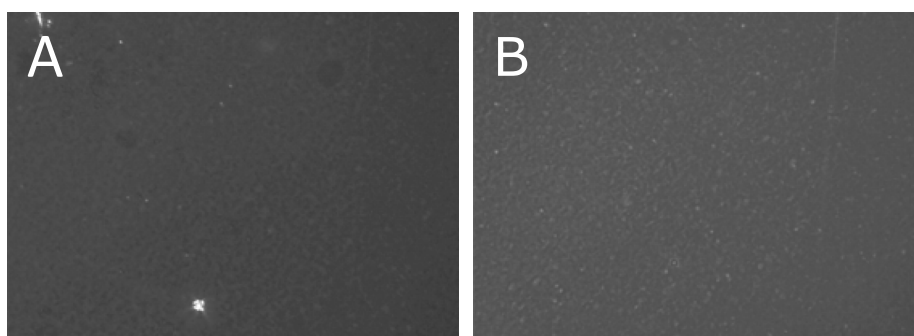


Figure 3. 15 Photographs from the polarized optical microscopy of Pebax®2533 a) molten state and b) in the equilibrium of the spherulite formation at 80°C.

Pebax2533-[C₈MIM][Cl]



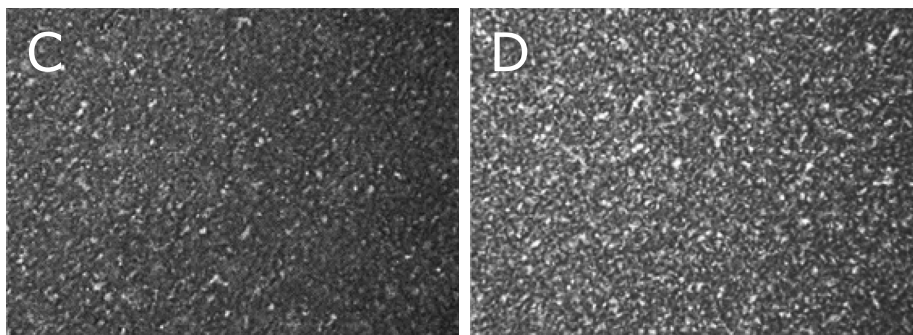


Figure 3. 16 Photographs from the polarized optical microscopy of Pebax2533-[C₈MIM][Cl] . Gradient of temperatures until spherulite observation a) molten state, b) 80°C, c) 50°C and d) 40°C.

Considering that previous characterization techniques have provided information about the interactions between the copolymer and the ILs in terms of thermal stability and semi-crystallinity behaviour, we expected that spectroscopic techniques such as FTIR could provide more explicit data on the possible interactions taking place between the ILs and the base polymer.

3.2.3 Spectroscopic Characterization

Infrared spectroscopy is one of the most powerful methods for studying molecular interactions in polymer systems. As an example, D. Miranda *et al.* showed by FTIR that [BMIM][PF₆] mostly interacts with PEO blocks when being mixed with di or tri-block copolymers [13].

The influence of the interaction with water on the properties of polyamides has also been widely studied by FTIR. Vergelaty [88], Fukuda [89] and Kusanagi [90] have observed that the -OH stretching of sorbed water shifts the frequency band depending on the nature of the amide polymer. Michael Coleman *et al.* have also studied hydrogen bonding in polymers by FTIR [91], [92].

Since our polymer base material, Pebax®, is known to show microphase separation [45], [93] the population of hydrogen-bonded ester carbonyl can be regarded as an indicator for the mixing of the soft and hard segments.

Figure 3. 17 depicts the FTIR spectra of pristine Pebax®2533 and the IL/polymer membranes. The characteristic peaks at 1740 and 1100 cm^{-1} in Pebax®2533 are attributed to ester -C=O and -C-O-C stretching vibrations of the PA and PE respectively segments (for a better comprehension its monomeric structure was depicted previously in Figure 3. 4). As can be seen, these two bands do not suffer any significant change comparing the pristine membrane and those membranes containing ILs.

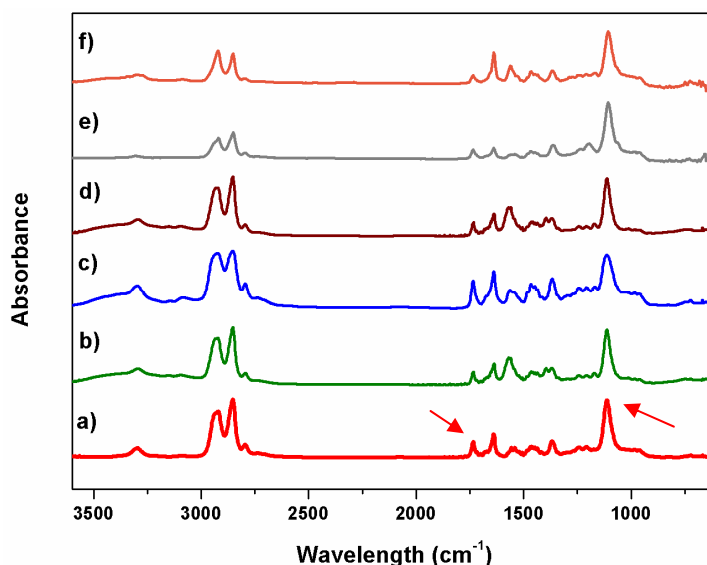


Figure 3. 17 Comparison of FTIR spectra of Pebax®2533 and its mixed membranes. a) Pebax®2533, b) Pebax2533-[C₈MIM][Cl], c) Pebax2533-[BMIM][BF₄], d) Pebax2533-[BMIM][Ac], e) Pebax2533-[BMIM][Tf₂N] and Pebax2533-[TMG][BF₄]

The other two peaks at 1641 and 3290 cm^{-1} indicate the presence of amide H-N-C=O and N-H groups respectively [94]. It is expected that the N-H groups would have preferential interaction with water present in the feed solutions through hydrogen bonding. In this case, for all membranes containing ILs, the bands situated at this position become partially wider (their baseline gets not so defined than in pristine Pebax®2533), assuming possible interactions between the N-H group of hard segment of Pebax®2533 and the water content of the IL.

The band at 1641 cm^{-1} , corresponding to the C=O of H-N-C=O group could be considered to be the most sensitive to interactions due to its mesomeric effect, however no alterations of this band are observed.

The C=O stretching band in amide group of Pebax®2533 consists of two types, the hydrogen-bonded amide peak at 1641 cm^{-1} and the free amide C=O peak at 1656 cm^{-1} , as a tail attached to the former, indicating that the PA block of Pebax®2533 is significantly self-associated via hydrogen bonding [95].

Thus, focusing on this most sensitive area to IL-water interactions (involved C=O stretching bands of ester groups as well as amide ones) between 1500 and 1800 cm^{-1} , (see Figure 3. 17 and Figure 3. 18), we can discern some differences between the blended membranes and Pebax®2533.

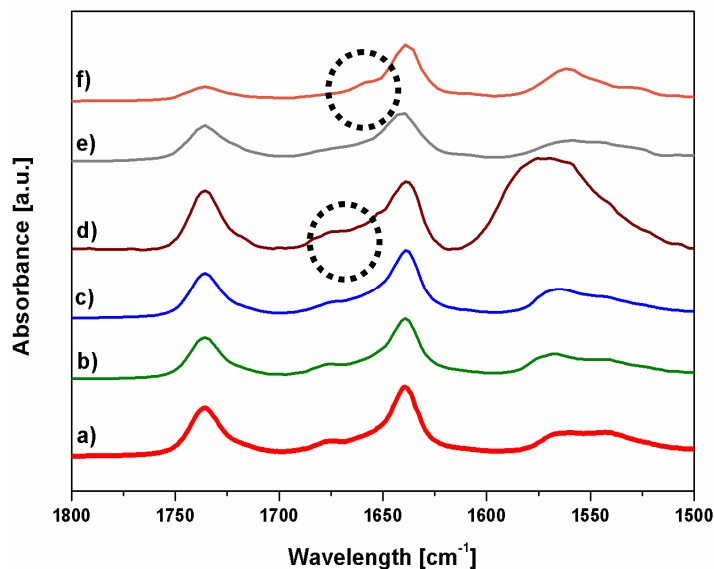


Figure 3. 18 IR spectra focused on amidecarbonyl bands. a) Pebax®2533, b) Pebax2533[BMIM][BF₄], c) Pebax2533-[C₈MIM][Cl], d)Pebax2533-[BMIM][Ac], e) Pebax2533-[BMIM][Tf₂N] and f) Pebax2533-[TMG][BF₄].

It should first be noted that evidences by infrared spectroscopy seem in general not to be extremely clear in such systems as detailed also in literature by Iwamoto et al. where the interactions between amide groups and water [96] showed only very small changes in IR-bands .

Nevertheless, in the case of Pebax®2533, Pebax-[BMIM][BF₄], Pebax-[C₈MIM][Cl] and Pebax-[BMIM][Tf₂N], the free carbonyl amide band has disappeared meaning that the PA block is likely to be forming H-bonds with the water omnipresent in the ILs.

Furthermore, for the cases of Pebax-[BMIM][Ac] and Pebax-[TMG][BF₄], (a zoom has been plotted in Figure 3. 19 for a better observation), a small tail near 1656cm⁻¹ could be identified. This means that both ILs could be intercalated between the copolymer chains producing an effect in the microcrystalline structure of Pebax®2533 [97], causing a bigger distance between both segments.

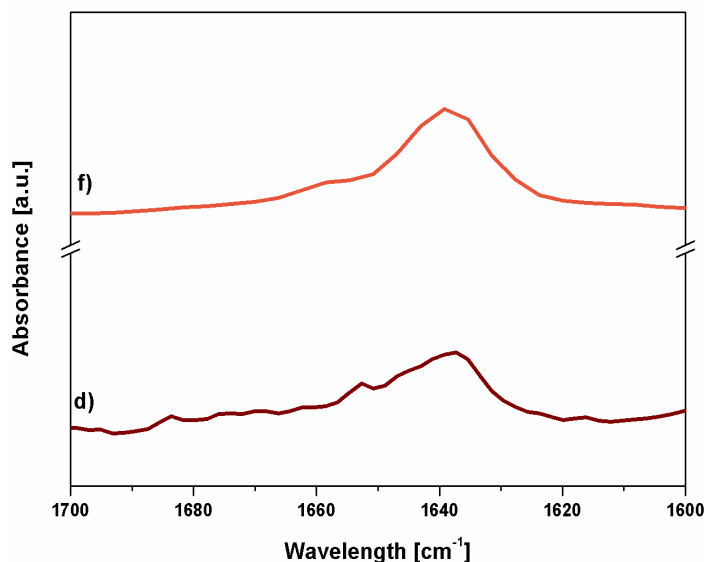


Figure 3. 19 Evidence of the small tail in the free carbonyl band in d) Pebax®2533- [BMIM][Ac] and f) Pebax2533-[TMG][BF₄] as a consequence of the intercalation of the ILs

The PTMO phase of the copolymer is a potential H-bond acceptor. If the ether group would be a stronger hydrogen bond acceptor than the anion of the imidazolium based ILs, the absorbance peaks of the C-H stretching vibrations should suffer a red-shift (shift to lower wavenumbers). This would provide a clear indication of a hydrogen bond being formed between the IL and PTMO. However, no shifts have been observed in the rest of the spectra with any of the IL added.

Other studies in literature [94], [98] have shown rather evident changes in bands [13] (shifts of about 45cm^{-1} in some cases) as a consequence of the hydrogen bond interactions or electron donations by the C=O oxygen to some ions. However, in the case of the mixed-matrix-membranes studied here, we have not seen any significant displacements in the respective bands.

Thus, as a general summary, we can state that while DSC and TGA have shown that [BMIM][BF₄] and [TMG][BF₄] are probably to be those ILs that least modify the thermal

properties of the block copolymer, FTIR reveals for the cases of [BMIM][Ac] and [TMG][BF₄] they indeed modify the copolymer's structure mainly in the PA phase where the interchain distance seems to become bigger due to intercalation. Furthermore, the water present in the other three ILs: [C₈MIM][Cl], [BMIM][BF₄] and [BMIM][Tf₂N] seems to interact with the free carbonyl groups of Pebax®2533 by H-bonding association.

In order to get a deeper knowledge of the effect of each IL into the base copolymer matrix, solid state ¹³C-NMR was also employed as an additional technique. As reported previously by G.R. Hatfield *et al.* [99], this technique has become an ideal method for describing the structure and morphology of polymers.

Literature reveals [100] three specific regions in the Pebax®2533 spectra (see Figure 3. 20) located at:

- **Zone A:** 17-40ppm: polyamide methylene carbons and polyether methylene or methyl carbons in β-position of oxygen atom.
- **Zone B:** 63-76ppm: polyether carbons in α-position of oxygen atom.
- **Zone C:** ~173ppm: polyamide carbonyl group.

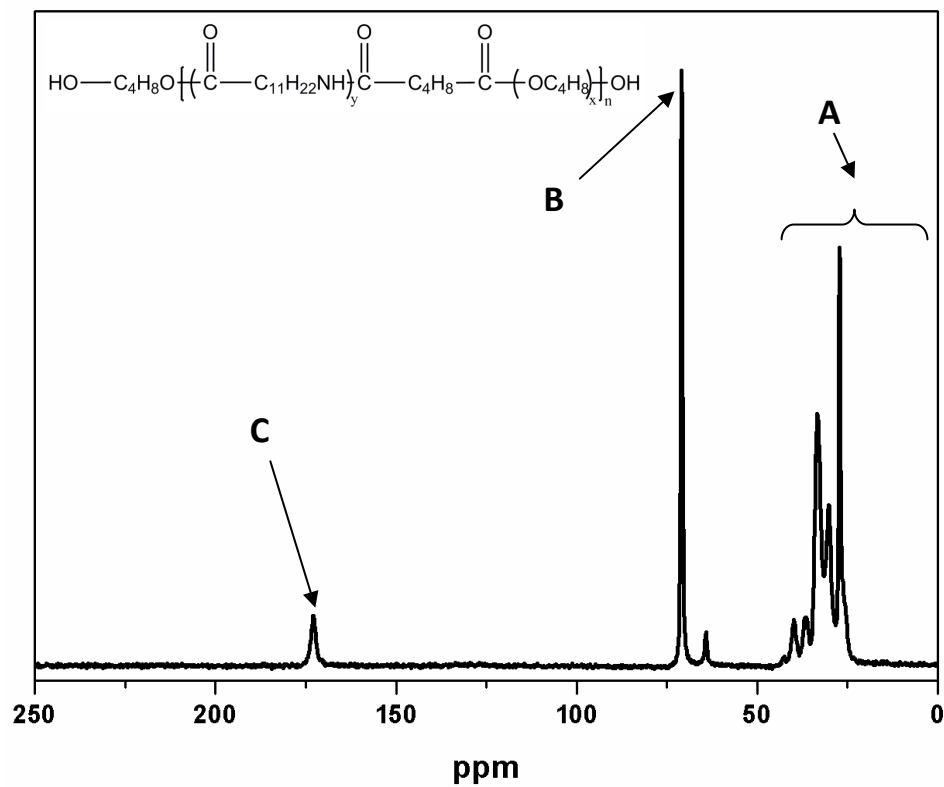


Figure 3. 20 ¹³C-NMR spectra of Pebax®2533 membrane

In order to study the effect of the ILs on the polymer structure, Figure 3. 21 collects the pristine Pebax®2533 membrane compared with IL blended membranes.

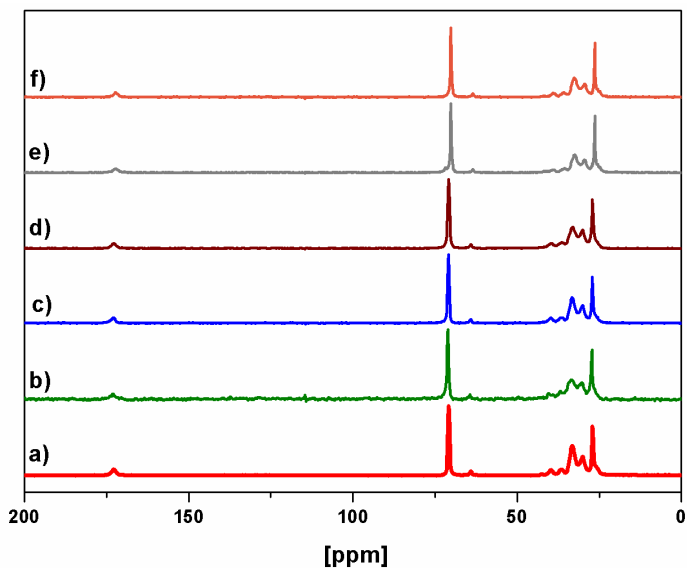


Figure 3. 21 Comparison of ^{13}C -NMR spectra of all mixed membranes. a) Pebax®2533, b) Pebax2533-[BMIM][BF₄], c) Pebax2533-[C₈MIM][Cl], d) Pebax2533-[BMIM][Ac], e) Pebax2533-[BMIM][Tf₂N] and f) Pebax2533-[TMG][BF₄].

At first sight, no significant differences are observed between pristine Pebax®2533 and IL blended membranes. Thus, in order to obtain more details, the most significant areas of the spectra were amplified (areas A and B as detailed in Figure 3. 22).

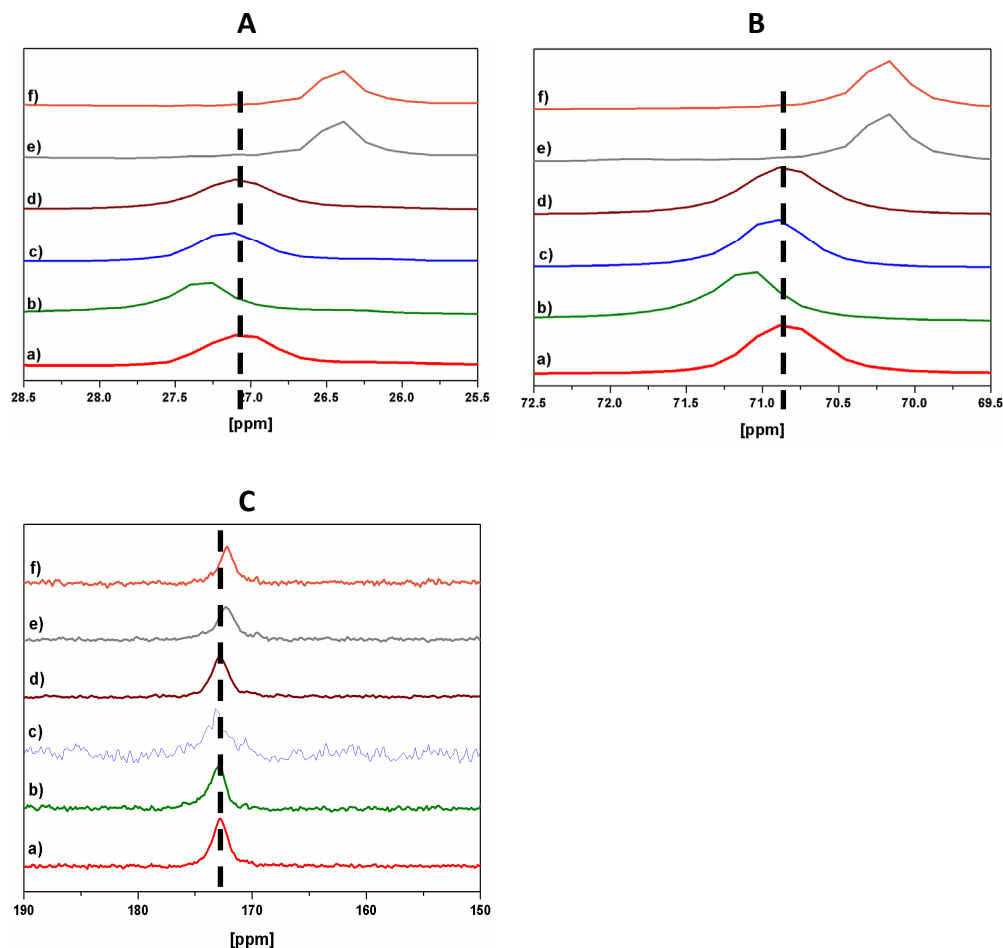


Figure 3. 22 Zoom of the maximum of the peak that corresponds to zone A (left) and zone B (right) for a) Pebax[®]2533, b) Pebax2533-[C₈MIM][Cl], c) Pebax2533-[BMIM][BF₄], d) Pebax2533-[BMIM][Ac], e) Pebax2533-[BMIM][Tf₂N] and f) Pebax2533-[TMG][BF₄].

It can be seen that the shifts observed for both A, B and C peaks are tendentially similar for each IL which means that the ILs interacted in similar ways with the polyamide methylene carbons and polyether carbons. For all peaks, [BMIM][Tf₂N] and [TMG][BF₄] caused identical upfield shifts (shielding) of about $\delta = -0,7$ ppm. Hardly any measureable shift was observed for [BMIM][Ac]. [BMIM][BF₄] and mainly [C₈MIM][Cl] result in downfield shifts (deshielding) the magnitude of which depends on the peak zone: while [C₈MIM][Cl]

generates a downfield shift of around $\delta=0,2$ ppm for the zone A and B but only a minor shift in zone C of $\delta=0,1$ ppm, [BMIM][BF₄] triggers a shift of about $\delta=0,3$ ppm in zone C but only a shift of $\delta=0,1$ ppm in zone A and B, respectively. From these results no clear tendency in interaction can be observed, neither as a function of the cation (see ILs with [BMIM]) nor the anion (see ILs with [BF₄]) of the IL. The shielding observed by [TMG][BF₄] could mean a higher electron density around the methylene and polyether carbons due to intercalation as was also deduced from IR-spectra. The latter indicated a similar interaction with [BMIM][Ac] which, however, might not result in a shift in ¹³C NMR as [Ac] has a lower electron density than [BF₄]. It then remains unclear why [BMIM][Tf₂N] causes a shielding in A and B without any apparent band shift observable in IR. [C₈MIM][Cl] results in deshielding in these regions which could be due to stacking. This is interesting as it would occur via the cation which is similar for several ILs tested but apparently does not always result in the same interactions. Here the long alkyl-chain may indeed make a difference and align with the polymer carbons as has been speculated before.

The spectra for zone C show similar tendencies in shifts like zone A and B. Representing the carbonyl groups of Pebax®2533, it would be expected to be the most sensitive to hydrogen bond formation which would then be noticeable through a downfield shift. In this zone of the spectra it would also be assumed that the cation of the imidazolium ring could partially interact with the free carbonyl of Pebax®2533. As can be seen in Table 3. 4, the most significant downfield shift is observed for [BMIM][BF₄]. Due to the hydrophilic character of this IL it could be caused due to possible hydrogen bonding formation between the water inside the IL and the polyamide carbonyl groups [101], [102]. The same might apply for [C₈MIM][Cl], although at a smaller scale. Interestingly, for [BMIM][Ac] no shift was observed at all, as occurred in zone B. On the contrary, [TMG][BF₄] and [BMIM][Tf₂N] cause significant shielding: with [BMIM][Tf₂N] being hydrophobic as opposed to [BMIM][BF₄] which is hydrophilic, this might indicate interaction with the cation. It is interesting to note that both ILs share either the anion or cation of [BMIM][BF₄] but result in entirely opposed shifts. This stresses once more how prediction of interactions between ILs and the block copolymer are not straightforward (see Table 3. 4).

Table 3. 4 collects quantitatively the shifts observed for blended membranes in the three zones A, B and C of the spectra when taking the positions of pristine Pebax®2533 as reference.

Table 3. 4 Detailed Shifts of each characteristic peaks in each region of the spectra using pristine Pebax®2533 positions peaks as reference. (negative value means an “upfield” shift-shielding)

	A (ppm)	B (ppm)	C (ppm)
Pebax®2533	0	0	0
δ Pebax®2533: [C₈MIM][Cl]	0.24	0.21	0.09
δ Pebax®2533: [BMIM][BF₄]	0.06	0.05	0.26
δ Pebax®2533: [BMIM][Ac]	0.04	0	0
δ Pebax®2533: [BMIM][Tf₂N]	-0.67	-0.70	-0.59
δ Pebax®2533: [TMG][BF₄]	-0.69	-0.70	-0.68

Summarizing results from FTIR and ¹³C-NMR measurements, the most significant changes were observed for Pebax2533-[C₈MIM][Cl] with the disappearance of the free carbonyl band in FTIR and suffering biggest peak displacements in ¹³C-NMR when compared to pristine polymer. This would make think that [C₈MIM][Cl] would be the IL that most interacts with the block copolymer.

On the other hand, DSC measurements, showed that [BMIM][Tf₂N] was the IL that most modified the PA lamellae structure of the copolymer. This apparent incongruence, could be due to water present in the IL, primarily in [C₈MIM][Cl], and which results in shift of the carbonyl group in the ¹³C-NMR spectra although the IL itself does not undergo any detectable interactions.

It also becomes apparent that FTIR and ¹³C-NMR are for this study analytical techniques far less helpful for identifying IL-polymer interactions than thermal and calorimetric analysis.

3.2.4 Organic Vapour Permeation Tests

The aforementioned analyses served for characterizing the changes the ILs would cause in the morphology of the polymer membrane. On one hand, it was expected that the IL phase would change the selectivity of the membrane for certain permeants. On the other hand, the changes in semi-crystallinity of the base polymer which had been determined would be expected to also increase the membrane permeability. Permeability studies were therefore carried out using the gravimetric permeation setup (for details see Chapter 2) with five organic solvents: water, ethanol, ethyl acetate, hexane and toluene. The permeabilities measured are listed in Table 3. 5 and depicted in Figure 3. 23.

Table 3. 5 Saturated organic vapour permeabilities measured for all blended membranes in $[\text{cm}^3 \cdot \text{cm} \cdot \text{cm}^{-2} \cdot \text{s}^{-1} \cdot \text{cmHg}^{-1}] \times 10^{10}$ (Barrer) together with the experimentally observed error.

	Pebax- Pebax2533	Pebax- [C ₈ MIM] [Cl]	Pebax- [BMIM] [BF ₄]	Pebax- [BMIM] [Ac]	Pebax- [BMIM] [Tf ₂ N]	Pebax- [TMG] [BF ₄]
Hexane	10±1	7±1	8±2	6±1	8±2	7±2
EtOH	12±4	19±2	20±6	23±7	26±6	27±5
Water	24±7	35±4	28±8	30±5	74±15	32±7
Ethyl Acetate	19±3	14±3	21±8	9±2	42±10	23±8
Toluene	25±5	16±3	27±9	6±1	34±11	24±7

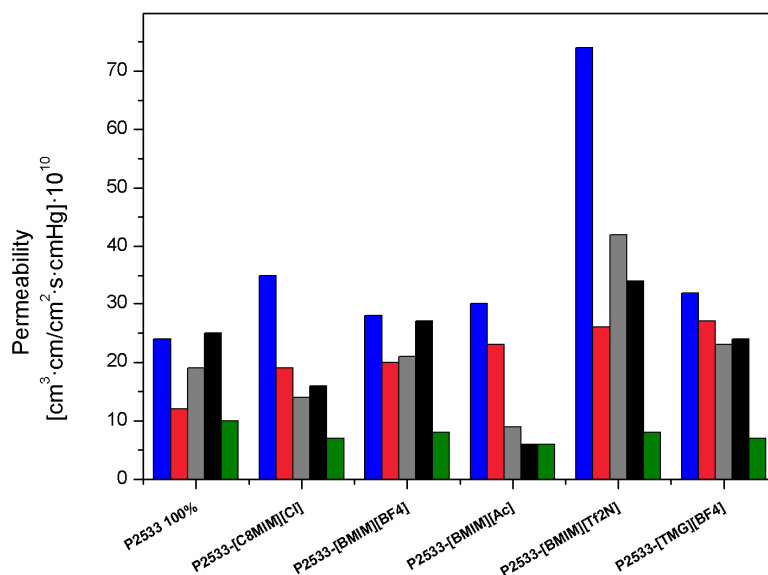


Figure 3. 23 Vapour permeabilities measured for pristine Pebax®2533 and IL-blended membranes. Blue: water, red: ethanol, grey: ethyl acetate, black: toluene and green: hexane

As can be seen from Figure 3. 23 and Table 3. 5, pristine Pebax®2533 has similar permeabilities for saturated organic vapours of water and toluene, as well as ethanol and hexane, respectively. This illustrates the presence of both hydrophilic and hydrophobic domains in the pristine polymer. Upon incorporation of ILs, all blended membranes reveal a permeability for water and ethanol higher than those obtained with the pristine membrane, reflecting the high affinity of the ILs for these compounds ILs but possibly also as a consequence of the diminished semi-crystallinity. For better visualization of how individual ILs affected the permeability of the Pebax®2533 base polymer, the solvent permeabilities of the blended membranes are represented in Figure 3. 24 offset against the respective permeabilities of the pristine membrane (Pebax®2533) (hence, pristine membrane permeabilities become equal to zero).

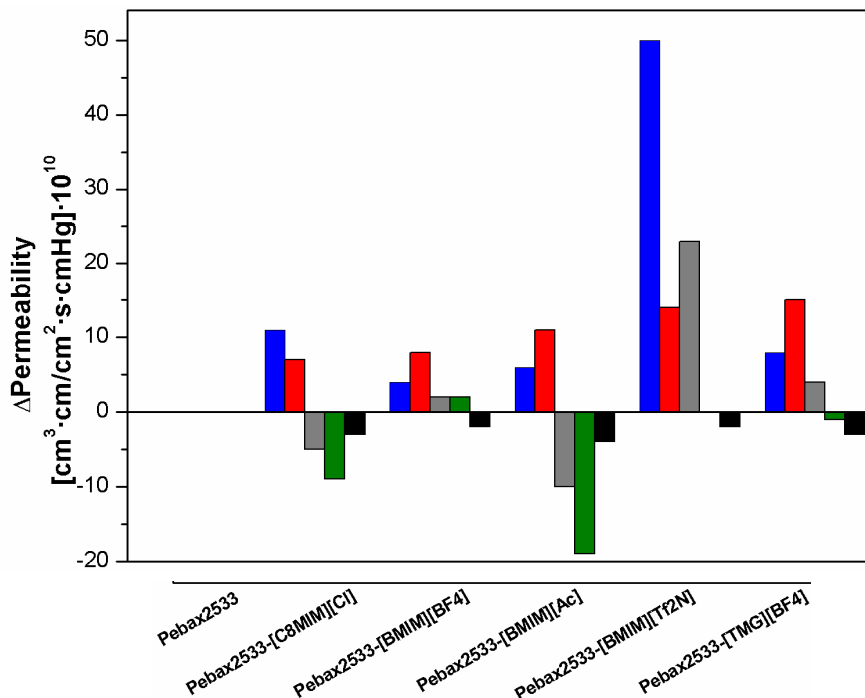


Figure 3. 24 Organic vapour permeability experiments of the Pebax2533-IL membranes. Solvent permeabilities in the Pebax2533 blends were offset against respective permeabilities of pristine Pebax®2533. Blue: water, red: ethanol, grey: ethyl acetate, black: toluene and green: hexane.

At a first glance it can be seen that the transport properties of the membranes varied depending on the nature of the IL incorporated in the block copolymer when being in contact with different vapours. Taking the values given by the pristine membrane as a reference, it is observed that according to the nature of the vapour of interest the membrane permeability is either increased or even decreased. Most remarkable differences can be found between the polar compounds water and ethanol on one hand, and the less polar or apolar ones: ethyl acetate, toluene and hexane, on the other. This is in line with observations reported in literature [16].

Interestingly, the water permeability with [BMIM][Tf₂N] was the highest for all membranes, although this IL was the only hydrophobic one [103]. This behavior may therefore possibly be explained as a lower interaction of [BMIM][Tf₂N] with water while at the same time increasing diffusivity more than the rest of the blended membranes. This

observation would need to be confirmed by separate sorption and diffusion experiments which also would allow to understand in more detail whether the respective ILs changed the overall permselectivity based on changes in sorption, diffusion, or both.

In practical terms, the results obtained could not be considered to be relevant for separation processes; however it is appreciable that the selectivity of the membranes has significantly changed for various solutes when incorporating a 20 wt% of the IL. This seems to indicate that once a high-affinity solvent is identified, it may be incorporated into a base structure so as to increase its permselectivity.

3.2.5 ^{13}C NMR experiments with organic solvents

It had been shown that in ^{13}C -NMR spectra small shifts indicated some interaction between certain ILs and Pebax[®]2533. In order to provide a context for this experimental evidence, pristine Pebax[®]2533 was contacted with five different conventional organic solvents (water, ethanol, ethyl acetate, hexane and toluene) for 36h. During this period of time, it was expected that the sorption equilibrium was reached. Subsequently, the polymeric film was superficially dried and then the ^{13}C -NMR spectra measured. The aim was to observe whether organic solvents would cause NMR-shifts comparable to those observed with ILs, or higher, and in this way create a context for interpreting IL-polymer interactions. All ^{13}C -NMR spectra measured are shown in Figure 3. 25.

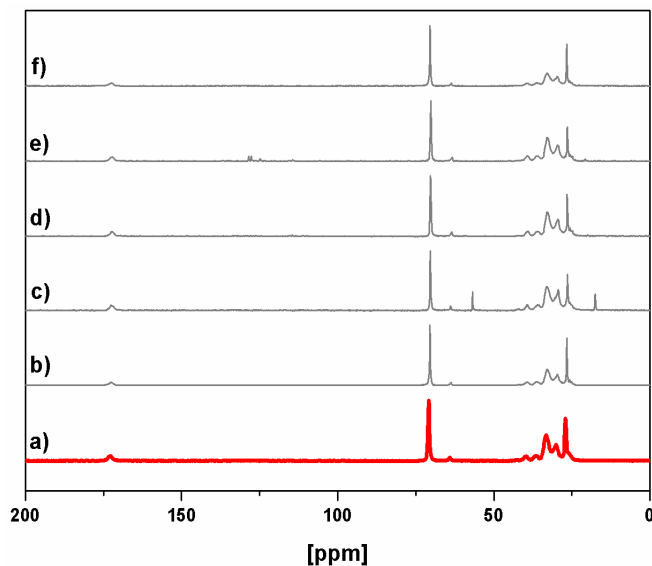


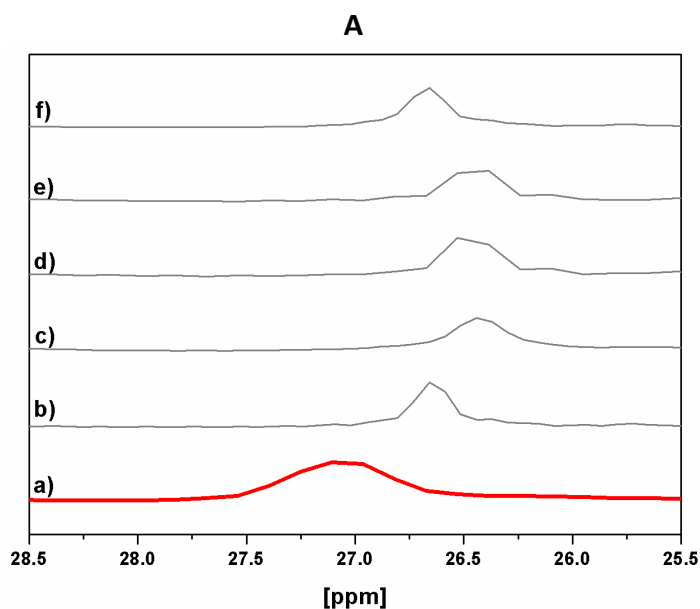
Figure 3. 25 Comparison of Pebax®2533 membrane with Pebax®2533 membranes in contact with several organic solvents. a) Pebax®2533, b) Pebax®2533-water, c) Pebax®2533-ethanol, d) Pebax®2533-ethyl acetate, e) Pebax®2533-toluene and f) Pebax®2533-hexane.

Processing the data as done before, and zooming into the three areas of main interest of the spectra (see Figure 3. 20), the shifts are listed in Table 3. 6 and depicted in Figure 3. 26.

Table 3. 6 Shifts of the characteristic bands as identified in Figure 3. 25 observed when contacting Pebax®2533 with different organic solvents

	A (ppm)	B (ppm)	C (ppm)
Pristine Pebax®2533	0	0	0
δ Pebax®2533-Water	-0.50	-0.50	-0.35
δ Pebax®2533-Ethanol	-0.72	-0.57	-0.39
δ Pebax®2533-Ethyl Acetate	-0.58	-0.58	-0.59
δ Pebax®2533-Toluene	-0.71	-0.71	-0.63
δ Pebax®2533-Hexane	-0.5	-0.5	-0.5

As can be seen, the shifts observed when Pebax®2533 contacts with the organic solvents are in the range of those occurring with some ILs but without exception toward lower frequencies, i.e., an upfield shift and indicating in general a shielding effect. Given that despite of the diversity of the solvents tested they follow the same general tendency, this indicates that ILs must not be considered as a class of solvents and may possibly not even be compared with solvents in their interactions with the base polymer. It also shows that some ILs undergo interactions similar in strength to that of common solvents. Table 3. 6 provides the valuable insight that highly polar or apolar compounds, such as water and hexane, respectively, generate identical upfield shifts in the region A and B, thus revealing that possibly the shifts observed are not due to solvent-polymer interactions but mainly due to the intercalation of the solvent within the polymer structure and hence increasing distance between polymer carbon chains. As a consequence and seen in this context, previous observations on IL-polymer interactions from ^{13}C NMR spectra might not be conclusive.



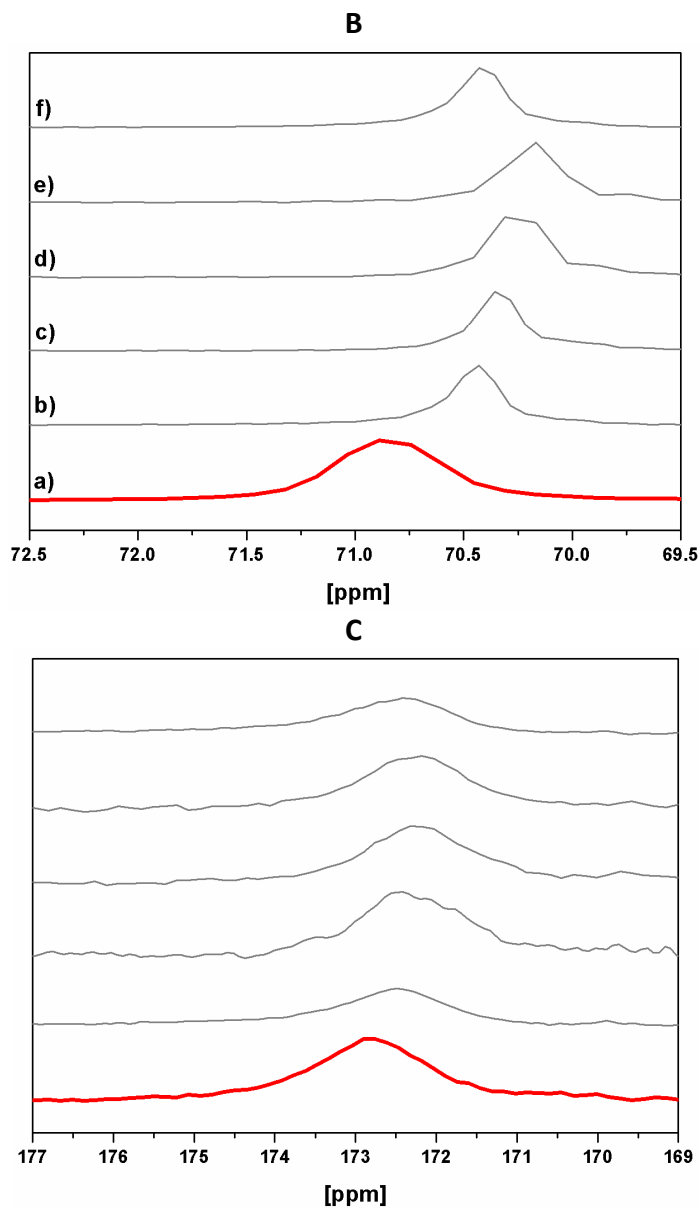


Figure 3. 26 A: polyamide methylene carbons and polyether methylene or methyl carbons in β -position of oxygen atom and B: polyether carbons in α -position of oxygen atom. C: polyamide carbonyl group. a) Pristine Pebax®2533, b) Pebax®2533-Water c) Pebax®2533-ethanol, d) Pebax®2533-ethyl acetate, e) Pebax®2533-hexane and f) Pebax®2533-toluene.

With regard to region "C" (carbonyl groups), one would have expected pronounced downfield shifts for both water and ethanol due to formation of hydrogen bonds with the carbonyl amide group. However, no relevant differences between solvents are observed and, in fact water exhibits an upfield shift similar to the alkane hexane. As opposed to the IL-polymer studies which were conducted with a defined and fixed amount of IL added to the base polymer, here concentration effects might come into play as the polymer was saturated in solvent according to its thermodynamic sorption equilibrium. Nevertheless, the results obtained seem to indicate that from the current results no conclusive data can be obtained from ^{13}C NMR on how exactly the polymer chains rearrange or interact in presence of ILs.

3.2.5.1 *Pebax[®]2533-[BMIM][BF₄]* with organic solvents

Previous tests have shown that the block-copolymer shows good swelling capacity meaning that it is interacting with the solvents in contact. The aim was not to see in how far polymer-solvent interactions would change upon incorporation of an IL into the polymer matrix. As an example, [BMIM][BF₄] was studied as a model system in order to investigate in how far the presence of 20 wt% of IL in the base polymer could possibly affect its overall interaction with organic solvents. For this purpose, ^{13}C NMR spectra were taken after reaching to an equilibrium of Pebax[®]2533 with ethanol, ethyl acetate and toluene, respectively, and with and without [BMIM][BF₄], respectively. The sample preparation of the Pebax2533-[BMIM][BF₄] blend membrane was the same as in the previous tests.

Figure 3. 27 is only focused on the peak at around $\delta=70\text{ppm}$. The other areas are not showed for simplification as no relevant shifts have been observed.

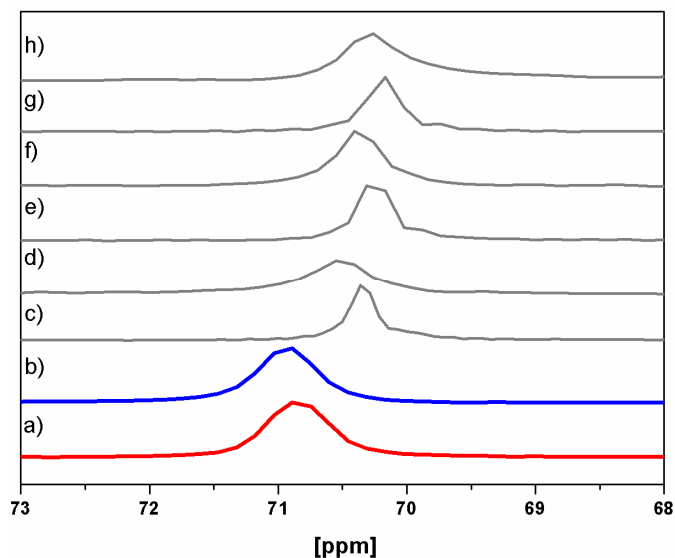


Figure 3. 27 ^{13}C NMR Evidence of shifts observed for Pebax®2533 with different organic solvents and compared to Pebax®2533 containing 20 wt% [BMIM][BF₄]. a) Pebax®2533 and b) Pebax2533-[BMIM][BF₄]. c) Pebax®2533-Ethanol, d) Pebax2533-[BMIM][BF₄]-Ethanol, e) Pebax®2533-Ethyl acetate, f) Pebax2533-[BMIM][BF₄]-Ethyl Acetate, g) Pebax®2533-Toluene, h) Pebax2533-[BMIM][BF₄]-Toluene

As mentioned above, the presence of [BMIM][BF₄] into the polymer structure produced a minor deshielding effect (downfield shift) since the peak that corresponds to polyether carbons in α -position of oxygen atom (the most representative ones to show this effect) are shifted to higher frequencies (Figure 3. 22B). This displacement compared to the pristine polymer was also maintained when contacting with the solvents. As can be seen from Figure 3. 27 and Table 3. 7, [BMIM][BF₄] did apparently not change at all the interactions between the polymer chains and the solvents, neither that of the IL with the polymer.

Table 3. 7 List of the shifts observed in ^{13}C NMR (zone B of the spectra) when contacting organic solvents with Pebax[®]2533 or Pebax[®]2533-[BMIM][BF₄]

	δ [ppm]	δ polymer/IL - δ polymer [-]	δ measured - δ polymer [ppm]
Pebax[®]2533	70.95		
		0.06	
Pebax2533- [BMIM][BF₄]	71.01		
Pebax[®]2533-Ethanol	70.40		-0.55
		0.13	
Pebax2533- [BMIM][BF₄]-Ethanol	70.53		-0.42
Pebax[®]2533-Ethyl Acetate	70.35		-0.60
		0.03	
Pebax2533- [BMIM][BF₄]-Ethyl Acetate	70.38		-0.63
Pebax[®]2533-Toluene	70.24		-0.71
		0.03	
Pebax2533- [BMIM][BF₄]-Toluene	70.27		-0.74

^{13}C NMR experiments did, hence, provides the following insights: (1) the intensity of IL-polymer interactions are in the range of interactions the polymer has with common solvents; (2) ILs do not interact with the polymer as a group of a solvent but need to be evaluated on a case-to-case basis; (3) apparently the presence of the IL does not affect interactions with solvents compared to the pristine polymer.

3.3 Conclusions

Pebax®2533 has been used as a base polymer for physico-chemical modification by the incorporation of five different ILs. Membranes were successfully prepared by a casting method and maintained mechanically stable with a 20 wt% of IL.

It has been demonstrated that the incorporation of ILs in a polymer matrix as Pebax®2533 could be a new alternative to the development of SILMs. Since apart from avoiding some of the disadvantages SILMs present, these polymer/IL blends have confirmed not only good stabilities but also acceptable thermal stabilities.

Thermal measurements have demonstrate that for the case of DSC, the most affected phase in the copolymer would be the one that corresponds to the PA phase while TGA measurements indicate that despite the thermal stability of the mixed-matrix-membranes are partially lowered, they still reveal acceptable decomposition temperatures. [BMIM][Tf₂N] and [C₈MIM][Cl] seem to be the ILs that most modify the semi-crystalline structure of the block-copolymer but FITR experiments have also shown that [BMIM][BF₄] and [TMG][BF₄], although not likely to interact with the copolymer, indeed produce microphase separation of the base material.

FTIR measurements demonstrate that [BMIM][Ac] and [TMG][BF₄] are those ILs that induce the microphase separation by modifying the crystalline structure and distancing both segments in the copolymer. On the contrary, [BMIM][BF₄], [C₈MIM][Cl], and [BMIM][Tf₂N] in the blended membranes seem to self-associate via H-bonding. Although not for all cases, ¹³C NMR has also shown a complementary evidence in [BMIM][Tf₂N] being reflected in the amide carbonyl shift.

Even so, FTIR and ¹³C NMR seem to have very limited sensitivity for the detection of these low interactions taking place between Pebax®2533 and the ILs.

Chapter 3

From now on, the following chapters will be focused on the efficiency of these blended membranes for separation processes and the study of their interactions with solutes as well as how ILs place between the copolymer chains in the base matrix.

3.4 References

- [1] M. J. A. Shiddiky and A. A. J. Torriero, "Application of ionic liquids in electrochemical sensing systems," *Biosens. Bioelectron.*, vol. 26, no. 5, pp. 1775–1787, **2011**.
- [2] F. Faridbod, M. R. Ganjali, B. Larijani, and P. Norouzi, "Multi-walled carbon nanotubes (MWCNTs) and room temperature ionic liquids (RTILs) carbon paste Er(III) sensor based on a new derivative of dansyl chloride," *Electrochim. Acta*, vol. 55, no. 1, pp. 234–239, **2009**.
- [3] R. T. Kachoosangi, M. M. Musameh, I. Abu-Yousef, J. M. Yousef, S. M. Kanan, L. Xiao, S. G. Davies, A. Russell, and R. G. Compton, "Carbon Nanotube–Ionic Liquid Composite Sensors and Biosensors," *Anal. Chem.*, vol. 81, no. 1, pp. 435–442, **2009**.
- [4] L. J. Lozano, C. Godínez, A. P. de los Ríos, F. J. Hernández-Fernández, S. Sánchez-Segado, and F. J. Alguacil, "Recent advances in supported ionic liquid membrane technology," *J. Memb. Sci.*, vol. 376, no. 1–2, pp. 1–14, **2011**.
- [5] M. Matsumoto, Y. Inomoto, and K. Kondo, "Selective separation of aromatic hydrocarbons through supported liquid membranes based on ionic liquids," *J. Memb. Sci.*, vol. 246, no. 1, pp. 77–81, **2005**.
- [6] N. M. Kocherginsky, Q. Yang, and L. Seelam, "Recent advances in supported liquid membrane technology," *Sep. Purif. Technol.*, vol. 53, no. 2, pp. 171–177, **2007**.
- [7] J. Ilconich, C. Myers, H. Pennline, and D. Luebke, "Experimental investigation of the permeability and selectivity of supported ionic liquid membranes for CO₂/He separation at temperatures up to 125 °C," *J. Memb. Sci.*, vol. 298, no. 1–2, pp. 41–47, **2007**.
- [8] M. Matsumoto, A. Panigrahi, Y. Murakami, and K. Kondo, "Effect of ammonium-

- and phosphonium-based ionic liquids on the separation of lactic acid by supported ionic liquid membranes (SILMs)," *Membranes (Basel)*, vol. 1, no. 2, pp. 98–108, **2011**.
- [9] M. Teramoto, Y. Sakaida, S. S. Fu, N. Ohnishi, H. Matsuyama, T. Maki, T. Fukui, and K. Arai, "An attempt for the stabilization of supported liquid membrane," *Sep. Purif. Technol.*, vol. 21, no. 1, pp. 137–144, **2000**.
- [10] M. Joskowska, I. Kopczynska, B. Debski, D. Holownia-Kedzia, R. Aranowski, and J. Hupka, "Wetting of supports by ionic liquids used in gas separation processes," *Physicochem. Probl. Miner. Process.*, vol. 48, no. 1, pp. 129–140, **2012**.
- [11] P. Cserjési, N. Nemestóthy, and K. Bélafi-Bakó, "Gas separation properties of supported liquid membranes prepared with unconventional ionic liquids," *J. Memb. Sci.*, vol. 349, no. 1–2, pp. 6–11, **2010**.
- [12] K. Simons, K. Nijmeijer, J. E. Bara, R. D. Noble, and M. Wessling, "How do polymerized room-temperature ionic liquid membranes plasticize during high pressure CO₂ permeation?," *J. Memb. Sci.*, vol. 360, no. 1–2, pp. 202–209, **2010**.
- [13] D. F. Miranda, T. P. Russell, and J. J. Watkins, "Ordering in mixtures of a triblock copolymer with a room temperature ionic liquid," *Macromolecules*, vol. 43, no. 24, pp. 10528–10535, **2010**.
- [14] S. Livi, V. Bugatti, B. G. Soares, and J. Duchet-Rumeau, "Structuration of ionic liquids in a poly(butylene-adipate-co-terephthalate) matrix: its influence on the water vapour permeability and mechanical properties," *Green Chem.*, vol. 16, no. 8, p. 3758, **2014**.
- [15] M. Kárászová, M. Kacirková, K. Friess, and P. Izák, "Progress in separation of gases by permeation and liquids by pervaporation using ionic liquids: A review," *Sep. Purif. Technol.*, vol. 132, pp. 93–101, **2014**.

- [16] K. Friess, J. C. Jansen, F. Bazzarelli, P. Izák, V. Jarmarová, M. Kacirková, J. Schauer, G. Clarizia, and P. Bernardo, "High ionic liquid content polymeric gel membranes: Correlation of membrane structure with gas and vapour transport properties," *J. Memb. Sci.*, vol. 415–416, pp. 801–809, **2012**.
- [17] P. Bernardo, J. C. Jansen, F. Bazzarelli, F. Tasselli, A. Fuoco, K. Friess, P. Izák, V. Jarmarov, M. Kacirková, and G. Clarizia, "Gas transport properties of Pebax??/room temperature ionic liquid gel membranes," *Sep. Purif. Technol.*, vol. 97, pp. 73–82, **2012**.
- [18] M. P. Scott, M. Rahman, and C. S. Brazel, "Application of ionic liquids as low-volatility plasticizers for PMMA," *Eur. Polym. J.*, vol. 39, no. 10, pp. 1947–1953, **2003**.
- [19] M. P. Scott, C. S. Brazel, M. G. Benton, J. W. Mays, J. D. Holbrey, and R. D. Rogers, "Application of ionic liquids as plasticizers for poly(methyl methacrylate)," *Chem. Commun.*, no. 13, pp. 1370–1371, **2002**.
- [20] M. Rahman and C. S. Brazel, "Ionic liquids: New generation stable plasticizers for poly(vinyl chloride)," *Polym. Degrad. Stab.*, vol. 91, no. 12, pp. 3371–3382, **2006**.
- [21] M. Rahman, H. W. Shoff, and C. S. Brazel, "Ionic Liquids as Alternative Plasticizers for Poly(vinyl chloride): Flexibility and Stability in Thermal, Leaching, and UV Environments," *ACS Symp. Ser.*, vol. Chapter 7, pp. 103–118, **2005**.
- [22] L. X. Hou and S. Wang, "Study on ionic liquid [bmim]PF₆ and [hmim]PF₆ as plasticizer for PVC paste resin," *Polym. Bull.*, vol. 67, no. 7, pp. 1273–1283, **2011**.
- [23] A. S. Wilson, "Plasticisers principles and practice," vol. London, no. Institute of materials, p. 316, **1995**.
- [24] J. Le Bideau, L. Viau, and A. Vioux, "Ionogels, ionic liquid based hybrid materials,"

Chem Soc Rev, vol. 40, no. 2, pp. 907–925, **2011**.

- [25] H. Rabiee, A. Ghadimi, S. Abbasi, and T. Mohammadi, “CO₂ separation performance of poly(ether-b-amide6)/PTMEG blended membranes: Permeation and sorption properties,” *Chem. Eng. Res. Des.*, vol. 98, pp. 96–106, **2015**.
- [26] D. F. Cadogan, “Plasticizers: A consideration of their impact on health and the environment,” *J. Vinyl Addit. Technol.*, vol. 13, no. 2, pp. 104–108, **1991**.
- [27] H. Z. Chen, P. Li, and T. S. Chung, “PVDF/ionic liquid polymer blends with superior separation performance for removing CO₂ from hydrogen and flue gas,” *Int. J. Hydrogen Energy*, vol. 37, no. 16, pp. 11796–11804, **2012**.
- [28] S. U. Hong, D. Park, Y. Ko, and I. Baek, “Polymer-ionic liquid gels for enhanced gas transport,” *Chem. Commun. (Camb)*, vol. 1, no. 46, pp. 7227–9, **2009**.
- [29] S. Kasahara, E. Kamio, a Yoshizumi, and H. Matsuyama, “Polymeric ion-gels containing an amino acid ionic liquid for facilitated CO₂ transport media,” *Chem. Commun. (Camb)*, vol. 50, no. 23, pp. 2996–9, **2014**.
- [30] A. Car, C. Stropnik, W. Yave, and K. V. Peinemann, “PEG modified poly(amide-b-ethylene oxide) membranes for CO₂ separation,” *J. Memb. Sci.*, vol. 307, no. 1, pp. 88–95, **2008**.
- [31] A. Car, C. Stropnik, W. Yave, and K. V. Peinemann, “Pebax??/polyethylene glycol blend thin film composite membranes for CO₂ separation: Performance with mixed gases,” *Sep. Purif. Technol.*, vol. 62, no. 1, pp. 110–117, **2008**.
- [32] W. Yave, A. Car, and K. V. Peinemann, “Nanostructured membrane material designed for carbon dioxide separation,” *J. Memb. Sci.*, vol. 350, no. 1–2, pp. 124–129, **2010**.
- [33] R. Surya Murali, S. Sridhar, T. Sankarshana, and Y. V. L. Ravikumar, “Gas permeation

behavior of pebax-1657 nanocomposite membrane incorporated with multiwalled carbon nanotubes," *Ind. Eng. Chem. Res.*, vol. 49, no. 14, pp. 6530–6538, **2010**.

- [34] J. H. Kim and Y. M. Lee, "Gas permeation properties of poly(amide-6-b-ethylene oxide)-silica hybrid membranes," *J. Memb. Sci.*, vol. 193, no. 2, pp. 209–225, **2001**.
- [35] a Gugliuzza and E. Drioli, "New performance of a modified poly(amide-12-b-ethyleneoxide)," *Polymer (Guildf)*, vol. 44, no. 7, pp. 2149–2157, **2003**.
- [36] Y. Cen, C. Staudt-bickel, and R. N. Lichtenthaler, "Sorption properties of organic solvents in PEBA membranes," *J. Memb. Sci.*, vol. 206, pp. 341–349, **2002**.
- [37] V. I. Bondar, B. D. Freeman, and I. Pinnau, "Gas transport properties of poly(ether-b-amide) segmented block copolymers," *J. Polym. Sci. Part B Polym. Phys.*, vol. 38, no. 15, pp. 2051–2062, **2000**.
- [38] A. Inc, "Pebax by ARKEMA (Polyether Block Amides)-Product range brochure," *Conception Publicis Activ.* [Online]. Available: <http://www.pebax.com/export/sites/pebax/.content/medias/downloads/literature/pebax-product-range-brochure.pdf>. [Accessed: 18-May-2016].
- [39] L. De Physique and D. Narbonne, "A thermally stimulated current technique for measuring the molecular parameters of Pebax, a polyether-block amide copolymer," *J. Mater. Sci.*, vol. 22, pp. 675–678, **1987**.
- [40] V. Barbi, S. S. Funari, R. Gehrke, N. Scharnagl, and N. Striebeck, "SAXS and the Gas Transport in Polyether- b lock -polyamide Copolymer Membranes," *Macromolecules*, vol. 36, no. 3, pp. 749–758, **2003**.
- [41] B. B. Sauer, R. S. McLean, D. J. Brill, and D. J. Londono, "Morphology and orientation during the deformation of segmented elastomers studied with small-angle X-ray scattering and atomic force microscopy," *J. Polym. Sci. Part B Polym.*

- Phys.*, vol. 40, no. 16, pp. 1727–1740, **2002**.
- [42] V. I. Bondar, B. D. Freeman, and I. Pinnau, “Gas Sorption and Characterization of Poly (ether-b-amide),” *J. Polym. Sci. Part B Polym. Phys.*, vol. 37, pp. 2463–2475, **1999**.
- [43] E. Tocci, A. Gugliuzza, L. De Lorenzo, M. Macchione, G. De Luca, and E. Drioli, “Transport properties of a co-poly(amide-12-b-ethylene oxide) membrane: A comparative study between experimental and molecular modelling results,” *J. Memb. Sci.*, vol. 323, no. 2, pp. 316–327, **2008**.
- [44] S. Sridhar, S. Kalyani, Y. V. L. Ravikumar, and T. Muralikrishna, “Performance of Composite Membranes of Poly(ether-block-amide) for Dehydration of Ethylene Glycol and Ethanol,” *Sep. Sci. Technol.*, vol. 45, no. 3, pp. 322–330, **2010**.
- [45] J. P. Sheth, J. Xu, and G. L. Wilkes, “Solid state structure-property behavior of semicrystalline poly(ether-block-amide) PEBAX® thermoplastic elastomers,” *Polymer (Guildf.)*, vol. 44, no. 3, pp. 743–756, **2002**.
- [46] M. F. Champagne, M. M. Dumoulin, L. A. Utracki, and J. P. Szabo, “Generation of fibrillar morphology in blends of block copolyetheresteramide and liquid crystal polyester,” *Polym. Eng. Sci.*, vol. 36, no. 12, pp. 1636–1646, **1996**.
- [47] X. Jiang, C. J. Brinker, D. L. Li, H. S. Zhou, I. Honma, T. Waitz, M. Tiemann, P. J. Klar, J. Sann, J. Stehr, B. K. Meyer, J. Sun, L. Gao, Q. Zhang, D. M. Blake, P. C. Maness, Z. Huang, E. J. Wolfrum, J. Huang, W. A. Jacoby, V. I. Parvulescu, P. Grange, B. Delmon, H. Keskinen, J. M. Mäkelä, S. Hellsten, M. Aromaa, E. Levänen, T. Mäntylä, J. S. Beck, J. C. Vartuli, W. J. Roth, M. E. Leonowicz, C. T. Kresge, K. D. Schmitt, C. T.-W. Chu, D. H. Olson, E. W. Sheppard, S. B. McCullen, J. B. Higgins, J. L. Schlenkert, G. J. D. A. Soler-Illia, E. L. Crepaldi, D. Grosso, C. Sanchez, D. Zhao, J. Feng, Q. Huo, N. Melosh, G. H. Fredrickson, B. F. Chmelka, G. D. Stucky, S. H. Tolbert, A. Firouzi, G. D. Stucky, B. F. Chmelka, K. Yu, C. Bartels, A. Eisenberg, B. Smarsly, M. Antonietti, S.

H. Park, Y. N. Xia, J. H. Schattka, E. H. M. Wong, M. Antonietti, R. A. Caruso, R. A. Zoppi, S. das Neves, S. P. Nunes, J. H. Kim, Y. M. Lee, S. Sridhar, T. M. Aminabhavi, S. J. Mayor, M. Ramakrishna, J. Müller, K.-V. Peinemann, J. Müller, Z. L. Xu, L. Y. Yu, L. F. Han, M. Niederberger, G. Garnweitner, J. H. Ba, J. Polleux, N. Pinna, Z. S. Jing, X. M. Jiang, A. Pottier, C. Chaneac, E. Tronc, L. Mazerolles, J. P. Jolivet, C. J. Homer, X. M. Jiang, T. L. Ward, C. J. Brinker, J. P. Reid, X. M. Jiang, T. L. Ward, F. van Swol, C. J. Brinker, A. Di Paola, M. Bellardita, R. Ceccato, L. Palmisano, F. Parrino, M. Koelsh, S. Cassaignon, J. P. Jolivet, D. Gomes, S. P. Nunes, and K. V. Peinemann, "Rigid templating of high surface-area, mesoporous, nanocrystalline rutile using a polyether block amide copolymer template," *Chem. Commun.*, vol. 46, no. 33, p. 6123, **2010**.

- [48] R. Singh and R. Singh, "Chapter 3 – Hybrid membrane systems – applications and case studies," *Hybrid Membr. Syst. Water Purif.*, vol. Chapter 3, pp. 131–196, **2005**.
- [49] S. B. Hamouda, a. Boubakri, Q. T. Nguyen, and M. B. Amor, "PEBAX membranes for water desalination by pervaporation process," *High Perform. Polym.*, vol. 23, no. 2, pp. 170–173, **2011**.
- [50] T. Asada, K. Inoue, and S. Onogi, "Diffusion in the Nylon 12 and water systems_Polymer Journal_T.Asada_1976.pdf," *Polym. J.*, vol. 8, no. 1, pp. 21–29, **1976**.
- [51] J. H. Park and Y. H. Bae, "Hydrogels based on poly (ethylene oxide) and poly (tetramethylene oxide) or poly (dimethyl siloxane): synthesis , characterization , in vitro protein adsorption and platelet adhesion," *Biomaterials*, vol. 23, pp. 1797–1808, **2002**.
- [52] A. Gugliuzza, R. Fabiano, M. G. Garavaglia, A. Spisso, and E. Drioli, "Study of the surface character as responsible for controlling interfacial forces at membrane-feed interface," *J. Colloid Interface Sci.*, vol. 303, no. 2, pp. 388–403, **2006**.

- [53] I. Corzani and E. Russo, "Thermoplastic hydrophilic, polymeric compositions with improved adhesive properties for moisture vapour permeable structures," p. EP1180533 (A1), **2000**.
- [54] V. Na and M. Ha, "Development of Nanocomposite Membranes Containing Modified Si Nanoparticles in PEBA-2533 as a Block Copolymer and 6FDA-Durene Diamine as a Glassy Polymer," *Appl. Mater. Interfaces*, **2014**.
- [55] G. Wypych, "Plasticizers Use and Selection for Specific Polymers," *Handb. Plast.*, pp. 273–379, **2004**.
- [56] S. Güngör, M. S. Erdal, and Y. Özsoy, "Plasticizers in transdermal drug delivery systems," *Recent Adv. Plast.*, pp. 91–112, **2012**.
- [57] H. A. Schneider, "Are kinetic parameters of non-isothermal of polymers," *J. Therm. Anal.*, vol. 40, pp. 677–687, **1993**.
- [58] H. P. S. Missan, B. S. Lalia, K. Karan, and A. Maxwell, "Polymer-ionic liquid nanocomposites electrolytes: Electrical, thermal and morphological properties," *Mater. Sci. Eng. B Solid-State Mater. Adv. Technol.*, vol. 175, no. 2, pp. 143–149, **2010**.
- [59] C. Maton, N. De Vos, and C. V. Stevens, "Ionic liquid thermal stabilities: decomposition mechanisms and analysis tools," *Chem. Soc. Rev.*, vol. 42, no. 13, pp. 5963–77, **2013**.
- [60] M. E. Mahmoud, "Surface loaded 1-methyl-3-ethylimidazolium bis(trifluoromethylsulfonyl)imide [EMIM+Tf₂N⁻] hydrophobic ionic liquid on nano-silica sorbents for removal of lead from water samples," *Desalination*, vol. 266, no. 1–3, pp. 119–127, **2011**.
- [61] H. M. Al-bishri, T. M. Abdel-Fattah, and M. E. Mahmoud, "Immobilization of [Bmim +Tf₂N⁻] hydrophobic ionic liquid on nano-silica-amine sorbent for implementation

in solid phase extraction and removal of lead," *J. Ind. Eng. Chem.*, vol. 18, no. 4, pp. 1252–1257, **2012**.

- [62] M. C. Kroon, W. Buijs, C. J. Peters, and G. J. Witkamp, "Quantum chemical aided prediction of the thermal decomposition mechanisms and temperatures of ionic liquids," *Thermochim. Acta*, vol. 465, no. 1–2, pp. 40–47, **2007**.
- [63] H. L. Ngo, K. LeCompte, L. Hargens, and A. B. McEwen, "Thermal properties of imidazolium ionic liquids," *Thermochim. Acta*, vol. 357–358, pp. 97–102, **2000**.
- [64] H. Tokuda, K. Hayamizu, K. Ishii, A. Bin, H. Susan, and M. Watanabe, "Physicochemical Properties and Structures of Room Temperature Ionic Liquids . 2 . Variation of Alkyl Chain Length in Imidazolium Cation Physicochemical Properties and Structures of Room Temperature Ionic Liquids . 2 . Variation of Alkyl Chain Length in Im," *J. Phys. Chem. B*, vol. 109, pp. 6103–6110, **2005**.
- [65] E. I. Privalova, P. Mäki-Arvela, D. Y. Murzin, and J. P. Mikkhola, "Capturing CO₂: Conventional Versus Ionic-Liquid Based Technologies," *Russ. Chem. Rev.*, vol. 81, no. 5, pp. 435–457, **2012**.
- [66] J. D. Holbrey and K. R. Seddon, "Ionic Liquids," *Clean Technol. Environ. Policy*, vol. 1, no. 4, pp. 223–236, **1999**.
- [67] S. Armstrong, B. Freeman, A. Hiltner, and E. Baer, "Gas permeability of melt-processed poly(ether block amide) copolymers and the effects of orientation," *Polymer (Guildf.)*, vol. 53, no. 6, pp. 1383–1392, **2012**.
- [68] Paul J. Flory., "Principles of Polymer Chemistry. Paul J. Flory.," p. 688, **1954**.
- [69] B. Lotz and A. J. Kovacs, "Phase transitions in block-copolymers of polystyrene and polyethylene oxide," *Abstr. Pap. Am. Chem. Soc.*, p. P048, **1969**.
- [70] C. Robitaille and J. Prud'homme, "Thermal and mechanical properties of a

poly(ethylene oxide-b-isoprene-b-ethylene oxide) block polymer complexed with sodium thiocyanate," *Macromolecules*, vol. 16, no. 4, pp. 665–671, **1983**.

- [71] R. L. Miller and L. E. Nielsen, "Crystallographic data for various polymers," *J. Polym. Sci.*, vol. 44, no. 144, pp. 391–395, **1960**.
- [72] Y. C. Yu and W. H. Jo, "Segmented block copolyetheramides based on nylon 6 and polyoxypropylene. I. Synthesis and characterization," *J. Appl. Polym. Sci.*, vol. 54, no. 5, pp. 585–591, **1994**.
- [73] Y. C. Yu and W. H. Jo, "Segmented block copolyetheramides based on nylon 6 and polyoxypropylene. II. Structure and properties," *J. Appl. Polym. Sci.*, vol. 56, no. 8, pp. 895–904, **1995**.
- [74] B. Wunderlich, "Thermodynamics and properties of nanophases," *Thermochim. Acta*, vol. 492, no. 1–2, pp. 2–15, **2009**.
- [75] T. Hatakeyama and F. X. Quinn, "Thermal analysis: fundamentals and applications to polymer science," p. 180, **1999**.
- [76] M. Kretz, B. Meurer, B. Lotz, and G. Weill, "Plastic deformation of polytetramethylene oxide. I. Influence of molecular weight distribution, crystallinity, and structure," *J. Polym. Sci. Part B Polym. Phys.*, vol. 26, no. 3, pp. 663–675, **1988**.
- [77] J. E. Mark, "Polymer data handbook," *Oxford Univ. Press*, p. 1250, **2009**.
- [78] S.-C. Chao, M. Chen, and C.-T. Chung, "Isothermal crystallization and melting behavior of short carbon fiber reinforced poly(ether ether ketone) composites," *J. Polym. Res.*, vol. 5, no. 4, pp. 221–226, **1998**.
- [79] D. F. Miranda, "Interactions and morphology of triblock copolymer - ionic liquid mixtures and applications for gel polymer electrolytes," **2012**.

- [80] A. J. . A. G. C. S. Kovacs, "Isothermal growth, thickening and melting of PEO single crystals in the bulk_JPolSciPolSymposia_A.J.Kovacs_1975.pdf," *J. Polym. Sci.*, vol. 50, pp. 283–325, **1975**.
- [81] A. J. . A. G. C. S. Kovacs, "Isothermal growth, thickening and melting of PEO single crystals in the bulk II_JPolSciPolSymposia_A.J.Kovacs_1977.pdf," *J. Polym. Sci.*, vol. 59, pp. 31–54, **1977**.
- [82] E. D. T. Atkins, M. J. Hill, N. A. Jones, and P. Sikorski, "Chain-folding and structures in nylon 6 oligoamide lamellar crystals," *J. Mater. Sci.*, vol. 35, no. 20, pp. 5179–5186, **2000**.
- [83] L. Li, Z. Zhong, W. H. de Jeu, P. J. Dijkstra, and J. Feijen, "Crystal Structure and Morphology of Poly(L-lactide-b-D-lactide) Diblock Copolymers," *Macromolecules*, pp. 8641–8646, **2004**.
- [84] Arza Seidel, "Characterization and Analysis of Polymers," *Wiley*, p. 553 of 977, **2008**.
- [85] M. G. Freire, P. J. Carvalho, A. M. Fernandes, I. M. Marrucho, A. J. Queimada, and J. A. P. Coutinho, "Surface tensions of imidazolium based ionic liquids: Anion, cation, temperature and water effect," *J. Colloid Interface Sci.*, vol. 314, no. 2, pp. 621–630, **2007**.
- [86] H. Alter, "A critical investigation of polyethylene gas permeability," *J. Polym. Sci.*, vol. 57, no. 165, pp. 925–935, **1962**.
- [87] E. L. Lawton, "Nucleation of crystallization of polyester by catalyst remnants—a review," *Polym. Eng. Sci.*, vol. 25, no. 6, pp. 348–354, **1985**.
- [88] C. Vergelati, A. Imberty, and S. Perez, "Water-induced crystalline transition of polyamide 66: a combined x-ray and molecular modeling approach,"

- Macromolecules*, vol. 26, no. 17, pp. 4420–4425, **1993**.
- [89] M. Fukuda, M. Miyagawa, H. Kawai, N. Yagi, O. Kimura, and T. Ohta, “Fundamental studies on the interactions between moisture and textiles. V: FT-IR study of the moisture sorption isotherm of nylon 6,” *Polym. J.*, vol. 19, no. 7, pp. 785–804, **1987**.
- [90] H. Kusanagi and S. Yukawa, “Fourier transform infra-red spectroscopic studies of water molecules sorbed in solid polymers,” *Polymer (Guildf.)*, vol. 35, no. 26, pp. 5637–5640, **1994**.
- [91] M. M. Coleman, D. J. Skrovanek, J. Hu, and P. C. Painter, “Hydrogen bonding in polymer blends. 1. FTIR studies of urethane-ether blends,” *Macromolecules*, vol. 21, no. 1, pp. 59–65, **1988**.
- [92] D. J. Skrovanek, S. E. Howe, P. C. Painter, and M. M. Coleman, “Hydrogen bonding in polymers: infrared temperature studies of an amorphous polyamide,” *Macromolecules*, vol. 18, no. 9, pp. 1676–1683, **1985**.
- [93] E. V. Konyukhova, A. I. Buzin, and Y. K. Godovsky, “Melting of polyether block amide (Pebax): The effect of stretching,” *Thermochim. Acta*, vol. 391, no. 1–2, pp. 271–277, **2002**.
- [94] T. Kamal, S.-Y. Park, M.-C. Choi, Y.-W. Chang, W.-T. Chuang, and U.-S. Jeng, “An in-situ simultaneous SAXS and WAXS survey of PEBA[®] nanocomposites reinforced with organoclay and POSS during uniaxial deformation,” *Polymer (Guildf.)*, vol. 53, no. 15, pp. 3360–3367, **2012**.
- [95] R. Surya Murali, K. Yamuna Rani, T. Sankarshana, A. F. Ismail, S. Sridhar, and S. Sridhar, “Separation of Binary Mixtures of Propylene and Propane by Facilitated Transport through Silver Incorporated Poly(Ether-Block-Amide) Membranes,” *Oil Gas Sci. Technol. – Rev. d’IFP Energies Nouv.*, vol. 70, no. 2, pp. 381–390, **2015**.

- [96] R. Iwamoto and H. Murase, "Infrared Spectroscopic Study of the Interactions of Nylon-6," *J. Polym. Sci. Part B Polym. Phys.*, vol. 41, pp. 1722–1729, **2003**.
- [97] E. S. Manas, Z. Getahun, W. W. Wright, W. F. DeGrado, and J. M. Vanderkooi, "Infrared spectra of amide groups in α -helical proteins: Evidence for hydrogen bonding to water," *J. Am. Chem. Soc.*, vol. 122, no. 41, pp. 9883–9890, **2000**.
- [98] S. Ben Hamouda, Q. T. Nguyen, D. Langevin, C. Chappey, and S. Roudesli, "Polyamide 12-polytetramethyleneoxide block copolymer membranes with silver nanoparticles - Synthesis and water permeation properties," *React. Funct. Polym.*, vol. 67, no. 10, pp. 893–904, **2007**.
- [99] G. R. Hatfield, Y. Guo, W. E. Killinger, R. A. Andrejak, and P. M. Roubicek, "Characterization of structure and morphology in two poly(ether-block-amide) copolymers," *Macromolecules*, vol. 26, no. 24, pp. 6350–6353, **1993**.
- [100] A. Boulares, M. Tessier, and E. Maréchal, "Synthesis and characterization of poly(copolyethers-block-polyamides) II. Characterization and properties of the multiblock copolymers," *Polymer (Guildf.)*, vol. 41, no. 10, pp. 3561–3580, **2000**.
- [101] J. R. Wagner, E. M. Mount, and H. F. Giles, "Extrusion (Second Edition)," *Extrusion*, **2014**.
- [102] B. L. Deopura and E. Textile Institute (Manchester), "Polyesters and polyamides," *Elsevier*, p. 608, **2008**.
- [103] M. G. Freire, P. J. Carvalho, R. L. Gardas, I. M. Marrucho, L. M. N. B. F. Santos, and J. A. P. Coutinho, "Mutual solubilities of water and the [C(n)mim][Tf(2)N] hydrophobic ionic liquids," *J. Phys. Chem. B*, vol. 112, no. 6, pp. 1604–10, **2008**.

Chapter 4

Interactions of Pebax2533-Ionic Liquid Composites with solutes

4.1	Introduction	135
4.2	Results and Discussion.....	135
4.2.1	Vapour Sorption Experiments.....	135
4.2.2	Gas Permeation Studies.....	151
4.3	References	156

4.1 Introduction

Chapter 3 has focused on characterizing the effect of different ILs on the morphology of a base block copolymer such as Pebax®2533. It was also demonstrated that the incorporation of ILs does indeed alter transport properties when compared to pure Pebax®2533. This Chapter investigates the possible interactions these composite blends undergo when submitted to a third component such as gas or vapour, as well as their sorption coefficients.

4.2 Results and Discussion

4.2.1 Vapour Sorption Experiments

The sorption of ethanol, water and ethyl acetate by the base polymer Pebax®2533, the pristine ILs as well as the composite membranes was determined in a Cahn electrobalance under equilibrium conditions, consisting in a weight gain of the sample under study as a consequence of the vapour sorption.

4.2.1.1 Solubility parameter of each vapour

Each vapour experiment was repeated three times. Therefore, data shown in Table 4.1 comprise an average of the values obtained for the vapour solubility expressed as mass fraction or mole fraction according to Equation 2. 1 (Chapter 2). It is emphasized that the conversion to mole fraction was done taking into consideration the molecular weight of the repetitive unit of Pebax®2533. In the case of composite membranes, the same approach was followed but accounting for the percentage of each component, namely 20% for IL and 80% for block copolymer, respectively.

Table 4. 1 summarizes the ILs employed with their respective molecular weights as well as the calculation of the average molecular weight of the composite membranes.

Table 4. 1 Molecular weight [g/mol] of the repetitive unit of Pebax®2533 and pristine ILs. Calculation of the average molecular weight of the IL-blended membranes.

	Molecular Weight [g/mol]	Average Molecular Weight
Pebax®2533 (repetitive unit)	315	
[C₈MIM][Cl]	230.78	
Pebax2533-[C₈MIM][Cl]		$\frac{0.80 * m_{initialPebax2533-[C8MIM][Cl]}}{M_w Pebax2533} + \frac{0.20 * m_{initialPebax2533-[C8MIM][Cl]}}{M_w [C8MIM][Cl]}$
[BMIM][BF₄]	226.03	
Pebax2533-[BMIM][BF₄]		$\frac{0.80 * m_{initialPebax2533-[BMIM][BF4]}}{M_w Pebax2533} + \frac{0.20 * m_{initialPebax2533-[BMIM][BF4]}}{M_w [BMIM][BF4]}$
[BMIM][Ac]	198.26	
Pebax2533-[BMIM][Ac]		$\frac{0.80 * m_{initialPebax2533-[BMIM][Ac]}}{M_w Pebax2533} + \frac{0.20 * m_{initialPebax2533-[BMIM][Ac]}}{M_w [BMIM][Ac]}$
[BMIM][Tf₂N]	419.36	
Pebax2533-[BMIM][Tf₂N]		$\frac{0.80 * m_{initialPebax2533-[BMIM][Tf2N]}}{M_w Pebax2533} + \frac{0.20 * m_{initialPebax2533-[BMIM][Tf2N]}}{M_w [BMIM][Tf2N]}$
[TMG][BF₄]	202.99	
Pebax2533-[TMG][BF₄]		$\frac{0.80 * m_{initialPebax2533-[TMG][BF4]}}{M_w Pebax2533} + \frac{0.20 * m_{initialPebax2533-[TMG][BF4]}}{M_w [TMG][BF4]}$

Table 4. 2 compiles all the data obtained for vapour sorption studies in ethanol, water and ethyl acetate in units of mass fraction and mole fraction, respectively.

Table 4. 2 Vapour sorption data for pristine Pebax®2533, pristine ILs and mixed membranes expressed in mass fraction and mole fraction. The respective original sorption curves can be found in the I. - ANNEX 4.1 (for clarification only one sorption curve of each material/vapour was plotted)

	ETHANOL		WATER		ETHYL ACETATE	
	Mass Fraction (w _i)	Mole Fraction (x _i)	Mass Fraction (w _i)	Mole Fraction (x _i)	Mass Fraction (w _i)	Mole Fraction (x _i)
Pebax®2533	0.12	0.48	0.01	0.15	0.04	0.11
Pebax2533-[C₈MIM][Cl]	0.22	0.65	0.02	0.24	0.03	0.10
[C₈MIM][Cl]	0.51	0.84	0.26	0.81	0.09	0.22
Pebax2533-[BMIM][BF₄]	0.13	0.49	0.02	0.20	0.02	0.05
[BMIM][BF₄]	0.13	0.43	0.07	0.49	0.06	0.14
Pebax2533-[BMIM][Ac]	0.30	0.73	0.04	0.42	0.05	0.16
[BMIM][Ac]	0.61	0.87	0.33	0.85	0.10	0.20
Pebax2533-[BMIM][Tf₂N]	0.12	0.51	0.01	0.19	0.07	0.23
[BMIM][Tf₂N]	0.13	0.59	0.01	0.16	0.11	0.38
Pebax2533-[TMG][BF₄]	0.39	0.80	0.02	0.21	0.04	0.11
[TMG][BF₄]	0.22	0.56	0.15	0.66	0.06	0.14

Table 4. 2 demonstrates how the incorporation of each of the ILs in the block copolymer structure produces an increase of the sorption coefficient for the majority of the solutes studied. The sorption data given in this work are in accordance with those obtained by Mary E. Rezac et al. [1] for same compounds. For better visualization, the data of Table 4. 2

were plotted in Figure 4. 1 representing the sorption coefficient in pristine Pebax®2533 as well as for the blend membranes with the three solutes studied. Figure 4. 2 depicts the change of the sorption capacity of the blend membranes expressed as a factor of variation with pristine Pebax®2533 as a reference.

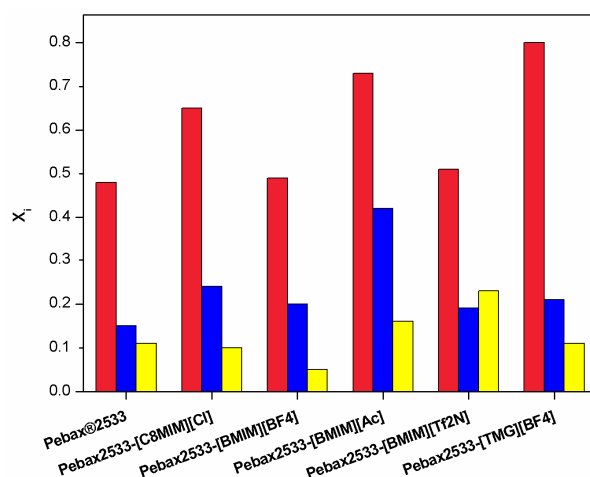


Figure 4. 1 Molar fraction x_1 of pristine Pebax®2533 and Pebax2533-IL blend membranes for each saturated vapour. (Red for ethanol, blue for water and yellow for ethyl acetate).

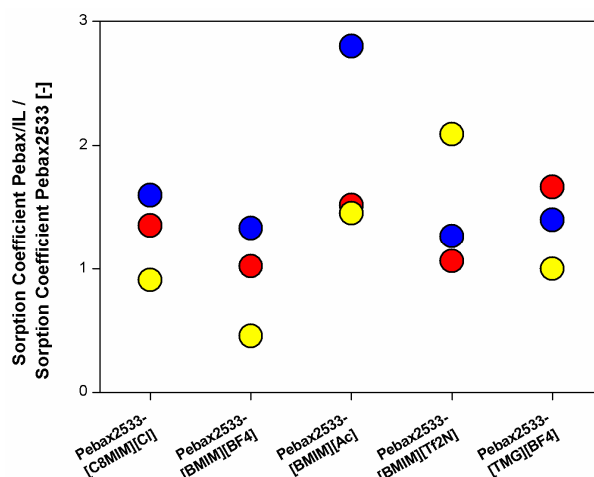


Figure 4. 2 Variation of the sorption capacity of Pebax2533-IL composites [mole fraction] in comparison with pristine Pebax®2533. (Red for ethanol, blue for water and yellow for ethyl acetate). The measured sorption of ethanol, water and ethyl acetate in pristine Pebax®2533 are 0.48, 0.15 and 0.11 respectively. A ratio of "1" means same value as obtained with pristine Pebax®2533.

An evident increase in the sorption coefficient can be seen for all the IL blended membranes as regards ethanol and also water. The ethanol vapour sorption increase is roughly similar for all blend membranes covering a range of up to 1.7. The increase of the sorption coefficient of water in Pebax2533-[BMIM][Ac] reaches a factor of almost 3, demonstrating the strong hydrophilicity of [BMIM][Ac].

As opposed to water and ethanol, those polymer blends containing [C₈MIM][Cl] and [BMIM][BF₄] suffer a decrease in the sorption coefficient of ethyl acetate while for the ILs [BMIM][Ac], [TMG][BF₄] and [BMIM][Tf₂N] an increase is observed, doubled for the latter.

All in all, it can be seen that all ILs used in this study increased the sorption of the polar compounds water and ethanol, which might be expected owing to the charged character of ILs. On the other hand, the change in the sorption of ethyl acetate partially differs depending on the IL used which evidences the general possibility to identify ILs with particular affinities to distinct solvent vapours.

4.2.1.2 Diffusivity of vapours

From the vapour sorption kinetics, the diffusion coefficient can be obtained by indirect methods such as described in Chapter 2 (Materials and Methods, Section 2.3.3.1, Cahn Data Processing). Hereby, two methods for obtaining the diffusion coefficient were employed based on Fick's second law: the first is based on analytical solutions yielding the so-called "short" and "long time" diffusion coefficients [2] while the second consists of a fit to the overall sorption curve. Both assume within their range of application a constant diffusion coefficient, i.e., diffusivity does not depend on the solute concentration. With regard to the former, diffusivity coefficients obtained using the "short" and "long time" methods are reported in literature to be very similar [3]. However, this latter approximation of Crank and Park [2] can be of limited applicability when saturated vapours

are employed because under such experimental conditions block copolymers are expected to undergo significant swelling [4], [5]. As a consequence, the polymer chains may re-organize, adjust to host a significant amount of solutes, increase the free volume between polymer chains and consequently reach the state where the diffusion of solutes across the polymer/solute mixture is considerably different as compared to the pristine polymer. Table 4. 3 summarizes in the first and second column the analytical solution from the "short" and "long" times, respectively, as well as in a third column the fit to the entire sorption kinetics according to Fick's second law.

Table 4. 3 Diffusion coefficient given in $10^{-12} \text{ m}^2/\text{s}$ for pristine Pebax®2533, pristine IIs and mixed membranes obtained by different analytical methods (analytical solutions and overall fit to the sorption kinetics, respectively, according to Fick's Second Law)

	ETHANOL			WATER			ETHYL ACETATE		
	$\cdot 10^{-12} (\text{m}^2/\text{s})$								
	Short times	Long times	Fit Fick's law	Short times	Long times	Fit Fick's law	Short times	Long times	Fit Fick's law
Pebax®2533	0.4	0.4	1.7	1.0	0.9	1.2	1.9	1.9	2.6
Pebax2533-[C ₈ MIM][Cl]	1.6	1.3	1.9	0.1	0.1	0.2	0.8	0.5	1.0
[C ₈ MIM][Cl]	195.0	182.0	1120.0	42.9	34.5	250.0	86.4	95.8	410.0
Pebax2533-[BMIM][BF ₄]	2.1	1.8	2.2	0.3	0.1	0.4	0.5	0.6	0.6
[BMIM][BF ₄]	60.1	60.5	220.0	201.0	160.0	1100.0	299.0	278.0	114.0
Pebax2533-[BMIM][Ac]	2.1	1.7	2.4	0.1	0.2	0.2	5.1	7.6	2.0
[BMIM][Ac]	33.4	76.6	158.0	78.3	72.0	755.0	111.0	133.0	520.0
Pebax2533-[BMIM][Tf ₂ N]	1.0	0.8	1.0	0.4	0.4	0.5	4.6	5.4	3.6

Interactions of Pebax2533-IL composites with solutes

[BMIM][Tf₂N]	61.0	53.8	275.0	296.0	224.0	1250.0	252.0	288.0	700.0
Pebax2533- [TMG][BF₄]	1.3	0.5	1.4	0.3	0.3	0.5	1.6	0.7	0.9
[TMG][BF₄]	25.8	19.6	145.0	113.0	96.2	680.0	190.0	146.0	1100.0

All diffusion curves and fits to Fick's Second law fit can be found in ANNEX 4.1 (where for clarification only one sorption curve of each material/vapour is depicted).

As a summary of the values compiled in Table 4. 3, we may state that the data obtained by both analytical solutions (short and long times) are in the same order of magnitude for all components, be it in pristine Pebax®2533, pristine ILs, or Pebax2533-IL blends. This would in principle indicate that no significant rearrangement or swelling occurred in any of the materials under study and/or that the diffusion coefficient would be independent of solute concentration until reaching equilibrium sorption. However, comparing the analytical solutions with the fit to the sorption kinetics, discrepancies are more evident in some of the materials studied. For example, the fitted diffusion coefficient determined for ethyl acetate in Pebax2533-[BMIM][Ac] is about three to four times smaller than the one obtained by the analytical solution; in the case of [C₈MIM][Cl] it is eight times bigger, almost an order of magnitude. In fact, in the case of pristine ILs, this variation is rather noticeable and for most cases the fit provides values on average about five times higher than the ones obtained by the short and long times approximation, the only exception being the case of [BMIM][BF₄] where the fit underestimates the data from the analytical solutions.

The almost general overestimation of the diffusion coefficient by about five times through the fit for the ILs might stem from a systematic error in the determination of the diffusional length. As a matter of fact, the diffusional length of polymer films can be determined easier and with higher accuracy than the diffusional length of a small volume of IL deposited in the scale pan. It was found that overestimating the diffusional length by a

factor of about two would explain the overestimation of the diffusion coefficient by a factor of five. Considering the difficulty in determining the average diffusional length of a drop of IL spreading over the scale pan, this systematic error seems very plausible. However, due to a lack of experimental evidence that this is the case, the diffusion coefficients will be further compared in the following with each other based on the data presented in Table 4. 3 and given that the systematic error is very similar for almost all of them.

Furthermore, it is important to stress that for the case of the fit according to Fick's second law, the experimental sorption curves have been fitted to the initial phase of the sorption curve with the consequence that the final plateau (final sorption equilibrium) remains in most cases below the prediction (see figures in ANNEX 4.1). This indicates a significant re-organization of the polymer chains in the material and, hence, a diffusion coefficient which is not independent of the solute concentration, although this does not become evident from the "short" and "long time" analysis.

Figure 4. 3 depicts the diffusion coefficients of the different solutes in Pebax®2533 pristine membrane and Pebax2533-IL blend membranes taking into consideration only the diffusion coefficients obtained from the fit over the whole sorption curve (respective third column for each solvent in Table 4. 3).

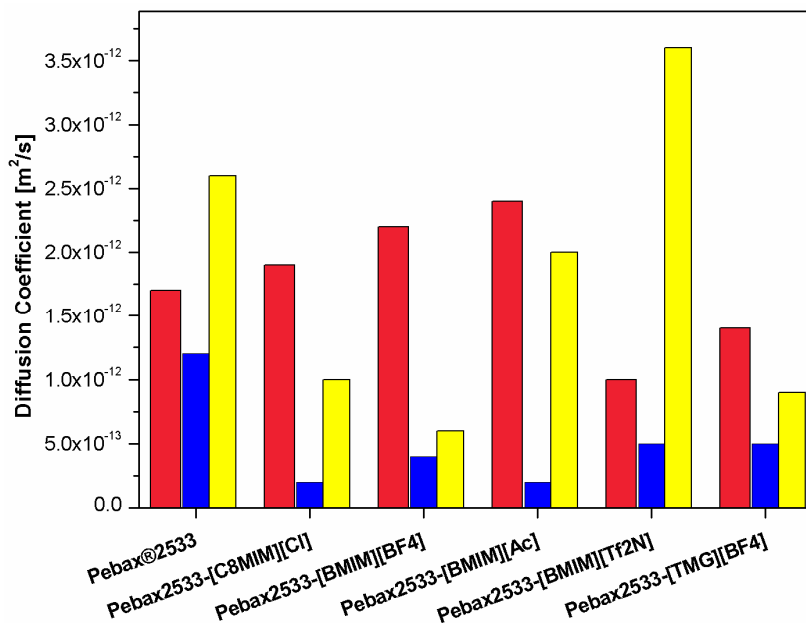


Figure 4. 3 Diffusion Coefficient of pristine Pebax®2533 and Pebax2533-IL blend membranes for each saturated vapour. (Red for ethanol, blue for water and yellow for ethyl acetate)

As can be seen from Figure 4. 3, the incorporation of 20 wt% of the IL modifies the diffusion coefficient of the overall membrane but indeed to a minor extent, particularly when taking into consideration that the determination of absolute diffusion coefficients in polymers and ILs is intrinsically difficult and variations within an order of magnitude are common. This is also illustrated by the fact that the measured diffusion coefficient of water in Pebax®2533 is slightly lower than the one of ethanol and half of that of ethyl acetate. According to the Stokes-Einstein equation the inverse would be expected. This indicates that other phenomena affect the diffusion measurement, e.g. internal reorganization of molecules or external boundary layer mass transport phenomena. Nevertheless, it is interesting to note that the diffusion of the smallest solute tested, water, is decreased in all blend membranes compared to pristine Pebax®2533. No clear tendency can be observed for the other two solvents depending on the IL employed.

Moreover, it can also be seen that the diffusion coefficient of Pebax2533/IL blends and the Pebax®2533 pristine membrane do not differ by more than one order of magnitude. On

the other hand, diffusion coefficients of solutes in pristine Pebax[®]2533 and IL, respectively, differ by two to three orders of magnitude (Table 4. 3). This means that a 20 wt% addition of IL does not produce any significant variation in the mobility of the solutes tested within the membrane. In other words, the initially presented hypothesis that ILs added to the polymer matrix would increase the overall diffusion coefficient significantly toward the order of magnitude of diffusion coefficients in ILs could not be verified for the solutes tested under saturated vapour conditions. For example, the diffusion coefficients for ethanol, water and ethyl acetate in the ILs being studied exhibit values at a magnitude between 10^{-10} - 10^{-9} m²/s but are in the order of 10^{-13} - 10^{-12} m²/s in the composites (Table 4. 2 and Figure 4. 4). So what is the reason of the low increase of diffusion coefficient observed in the Pebax2533-IL blend membranes?

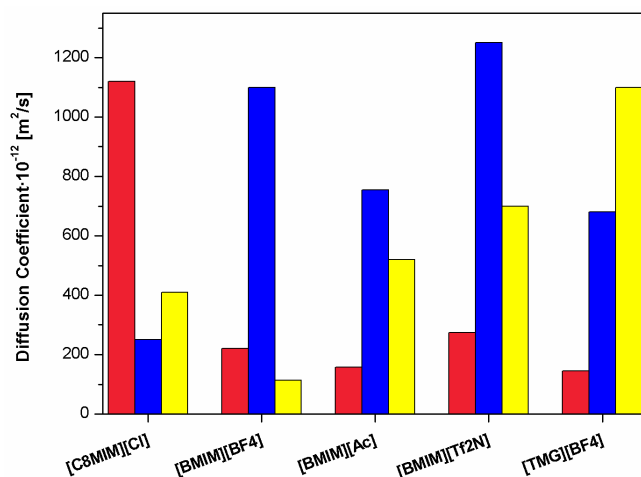


Figure 4. 4 Diffusion Coefficient of pristine ILs for each saturated vapour (Red for ethanol, blue for water and yellow for ethyl acetate).

For a better understanding, a calculation of the efficient diffusion coefficient in the blend membrane Pebax2533/IL was done following the work of J.R. Kalnin et al. [6]. For inhomogeneous 3D-media in which both phases are permeable and no rejection at the boundary of both phases occurs, Kalnin et al. showed that the efficient diffusion coefficient D_{eff} can be calculated by the diffusion coefficient in each medium, here $D_{\text{Pebax2533}}$ and D_{IL} ,

respectively, multiplied by the respective volume fraction $\Phi_{\text{Pebax2533}}$ and Φ_{IL} , assuming that $\Phi_{\text{Pebax2533}} + \Phi_{\text{IL}} = 1$, as described in Equation 4. 1:

$$\text{Equation 4. 1} \quad \frac{1}{D_{eff}} = \frac{1}{D_{PEBAX}} \cdot \Phi_{PEBAX} + \frac{1}{D_{IL}} \cdot \Phi_{IL}$$

In fact, this equation is the well-known approach of calculating an average overall conductivity by adding the inverse individual conductivities, weighed by the contribution of each to the whole. Using this equation implies that the individual conductivities are additive and not alternative, i.e., both phases participate in the solute mass transport rather than only the phase of less mass transfer resistance (exhibiting higher solute diffusivities). This is schematically illustrated in Figure 4. 5:

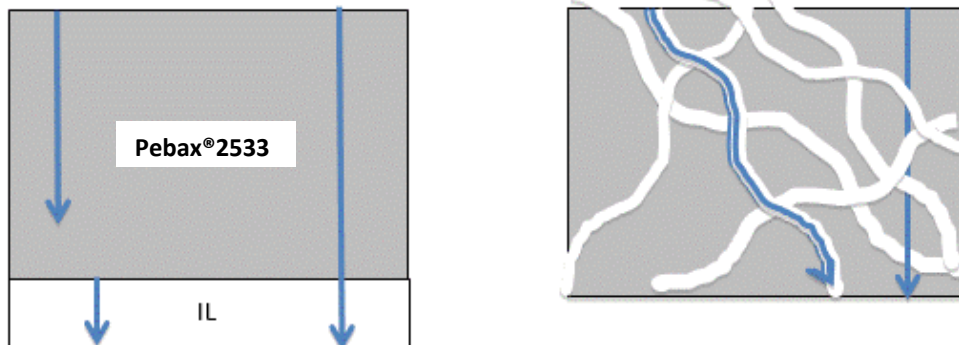


Figure 4. 5 Graphical illustration of how vapour molecules diffuse conceptually through the blend membrane

Figure 4. 6 represents the theoretic efficient diffusion coefficient calculated following Equation 4. 1 for blend membranes.

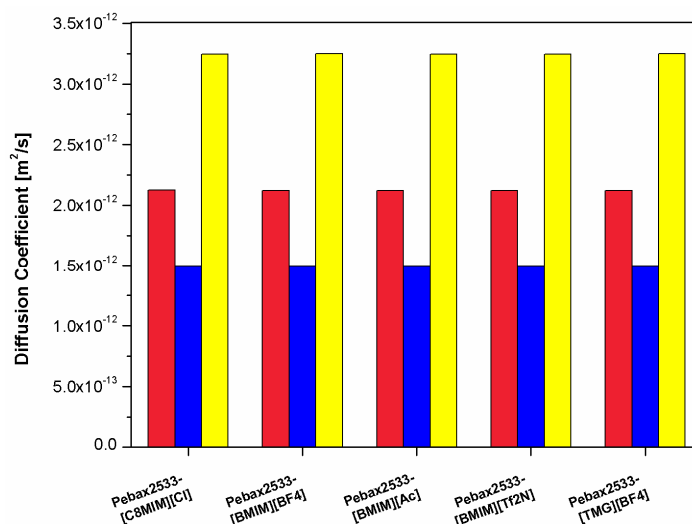


Figure 4. 6 Theoretic efficient diffusion in blend membranes. (Red for ethanol, blue for water and yellow for ethyl acetate).

As can be seen from the above figure, all the values of the D_{eff} are virtually the same for all the blend membranes.

This is further illustrated in

Figure 4. 7 Variation of the diffusion coefficient of Pebax2533/IL composite in comparison with pristine Pebax[®]2533. (Red for ethanol, blue for water and yellow for ethyl acetate).

comparing the results with the pristine Pebax[®]2533 membrane showing that the measured diffusion coefficients and those calculated do not differ significantly. The variation does not exceed a factor of 8 demonstrating that the contribution of the IL-phase in Equation 4. 1 is almost negligible.

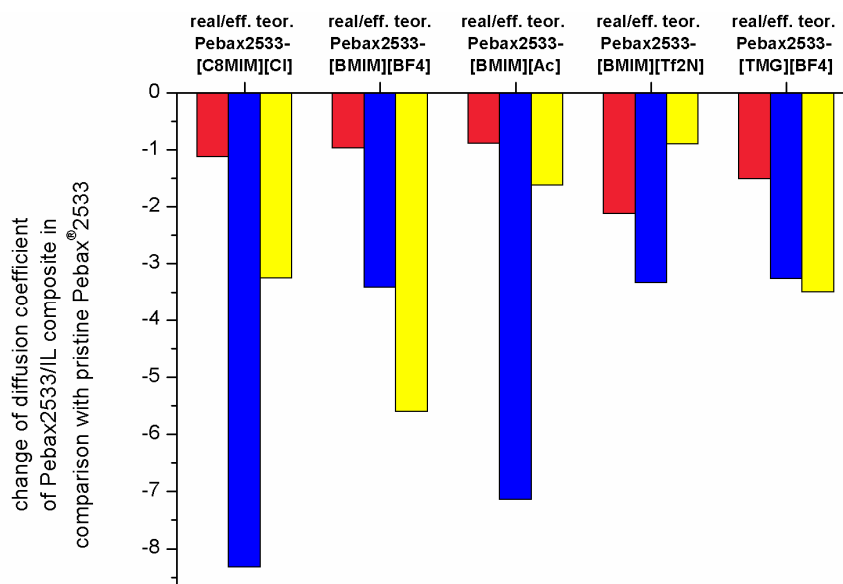


Figure 4. 7 Variation of the diffusion coefficient of Pebax2533/IL composite in comparison with pristine Pebax®2533. (Red for ethanol, blue for water and yellow for ethyl acetate).

This confirms that the diffusion occurs through both the polymer and the IL phase. Naturally, in such a situation the diffusion through the polymer-phase will be the rate-limiting step and the effect of the IL minor despite of the solutes' higher diffusivity. This reveals further information on how the IL is most probably distributed within the polymer matrix. At a first stage we expected that the IL would occupy the free volume between the polymeric chains such that the block copolymer would serve as a mere support matrix resulting in a blend membrane where the vapour solutes could pass preferentially through the inclusions of IL distributed across the dense polymer base material (block copolymer chains). Alternatively, one could imagine also micro-domains of IL within the polymer matrix as depicted in Figure 4. 5. However, in view of these experimental results, it is assumed that the IL molecules do not form defined channels or micro-clusters of IL within the polymer matrix, but that the IL will be rather entirely dispersed within the polymer structure. As a consequence, it will still be the polymeric structure that controls the mobility and hence diffusivity of the vapour solutes.

Based on this result, the parameter that governs the variation in solute permeability in polymer/IL blend membranes would be the solubility rather than the diffusivity. Therefore, the addition of ILs to form blend membranes will be useful just for those cases where ILs possess a particular and significant selectivity for a determined solute. Only in this case the permeability would be favoured as a consequence of the increase of the vapour sorption, but not owing to an increased diffusion coefficient.

4.2.1.3 Permeability of vapours

As long as the "Solution Diffusion Model" is fulfilled [7], then the permeability of vapours experimentally determined using a permeation cell should coincide with the permeability calculated on the basis of the individually measured diffusion and solubility coefficients. Figure 4. 8 depicts the experimentally determined change in permeability of different solutes in Pebax/IL blend membranes (detailed in Chapter 2- Materials and Methods, Section 2.6.1 Saturated vapour permeability measurements) with respect to pristine Pebax®2533. Figure 4. 9 represents the change in permeability as calculated on the basis of the sorption and diffusion coefficients measured (Table 4. 2 and Table 4. 3, respectively), again as the ratio between the respective permeabilities in Pebax/IL blend membranes and pristine Pebax®2533. A ratio of "1" indicates that no change in membrane permeability occurred.

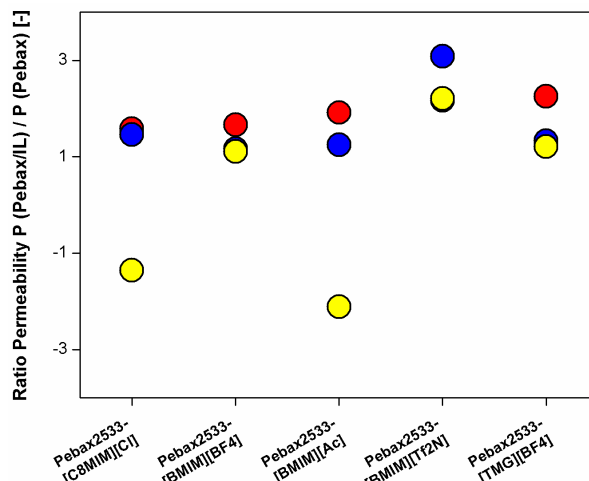


Figure 4. 8 Ratio of the permeability of the Pebax/IL blend membranes and the permeability of the pristine Pebax®2533 membranes. Values obtained experimentally using the Teflon permeation cell. Red: ethanol; blue: water; yellow: ethyl acetate. The measured permeabilities of ethanol, water and ethyl acetate in pristine Pebax®2533 are 12, 24 and 19 Barrer respectively. A ratio of "1" means same value as obtained with pristine Pebax®2533.

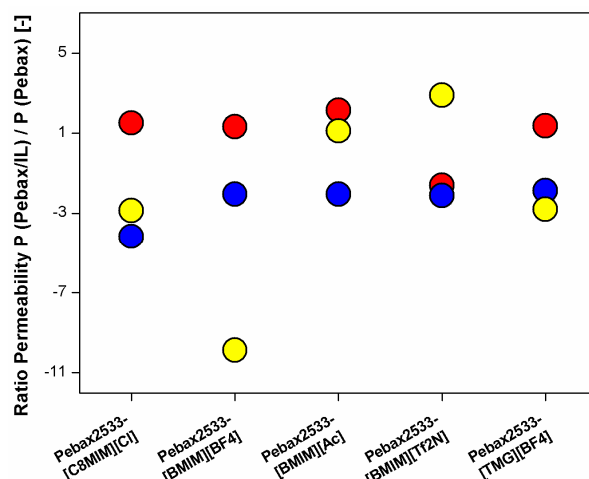


Figure 4. 9 Difference in permeability of the Pebax/IL blend membrane with respect to pristine Pebax®2533 membranes. Values calculated as the product of the sorption and diffusion coefficient measured (values from Table 4. 2 and Table 4. 3). Red: ethanol; blue: water; yellow: ethyl acetate. The calculated permeabilities of ethanol, water and ethyl acetate in pristine Pebax®2533 are 0.08, 0.02 and 0.03, respectively. A ratio of "1" means same value as obtained with pristine Pebax®2533.

On first sight it becomes evident that (1) in many cases the solute permeability is not dramatically altered by incorporating the IL into the polymer membrane and (2) the experimentally determined effect of ILs on the membrane permeability is very different from that obtained by calculating the permeability on the basis of experimental sorption and diffusion data. This is not entirely surprising given that each experimental method has its limitations. It also shows that permeability data obtained with different experimental approaches may be comparable in their tendency but might not agree in absolute, as much as the operating conditions might appear to be similar. The reason for this divergence are, for example, possible limiting mass transport phenomena that cannot be overcome and therefore affect the determination of directly obtained permeability data as opposed to the solution-diffusion model which assumes that such phenomena are avoided in the experimental set-up. Yet, data sets obtained via different experimental approaches should still reflect the same tendency.

Comparing Figure 4. 8. and Figure 4. 9, it can be seen that only the permeability of ethanol shows quite similar results for all IL/blend membranes in both plots, with its value from pristine Pebax®2533 being roughly duplicated. Only in the case of the calculated permeability in Pebax2533-[BMIM][Tf₂N] a decrease in permeability is observed. This means that the solution diffusion model would predict less ethanol flux than actually measured. The reason is a reduced diffusivity of ethanol (Table 4. 3) as compared to its diffusivity in Pebax®2533, given that its sorption coefficient (Table 4. 2) was in fact determined slightly higher

Water permeabilities show an absolutely opposed trend in both cases. Experimentally determined water permeabilities are all higher for the blends than for the pristine polymer, even in presence of the hydrophobic IL [BMIM][Tf₂N], whilst the calculated water permeabilities are all lower. The latter results mainly from strongly decreased diffusivities (Table 4. 3) which were determined in the Pebax/IL blends during sorption experiments. During permeation studies the permeability is obtained from steady-state fluxes with the membrane being in equilibrium with the sample vapour. During sorption experiments the

diffusivity is determined from the transient leading eventually to the equilibrium. Given the particular interactions between ILs and water, this might explain the difference in the resulting permeabilities.

Tendencies for ethyl acetate permeabilities also differ somewhat depending on the employed method. Particularly in the case of [BMIM][BF₄], the calculated ethyl acetate permeability is significantly lowered resulting from both a lower sorption and diffusion coefficient.









As observed it cannot be established any consistent conclusion based on these two methods of determining the permeability. Variations observed cannot be considered to be very significant as they in most cases do not exceed a factor of 3 with respect to Pebax®2533 membranes.

Finally, it remains to be shown whether the increase in diffusivity observed in some cases is due to an increase of the free volume between the copolymer chains. This will be further investigated in Chapter 8.

4.2.2 Gas Permeation Studies

Gas permeation experiments (CO₂ and N₂) have been carried out in order to determine the selectivity of the composite materials for carbon dioxide given that both ILs and Pebax®2533 are known to have a certain permselectivity for CO₂ over N₂. Additionally, these tests were also carried out with pristine Pebax®2533 and Pebax2533-[C₈MIM][Cl] obtained from a melting compression procedure. The aim was hereby to evaluate whether the use of solvents during membrane casting as a third phase could possibly have an impact on membrane morphology and, hence, on the final mass transport properties. Data obtained from the experiments are summarized in Table 4. 4.

Table 4. 4 : CO₂ and N₂ permeability and selectivity values of pristine Pebax®2533 and its IL-blended membranes

	P_{CO2} (Barrer)	P_{N2} (Barrer)	α_{CO2/N2}	Ref
Pebax®2533	270±52	12±1	23	
Pebax2533- [C₈MIM][Cl]	219±50	8±1	27	
Pebax®2533 (compressed)	376±64	16±2	24	
Pebax2533- [C₈MIM][Cl] (compressed)	239±50	12±3	20	
Pebax2533- [BMIM][BF₄]	291±54	6±2	49	
Pebax2533- [BMIM][Ac]	196±30	9±2	22	
Pebax2533- [BMIM][Tf₂N]	138±27	7±1	20	
Pebax2533- [TMG][BF₄]	242±18	7±1	35	

Values obtained in our research group correlate with those obtained previously from Rahman [8] and Dong [9]. In addition, it is remarkable that for all membranes containing ILs in their structure, it is observed both in Table 4. 4 and in the Robeson Plot (see Figure 4. 10) that while they maintain or even exceed the CO₂/N₂ selectivity of pristine Pebax®2533, their permeability is improved only in the case of [BMIM][BF₄].

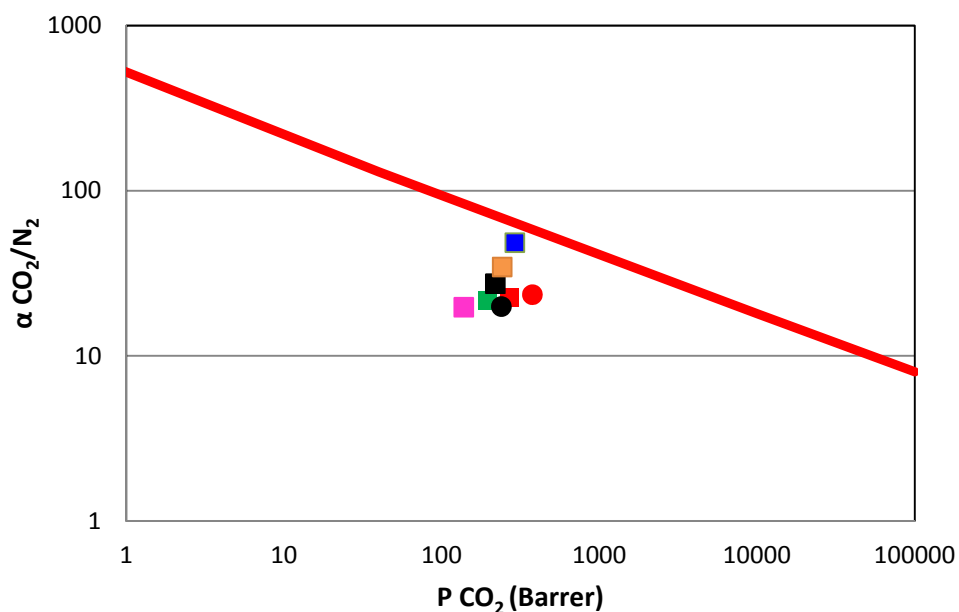


Figure 4. 10 Upper bound correlation for CO₂/N₂ separations in the synthesized membranes [upper bound from Robeson updated in 2008]

In fact, the CO₂/N₂ selectivity was only improved by the incorporation of ILs such as [BMIM][BF₄] and [TMG][BF₄]. Anyhow, it should bear in mind that this conclusion appears less negative in view of the fact that works published in literature concerning the improvement of gas selectivities in polymer-ILs composites are in the same range as the ones shown in this work [10]–[12]. This reveals once more that ILs may be far less apt for CO₂ separation than is widely considered. Polymer/IL blends of high CO₂-permselectivity would therefore be expected to only be viable in the case of ILs with outstandingly high CO₂ sorption capacity.

At the same time, it is remarkable that the Pebax[®]2533 and Pebax2533-[C₈MIM][Cl] membranes obtained by a thermal compression method do not dramatically differ in the gas separation performance when compared to their homologues obtained by solvent casting. It seems that the possible differences in the reorganization of the copolymer

chains (fast cooling step in thermal compression while in solvent casting the copolymer chains adapt to their more favorable organization) hardly cause any difference in the gas selectivity. It might be concluded that the permeability to CO₂ is slightly increased in the case of pristine Pebax®2533 obtained by compression due to a possible decrease in the semicrystallinity of the polymer material. Since the latter also affects the permeability of N₂, the permselectivity of the membrane to CO₂ eventually remains unaltered.

The CO₂ diffusion constant has been reported in literature to be a difficult parameter to be measured [13]. Some works can be found where the diffusion coefficient has been determined via FTIR measurements [14], NMR techniques [13], and also by gravimetric measurements [15], but it seems that no measurement method provides consistent values.

The CO₂ diffusion coefficients in the pristine and IL-blended membranes obtained in this work and listed in Table 4. 5 were determined by the time-lag method which in itself also can bear a significant error. Bearing this in mind, the values listed do not vary significantly between pristine Pebax®2533 membrane and IL-doped membranes.

Table 4. 5 CO₂ diffusion coefficients measured by time lag method

	D_{CO2} (m²/s)
Pebax®2533	2.4·10 ⁻¹¹
Pebax2533-[C₈MIM][Cl]	3.5·10 ⁻¹¹
Pebax®2533 (compressed)	2.2·10 ⁻¹¹
Pebax2533-[C₈MIM][Cl]	8.6·10 ⁻¹¹

Interactions of Pebax2533-IL composites with solutes

(compressed)	
Pebax2533-[BMIM][BF₄]	8.5·10⁻¹¹
Pebax2533-[BMIM][Ac]	3.2·10⁻¹¹
Pebax2533-[BMIM][Tf₂N]	5.6·10⁻¹¹
Pebax2533-[TMG][BF₄]	3.6·10⁻¹¹

It can be seen that the use of a solvent during membrane casting does not alter the diffusivity of CO₂ in the resulting pristine Pebax[®]2533 or Pebax2533-[C₈MIM][Cl] films when compared with the ones obtained by compression. This rules out that the solvent as a third phase could possibly interfere with how the IL disperses within the polymer matrix. Based on the minor variations of the diffusivity values listed in Table 4. 5, it furthermore appears that the decrease in crystallinity of the PA phase reported in Chapter 3 for the blend membranes containing [BMIM][BF₄], [BMIM][Ac] and [TMG][BF₄] could not be directly correlated with an increased diffusivity. Chapter 8 will further investigate in how far changes in free volume might have occurred upon incorporation of ILs.

4.3 References

- [1] M. E. Rezac, T. John, and P. H. Pfromm, "Effect of copolymer composition on the solubility and diffusivity of water and methanol in a series of polyether amides," *J. Appl. Polym. Sci.*, vol. 65, no. 10, pp. 1983–1993, **1997**.
- [2] H. L. Frisch, "Diffusion in polymers" edited by J. Crank and G. S. Park, Academic Press, London and New York, 1968; 452 pg," *J. Appl. Polym. Sci.*, vol. 14, no. 6, pp. 1657–1657, **1970**.
- [3] M. E. Rezac and T. John, "Correlation of penetrant transport with polymer free volume: Additional evidence from block copolymers," *Polymer (Guildf)*, vol. 39, no. 3, pp. 599–603, **1998**.
- [4] A. Jonquière, R. Clément, and P. Lochon, "Permeability of block copolymers to vapors and liquids," *Prog. Polym. Sci.*, vol. 27, no. 9, pp. 1803–1877, **2002**.
- [5] R. Surya Murali, S. Sridhar, T. Sankarshana, and Y. V. L. Ravikumar, "Gas permeation behavior of pebax-1657 nanocomposite membrane incorporated with multiwalled carbon nanotubes," *Ind. Eng. Chem. Res.*, vol. 49, no. 14, pp. 6530–6538, **2010**.
- [6] J. R. Kalnin, E. A. Kotomin, and J. Maier, "Calculations of the effective diffusion coefficient for inhomogeneous media," *J. Phys. Chem. Solids*, vol. 63, no. 3, pp. 449–456, **2002**.
- [7] J. G. Wijmans and R. W. Baker, "The solution-diffusion model: a review," *J. Memb. Sci.*, vol. 107, no. 1–2, pp. 1–21, **1995**.
- [8] M. M. Rahman, V. Filiz, S. Shishatskiy, C. Abetz, S. Neumann, S. Bolmer, M. M. Khan, and V. Abetz, "PEBAX® with PEG functionalized POSS as nanocomposite membranes for CO₂ separation," *J. Memb. Sci.*, vol. 437, pp. 286–297, **2013**.
- [9] L. Dong, C. Zhang, Y. Zhang, Y. Bai, J. Gu, Y. Sun, and M. Chen, "Improving CO₂ /N₂ separation performance using nonionic surfactant Tween containing polymeric gel membranes," *RSC Adv.*, vol. 5, no. 7, pp. 4947–4957, **2015**.

- [10] L. C. Tomé, D. Mecerreyes, C. S. R. Freire, L. P. N. Rebelo, and I. M. Marrucho, "Pyrrolidinium-based polymeric ionic liquid materials: New perspectives for CO₂ separation membranes," *J. Memb. Sci.*, vol. 428, pp. 260–266, **2013**.
- [11] S. Kasahara, E. Kamio, a Yoshizumi, and H. Matsuyama, "Polymeric ion-gels containing an amino acid ionic liquid for facilitated CO₂ transport media.," *Chem. Commun. (Camb)*., vol. 50, no. 23, pp. 2996–9, **2014**.
- [12] Y. Gu, "Block Copolymer Ion Gels for CO₂ Separations," *PhD Thesis*, **2013**.
- [13] J. Allen and K. Damodaran, "High-resolution slice selection NMR for the measurement of CO₂ diffusion under non-equilibrium conditions.," *Magn. Reson. Chem.*, vol. 53, no. 3, pp. 200–2, **2015**.
- [14] K. Kortenbruck, B. Pohrer, E. Schluecker, F. Friedel, and I. Ivanovic-Burmazovic, "Determination of the diffusion coefficient of CO₂ in the ionic liquid EMIM NTf₂ using online FTIR measurements," *J. Chem. Thermodyn.*, vol. 47, pp. 76–80, **2012**.
- [15] C. Moya, J. Palomar, M. Gonzalez-Miquel, J. Bedia, and F. Rodríguez, "Diffusion Coefficients of CO₂ in Ionic Liquids Estimated by Gravimetry," *Ind. Eng. Chem. Res.*, vol. 53, no. 35, pp. 13782–13789, **2014**.

Chapter 5

CO₂ sorption capacity of ionic liquids

5.1	Introduction	161
5.2	Sorption of CO₂ in [C₈MIM][Cl] - a case study	167
5.2.1	Gas sorption tests	169
5.2.2	Chemical Characterization	175
5.3	References	187

5.1 Introduction

ILs are reported to have a high affinity for CO₂ and a low affinity for diatomic gases like N₂ and O₂ [1]. Historically, the most studied ILs up to date have been the imidazolium based ILs [2], [3] and several authors have been systematically determining the solubility of the CO₂ by observing the influence of the anion and the cation alkyl chain length of additional alkyl substitutes on the C₂ position of the cation ring.

In general, it has been observed that the solubility depends on the choice of anion as it generally dominates the interactions with the CO₂, with the cation playing a secondary role [4], [5]. High basicity or hydrogen bonding [6] were highlighted as warranting highest CO₂ solubilities in those ILs with fluoroalkyl groups in the anion [7]–[9]. The increase of the alkyl group chain length of the cation apparently slightly affects the CO₂ solubility, as demonstrated by an increase from butyl to octyl groups [10]. Additionally, the replacement of the C2 hydrogen of the cation by a methyl group produces a small decrease in the CO₂ solubility at low pressures due to a steric impediment [1] which became more apparent at higher pressures.

Despite the possibility to widely tune the physico-chemical properties of ILs, and in view of the unlimited synthetic variations of ILs, the research has been focusing during a long time on ILs with the same anions: [BF₄]⁻, [PF₆]⁻, [Tf₂N]⁻, [OTf]⁻ or [DCA]⁻. In the same way, regarding the cation, imidazolium based-ILs with different alkyl chain lengths have been the most studied ones [4], [11]–[19] while anions with different nature as: chloride [Cl]⁻, bromide [Br]⁻, acetate [Ac]⁻ [20] or tetracyanoborate [B(CN)₄]⁻ [21] and cations based on piridinium [22] pirrolidinium [21], [23], ammonium or phosphonium are much less studied and published data are scarce. Only recently, novel ILs found their way into the literature [24]–[28] finally broadening the choice of ILs.

The solubility of many gases in molecular solvents is in general quite low and can therefore - and only for dilute systems - be adequately described at or below ambient pressure by Henry's law, Equation 5. 1.

$$\text{Equation 5. 1} \quad p_{CO_2} = K_{H CO_2} \cdot x_{CO_2}$$

with p_{CO_2} denoting the partial pressure of the CO_2 , x_{CO_2} the molar fraction of the CO_2 in the IL, and $K_{H CO_2}$ the Henry's law constant of CO_2 . Thereby, a large Henry's law constant indicates low gas solubility, whereas a small one indicates high gas solubility.

Blanchard et al [29] were the first reporting a supposed high CO_2 solubility in ILs such as [BMIM][PF₆]; but to what extent is this solubility competitive in the context of other materials, such as polymers? In order to demonstrate the effectiveness of the separation capacity of ILs, some values have therefore been collected from literature and were compared with common polymer materials.

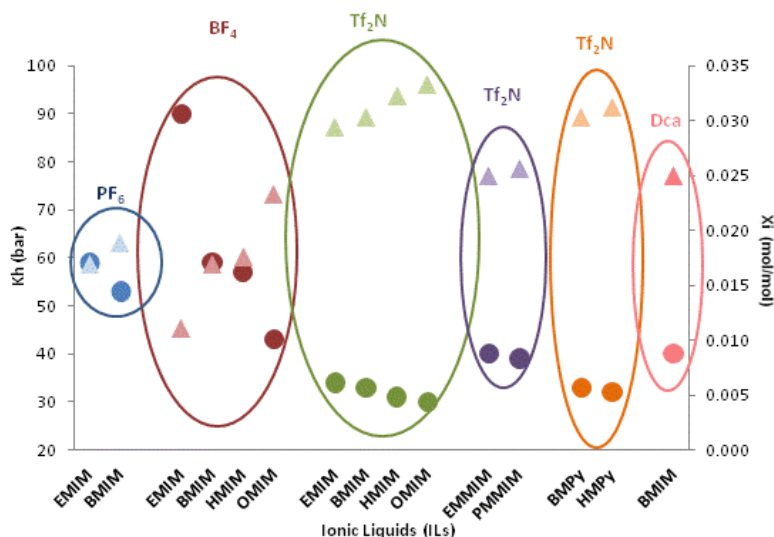


Figure 5. 1 Average Henry's law constants taken from literature data (circles) and as molar fractions (triangles) of commonly studied ILs. [3], [28], [30]–[38]

Figure 5. 1 shows, as already reported by Baltus et al. [10] that the CO₂ solubility of these ILs increase by increasing the length of the alkyl side chain in the cation ring and that the Tf₂N anion provides greater solubility values than of [BF₄]⁻ or [PF₆]⁻. Fluorination of the IL has been shown by several publications from the group of Joan F Brenecke [5], [9], [39], as well as from M. Costa-Gomes [40] to increase CO₂ solubility depending on the number of fluorine in the alkyl side chain.

At the same time, molecular dynamic simulations revealed that CO₂ is some 30% more soluble in ILs with a [CN₄]⁻ anion than that possessing a [Tf₂N]⁻ anion, the latter being ILs with a supposed high CO₂ solubility [41]. This was found to be due to a weaker cation-anion pair attraction which allows more CO₂ insertion into the free volume of the IL. This meant, hence, that weaker cation-anion interactions lead to a higher CO₂ solubility, however, not based on affinity between CO₂ and the IL.

On the other hand, ILs with fluorinated cations such as (1-methyl-3-(3,3,4,4,5,5,6,6,6-nonafluorohexyl)imidazolium bis(trifluoromethylsulfonyl)imide) [C6H4F9MIM][Tf2N] or 1-methyl-3-(3,3,4,4,5,5,6,6,6,7,7,8,8,8-tridecafluorooctyl)imidazolium bis(trifluoromethylsulfonyl)imide) [C8H4F13MIM][Tf2N] have shown Henry's law constants not higher than 28.4 and 27.3 bar at 25°C [9] and even the supposed effect of fluorinating the anion in order to achieve a higher CO₂ solubility [9][42][43] in ILs like [HMIM][eFAP]: 1-hexyl-3-methylimidazolium tris(pentafluoroethyl)trifluoro phosphate, [HMIM][pFAP]: 1-hexyl-3-methylimidazolium tris(heptafluoropropyl) trifluoro phosphate and [P₅MIM][bFAP]: 1-pentyl-3-methylimidazolium tris(nonafluorobutyl)trifluoro phosphate, that contain 18, 24 and 30 fluoride atoms, respectively, in each anion has yielded Henry's law constants as low as 25.2, 21.6 and 20.5 bar, respectively. The advantage of these FAP based anions was a higher stability with respect to moisture and air compared to other fluorinated ILs. On the other hand, it should be taken into consideration that fluorinated ILs may be less environmentally benign than some of non-fluorinated ones [44]. The high stability [45] and low reactivity of the fluorinated compounds also leads to a poor biodegradability and high persistency in the environment and only be justified by their particular suitability for a defined application [46].

As regards CO₂ solubility, the biggest and smallest Henry's Law constants for these ILs are 58 and 21.6 bar for [BMIM][BF₄] and [HMIM][pFAP], respectively, which translates into a sorption of 1.9 and 2.6 mg CO₂/g IL, respectively. These are CO₂ sorption values considered in the IL related literature to be "attractive and promising" for CO₂ separation processes. Our aim was to put these values into context with sorption values of widely known polymers.

As is in part also observed with sorption data of CO₂ reported in ILs, many data on CO₂ sorption in polymers have been obtained under different pressure and temperature conditions which can by no means be easily extrapolated to conditions similar to the ones used in this work, namely a pressure of 1bar and a temperature of 298K. We therefore focused only on data reported at or near these latter conditions.

Polymers of varied physico-chemical properties and structure have been studied for a long time with regard to their CO₂ removal capacity [47]–[53], such as poly(methyl methacrylate) PMMA, polypropylene PP, poly(styrene) PS, polyvinyl acetate PVAs poly(dimethylsiloxane) PDSM, poly(lactic)acid PLA, or polychlorotrifluoroethylene PCTFE, revealing as an example a CO₂ sorption average range between 5-50 mg CO₂/g in PMMA, PS and PVAs. This is significantly higher than the supposedly competitive sorption values reported for the, for example, fluorinated ILs (around 2 mg CO₂/g IL). However, it is important to remark that these values cannot be obtained at room temperature; they require high pressure and temperature conditions.

Data on CO₂ sorption in materials under certain experimental conditions cannot easily be extrapolated. For example, in early studies reported in literature on the sorption of CO₂ into polymers at high pressure, the anomalous behavior was found that a maximum sorption appeared in the proximity of the CO₂ critical pressure and temperature. While this behavior has not been entirely explained, yet, Strubinger and Parcher [54] reported that a maximum adsorption near the critical point was caused by both the surface excess adsorption and the pronounced change in the density of CO₂ and that they decreased with increasing temperature. Miura et al. [55] determined the solubility of CO₂ in a polystyrene (PS) film at 40 °C with the

QCM method where the PS film in the range of 500–1100 nm was coated on crystals by the dip-coating method. They also found that an anomalous solubility peak appeared in the proximity of the critical pressure. Otake et al. [56] reported that a similar maximum existed on the swelling curve of PS latex particles in an atmosphere of CO₂ at 25 °C and 0–35 MPa. Li and Vogt [57] found that the isothermal swelling of polymer thin films by supercritical CO₂ did not increase monotonically as pressure increased but rather generally exhibited a maximum value near the critical pressure where CO₂ would concentrate in the pores of polymer film. Sirard et al. [58] used ellipsometry to measure the sorption isotherm of CO₂ into PMMA film which also exhibited an anomalous maximum around the critical point of CO₂. They suggested that an inhomogeneity of the CO₂ concentration inside the film attributed to a phase separation.

Although all of these research efforts represented significant experimental and theoretical attempts to explain this anomalous sorption behavior, most of their conclusions were based on excess sorption theory. As the case may be, there are still some lacks of understanding regarding phenomena at the polymer/substrate interfaces, as well as possible morphology changes of polymer films. The general thought is that the origin of the anomalous behavior could be due to two factors: a change in the morphology of the interface between the polymer and the crystal surface and a pronounced change in the density and viscosity of CO₂ that results in a pronounced change in the viscosity of the CO₂/polymer mixture.

Hence, when comparing the solubility values between ILs and polymers, we can sum up saying that in view of the differences of the experimental conditions under which solubility data are reported, it is very difficult to make a comparison with a common polymer. Nevertheless, there exist commercial polymers that could indeed be an alternative to SILMs. According to data reported in literature, some of them provide a permeability of 75 Barrers and a selectivity of ~58 as it is the case of Pebax® [59]–[62]. For illustration, the values from block copolymers represented in the Robeson Plot in are compared with data of ILs compiled from SILMs.

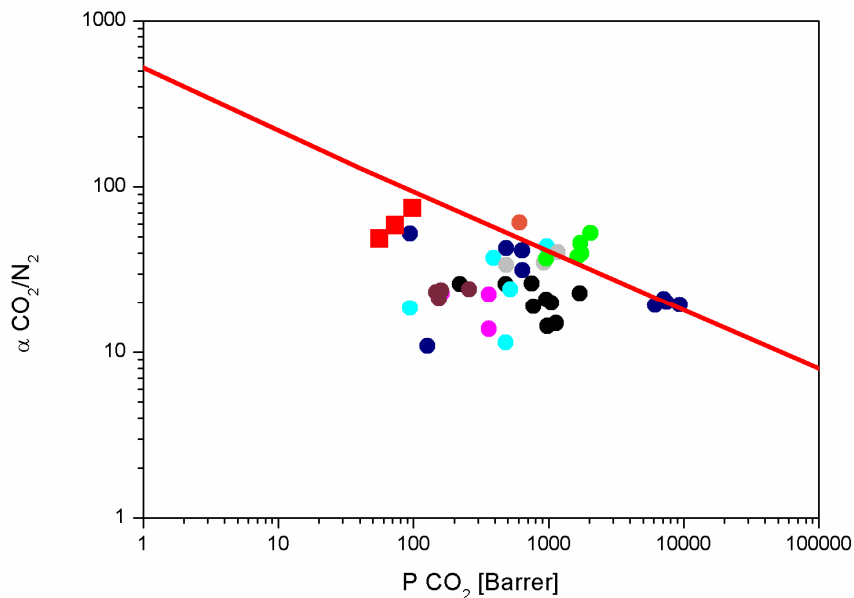


Figure 5. 2 Robeson Plot of several ILs (associated by the same anion) collected from literature. The squares correspond to block copolymer and circles to ILs. Red: Pebax®, Black: [Tf₂N] based ILs [3], [11], [36], [63], [64], Light blue: [BF₄] based ILs [31], [35], [36], [63], Light Grey: [CF₃SO₃] based ILs [11], [31], [64], [65], Orange: [dca] based ILs [30], Pink: [PF₆] based ILs [35], [63], Green: [B(CN)₄] based ILs [66], Dark blue: unconventional ILs [67], and Dark grey: magnetic ILs [32].

No significant differences are observed in the Robeson Plot between commercial block copolymers and ILs. Hence, it seems that the use of SILMs is not economically profitable since ILs do not provide extremely promising values for CO₂ capture in view of the higher complexity of membrane fabrication and membrane stability.

In order to exceed the upper bound limit, it would seem reasonable to focus on a new type of polymers such as PIMs (polymers of intrinsic microporosity) [68], [69], TR polymers (thermally rearranged polymers)[70]–[72], MMMs (mixed matrix membranes) [73]–[75], or the use of MOFs [76], [77] which are some of the alternatives that can be found in literature and which seem to be more promising than the use of ILs.

5.2 Sorption of CO₂ in [C₈MIM][Cl] - a case study

Separation of CO₂ from other gases has become an increasingly important task during the last years, largely due to the demand of reducing green house gas emissions [4]. One approach being considered for such task is the use of nonvolatile solvents. As an example, with the aim of replacing traditional organic solvents, ILs have received much attention due to their potential application in separation technologies [78], [79]. CO₂ capture by ILs is based on either chemi- or physisorption. Chemisorption relies on a reversible chemical reaction between the CO₂ and, for example, an amine group in the cation of the IL [80]. It has several advantages, such as high separation capacity [81] and rapid kinetics. Unfortunately, amine-group containing ILs for separations present some intrinsic disadvantages such as solvent loss or degradation, but the most relevant one is the energy penalty paid for the regeneration step [82]. On the contrary, physisorption is dominated by entropic effects [83] and weak interactions between CO₂ and the IL [84]. During this process, the CO₂ interacts with the ions [1] without significantly affecting the structure of the IL [85]. The main advantage of physisorption is the low enthalpy of sorption which implies a low energy requirement to recover the absorbed gas. However, its main drawback is the low solubility values reported in literature. As an example, for the case of [BMIM][BF₄] CO₂ solubility values between 2.9 [13] and 3.6 mg CO₂/g IL [20] are reported at ambient pressure and for the case of [HMIM][Tf₂N] it does not exceeded 4 mg CO₂/g IL [86]. On the other hand, for the case of chemisorbed ILs, the values reached are several orders of magnitude higher as is the case of [EMIM][Ac], where values of 70 mg CO₂/g IL [86] are obtained or even higher values of about 105 mg CO₂/g IL [87] with different structures of ILs such as [C₂OMIM][Tf₂N].

So, are ILs indeed excellent sorbents for CO₂? [1]

In fact it will depend on what materials they are compared with. As an example, in the last two decades Metal-Organic Frameworks (MOFs) have attracted intense research due to their capability for CO₂ capture and mass storage since they

present several advantages such as ordered structures, high thermal stability, adjustable chemical functionality or extra high porosity [88], [89].

Literature related to MOFs [90] can provide a wide range of CO₂ solubility values depending on the MOF being studied. As an example, data collected at a pressure of 1bar and 298K reveals CO₂ solubilities under physisorption of about 25mg CO₂/g for MOF-2, 144 mg CO₂/g for MOF-505 and 214 mg CO₂/g for MOF-74.

When assessing CO₂ solubility in literature, it is important to focus on the experimental conditions as they are sometimes completely different, but can still be found compared. As an example, J. Jacquemin et al [18] have reported that although carbon dioxide is a widely studied gaseous solute, it is shown that values reported in literature for the Henry's law constants agree to within $\pm 20\%$. Z. Lei et al [91] have reported an extensive review about several types of ILs studied in literature for gas sorption describing for each material the temperature and pressure conditions as well as the experimental technique used in each test. Although data from literature of CO₂ solubility do not always show the same values, we observe that there is a reasonable agreement between different authors. Purity of ILs before the sorption tests is also important. Therefore, it is necessary to thoroughly desorb any impurity, particularly water, from an IL before sorption studies as they have significant effect in several properties such as viscosity, gas solubility, and certainly interaction with the sorbent [92]–[95]. Several experimental techniques can be applied to measure CO₂ solubility. R.E. Baltus et al have used a Quartz Crystal Microbalance [10], J. L. Anthony [5] as well as X. Zhang [96] used a gravimetric microbalance (IGA 003, Hiden Analytical), and finally another technique widely employed in literature [18], [97], [98] is the determination of gas solubility by the isochoric saturation method.

Herein, we show in two independent sorption experiments of CO₂ in [C₈MIM][Cl] that - although being based on a physisorption process - the sorption capacity of this IL can reach CO₂ solubility values of the same order of magnitude of a chemisorption processes.

5.2.1 Gas sorption tests

The experimental procedure, desorption and sorption steps have been detailed in chapter 2-Section 2.6.3.2- Gas sorption studies (static process).

Two very different samples masses were employed in order to understand whether the conditioning of the sample (desorption) would affect the amount of gas sorbed. A first sample (a) of about 100mg had undergone a previous degasification step. A second one of about 3 mg was placed directly in the sample holder (b) without previous degasification.

Data from the desorption process are represented in . It is observed that for the smaller sample quantity of IL, the “total” desorption is reached earlier, as would be expected, i.e., 27 days for the sample of ~100 mg versus 6 days for the ~3mg sample.

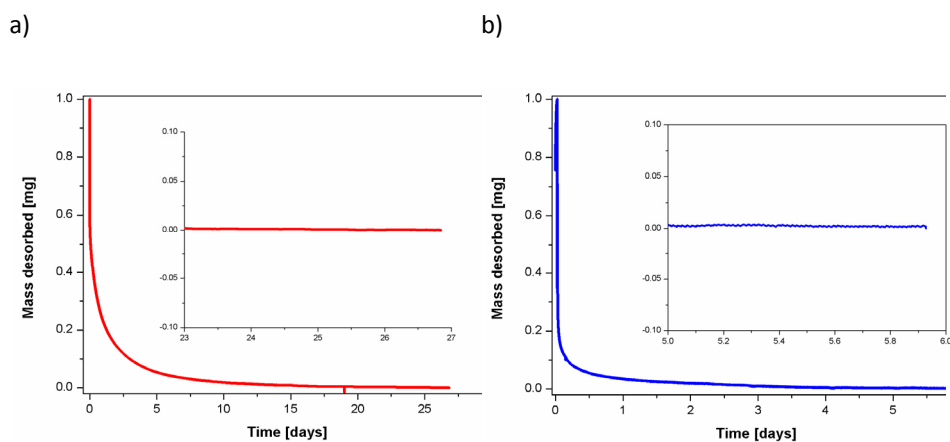


Figure 5. 3 First desorption step in both samples. a) 100mg sample, b) 3mg sample. Inlet: magnification of the final desorption data.

"Total" desorption was considered to be achieved when the variation of the sample mass was $<10^{-2}\%/h$. This rule used during the desorption is the same as the one commercially established by IGA Hyden balance analyzer[99].

The desorption step was then followed by the CO₂ sorption measurement, of which the first twenty hours are depicted in :

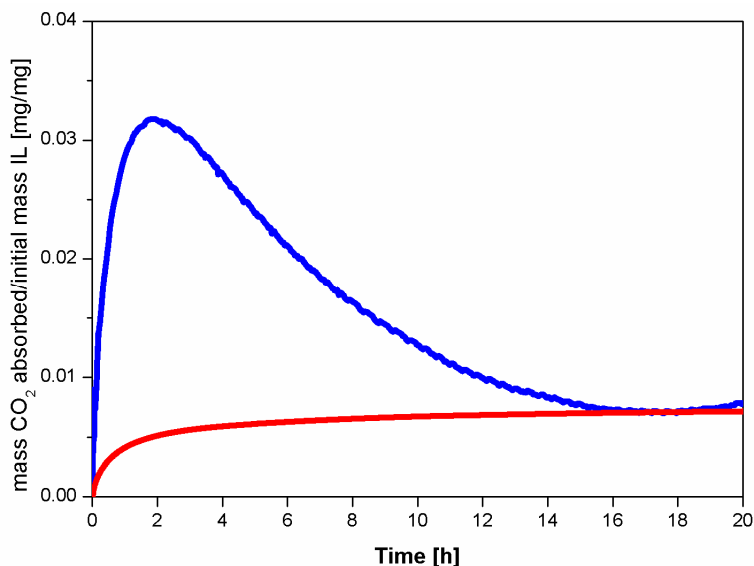


Figure 5. 4 Red line for 100mg sample (prior desorption) and blue one for 3mg sample (no prior desorption). The effect of overshoot can be observed in the sample that had not been desorbed previously (blue line).

It can be seen that depending on the sample the CO_2 sorption transient is different. The first sample (red line) of about 100mg had undergone a previous degasification step followed by the desorption under vacuum. The second one was placed directly in the sample holder from the bottle. This last one shows an anomalous overshoot as soon as being in contact with the CO_2 followed by a decrease in the uptake and a gradual attainment of the equilibrium. This sorption overshoot, already reported in the case of hydrophilic polymers in previous works carried out by our research group [100]–[102], takes place due to a rearrangement of the polymer chains as a consequence of a slow relaxation of the polymer chains to a more compact structure as can be observed in the case of the 3mg sample. Nevertheless, irrespective of the "history" of the IL, the final sorption of CO_2 is almost the same as both samples reach the same sorption equilibrium. However, it is worthwhile mentioning that in the case of samples with an overshoot a less careful data processing and premature ending of the experiment might suggest a higher sorption capacity of the IL than is actually true (here, an almost five times higher sorption could be determined based on the overshoot).

As an impurity, mainly water is expected to be present in the IL. Therefore, once the desorption equilibrium is achieved, we can make a simple mass balance over the volatile compounds lost all of which can be assumed to be water. The water content as determined by Karl Fischer measurements showed a value of 13±0.1%. The exact initial amount of IL loaded in the microbalance was in one case **113.3740 mg**. The IL was then degassed using the vacuum of an oil-pump for 27 days and the stabilized mass before sorption was **106.0278mg**. Hence, the mass lost after desorption was 113.3740-106.0278= 7.3462mg. The initial water content of about 13% corresponds to 14.7386mg of water considering the initial quantity of sample mass of 113.3740 mg . Hence, the remaining water content in the sample after desorption corresponds to 14.7386(total water)-7.3462(mass desorbed) =**7.3924mg** of water remaining in the sample. As a consequence, the amount of [C₈MIM][Cl] was 106.0278mg-7.3924 mg=98.6354mg, which corresponds to: **0.43 mmol of [C₈MIM][Cl]**. At the same time, 7.3924 mg of remaining water in the sample correspond to **0.41 mmol H₂O**. This means that we have one molecule of water for each molecule of IL even under the desorption conditions and although the desorption curve suggests a "clean sample", i.e., a molar fraction of 0.49 for water.

$$X_{H_2O-[C_8MIM][Cl]} = \frac{0.41}{0.41 + 0.43} \cdot 100 = 0.49$$

In other words, despite the degasification step under vacuum of the IL, two different types of water seem to exist in the IL. On the one hand, we find the "free-water" which has an activity high enough to be eliminated under the desorption conditions. And on the other one, we find "associated-water" with a very low activity and which cannot be removed from the IL sample under the desorption conditions. Therefore, although the sample mass reaches a stable plateau value, we cannot guarantee to have dried ILs [103] and there might still be a considerable quantity of water that has not been removed even under standard desorption conditions as they are widely used experimentally. Similar observations had been

made in the past with hydrophilic polymers. This has two consequences: firstly, the purity of the IL cannot be controlled as is widely considered and secondly, experimental data might be obtained from an IL/water mixture and not pristine IL, which makes a considerable difference. Therefore, regarding that most ILs are hygroscopic [104] we should be aware that when talking about supposedly "pure" and "dried" ILs in literature [105] this may indeed not be the case, consequently affecting the reliability of the data obtained in such systems.

The mass fraction of CO₂ determined for both samples of [C₈MIM][Cl] was 0.0065 mg/mg with 0.74 mg of CO₂ being sorbed by 106 mg of IL (still containing water despite of the previous desorption). Hence, and according to previous calculations, 0.019 mmol of CO₂ are sorbed by a mixture of 0.43 mmol of [C₈MIM][Cl] and 0.41 mmol of H₂O, resulting in a molar fraction of 0.019/ (0.019+0.43+0.41)=0.016 mmol/mmol which is similar to values depicted in Figure 5.1. In the case of not accounting for water and assuming all the sample mass being [C₈MIM][Cl], the sorbed molar fraction of CO₂ in the IL would be 0.035 mmol/mmol, still within the range of values of . Hence, roughly 1 molecule of CO₂ per 25 molecules of IL is sorbed which can be considered very low and is in line with the assumptions that many ILs are not high affinity sorbents for CO₂ as long as the interaction is non-covalent.

Normally, after reaching the plateau values as depicted in the experiment would be stopped. However, for curiosity we maintained the CO₂ and the IL in contact for a longer time with the aim of simulating prolonged contact between the gas and the IL as it would occur in a separation process in a possible future application. To our great surprise, we could observe at some point a very slow but steady increase in the mass up to a new equilibrium plateau was reached (). Hereby, the experiment with 3mg of sample showed almost the same tendency as the 100mg sample. For the latter, the overall experimental duration amounted to 130 days.

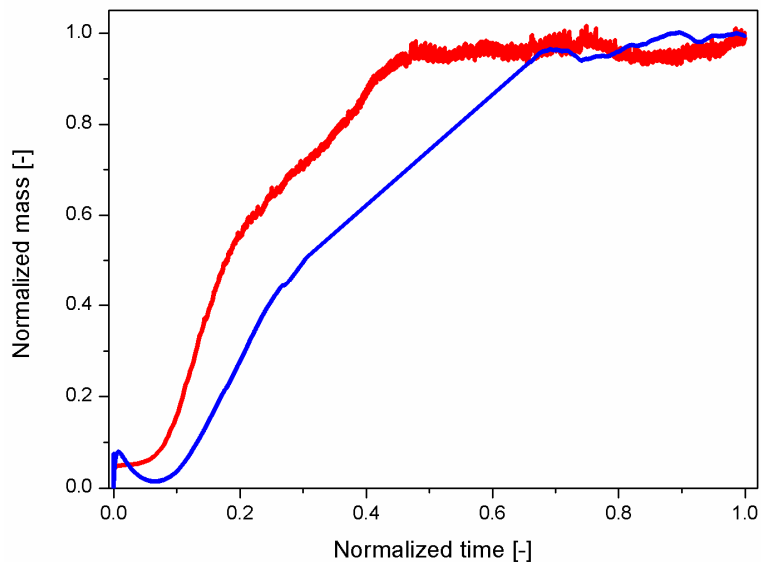


Figure 5. 5 CO₂ sorption of [C₈MIM][Cl] (red line for 100mg sample and blue line for 3mg sample) exposed to CO₂ during a 130 days (red line) and 28 days (blue line) experiment.

Just for ensuring that this result was not based on an experimental artifact, a blank experiment under the same conditions was carried out for 28 days. shows that in absence of the IL and under a CO₂ atmosphere, no sorption of the gas was registered:

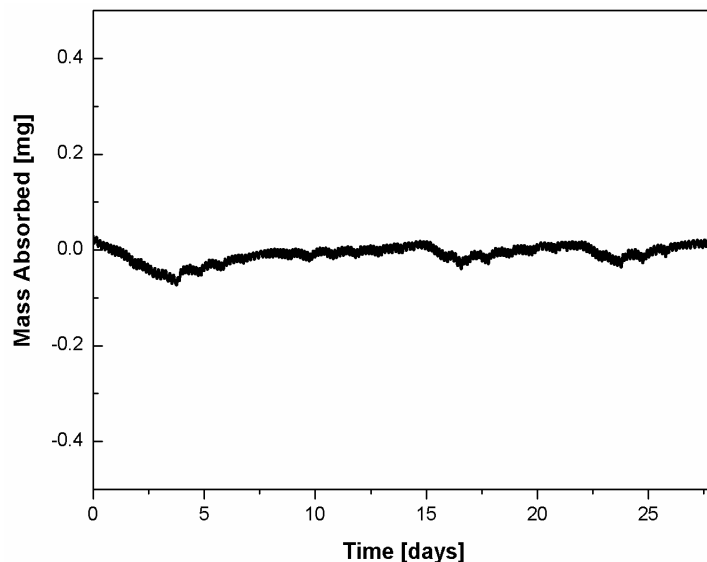


Figure 5. 6 Blank experiment with 1 bar of CO₂ in the Cahn electrobalance.

Thus, despite the seemingly low solubility of [C₈MIM][Cl] for CO₂ as shown in , under prolonged exposure to CO₂ as it would occur in practice we actually do reach a sorption mass fraction of about 200 mg CO₂/g IL. This means In our case a practical equimolar ration CO₂:IL in supposed absence of any reaction. This value is in the same order of magnitude as those observed in MOFs which are considered to be amongst the most effective materials in CO₂ capture up to now [90], [106], [107] and it corresponds to an almost equimolar ratio of CO₂ and IL under equilibrium sorption conditions.

We speculated how this phenomenon, observed only under prolonged contact of the IL with CO₂, could be explained. Our considerations were that either a slow reaction would be taking place (1) between the CO₂ and the IL, or (2) between the H₂O inside the IL and the CO₂, or that (3) the observed phenomenon would somehow be related to a slow physical rearrangement of the IL matrix.

Hypothesis (1) would be a chemisorption mechanism giving rise to a new chemical compound [20], [108], [109]. Some conventional ILs can undergo chemisorptions of CO₂. This is the case, for example, for ILs with an amino acid anion [110] or ILs with a sufficiently basic anion, as it is the case of acetate anions. The analysis of the

behavior of these ILs in absorption of CO₂ has led to the proposal of different mechanisms. For example, Maggin et al [111] suggested a de-protonation of the imidazolium cation by the action of the acetate anion, thus enabling the CO₂ binding to the N-heterocyclic carbene (NHC) generated in the imidazolium cation [112], [113]. Based on the same carbene formation principle, Yokozeki et al [20] and Gurau et al [114] proposed the formation of a complex acetic acid-acetate ion. In these cases, the formation of such compounds should be detected by spectroscopic techniques and we therefore resorted to spectroscopic analysis in order to be able to explain the unusual high sorption observed. We therefore investigated whether any reaction products could be detected in the IL at the final equilibrium plateau during CO₂ sorption.

5.2.2 Chemical Characterization

The samples submitted to CO₂ into the Cahn electrobalance were characterized as quickly as possible so as to avoid any possible alteration of the chemical composition of the sample. Furthermore, in order to avoid any exposure to the atmosphere, as soon as the samples were taken from the Cahn sample holder they were placed in a hermetically closed vial until analysis.

5.2.2.1 Fourier transform infrared spectroscopy (FTIR):

Transmission infrared spectra were recorded at room temperature using a FTIR Nicolet 6700 Thermo scientific spectrophotometer. Measurements were obtained at room temperature in the scanning range of 4000 to 400cm⁻¹ during 32 scans to obtain a high signal-to-noise ratio, with 2cm⁻¹ nominal resolution. The spectra were taken by placing a small drop of [C₈MIM][Cl] onto a KBr pellet.

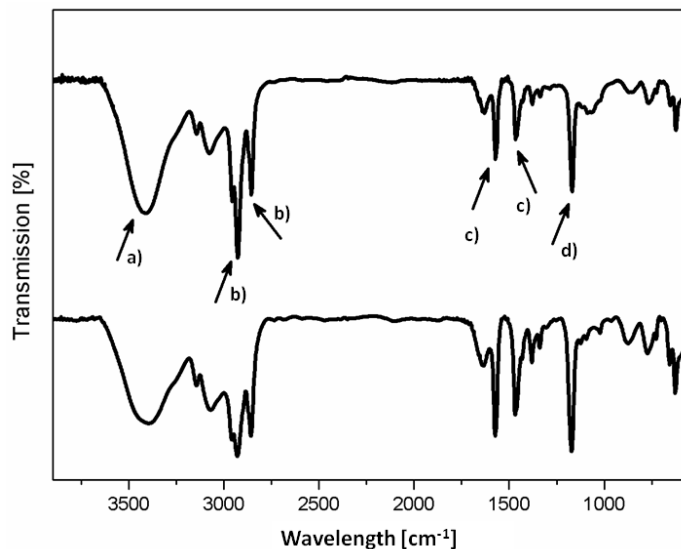


Figure 5. 7 FTIR spectrum of the $[\text{C}_8\text{MIM}][\text{Cl}]$ used in this study. Reference $[\text{C}_8\text{MIM}][\text{Cl}]$ sample up and $[\text{C}_8\text{MIM}][\text{Cl}]$ sample submitted to CO_2 down.

The FTIR spectrum in , shows the most relevant peaks of $[\text{C}_8\text{MIM}][\text{Cl}]$. The wide peak around $3300\text{-}3600\text{cm}^{-1}$ (a) corresponds to O-H bonds, probably belonging to the water inside the IL and whose existence had been verified earlier. Peaks of wavenumbers between 2800 and 3000cm^{-1} (b) originated from the butyl chain attached to the imidazolium ring and are attributed to the aliphatic symmetric and antisymmetric (C-H) stretching vibrations of the CH_2 and CH_3 groups.

Peaks at 1635cm^{-1} and 1600cm^{-1} (c) are due to C=C and C=N stretching vibrations respectively. And finally, the peak at around 1250cm^{-1} (d) belongs to C-N vibration.

No significant differences were detectable in FTIR spectra between the samples submitted to CO_2 and the one as reference.

5.2.2.2 ¹³C Nuclear Magnetic Resonance Spectroscopy (¹³C-NMR):

The ¹³C-NMR spectrum of pristine [C₈MIM][Cl] and [C₈MIM][Cl] exposed to CO₂ were taken by dissolving the IL in an appropriate deuterated solvent (CDCl₃), up to a final volume of 500 μl. The two spectra are compared in .

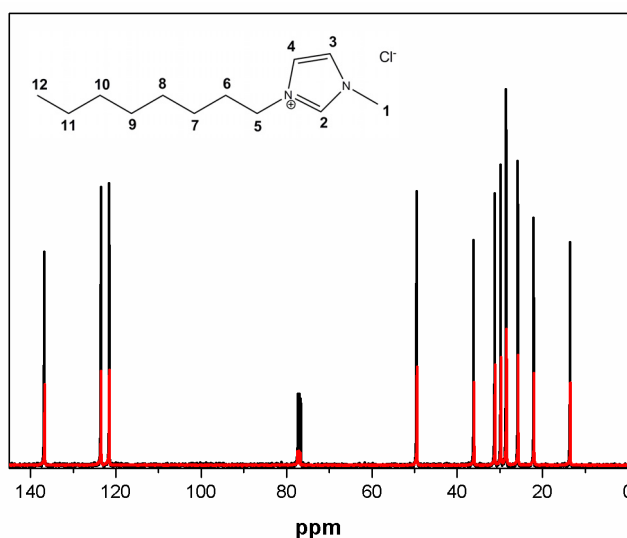


Figure 5. 8 black: ¹³C-NMR spectra of pristine [C₈MIM][Cl] and red: the one exposed to CO₂ during 130 days in the Cahn electrobalance.

For a better understanding, Table 5. 1 collects the peak displacements in ¹³C NMR, both in neat [C₈MIM][Cl] taken as reference and the [C₈MIM][Cl] sample submitted to CO₂. The peak positions are in accordance with data from literature [92]. The sample submitted to CO₂ reveals a very small deshielding (shift to downfield-highest chemical bonding) when being compared with the reference. Only for the case of C2 of the IL a small shielding is occurring.

Table 5. 1 Position of each peak in ^{13}C NMR spectra which and its respective displacement

	$[\text{C}_8\text{MIM}][\text{Cl}]_{\text{ref}}$ [ppm]	$[\text{C}_8\text{MIM}][\text{Cl}]_{\text{CO}_2}$ [ppm]	δ [ppm]
1	36.17	36.28	0.11
2	136.77	136.64	-0.13
3	121.55	121.63	0.08
4	123.55	123.68	0.13
5	49.50	49.59	0.09
6	29.86	29.96	0.1
7	25.85	25.98	0.13
8, 9	28.58	28.76	0.18
9, 8	28.52	28.71	0.19
10	31.25	31.39	0.14
11	22.10	22.26	0.16
12	13.60	13.74	0.14

The shift of the C2 carbon is depicted in as a detail for clarity.

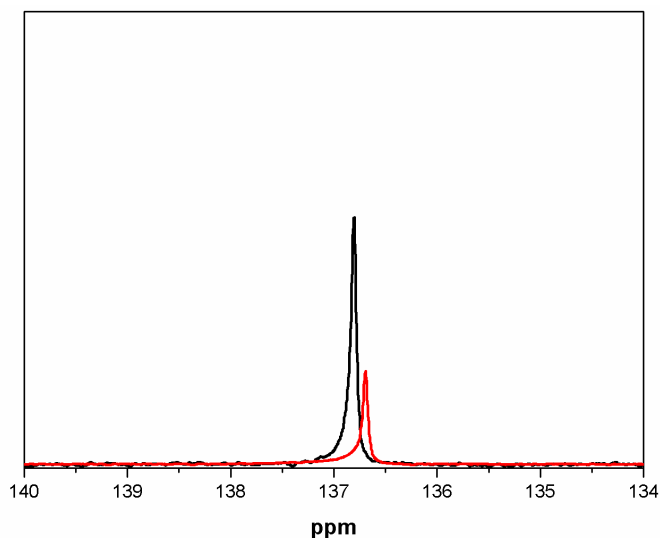


Figure 5. 9 Shift of the peak of the C2 carbon in the ¹³C NMR spectrum

However, most importantly, it could be seen that no newly formed compounds were detected. Therefore, hypothesis (1) should be rejected. If a chemical bond between the CO₂ and the C2 in the imidazolium ring had taken place, we would have observed a peak in ¹³C NMR between 140-145 ppm as it is the case of several studies reported in literature, involving CO₂-[BMIM][Ac] mixtures [115], [116].

As regards the small shifts observed, these small displacements can arise due to various factors, such as instrumental instabilities, variations in pH, ionic strength or temperature among others [117] that could partially modify the real position of each peak in the NMR spectra and can lead to incorrect interpretation of results [118]–[120]. It could also be explained as a consequence of the presence of water in the IL. As commented before, there are two types of water in the IL, the “free water” that can be removed under standard desorption conditions or a preliminary degasification step, and the “associated-water” with a much lower activity. It is known that the anion in the IL preferentially interacts with the C2 of the IL [121]–[123]. The shielding observed in ¹³C NMR could therefore stem from a formation of hydrogen bonds between the Cl⁻ and the water, originating a decrease of the Coulombic interactions between the anion and the cation and therefore a bigger distance between both which is why the peak at about 136.7ppm in the reference

sample suffers a shielding (a displacement to upfield) when submitted to CO₂. In addition to the effect of water, we assume that the presence of CO₂ could in fact also promote an interaction between the CO₂ and the anion increasing causing thus the downfield shift.

Our second hypothesis was a reaction taking place between water and CO₂ resulting in the formation of carbonates. ¹³C NMR is sensitive to the carboxilate group at higher wavelengths as can be observed in depicting the peak of the CO₃²⁻ group when dissolving NaHCO₃ in water. The absence of this peak in the previous figures proves that neither carbonate formation occurred during prolonged contact of the IL with CO₂. This rules out the possibility of any reaction being responsible for the high sorption of CO₂ observed.

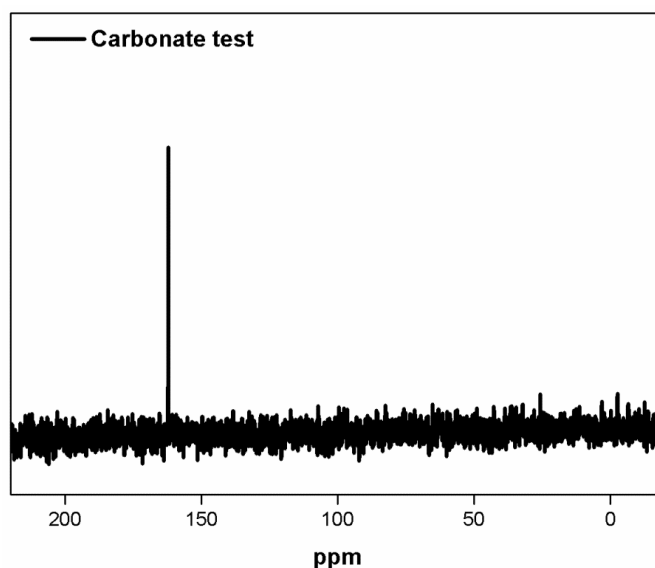


Figure 5. 10 Peak of CO₃²⁻ in ¹³C NMR

5.2.2.3 Theoretical calculations

Therefore, and in order to better understand possible interactions taking place between CO₂ and the IL, we conducted theoretical calculation studies in collaboration with Prof. Elixabete Rezabal from UPV/EHU. Density Functional Theory (DFT) calculations were carried out on CO₂-(H₂O)₂-([BMIM][Cl])₂ complexes. M06 [124] density functional was chosen, combined with the TZVP [125], [126] basis set as implemented in Gaussian09 [127]. Geometry optimizations and frequency calculations, in order to ensure the absence of imaginary modes, were carried out in the gas phase and in bulk IL. Gas phase represents the interactions that take place at the surface of the IL while the bulk refers strictly to the liquid phase. The latter was simulated by means of the SMD [128] implicit solvation method.

In this work, we did not aim at a complete exploration of the potential energy surface, but rather an overview of the preferred interaction sites for the solute and the influence of the solvent on the coordination preferences and the overall affinity, with this purpose, several complexes were characterized within 4 Kcal/mol above the overall minimum. The affinity of the solute was defined as the energy balance of the reaction in where the reactants keep the geometry they have in the product.

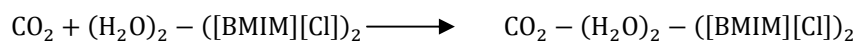


Figure 5. 11 Reaction of energy balance between a molecule of CO₂ and a 2 molecules of IL

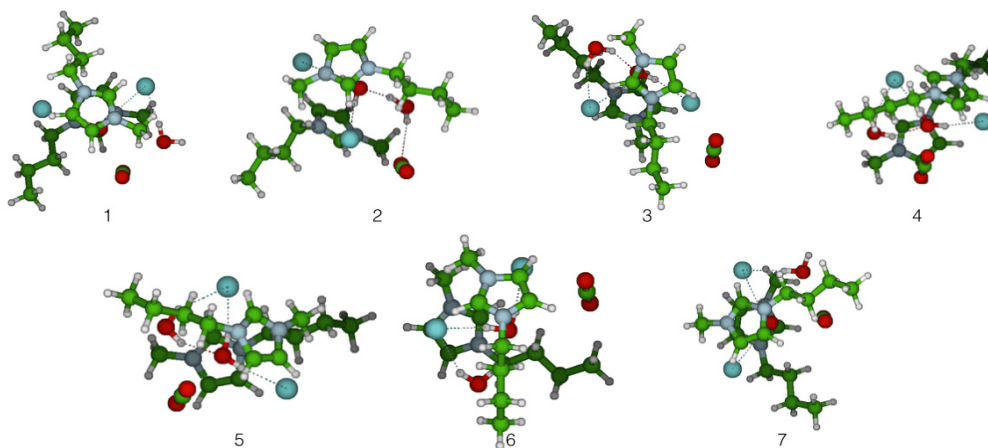


Figure 5. 12 $\text{CO}_2\text{-(H}_2\text{O)}_2\text{-}([\text{BMIM}][\text{Cl}])_2$ structures optimized in gas phase

Table 5. 2 Affinity (in kcal/mol) of the gas phase complexes, together with selected angle O-C-O (interaction $\text{CO}_2\text{-Water}$) (in degrees)

	Affinity	angle (C-O)
1	-12.0	174.9
2	-7.4	175.3
3	-7.3	175.1
4	-6.1	176.4
5	-7.2	176.8
6	-6.8	175.6
7	-12.7	174.7

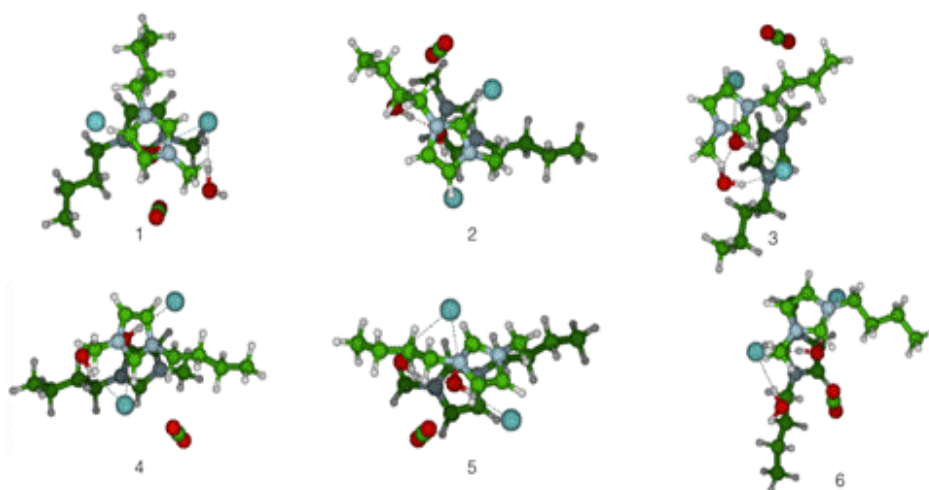


Figure 5. 13 CO₂-(H₂O)₂-([BMIM][Cl])₂ structures optimized in IL phase

Table 5. 3 Affinity (in kcal/mol) of the IL phase complexes (bulk), together with selected angle O-C-O (interaction CO₂-Water) (in degrees)

	Affinity	angle (C-O)
1	-7.2	175.2
2	-7.7	176.8
3	-5.6	176.4
4	-5.1	177.3
5	-5.6	177.7
6	-7.5	175.1

According to theoretical calculations, the dielectric constant of the IL environment changes significantly the interaction energy and preferences of CO₂ towards the IL and H₂O [129].

In the gas phase and in absence of water, it has been seen that CO_2 interacts mainly with the anion of the IL. As opposed, in presence of water, we observe that CO_2 prefers to interact with the oxygen atom of the water molecule, establishing a dipole induced dipole interaction of around -12 kcal/mol as also evidenced in $\text{O}=\text{C}=\text{O}$ angles in complexes 1 and 7 in Table 5. 2. Therefore, CO_2 interacts more favorably with the oxygen atom of the water molecule due to its polarity, which in turn does not establish specific interactions with the surrounding molecules and is partially negatively charged. In fact, the interaction between CO_2 and H_2O could be enhanced by a Cl^- - H_2O interaction which further polarizes the water, giving rise to collaborative effects and increasing the CO_2 affinity for the system. (see scheme in Figure 5. 14). This is the situation that we encounter at the IL/gas interphase.

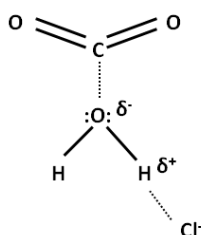


Figure 5. 14 Scheme of the collaborative effect of the interaction between the anion of the IL and water and its effect in the CO_2

Literature reports [129], [130] have studied the effect of increasing the alkyl length in ILs with the same anion and also the water content showing that at lower water quantities, and the more carbons are in the IL structure, the more perpendicular to the liquid surface they remain; on the contrary, when increasing the water content, the alkyl chains move to the bulk with the anions move to the liquid interphase.

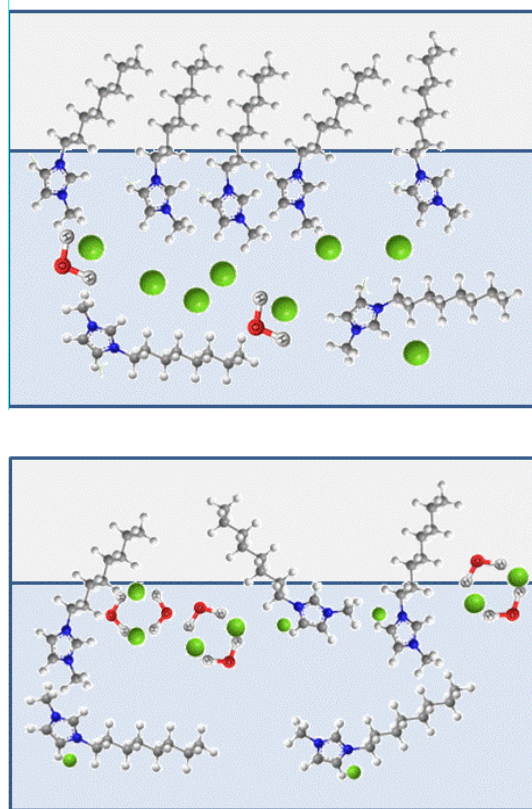


Figure 5. 15 Arrangement of the IL (cation and anion) and water molecules a) for low water content and b) high water content [129]

According to this theory, and considering that the IL used in our study has a long alkyl chain and elevated water content, this supposes that CO₂ molecules will tend to interact with water in the interphase, representing the fast gas absorption in our first hours of the experiment (about 10h).

Subsequently, and considering the bulk IL environment, the higher dielectric constant of the latter stabilizes the charges and weakens the charge-H₂O/CO₂ interactions. Consequently, the anion-cation and anion-H₂O interactions are weakened, and CO₂ shows similar binding preference for the different possible binding sites which are the ions and the water molecules, with a weaker interaction energy (between 5 and 7 kcal/mol) than in the gas phase.

In fact, it has previously been seen that CO₂ has less affinity for bulk neat IL than for IL molecules in gas phase, establishing only non specific dispersion interactions with the surrounding IL [131]. Our results indicate that this is also applicable to bulk H₂O-IL mixtures. Therefore, in the bulk, the interaction of CO₂ for both ions or water gets lowered to similar values, resulting in an existing but very low interaction network H₂O-IL-CO₂ possibly explaining why the equilibrium is reached only very slowly as experimentally observed. It also would explain why the equilibrium is reached precisely when the ratio H₂O:IL:CO₂ is about 1:1:1.

All in all, the experimental data prove that an IL needs to be considered together with its water content and that the latter can precisely lead to unexpected and surprisingly high sorption values for carbon dioxide. This is extremely interesting as the system studied reflects long-term applications of IL in, for example, separations, where humidity might be omnipresent. It also reveals that short-term experiments might disregard long-term effects of significant importance, such as the very high sorption capacity of the IL/water mixture under study.

5.3 References

- [1] C. Cadena, J. L. Anthony, J. K. Shah, T. I. Morrow, J. F. Brennecke, and E. J. Maginn, "Why Is CO₂ So Soluble in Imidazolium-Based Ionic Liquids?," *J. Am. Chem. Soc.*, vol. 126, no. 16, pp. 5300–5308, **2004**.
- [2] S. n. v. k. Aki, B. R. Mellein, E. M. Saurer, and J. F. Brennecke, "High-pressure phase behavior of carbon dioxide with imidazolium-based ionic liquids, J," *Phys. Chem. B*, vol. 108, pp. 5–20365, **2004**.
- [3] J. E. Bara, T. K. Carlisle, C. J. Gabriel, A. Finotello, D. L. Gin, R. D. Noble, and D. Camper, "Guide to CO Separations in Imidazolium-Based Room-Temperature Ionic Liquids Guide to CO₂ Separations in Imidazolium-Based Room-Temperature Ionic Liquids," *Ind. Eng. Chem. Res.*, vol. 48, no. 6, pp. 2739–2751, **2009**.
- [4] J. L. Anthony, E. J. Maginn, and J. F. Brennecke, "Solubilities and Thermodynamic Properties of Gases in the Ionic Liquid 1- n -Butyl-3-methylimidazolium Hexafluorophosphate," *J. Phys. Chem. B*, vol. 106, no. 29, pp. 7315–7320, **2002**.
- [5] J. L. Anthony, J. L. Anderson, E. J. Maginn, and J. F. Brennecke, "Anion Effects on Gas Solubility in Ionic Liquids," *J. Phys. Chem. B*, vol. 109, pp. 6366–6374, **2005**.
- [6] B. L. Bhargava and S. Balasubramanian, "Probing anion-carbon dioxide interactions in room temperature ionic liquids: Gas phase cluster calculations," *Chem. Phys. Lett.*, vol. 444, no. 4–6, pp. 242–246, **2007**.
- [7] S. N. V. K. Aki, B. R. Mellein, E. M. Saurer, and J. F. Brennecke, "High-Pressure Phase Behavior of Carbon Dioxide with Imidazolium-Based Ionic Liquids," *J. Phys. Chem. B*, vol. 108, no. 52, pp. 20355–20365, **2004**.
- [8] D. Morgan, L. Ferguson, and P. Scovazzo, "Diffusivities of gases in room-temperature ionic liquids: Data and correlations obtained using a lag-time technique," *Ind. Eng. Chem. Res.*, vol. 44, no. 13, pp. 4815–4823, **2005**.
- [9] M. J. Muldoon, S. N. V. K. Aki, J. L. Anderson, J. K. Dixon, and J. F.

- Brennecke, "Improving carbon dioxide solubility in ionic liquids," *J. Phys. Chem. B*, vol. 111, no. 30, pp. 9001–9009, **2007**.
- [10] R. E. Baltus, B. H. Culbertson, S. Dai, H. Luo, and D. W. DePaoli, "Low-Pressure Solubility of Carbon Dioxide in Room-Temperature Ionic Liquids Measured with a Quartz Crystal Microbalance," *J. Phys. Chem. B*, vol. 108, no. 2, pp. 721–727, **2004**.
- [11] P. Scovazzo, D. Camper, J. Kieft, J. Poshusta, C. Koval, and R. Noble, "Regular Solution Theory and CO₂ Gas Solubility in Room-Temperature Ionic Liquids," *Ind. Eng. Chem. Res.*, vol. 43, no. 21, pp. 6855–6860, **2004**.
- [12] J. Blath, M. Christ, N. Deubler, T. Hirth, and T. Schiestel, "Gas solubilities in room temperature ionic liquids - Correlation between RTiL-molar mass and Henry's law constant," *Chem. Eng. J.*, vol. 172, no. 1, pp. 167–176, **2011**.
- [13] J. Zhang, Q. Zhang, B. Qiao, and Y. Deng, "Solubilities of the gaseous and liquid solutes and their thermodynamics of solubilization in the novel room-temperature ionic liquids at infinite dilution by gas chromatography," *J. Chem. Eng. Data*, vol. 52, no. 6, pp. 2277–2283, **2007**.
- [14] S. Supasitmongkol and P. Styring, "High CO₂ solubility in ionic liquids and a tetraalkylammonium-based poly(ionic liquid)," *Energy Environ. Sci.*, vol. 3, no. 12, p. 1961, **2010**.
- [15] A. Finotello, J. E. Bara, S. Narayan, D. Camper, and R. D. Noble, "Ideal gas solubilities and solubility selectivities in a binary mixture of room-temperature ionic liquids," *J. Phys. Chem. B*, vol. 112, no. 8, pp. 2335–2339, **2008**.
- [16] A. Finotello, J. E. Bara, D. Camper, and R. D. Noble, "Room-Temperature Ionic Liquids: Temperature Dependence of Gas Solubility Selectivity," *Ind. Eng. Chem. Res.*, vol. 47, no. 10, pp. 3453–3459, **2007**.
- [17] D. Kerlé, R. Ludwig, A. Geiger, and D. Paschek, "Temperature dependence of the solubility of carbon dioxide in imidazolium-based ionic liquids.," *J. Phys. Chem. B*, vol. 113, pp. 12727–12735, **2009**.

- [18] J. Jacquemin, P. Husson, V. Majer, and M. F. Costa Gomes, "Influence of the cation on the solubility of CO₂ and H₂ in ionic liquids based on the bis(trifluoromethylsulfonyl)imide anion," *J. Solution Chem.*, vol. 36, no. 8, pp. 967–979, **2007**.
- [19] B.-C. Lee and S. L. Outcalt, "Solubilities of Gases in the Ionic Liquid 1-n-Butyl-3-methylimidazolium Bis(trifluoromethylsulfonyl)imide," *J. Chem. Eng. Data*, vol. 51, no. 3, pp. 892–897, **2006**.
- [20] A. Yokozeki, M. B. Shiflett, C. P. Junk, L. M. Grieco, and T. Foo, "Physical and chemical absorptions of carbon dioxide in room-temperature ionic liquids.," *J. Phys. Chem. B*, vol. 112, no. 51, pp. 16654–63, **2008**.
- [21] S. M. Mahurin, P. C. Hillesheim, J. S. Yeary, D. Jiang, and S. Dai, "High CO₂ solubility, permeability and selectivity in ionic liquids with the tetracyanoborate anion," *RSC Adv.*, vol. 2, pp. 11813–11819, **2012**.
- [22] N. M. Yunus, M. I. A. Mutalib, Z. Man, M. A. Bustam, and T. Murugesan, "Solubility of CO₂ in pyridinium based ionic liquids," *Chem. Eng. J.*, vol. 189–190, pp. 94–100, **2012**.
- [23] G. Hong, J. Jacquemin, M. Deetlefs, C. Hardacre, P. Husson, and M. F. Costa Gomes, "Solubility of carbon dioxide and ethane in three ionic liquids based on the bis((trifluoromethyl)sulfonyl)imide anion," *Fluid Phase Equilib.*, vol. 257, no. 1, pp. 27–34, **2007**.
- [24] W. Mroziak, C. Jungnickel, M. Paszkiewicz, and P. Stepnowski, "Interaction of Novel Ionic Liquids with Soils.," *Water. Air. Soil Pollut.*, vol. 224, p. 1759, **2013**.
- [25] B. Yang, F. Zhou, S. Liu, P. Wang, A. S. Alshammari, and Y. Deng, "Interaction between CO₂ and ionic liquids confined in the nanopores of SAPO-11," *RSC Adv.*, vol. 5, no. 60, pp. 48908–48915, **2015**.
- [26] R. Ferraz, L. C. Branco, I. M. Marrucho, J. M. M. Araújo, L. P. N. Rebelo, M. N. da Ponte, C. Prudêncio, J. P. Noronha, and Ž. Petrovski, "Development of novel ionic liquids based on ampicillin," *Medchemcomm*, vol. 3, p. 494,

2012.

- [27] A. L. Chong, M. Forsyth, and D. R. Macfarlane, "Novel imidazolium ionic liquids and organic salts," *Electrochim. Acta*, vol. 159, pp. 219–226, **2015**.
- [28] X. Lu, J. Yu, J. Wu, Y. Guo, H. Xie, and W. Fang, "Novel Guanidinium–Based Ionic Liquids for Highly Efficient SO₂ Capture," *J. Phys. Chem. B*, no. May, p. 150528132206002, **2015**.
- [29] L. A. Blanchard, D. Hancu, E. J. Beckman, and J. F. Brennecke, "Green processing using ionic liquids and CO₂," vol. 399, no. 6731, pp. 28–29, **1999**.
- [30] P. Scovazzo, J. Kieft, D. A. Finan, C. Koval, D. DuBois, and R. Noble, "Gas separations using non-hexafluorophosphate [PF₆]- anion supported ionic liquid membranes," *J. Memb. Sci.*, vol. 238, no. 1–2, pp. 57–63, **2004**.
- [31] P. Scovazzo, D. Havard, M. McShea, S. Mixon, and D. Morgan, "Long-term, continuous mixed-gas dry fed CO₂/CH₄ and CO₂/N₂ separation performance and selectivities for room temperature ionic liquid membranes," *J. Memb. Sci.*, vol. 327, no. 1–2, pp. 41–48, **2009**.
- [32] J. Albo, E. Santos, L. A. Neves, S. P. Simeonov, C. A. M. Afonso, J. G. Crespo, and A. Irabien, "Separation performance of CO₂ through Supported Magnetic Ionic Liquid Membranes (SMILMs)," *Sep. Purif. Technol.*, vol. 97, pp. 26–33, **2012**.
- [33] P. Luis, L. A. Neves, C. A. M. Afonso, I. M. Coelho, J. G. Crespo, A. Garea, and A. Irabien, "Facilitated transport of CO₂ and SO₂ through Supported Ionic Liquid Membranes (SILMs)," *Desalination*, vol. 245, no. 1–3, pp. 485–493, **2009**.
- [34] J. Ilconich, C. Myers, H. Pennline, and D. Luebke, "Experimental investigation of the permeability and selectivity of supported ionic liquid membranes for CO₂/He separation at temperatures up to 125 °C," *J. Memb. Sci.*, vol. 298, no. 1–2, pp. 41–47, **2007**.
- [35] L. A. Neves, J. G. Crespo, and I. M. Coelho, "Gas permeation studies in

supported ionic liquid membranes," *J. Memb. Sci.*, vol. 357, no. 1–2, pp. 160–170, **2010**.

- [36] P. Cserjési, N. Nemestóthy, and K. Bélafi-Bakó, "Gas separation properties of supported liquid membranes prepared with unconventional ionic liquids," *J. Memb. Sci.*, vol. 349, no. 1–2, pp. 6–11, **2010**.
- [37] J. E. Bara, C. J. Gabriel, T. K. Carlisle, D. E. Camper, A. Finotello, D. L. Gin, and R. D. Noble, "Gas separations in fluoroalkyl-functionalized room-temperature ionic liquids using supported liquid membranes," *Chem. Eng. J.*, vol. 147, no. 1, pp. 43–50, **2009**.
- [38] S. D. Hojniak, A. L. Khan, O. Hollóczki, B. Kirchner, I. F. J. Vankelecom, W. Dehaen, and K. Binnemans, "Separation of Carbon Dioxide from Nitrogen or Methane by Supported Ionic Liquid Membranes (SILMs): Influence of the Cation Charge of the Ionic Liquid," *J. Phys. Chem. B*, vol. 117, pp. 15131–15140, **2013**.
- [39] J. L. Anderson, J. K. Dixon, and J. F. Brennecke, "Solubility of CO₂, CH₄, C₂H₆, Bis(trifluoromethylsulfonyl)imide: Comparison to Other Ionic Liquids," *Acc. Chem. Res.*, vol. 40, no. 11, pp. 1208–1216, **2007**.
- [40] D. Almantariotis, T. Gefflaut, A. A. H. Pádua, J.-Y. Coxam, and M. F. Costa Gomes, "Effect of fluorination and size of the alkyl side-chain on the solubility of carbon dioxide in 1-alkyl-3-methylimidazolium bis(trifluoromethylsulfonyl)amide ionic liquids," *J. Phys. Chem. B*, vol. 114, no. 10, pp. 3608–17, **2010**.
- [41] R. Babarao, S. Dai, and D. E. Jiang, "Understanding the high solubility of CO₂ in an ionic liquid with the tetracyanoborate anion," *J. Phys. Chem. B*, vol. 115, no. 32, pp. 9789–9794, **2011**.
- [42] A. H. Jalili, M. Shokouhi, G. Maurer, and M. Hosseini-Jenab, "Solubility of CO₂ and H₂S in the ionic liquid 1-ethyl-3-methylimidazolium tris(pentafluoroethyl)trifluorophosphate," *J. Chem. Thermodyn.*, vol. 67, pp. 55–62, **2013**.

- [43] D. Almantariotis, S. Stevanovic, O. Fandino, A. S. Pensado, A. A. H. Padua, J.-Y. Coxam, and M. F. Costa Gomes, "Absorption of Carbon Dioxide, Nitrous Oxide, Ethane and Nitrogen by 1-Alkyl-3-methylimidazolium (C," *J. Phys. Chem. B*, vol. 116, pp. 7728–7738, **2012**.
- [44] A. B. Pereira, J. M. M. Araujo, S. Martinho, F. Alves, S. Nunes, A. Matias, C. M. M. Duarte, L. P. N. Rebelo, and I. M. Marrucho, "Fluorinated ionic liquids: Properties and applications," *ACS Sustain. Chem. Eng.*, vol. 1, no. 4, pp. 427–439, **2013**.
- [45] J. J. Tindale and P. J. Ragona, "Highly fluorinated phosphonium ionic liquids: novel media for the generation of superhydrophobic coatings.," *Chem. Commun. (Camb)*, no. 14, pp. 1831–1833, **2009**.
- [46] M. Ramdin, T. Z. Olasagasti, T. J. H. Vlugt, and T. W. De Loos, "High pressure solubility of CO₂ in non-fluorinated phosphonium-based ionic liquids," *J. Supercrit. Fluids*, vol. 82, pp. 41–49, **2013**.
- [47] H. Eslami, M. Kesik, H. A. Karimi-Varzaneh, and F. Müller-Plathe, "Sorption and diffusion of carbon dioxide and nitrogen in poly(methyl methacrylate).," *J. Chem. Phys.*, vol. 139, no. 12, p. 124902, **2013**.
- [48] K. F. Webb and A. S. Teja, "Solubility and diffusion of carbon dioxide in polymers," *Fluid Phase Equilib.*, vol. 158–160, pp. 1029–1034, **1999**.
- [49] A. Kasturirangan, "Specific Interactions in Carbon Dioxide + Polymer Systems," *PhD Thesis*, pp. 1–185, **2007**.
- [50] Y. Wu, B. Liu, M. Li, K. Tang, and Y. Wu, "Prediction of CO₂ Solubility in Polymers by Radial Basis Function Artificial Neural Network Based on Chaotic Self-adaptive Particle Swarm Optimization and Fuzzy Clustering Method," *Chinese J. Chem.*, vol. 31, no. 12, pp. 1564–1572, **2013**.
- [51] Y. Sato, T. Takikawa, S. Takishima, and H. Masuoka, "Solubilities and diffusion coefficients of carbon dioxide in poly(vinyl acetate) and polystyrene," *J. Supercrit. Fluids*, vol. 19, no. 2, pp. 187–198, **2001**.
- [52] J. H. Aubert, "Solubility of carbon dioxide in polymers by the quartz crystal

microbalance technique," *J. Supercrit. Fluids*, vol. 11, no. 3, pp. 163–172, **1998**.

- [53] X. Li, G. Cao, L. Chen, R. Zhang, H. Liu, and Y. Shi, "Study of the Anomalous Sorption Behavior of CO₂ into Poly(methyl methacrylate) Films in the Vicinity of the Critical Pressure and Temperature Using a Quartz Crystal Microbalance (QCM)," *Langmuir*, vol. 29, pp. 14089–14100, **2013**.
- [54] J. R. Strubinger and J. F. Parcher, "Surface excess (Gibbs) adsorption isotherms of supercritical carbon dioxide on octadecyl-bonded silica stationary phases," *Anal. Chem.*, vol. 61, no. 9, pp. 951–955, **1989**.
- [55] K. Miura, K. Otake, S. Kurosawa, T. Sako, T. Sugeta, T. Nakane, M. Sato, T. Tsuji, T. Hiaki, and M. Hongo, "Solubility and adsorption of high pressure carbon dioxide to poly(styrene)," *Fluid Phase Equilib.*, vol. 144, no. 1–2, pp. 181–189, **1998**.
- [56] K. Otake, S. E. Webber, P. Munk, and K. P. Johnston, "Swelling of Polystyrene Latex Particles in Water by High-Pressure Carbon Dioxide," *Langmuir*, vol. 13, no. 11, pp. 3047–3051, **1997**.
- [57] X. Li and B. D. Vogt, "Impact of thickness on CO₂ concentration profiles within polymer films swollen near the critical pressure," *Polymer (Guildf.)*, vol. 50, no. 17, pp. 4182–4188, **2009**.
- [58] S. M. Sirard, K. J. Ziegler, I. C. Sanchez, P. F. Green, and K. P. Johnston, "Anomalous Properties of Poly(methyl methacrylate) Thin Films in Supercritical Carbon Dioxide," *Macromolecules*, vol. 35, no. 5, pp. 1928–1935, **2002**.
- [59] V. I. Bondar, B. D. Freeman, and I. Pinnau, "Gas transport properties of poly(ether-b-amide) segmented block copolymers," *J. Polym. Sci. Part B Polym. Phys.*, vol. 38, no. 15, pp. 2051–2062, **2000**.
- [60] A. Car, C. Stropnik, W. Yave, and K. V. Peinemann, "PEG modified poly(amide-b-ethylene oxide) membranes for CO₂ separation," *J. Memb. Sci.*, vol. 307, no. 1, pp. 88–95, **2008**.

- [61] R. Surya Murali, S. Sridhar, T. Sankarshana, and Y. V. L. Ravikumar, "Gas permeation behavior of pebax-1657 nanocomposite membrane incorporated with multiwalled carbon nanotubes," *Ind. Eng. Chem. Res.*, vol. 49, no. 14, pp. 6530–6538, **2010**.
- [62] V. I. Bondar, B. D. Freeman, and I. Pinnau, "Gas Sorption and Characterization of Poly (ether-b-amide)," *J. Polym. Sci. Part B Polym. Phys.*, vol. 37, pp. 2463–2475, **1999**.
- [63] Y. Y. Jiang, Z. Zhou, Z. Jiao, L. Li, Y. T. Wu, and Z. B. Zhang, "SO₂ Gas Separation Using Supported Ionic Liquid Membranes," *J. Phys. Chem. B*, vol. 111, pp. 5058–5061, **2007**.
- [64] P. Scovazzo, "Determination of the upper limits, benchmarks, and critical properties for gas separations using stabilized room temperature ionic liquid membranes (SILMs) for the purpose of guiding future research," *J. Memb. Sci.*, vol. 343, no. 1–2, pp. 199–211, **2009**.
- [65] R. Condemarin and P. Scovazzo, "Gas permeabilities, solubilities, diffusivities, and diffusivity correlations for ammonium-based room temperature ionic liquids with comparison to imidazolium and phosphonium RTIL data," *Chem. Eng. J.*, vol. 147, no. 1, pp. 51–57, **2009**.
- [66] S. M. Mahurin, J. S. Lee, G. A. Baker, H. Luo, and S. Dai, "Performance of nitrile-containing anions in task-specific ionic liquids for improved CO₂/N₂ separation," *J. Memb. Sci.*, vol. 353, no. 1–2, pp. 177–183, **2010**.
- [67] P. Cserjésii, N. Nemestóthy, and K. Bélafi-Bakó, "Gas separation properties of supported liquid membranes prepared with unconventional ionic liquids," *J. Memb. Sci.*, vol. 349, no. 1–2, pp. 6–11, **2010**.
- [68] N. Du, G. P. Robertson, J. Song, I. Pinnau, S. Thomas, and M. D. Guiver, "Polymers of Intrinsic Microporosity Containing Trifluoromethyl and Phenylsulfone Groups as Materials for Membrane Gas Separation †," *Macromolecules*, vol. 41, no. 24, pp. 9656–9662, **2008**.
- [69] M. M. Khan, V. Filiz, G. Bengtson, S. Shishatskiy, M. Rahman, and V. Abetz,

“Functionalized carbon nanotubes mixed matrix membranes of polymers of intrinsic microporosity for gas separation,” *Nanoscale Res. Lett.*, vol. 7, no. 1, p. 504, **2012**.

- [70] S. Li, H. J. Jo, S. H. Han, C. H. Park, S. Kim, P. M. Budd, and Y. M. Lee, “Mechanically robust thermally rearranged (TR) polymer membranes with spirobisindane for gas separation,” *J. Memb. Sci.*, vol. 434, pp. 137–147, **2013**.
- [71] M. Calle, C. M. Doherty, A. J. Hill, and Y. M. Lee, “Cross-Linked Thermally Rearranged Poly(benzoxazole- co -imide) Membranes for Gas Separation,” *Macromolecules*, vol. 46, no. 20, pp. 8179–8189, **2013**.
- [72] H. J. Jo, C. Y. Soo, G. Dong, Y. S. Do, H. H. Wang, M. J. Lee, J. R. Quay, M. K. Murphy, and Y. M. Lee, “Thermally Rearranged Poly(benzoxazole- co -imide) Membranes with Superior Mechanical Strength for Gas Separation Obtained by Tuning Chain Rigidity,” *Macromolecules*, vol. 48, no. 7, pp. 2194–2202, **2015**.
- [73] M. Hussain and A. König, “Mixed-Matrix Membrane for Gas Separation: Polydimethylsiloxane Filled with Zeolite,” *Chem. Eng. Technol.*, vol. 35, no. 3, pp. 561–569, **2012**.
- [74] L. Dong, C. Zhang, Y. Zhang, Y. Bai, J. Gu, Y. Sun, and M. Chen, “Improving CO₂ /N₂ separation performance using nonionic surfactant Tween containing polymeric gel membranes,” *RSC Adv.*, vol. 5, no. 7, pp. 4947–4957, **2015**.
- [75] D. Eiras, Y. Labreche, and L. A. Pessan, “Ultem®/ZIF-8 Mixed Matrix Membranes for Gas Separation: Transport and Physical Properties,” *Mater. Res.*, vol. 19, no. 1, pp. 220–228, **2016**.
- [76] B. Seoane, J. Coronas, I. Gascon, M. E. Benavides, O. Karvan, J. Caro, F. Kapteijn, and J. Gascon, “Metal–organic framework based mixed matrix membranes: a solution for highly efficient CO₂ capture?,” *Chem. Soc. Rev.*, vol. 44, no. 8, pp. 2421–2454, **2015**.

- [77] X. Ling, N. R. Champness, and M. Schröder, "Functional Metal-Organic Frameworks: Gas Storage, Separation and Catalysis. Hydrogen, Methane and Carbon Dioxide Adsorption in Metal-Organic Framework Materials," *Springer*, vol. 293, **2010**.
- [78] X. Han and D. W. Armstrong, "Ionic liquids in separations," *Acc. Chem. Res.*, vol. 40, no. 11, pp. 1079–1086, **2007**.
- [79] S. A. Shamsi and N. D. Danielson, "Utility of ionic liquids in analytical separations.," *J. Sep. Sci.*, vol. 30, no. 11, pp. 1729–50, **2007**.
- [80] Z. Feng, F. Cheng-Gang, W. You-Ting, W. Yuan-Tao, L. Ai-Min, and Z. Zhi-Bing, "Absorption of CO₂ in the aqueous solutions of functionalized ionic liquids and MDEA," *Chem. Eng. J.*, vol. 160, no. 2, pp. 691–697, **2010**.
- [81] G. T. Rochelle, "Amine scrubbing for CO₂ capture.," *Science*, vol. 325, no. 5948, pp. 1652–4, **2009**.
- [82] Z.-Z. Yang, Y.-N. Zhao, and L.-N. He, "CO₂ chemistry: task-specific ionic liquids for CO₂ capture/activation and subsequent conversion," *RSC Adv.*, vol. 1, no. 4, p. 545, **2011**.
- [83] P. J. Carvalho and J. A. P. Coutinho, "On the Nonideality of CO₂ Solutions in Ionic Liquids and Other Low Volatile Solvents," *J. Phys. Chem. Lett.*, vol. 1, no. 4, pp. 774–780, **2010**.
- [84] H. Kolding, R. Fehrmann, and A. Riisager, "CO₂ Capture technologies: Current status and new directions using supported ionic liquid phase (SILP) absorbers," *Sci. China Chem.*, vol. 55, no. 8, pp. 1648–1656, **2012**.
- [85] F. Jutz, J.-M. Andanson, and A. Baiker, "Ionic liquids and dense carbon dioxide: a beneficial biphasic system for catalysis.," *Chem. Rev.*, vol. 111, no. 2, pp. 322–53, **2011**.
- [86] M. B. Shiflett and A. Yokozeki, "Phase Behavior of Carbon Dioxide in Ionic Liquids: [emim][Acetate], [emim][Trifluoroacetate], and [emim][Acetate] + [emim][Trifluoroacetate] Mixtures," *J. Chem. Eng. Data*, vol. 54, no. 1, pp. 108–114, **2009**.

- [87] P. Sharma, S. Do Park, K. T. Park, S. C. Nam, S. K. Jeong, Y. Il Yoon, and I. H. Baek, "Solubility of carbon dioxide in amine-functionalized ionic liquids: Role of the anions," *Chem. Eng. J.*, vol. 193–194, pp. 267–275, **2012**.
- [88] J.-R. Li, J. Sculley, and H.-C. Zhou, "Metal-organic frameworks for separations.," *Chem. Rev.*, vol. 112, no. 2, pp. 869–932, **2012**.
- [89] S. Qiu, M. Xue, and G. Zhu, "Metal-organic framework membranes: from synthesis to separation application.," *Chem. Soc. Rev.*, vol. 43, no. 16, pp. 6116–40, **2014**.
- [90] A. R. Millward and O. M. Yaghi, "Metal-organic frameworks with exceptionally high capacity for storage of carbon dioxide at room temperature.," *J. Am. Chem. Soc.*, vol. 127, no. 51, pp. 17998–9, **2005**.
- [91] Z. Lei, C. Dai, and B. Chen, "Gas Solubility in Ionic Liquids," *Chem. Rev.*, vol. 114, no. 2, pp. 1289–1326, **2013**.
- [92] J. G. Huddleston, A. E. Visser, W. M. Reichert, H. D. Willauer, G. a. Broker, and R. D. Rogers, "Characterization and comparison of hydrophilic and hydrophobic room temperature ionic liquids incorporating the imidazolium cation," *Green Chem.*, vol. 3, no. 4, pp. 156–164, **2001**.
- [93] K. R. Seddon, A. Stark, and M. J. Torres, "Influence of chloride, water, and organic solvents on the physical properties of ionic liquids," *Pure Appl. Chem.*, vol. 72, no. 12, pp. 2275–2287, **2000**.
- [94] Y. Chen, Y. Cao, and T. Mu, "A New Application of Acetate-Based Ionic Liquids: Potential Usage as Drying Materials," *Chem. Eng. Technol.*, vol. 37, no. 3, pp. 527–534, **2014**.
- [95] C. Cadena, "Molecular Modeling of the Thermodynamical and Transport Properties of Ionic Liquids," no. September, pp. 1–168, **2006**.
- [96] X. Zhang, Z. Liu, and W. Wang, "Screening of ionic liquids to capture CO₂ by COSMO-RS and experiments," *AIChE J.*, vol. 54, no. 10, pp. 2717–2728, **2008**.
- [97] P. Sharma, S.-H. Choi, S.-D. Park, I.-H. Baek, and G.-S. Lee, "Selective

- chemical separation of carbondioxide by ether functionalized imidazolium cation based ionic liquids," *Chem. Eng. J.*, vol. 181–182, pp. 834–841, **2012**.
- [98] W. Afzal, X. Liu, and J. M. Prausnitz, "Solubilities of some gases in four imidazolium-based ionic liquids," *J. Chem. Thermodyn.*, vol. 63, pp. 88–94, **2013**.
- [99] "IGA Series Gravimetric Gas Sorption Analyzers For Lab Testing." [Online]. Available: http://www.hidenisochema.com/our_products/iga_series/. [Accessed: 28-May-2016].
- [100] A. Etxeberria, C. Uriarte, M. J. Fernandez-Berridi, and J. J. Iruin, "Probing Polymer-Polymer Interaction Parameters in Miscible Blends by Inverse Gas Chromatography: Solvent Effects," *Macromolecules*, vol. 27, no. 5, pp. 1245–1248, **1994**.
- [101] J. A. Alfageme, M. Iriarte, J. J. Iruin, A. Etxeberria, and C. Uriarte, "Water-transport properties in polyetherimide blends with a liquid crystal polymer," *J. Appl. Polym. Sci.*, vol. 73, no. 3, pp. 323–332, **1999**.
- [102] N. Pantelić and C. J. Seliskar, "Anomalous Diffusion in Poly(vinyl alcohol)–Poly(acrylic acid) Thin Films," *J. Phys. Chem. C*, vol. 111, no. 5, pp. 2054–2062, **2007**.
- [103] L. Cammarata, S. G. Kazarian, P. A. Salter, and T. Welton, "Molecular states of water in room temperature ionic liquids," *Phys. Chem. Chem. Phys.*, vol. 3, no. 23, pp. 5192–5200, **2001**.
- [104] U. Domańska, E. Bogel-Łukasik, and R. Bogel-Łukasik, "1-Octanol/Water Partition Coefficients of 1Alkyl-3-methylimidazolium Chloride," *Chem. - A Eur. J.*, vol. 9, no. 13, pp. 3033–3041, **2003**.
- [105] M. Holzweber, R. Lungwitz, D. Doerfler, S. Spange, M. Koel, H. Hutter, and W. Linert, "Mutual Lewis acid-base interactions of cations and anions in ionic liquids," *Chemistry*, vol. 19, no. 1, pp. 288–93, **2013**.
- [106] Y. Liu, Z. U. Wang, and H.-C. Zhou, "Recent advances in carbon dioxide capture with metal-organic frameworks," *Greenh. Gases Sci. Technol.*, vol.

2, no. 4, pp. 239–259, **2012**.

- [107] Z. Zhang, Y. Zhao, Q. Gong, Z. Li, and J. Li, “MOFs for CO₂ capture and separation from flue gas mixtures: the effect of multifunctional sites on their adsorption capacity and selectivity.,” *Chem. Commun. (Camb)*, vol. 49, no. 7, pp. 653–61, **2013**.
- [108] J. Huang and T. Ruther, “Why are Ionic Liquids Attractive for CO₂ Absorption? An Overview,” *Aust. J. Chem.*, vol. 62, pp. 298–308, **2009**.
- [109] S. Shunmugavel, S. Kegnæs, J. Due-Hansen, T. Gretasdottir, A. Riisager, and R. Fehrmann, “Selective Gas Absorption by Ionic Liquids,” *ECS Trans.*, vol. 33, no. 7, pp. 117–126, **2010**.
- [110] J. Zhang, S. Zhang, K. Dong, Y. Zhang, Y. Shen, and X. Lv, “Supported absorption of CO₂ by tetrabutylphosphonium amino acid ionic liquids,” *Chem. - A Eur. J.*, vol. 12, no. 15, pp. 4021–4026, **2006**.
- [111] E. J. Maginn, “Design and Evaluation of Ionic Liquids as Novel CO₂ Absorbents,” *Final Rep. Proj. DE-FG26-04NT42122*, pp. 1–17, **2007**.
- [112] H. Rodríguez, G. Gurau, J. D. Holbrey, and R. D. Rogers, “Reaction of elemental chalcogens with imidazolium acetates to yield imidazole-2-chalcogenones: direct evidence for ionic liquids as proto-carbenes.,” *Chem. Commun. (Camb)*, vol. 47, no. 11, pp. 3222–4, **2011**.
- [113] S. Stevanovic, A. Podgoršek, A. A. H. Pádua, and M. F. Costa Gomes, “Effect of water on the carbon dioxide absorption by 1-alkyl-3-methylimidazolium acetate ionic liquids.,” *J. Phys. Chem. B*, vol. 116, no. 49, pp. 14416–25, **2012**.
- [114] G. Gurau, H. Rodríguez, S. P. Kelley, P. Janiczek, R. S. Kalb, and R. D. Rogers, “Demonstration of chemisorption of carbon dioxide in 1,3-dialkylimidazolium acetate ionic liquids.,” *Angew. Chem. Int. Ed. Engl.*, vol. 50, no. 50, pp. 12024–6, **2011**.
- [115] M. Besnard, M. I. Cabaço, F. V. Chávez, N. Pinaud, P. J. Sebastião, J. A. P. Coutinho, and Y. Danten, “On the spontaneous carboxylation of 1-butyl-3-

- methylimidazolium acetate by carbon dioxide.," *Chem. Commun. (Camb)*, vol. 48, no. 9, pp. 1245–7, **2012**.
- [116] M. Fèvre, P. Coupillaud, K. Miqueu, J.-M. Sotiropoulos, J. Vignolle, and D. Taton, "Imidazolium hydrogen carbonates versus imidazolium carboxylates as organic precatalysts for N-heterocyclic carbene catalyzed reactions.," *J. Org. Chem.*, vol. 77, no. 22, pp. 10135–44, **2012**.
- [117] S. A. A. Sousa, A. Magalhães, and M. M. C. Ferreira, "Optimized bucketing for NMR spectra: Three case studies," *Chemom. Intell. Lab. Syst.*, vol. 122, pp. 93–102, **2013**.
- [118] H. Winning, "Quantitative multivariable NMR spectroscopy in food science and nutrition," *PhD Thesis*, **2009**.
- [119] N. Trbovic, F. Dancea, T. Langer, and U. Günther, "Using wavelet de-noised spectra in NMR screening.," *J. Magn. Reson.*, vol. 173, no. 2, pp. 280–7, **2005**.
- [120] J. Forshed, R. J. O. Torgrip, K. M. Aberg, B. Karlberg, J. Lindberg, and S. P. Jacobsson, "A comparison of methods for alignment of NMR peaks in the context of cluster analysis.," *J. Pharm. Biomed. Anal.*, vol. 38, no. 5, pp. 824–32, **2005**.
- [121] E. Rezabal and T. Schäfer, "A First Principle Approach to Solvation by Methylimidazolium Based Ionic Liquids," *J. Phys. Chem. B*, vol. asap, **2013**.
- [122] K. Noack, P. S. Schulz, N. Paape, J. Kiefer, P. Wasserscheid, and A. Leipertz, "The role of the C2 position in interionic interactions of imidazolium based ionic liquids: a vibrational and NMR spectroscopic study.," *Phys. Chem. Chem. Phys.*, vol. 12, no. 42, pp. 14153–61, **2010**.
- [123] A. M. Fernandes, M. A. A. Rocha, M. G. Freire, I. M. Marrucho, J. A. P. Coutinho, and L. M. N. B. F. Santos, "Evaluation of cation-anion interaction strength in ionic liquids.," *J. Phys. Chem. B*, vol. 115, no. 14, pp. 4033–41, **2011**.
- [124] Y. Zhao and D. G. Truhlar, "The M06 suite of density functionals for main

group thermochemistry, thermochemical kinetics, noncovalent interactions, excited states, and transition elements: two new functionals and systematic testing of four M06-class functionals and 12 other functionals,” *Theor. Chem. Acc.*, vol. 120, no. 1–3, pp. 215–241, **2007**.

- [125] A. Schäfer, H. Horn, and R. Ahlrichs, “Fully optimized contracted Gaussian basis sets for atoms Li to Kr,” *J. Chem. Phys.*, vol. 97, no. 4, p. 2571, **1992**.
- [126] A. Schäfer, C. Huber, and R. Ahlrichs, “Fully optimized contracted Gaussian basis sets of triple zeta valence quality for atoms Li to Kr,” *J. Chem. Phys.*, vol. 100, no. 8, p. 5829, **1994**.
- [127] M. Frisch, G. Trucks, H. Schlegel, G. Scuseria, M. Robb, J. Cheeseman, G. Scalmani, V. Barone, B. Mennucci, G. Petersson, H. Nakatsuji, M. Caricato, X. Li, H. Hratchian, A. Izmaylov, J. Bloino, G. Zheng, J. Sonnenberg, M. Hada, M. Ehara, K. Toyota, R. Fukuda, J. Hasegawa, M. Ishida, T. Nakajima, Y. Honda, O. Kitao, H. Nakai, T. Vreven, J. Montgomery, J. Peralta, F. Ogliaro, M. Bearpark, J. Heyd, E. Brothers, K. Kudin, V. Staroverov, R. Kobayashi, J. Normand, K. Raghavachari, A. Rendell, J. Burant, S. Iyengar, J. Tomasi, M. Cossi, N. Rega, J. Millam, M. Klene, J. Knox, J. Cross, V. Bakken, C. Adamo, J. Jaramillo, R. Gomperts, R. Stratmann, O. Yazyev, A. Austin, R. Cammi, C. Pomelli, J. Ochterski, R. Martin, K. Morokuma, V. Zakrzewski, G. Voth, P. Salvador, J. Dannenberg, S. Dapprich, A. Daniels, Farkas, J. Foresman, J. Ortiz, J. Cioslowski, and D. Fox, “Gaussian 09, Revision B.01,” *Gaussian 09, Revis. B.01, Gaussian, Inc., Wallingford CT*, **2009**.
- [128] V. S. Bernales, A. V. Marenich, R. Contreras, C. J. Cramer, and D. G. Truhlar, “Quantum mechanical continuum solvation models for ionic liquids,” *J. Phys. Chem. B*, vol. 116, no. 30, pp. 9122–9, **2012**.
- [129] C. Ridings, V. Lockett, and G. Andersson, “Significant changes of the charge distribution at the surface of an ionic liquid due to the presence of small amounts of water,” *Phys. Chem. Chem. Phys.*, vol. 13, no. 48, pp. 21301–7, **2011**.
- [130] C. Ridings, V. Lockett, and G. Andersson, “Effect of the aliphatic chain

length on electrical double layer formation at the liquid/vacuum interface in the [C(n)mim][BF₄] ionic liquid series.," *Phys. Chem. Chem. Phys.*, vol. 13, no. 38, pp. 17177–84, **2011**.

- [131] E. Rezabal and T. Schäfer, "Ionic liquids as solvents of polar and non-polar solutes: affinity and coordination.," *Phys. Chem. Chem. Phys.*, vol. 17, no. 22, pp. 14588–97, **2015**.

Chapter 6

QCM-D as a method for measuring organic vapour sorption in ultra-thin polymer films. Comparison with the Cahn Electrobalance

6.1	Introduction to the QCM-D technique.....	206
6.1.1	Fundamental principles	206
6.1.2	The dissipation factor	208
6.1.3	Data Interpretation.....	211
6.2	Results and Discussion.....	215
6.2.1	Morphological and topographical characterization of Pebax®2533 and Pebax®2533-IL blended depositions on the quartz crystal	215
6.2.2	Reproducibility of the QCM-D technique	216
6.3	References	223

The main objective of chapters 6 and 7 consists in evaluating the reproducibility of sorption measurements conducted with a quartz crystal microbalance with monitoring of energy dissipation (QCM-D) when a Pebax®2533 copolymer deposited on its sensor surface is exposed to a common organic vapour, in this case ethanol (EtOH). First, the reproducibility of the Pebax®2533 depositions themselves will be studied. Secondly, it will be investigated in how far the layer thickness of the material could affect the experimental data obtained in terms of the intrinsic frequency and dissipation of the material. The underlying motivation is to be able to explore in how far sorption experiments with QCM-D using ultrathin polymer films can be compared with the ones obtained from bulk measurements in the widely known gravimetric Cahn electrobalance. The primary aim is therefore to identify in how far a free-standing film with a thickness of tenths of microns will differ from ultra-thin layers with a thickness of tenths of nanometers and attached to a quartz substrate.

This chapter starts with an introduction to the QCM-D technique by providing a short literature review and some applications, followed by the most important concepts of this technique. The most important differences to the Cahn electrobalance will also be highlighted. Finally, it will be determined in how far QCM-D is a viable alternative to the traditional electrobalance.

The aims of the experimental studies were the followings:

1. to characterize the morphology and roughness of Au-Pebax®2533 coated quartz crystals;
2. to determine the reproducibility and reliability of QCM-D when (a) different Pebax®2533 depositions with different layer thickness are submitted to increased EtOH vapour concentrations, and when (b) one and the same deposition of

Pebax®2533 is repeatedly being submitted to a cycle of several EtOH sorption-desorption steps;

3. to compare the amount sorbed and the sorption kinetics of EtOH in Pebax®2533 by QCM-D and Cahn electrobalance. These data were compared with data from literature.

6.1 Introduction to the QCM-D technique

The quartz crystal microbalance (QCM) has been used for a long time as a sensor to monitor thin film deposition in vacuum or gases. In 1980, T. Nomura and O. Hattori [1] showed that the QCM may be used in the liquid phase. In 1997 Hook [2], [3] reported on the experimental setup used in this work measuring simultaneously the frequency and the dissipation of energy in vacuum, air and liquid which completed the name of the device to the quartz crystal microbalance with monitoring of energy dissipation (QCM-D). This technique [4] represents an extension of the traditional QCM method and can provide unique and quantitative information on the viscoelastic properties of surface adsorbed layers [5]. The QCM-D allows to study the sorption of gases and vapours [6] the adsorption of biomolecules such as proteins [7], [8] as well as other surface-related processes such as cell adhesion [9], [10] surfactant adsorption [11] or enzymatic degradation studies [12]. Even conformational changes of DNA can be elucidated although this is possibly at the limit of the sensitivity of a QCM-D as employed in this study [13]–[15].

6.1.1 Fundamental principles

The quartz crystal microbalance (QCM) is a highly sensitive piezoelectric transducer (theoretically with a sensitivity at the order of ng/cm^2) whose operating principle is based on the alteration of the characteristics of acoustic shear waves propagating through a

medium. The core component of the QCM is a thin AT-cut quartz wafer that is sandwiched between two attached metal electrodes. Thus, due to the piezoelectric nature of the quartz crystal, the resonance frequency is induced by applying an alternating electric field that propagates across the thickness of the crystal [16]. As the sensor surface interacts with adsorbing molecules, its mass and mechanical properties are altered, which in turn leads to a phase shift and attenuation of the shear waves. The phase shift leads to a change in resonance frequency, ΔF , that depends on the mass change occurring at the interface.

QCMs became widely used as mass balance only after Sauerbrey demonstrated in 1959 [17] the linear relation between the frequency change of the oscillating crystal with the mass adsorbed on the surface. According to Sauerbrey, the relation between the change in frequency, ΔF , and the adsorbed mass per unit area, Δm , is given by Equation 6. 1:

$$\text{Equation 6. 1} \quad \Delta m = \frac{C_f}{n} \cdot \Delta F$$

with n : the overtone number ($n= 1,3,5\dots$). C_f : a constant that depends on the intrinsic properties of the quartz. $C_f=17.7 \text{ ng/cm}^2\cdot\text{Hz}$ (for the 5 MHz crystal used in these studies) and is defined as:

$$\text{Equation 6. 2} \quad C_f = \frac{t_q \rho_q}{f_0} \cdot \Delta F$$

with t_q : the thickness of the quartz; ρ_q : the density of the quartz; and f_0 : the fundamental resonant frequency.

For applying Sauerbrey's equation correctly, there are three main assumptions that must be fulfilled:

1. The adsorbed mass must be small relative to the mass of the quartz crystal.
2. The mass adsorbed is rigidly adsorbed.
3. The mass adsorbed is evenly distributed over the sensing area of the quartz.

In case the system does not obey Sauerbrey's equation, a viscoelastic model should be applied. Such a model takes into consideration the energy losses due to changes in viscoelasticity (i.e., by measuring the dissipation, D).

6.1.2 The dissipation factor

The QCM-D technique has proven to be well suited for *in situ* dynamic monitoring of both mass and mechanical properties such as viscoelasticity as a consequence of the adsorption/sorption phenomena occurring in gas, vapour or aqueous environments [3], [8], [18], [19]. For this purpose, the conventional QCM-technology is complemented with the measurement of the so-called "dissipation factor". For determining the dissipation factor, the electrical circuit in which the crystal is embedded is interrupted in millisecond intervals resulting in the piezoelectric crystal oscillator suffering a loss of energy which can be observed as an exponentially damped sinusoidal with time, t [3], [4]. The degree of loss of energy in the system depends on the medium surrounding the crystal and on the properties of the mass deposited onto the crystal.

Figure 6. 1 illustrates this idea: a soft material with a thicker layer deposited onto the crystal will result in a higher dissipation of energy during oscillations than a thin and more rigid film.

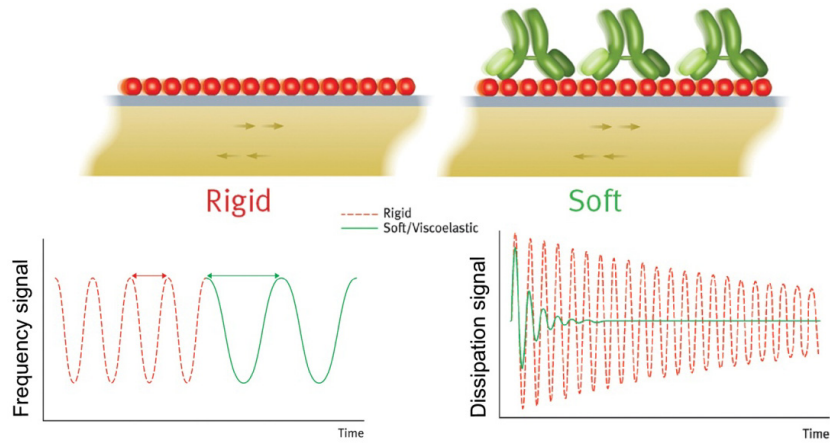


Figure 6. 1 Illustration of the difference in dissipation signal generated by a rigid and soft molecular layer, respectively, on the quartz crystal (Source: QCM-D product information brochure)

Hence, in the context of this work, a frequency change will result as a function of an incremental mass in the coating material while the dissipation factor, D , will provide information on possible concurrent changes in its viscoelastic properties [20]. The dissipation, D , is a dimensionless parameter that compares the time or decay of an oscillating physical system's amplitude to its oscillation period as defined by Equation 6. 3:

$$\text{Equation 6. 3} \quad D = \frac{1}{Q} = \frac{E_{\text{dissipated}}}{2 \cdot \pi \cdot E_{\text{stored}}}$$

with $E_{\text{dissipated}}$: the energy dissipated during one period of oscillation; E_{stored} : the energy stored in the oscillating system.

Non-rigid layers are a typical example for a system in which one of the three assumptions of Sauerbrey does not hold. In cases where Sauerbrey's equation is not satisfied, the value of mass calculated on the basis of the mere frequency change is expected to be underestimated. An example is the case of protein layers or layers that can suffer pronounced swelling, such as hydrogels [21]–[23]. Such viscoelastic systems require a more complex modeling in order to correctly determine mass changes occurring during adsorption. Within the several mathematical models that have been proposed for

simulation of the viscoelastic properties of materials, the two most commonly used ones are the Maxwell model [24] and Kelvin-Voigt model [5], [25]–[27]. The Maxwell model is usually applied to polymer solutions which can demonstrate purely liquid-like behaviour at least for low shear rates, whereas the Voigt model is applicable for polymers which conserve their shape and do not flow [25].

Overtone Sensitivity

The QCM-D used allows simultaneous measurements of the resonance frequencies and the dissipation shift at the fundamental $n=1$ (5MHz), third $n=3$ (15MHz), fifth $n=5$ (25MHz), seventh $n=7$ (35MHz) until the thirteenth $n=13$ (65MHz) overtone. These overtones represent different penetration depths of the harmonic acoustic frequencies into the film adjacent to the sensor surface (Figure 6. 2). They can therefore be used to retrieve, for example, information on a possible anisotropy of a layer deposited on the electrode surface during sorption of compounds. The higher the overtone number the smaller the penetration depth, i.e., the more sensitive it is to phenomena occurring in the layer close to the electrode surface, while lower overtone numbers are more sensitive to variations on the layer surface as they are further from the electrode.

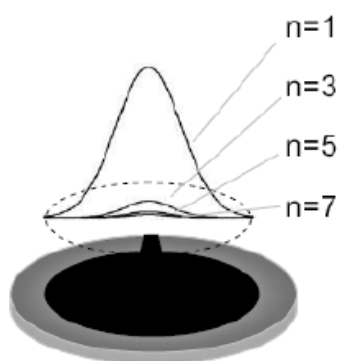


Figure 6. 2 Scheme of each overtone surface penetration in a quartz sensor (Source: QCM-D product information brochure)

The multiple harmonic data permit furthermore modeling the experimental data with a higher degree of confidence such as to extract meaningful data on ad/absorbed mass, change in thickness or density, viscoelastic properties or storage modulus. The viscoelastic data allows broader characterization of systems that fall outside of the scope of the linear Sauerbrey relationship between ΔF and Δm and makes QCM-D more than a simple gravimetric balance.

6.1.3 Data Interpretation

Typical vapour sorption measurements in QCM-D show an initial rapid frequency decrease (mass increase) due to the vapor adsorption, subsequently leveling off until a constant plateau is observed, as is illustrated in Figure 6. 3. Leveling off of the signal represents the equilibrium reached between the material deposited onto the sensor, and the vapour.

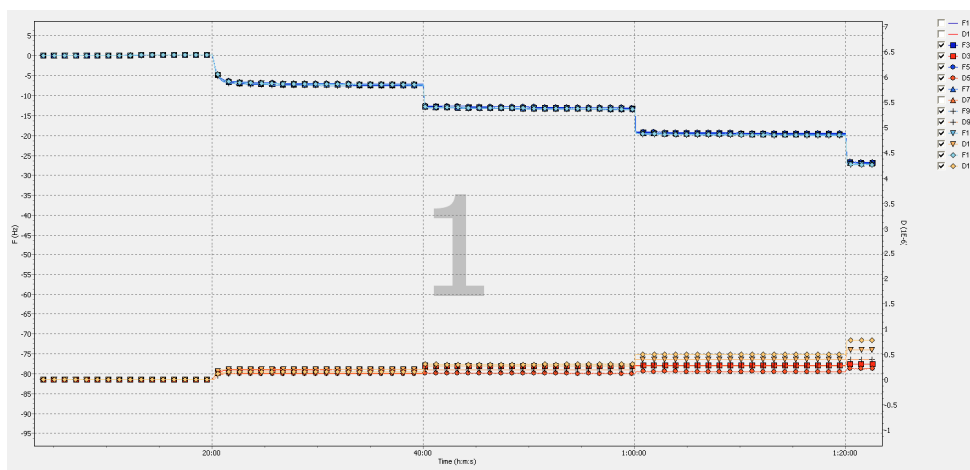


Figure 6. 3 A typical ΔF and ΔD versus time plot from a QCM-D measurement showing the response to an absorption of a vapour by varying its activity in the gas phase

The dissipation-shifts (D-shifts) are intrinsically positive since their reference value is the pristine sensor surface which in the most common case is a gold coated electrode and as such will always be more rigid than any soft matter deposited on top of it. During the measurements of the sorption of vapours in polymers, D-shifts display a kinetics similar to the F-shifts (see Figure 6. 3), but do not have to necessarily coincide. For example, the sorption of a vapour may reach its equilibrium faster than it takes the polymer to rearrange and change its viscoelastic property. On the contrary, a significant and fast polymer rearrangement may occur upon initial sorption of a vapour, only, while vapour sorption takes longer to reach equilibrium. The frequency (ΔF) and dissipation shift (ΔD) plotted are calculated as the difference between the initial reference value of the deposition ($F(t=0)$ and $D(t=0)$) for each overtone and the respective value at equilibrium. Therefore, and if knowing the exact mass of the layer deposited onto the quartz sensor according to Sauerbrey, these measurements allow calculating the sorption coefficient of an organic vapour when stepwise increasing its activity.

A helpful and elucidating manner of exploring the relationship between the sorbed mass (ΔF) and its effect on the viscoelastic properties of the film (ΔD) is to plot $\Delta D/\Delta F$ versus vapour activity (denoted herein "D-F plots"), where time is eliminated as an explicit parameter (Figure 6. 4)

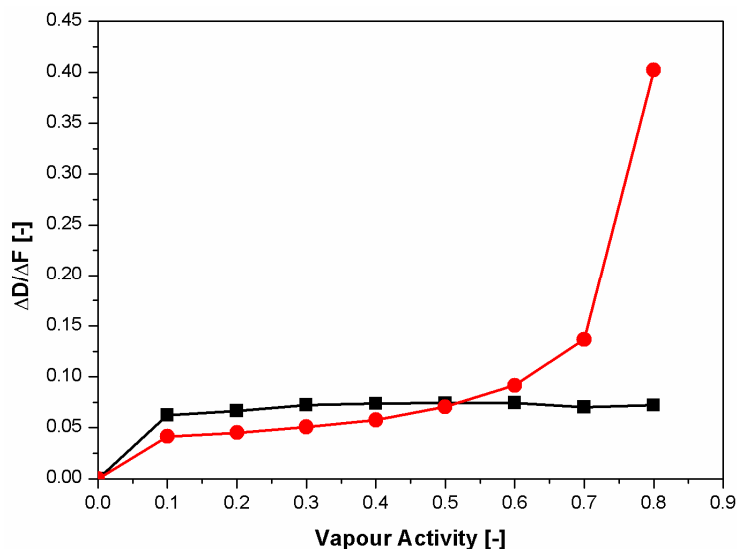


Figure 6. 4 Dissipation/Frequency versus vapour activity plot. A preliminary assay of sorption of water and toluene, respectively, in Pebax®2533. Black squares for water and red circles for toluene.

This plot is useful for evaluating the structural properties of the material deposited as it relates how much dissipation is caused per unit of frequency change (mass). Changes of the slope suggest structural alterations as the adsorption proceeds [28]. In other words, in this particular case this plot gives an estimate of how the sorption of vapour possibly affects the polymer structure: the higher the $\Delta D/\Delta F$ slope, the higher the dissipation per incremental mass sorbed, signaling that for the same incremental mass of vapour sorbed the polymer film undergoes more dramatic viscoelastic changes [2], [29], [30]. Figure 6. 4 depicts the value of such $\Delta D/\Delta F$ -plots resulting from the sorption of two solvents of very distinct physico-chemical property, namely water and toluene, in Pebax®2533. For simplicity, only harmonic number 5 is depicted. It can clearly be seen that while in the case of water $\Delta D/\Delta F$ is constant, in the case of toluene a dramatic increase in slope is registered when the same material gets in contact with higher activities of toluene. This means that toluene highly increases the dissipation of Pebax®2533 per unit added mass at high vapour activities, resulting in a softer material which is strongly swollen and therefore with totally different viscoelastic properties than when Pebax®2533 is submitted to the same activity of water. This strong swelling with toluene but not with water can only be qualitatively

evaluated thanks to the dissipation parameter of QCM-D, a task that the conventional Cahn electrobalance cannot perform.

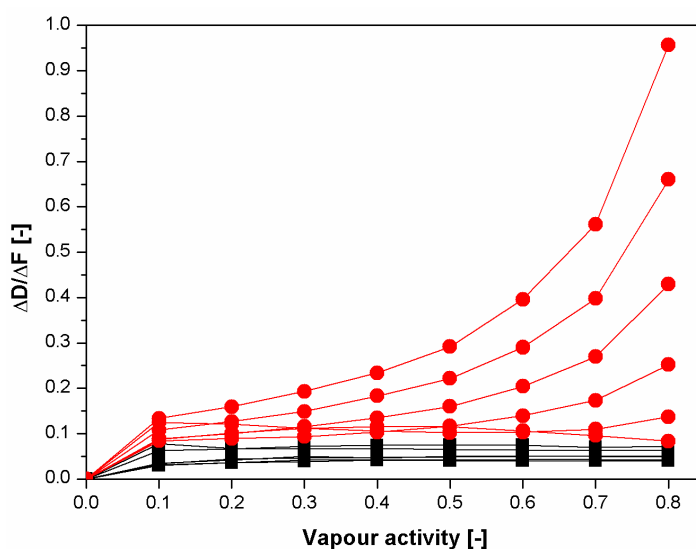


Figure 6. 5 Dissipation/frequency of the different harmonics versus vapour activity plot: evidence of the anisotropy of the material when increasing the vapour activity. Black squares for water and red circles for toluene.

A possible anisotropy of the material being studied can be determined by representing the dissipation/frequency of the different harmonics versus the vapour activity. Although being thin films, it will be shown later that the anisotropy of the material plays an important role in the vapour sorption process. Figure 6. 5 illustrates how the anisotropy of the material can be identified when focusing on the different harmonics. In the case of water sorption in Pebax®2533, the harmonics do not show any significant dispersion with increasing vapour activity. Toluene, on the contrary, causes a strong dispersion for higher harmonics from an activity of 0.5 on. The big exponential increase together with a strong dispersion of the $\Delta D/\Delta F$ values demonstrate that the anisotropy of the material is the consequence of the swelling of the material which on one side (facing the electrode) can swell less freely.

6.2 Results and Discussion

6.2.1 Morphological and topographical characterization of Pebax®2533 and Pebax2533-IL blended depositions on the quartz crystal

6.2.1.1 Atomic Force Microscopy

Atomic force microscopy (AFM) [31] was used to study the morphology of Pebax®2533 deposition onto a quartz substrate with the aim of obtaining information about how homogeneously the copolymer layer was deposited and whether there was any effect of the incorporation of ILs on the deposition quality and polymer surface.

AFM measurements were made with a Nanoscope IIIa Multimode scanning probe microscope (Digital Instruments Inc., Santa Barbara, CA, USA). The images were scanned in tapping mode in air using the deposited layers directly in the quartz crystal resonators as used for QCM-D measurements.

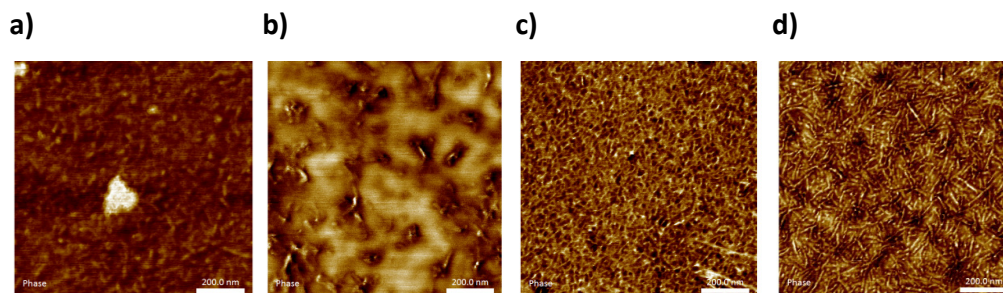


Figure 6. 6 AFM phase images of the surface of different polymer films of approximately 50nm thickness onto a QCM-D quartz crystal: a) Pebax®2533, b) Pebax-[C₈MIM][Cl], c) Pebax-[BMIM][Ac] and d) Pebax-[BMIM][Tf₂N]. The scale bar represents 200 nm.

The AFM photographs in Figure 6. 6 reveal that the whole sensor surface is covered homogeneously with the material. Therefore we can assume that when the quartz crystal

is exposed to the organic vapour, the whole area of the sensor will in principle respond under identical conditions, which is one of the important assumptions when applying the equation of Sauerbrey. Furthermore, these AFM images demonstrate undoubtedly that the copolymer surface gets altered when incorporating the ILs. From these AFM pictures, one certainly cannot differentiate whether the addition of the IL affected more predominantly any of the two phases of the polymer more preferably. However, it seems that the separation of the two phases of the copolymer, namely the PA and PE phases (Figure 6. 6 a), is modified depending on the IL used. Upon incorporation of the ILs, the surface roughness is also altered, as it was already demonstrated in Chapter 3 where DSC revealed how the addition of IL affected most the PA phase, causing a decrease in the semi-crystallinity of the material. This decrease in semi-crystallinity could reach values of 15-20% depending on the IL employed.

6.2.2 Reproducibility of the QCM-D technique

6.2.2.1 Pebax®2533 layer deposition of different thickness

Ultrathin polymer films (thickness <100 nm) can differ substantially from that of bulk polymers as far as their thermophysical properties [32] are concerned. With the aim of detecting if the layer thickness of Pebax®2533 can alter the responsiveness of the QCM-D system in absence of any sorption phenomena, several copolymer layers of varying thickness were deposited under identical spinning conditions as described previously and the response of the QCM-D monitored.

Although the spin-casting process seems to be conceptually simple, its effect on the polymer morphology is actually complex and mathematically challenging. As described by Bornside et al. [33], the spin-casting process can be divided into four steps: 1) polymer deposition, 2) spin-up, 3) spin-off and 4) solvent evaporation-reorganization of the polymer chains. During the first 3 stages, the film thickness is defined by the centrifugal forces, however during the final stage, the rheological properties and solvent evaporation

predominate [34]. For these reasons it is generally impossible to obtain a very high reproducibility in the polymer deposition thickness by spin coating.

The concentration of Pebax®2533 in solution were as follows: 0.10, 0.25, 0.30, 0.50, 0.65, 0.75, 0.85 and 1.00% wt, resulting in a polymer layer thickness from 26 to 230nm as calculated from the measured frequency change using the Sauerbrey equation and assuming a polymer density of 1g/cm^3 . Figure 6. 7 represents the variation of the frequency detected by QCM-D according to the concentration of the Pebax®2533-solution deposited during spin-coting. As expected, it is observed that the higher the initial Pebax®2533 concentration, the more polymer is deposited during spin-coating, with the resulting frequency describing a polynomial fit as a function of the polymer concentration in solution. This implies that the polymer layer formed during spin-coating can be roughly controlled by the concentration of the polymer in solution.

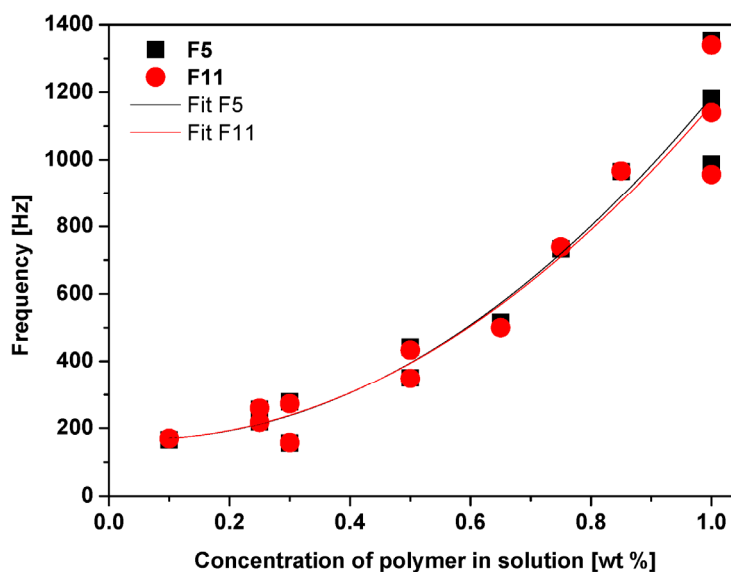


Figure 6. 7 Frequency (overtones 5 and 11) versus initial concentration of Pebax®2533 in solution.

While the mass deposited is correlated with the polymer concentration in solution, the question arises whether the polymer morphology is also roughly identical whatever the overall thickness. In order to answer this question we resort to the dissipation (D)

parameter. This value allows determining qualitatively the intrinsic viscoelasticity of the polymer film and its possible variation amongst different samples. In order to do so, the frequency (F) and dissipation (D) have been measured before (clean quartz) and after depositing Pebax®2533 while applying a flux of 50mL/min of N₂.

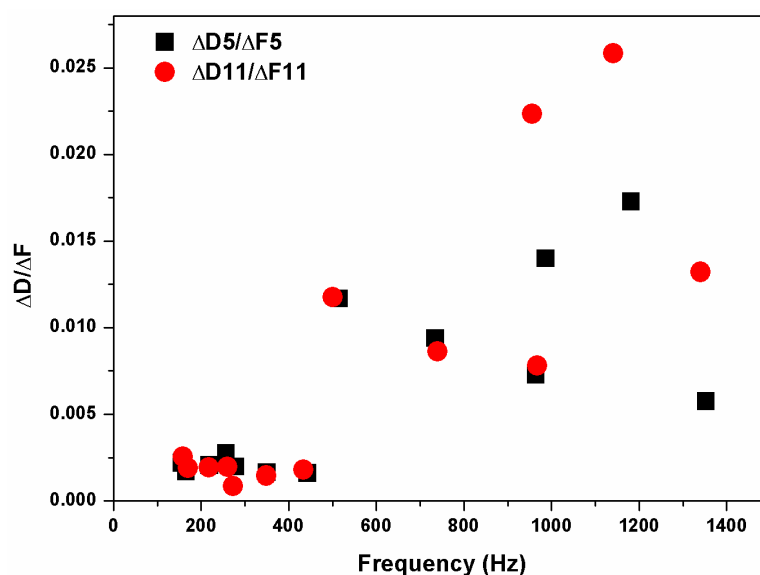


Figure 6. 8 Dissipation normalized by the respective frequency ($\Delta D/\Delta F$, overtones 5 and 11) versus mass deposited of Pebax®2533 (represented as frequency)

Figure 6. 8 shows how there seems to exist a limiting frequency, or mass deposited, which divides the plot in two different sections: below a frequency of 500 Hz, corresponding to a film thickness of about **100** nm, where hardly any variation of the normalized dissipation factor is observed in between samples. It is furthermore constant and independent of the mass deposited. The films formed therefore seem to be "rigid" and comparable in their morphology. This is also corroborated by harmonic 5 and 11 coinciding entirely. On the contrary, above 500Hz and **300** nm of film thickness, dissipation increases up to ten-fold and a strong scatter in the normalized dissipation is observed both between harmonics and samples in general. No clear dependency on the frequency, or mass deposited, can be detected. This "limiting" frequency or mass on the sensor surface may possibly be explained as the point from where on an "excess" of copolymer chains is created that do

not rigidly adhere to the gold substrate, as illustrated in Figure 6. 9. These polymer chains can dissipate the energy more freely and their high flexibility will also result in a higher degree of variation in dissipation. This indicates on an empirical basis that in order to achieve the highest possible reproducibility during QCM-D measurements, film layers deposited should not exceed 500 Hz which corresponds to an approximate film layer thickness of 100 nm in the case of Pebax®2533.

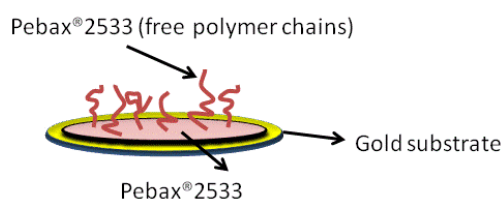
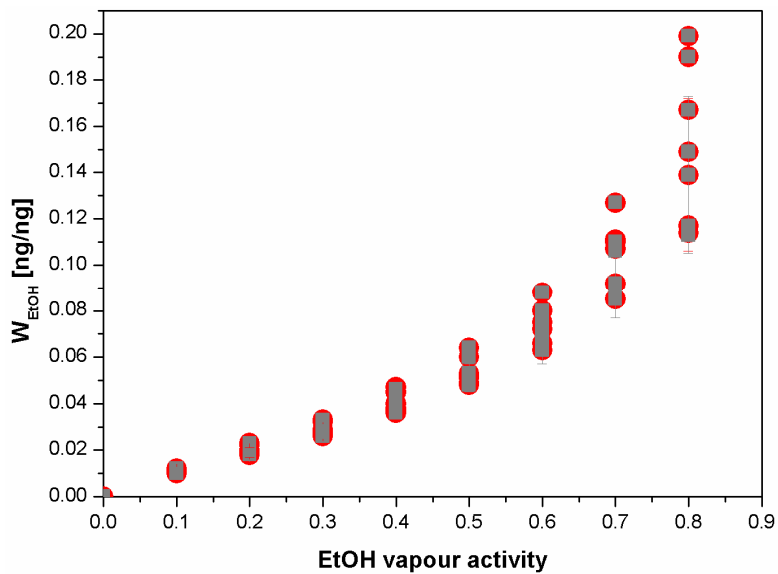


Figure 6. 9 Scheme of Pebax®2533 material deposited when the layer is thicker than 500Hz

6.2.2.2 Reproducibility of vapour sorption in one and the same Pebax®2533 layer deposition

The reproducibility has been investigated once the same layer deposition of the Pebax®2533 block copolymer was exposed to repeated EtOH vapour sorption and desorption cycles composed of series of successive measurements during which the vapour activity was stepwise increased to a maximum. A cycle consisted in a baseline measurement under N₂ atmosphere, followed by a gradient of EtOH vapour activities from 0 up to 0.8 at a flux of 50 mL/min with each vapour exposure lasting 20 min, followed by a desorption step with N₂ until baseline recovery. 6-7 of such cycles were conducted using two different depositions with a significantly different material thickness. The first deposition was about 25nm of thickness while the second was about 76nm (raw data can be found in ANNEX 6.2).

a)



b)

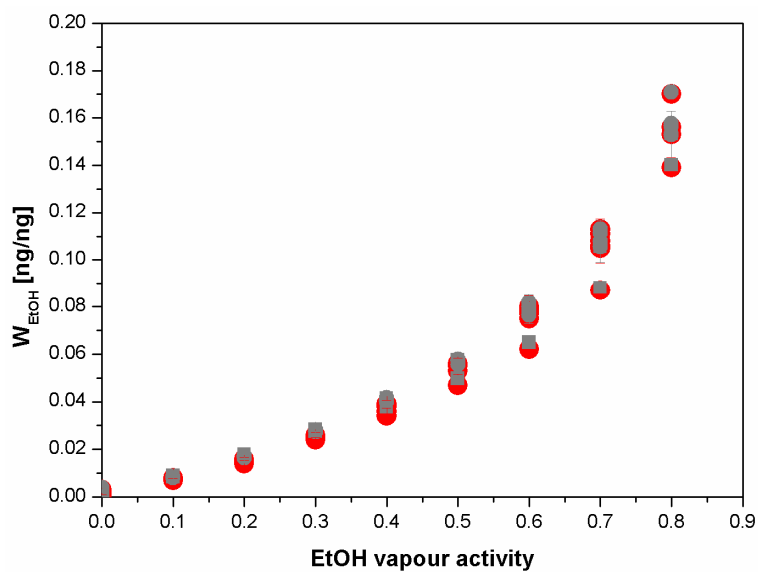


Figure 6. 10 EtOH vapour sorption by two samples of Pebax®2533 submitted to cyclic sorption-desorption processes. Thickness of a) 25nm and b) 76 nm. Grey squares: overtone 5, red circles: overtone 11.

Despite the variation in the thickness between the depositions, we can observe that both plots describe a very similar tendency. Figure 6. 10 depicts how at low vapour activities, from 0.1 up to 0.4, the mass sorbed increases almost linearly as a function of the vapour activity no matter the number of cyclic sorptions conducted. It can also be seen that for both layer thicknesses, the overtones number 5 and 11 widely coincide in this vapour activity range and are hardly dispersed. This implies that no major rearrangement within the polymer takes place upon vapour sorption for these activities. On the contrary, when increasing the vapour activity beyond 0.4, the exponential increase of the mass sorbed with vapour activity becomes evident. In this part of the vapour activity range, the results are less reproducible and particularly for the thinner layer there is a very dramatic dispersion of vapour sorption data obtained at highest vapour activities, demonstrating that the sorption history indeed influences in the EtOH sorption capacity in the polymer layer. In fact, it can be observed at highest vapour sorption that the vapour sorption capacity gradually increases first and then returns almost to its original value, as illustrated in Figure 6. 11.

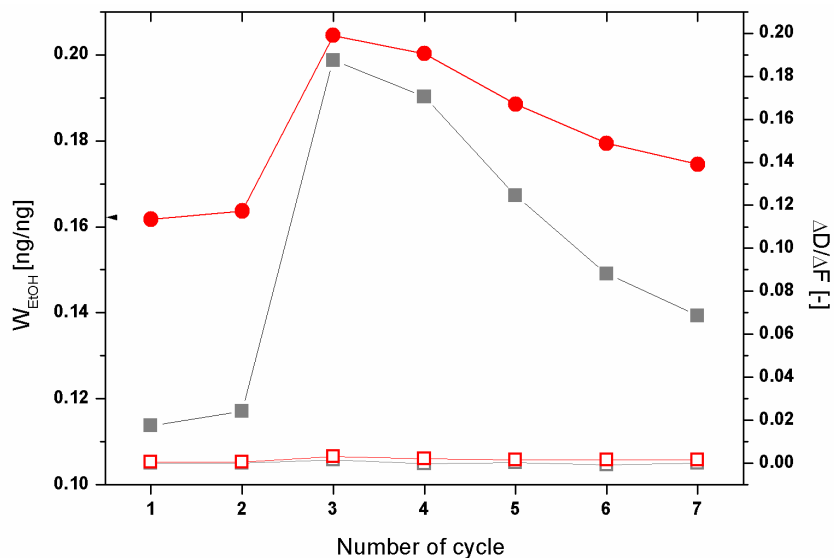


Figure 6. 11 Ethanol sorption behaviour (at an activity of 0.8) of a Pebax®2533 film of 25 nm as a function of the cycle being studied. Grey for overtone 5 and red for overtone 11. Filled legends for ethanol mass fraction and open ones for dissipation factor corrected by their respective frequency values.

This behavior could be explained due to the swelling behavior of the material which furthermore should result in a significant anisotropy across the layer since the polymer adheres on one side onto the sensor surface, an effect which will naturally be more pronounced at higher EtOH vapour activities when polymer swelling is maximum (thickness can be observed in ANNEX 6.2 for both samples respectively)

After each cycle and upon desorption with N_2 , it can be seen that the recovery is practically total (see Figures 1 and 2 in ANNEX 6.2) for all EtOH sorption repetitions implying that Pebax[®]2533 was entirely desorbed by passing N_2 . Based on these results, we can see that the reproducibility of both depositions after 6 and 7 cyclic sorption replicas can be considered acceptable as long as vapour activities do not exceed a vapour activity of 0.4. Beyond this activity and at the highest vapour activity measured (EtOH activity = 0.8), the sorption might show a variation of up to 100%. Therefore, for vapour activities equal or below 0.4, we confirm that QCM-D is an alternative technique to study vapour sorption in polymers such as Pebax[®]2533.

6.3 References

- [1] T. Nomura and O. Hattori, "Determination of micromolar concentrations of cyanide in solution with a piezoelectric detector," *Anal. Chim. Acta*, vol. 115, pp. 323–326, **1980**.
- [2] F. Höök, "Development of a Novel QCM Technique for Protein Adsorption Studies," *PhD Thesis*, **1997**.
- [3] M. Rodahl, F. Höök, A. Krozer, P. Brzezinski, and B. Kasemo, "Quartz crystal microbalance setup for frequency and Q-factor measurements in gaseous and liquid environments," *Rev. Sci. Instrum.*, vol. 66, no. 7, p. 3924, **1995**.
- [4] M. Rodahl and B. Kasemo, "A simple setup to simultaneously measure the resonant frequency and the absolute dissipation factor of a quartz crystal microbalance," *Rev. Sci. Instrum.*, vol. 67, no. 9, p. 3238, **1996**.
- [5] F. Höök, B. Kasemo, T. Nylander, C. Fant, K. Sott, and H. Elwing, "Variations in Coupled Water, Viscoelastic Properties, and Film Thickness of a Mefp-1 Protein Film during Adsorption and Cross-Linking: A Quartz Crystal Microbalance with Dissipation Monitoring, Ellipsometry, and Surface Plasmon Resonance Study," *Anal. Chem.*, vol. 73, no. 24, pp. 5796–5804, **2001**.
- [6] B. P. Regmi, N. C. Speller, M. J. Anderson, J. O. Brutus, Y. Merid, S. Das, B. El-Zahab, D. J. Hayes, K. K. Murray, and I. M. Warner, "Molecular weight sensing properties of ionic liquid-polymer composite films: theory and experiment," *J. Mater. Chem. C*, vol. 2, no. 24, pp. 4867–4878, **2014**.
- [7] M. Andersson, J. Andersson, A. Sellborn, M. Berglin, B. Nilsson, and H. Elwing, "Quartz crystal microbalance-with dissipation monitoring (QCM-D) for real time

- measurements of blood coagulation density and immune complement activation on artificial surfaces.," *Biosens. Bioelectron.*, vol. 21, no. 1, pp. 79–86, **2005**.
- [8] M. Thompson, C. L. Arthur, and G. K. Dhaliwal, "Liquid-phase piezoelectric and acoustic transmission studies of interfacial immunochemistry," *Anal. Chem.*, vol. 58, no. 6, pp. 1206–1209, **1986**.
- [9] C. Fredriksson, S. Kihlman, M. Rodahl, and B. Kasemo, "The Piezoelectric Quartz Crystal Mass and Dissipation Sensor: A Means of Studying Cell Adhesion," *Langmuir*, vol. 14, no. 2, pp. 248–251, **1998**.
- [10] J. Xi and J. Y. Chen, "Quartz Crystal Microbalance in Cell Biology Studies," *J. Biochips Tissue Chips*, vol. 5, **2013**.
- [11] N. Ballard, J. Urrutia, S. Eizagirre, T. Schäfer, G. Diaconu, J. C. de la Cal, and J. M. Asua, "Surfactant kinetics and their importance in nucleation events in (mini)emulsion polymerization revealed by quartz crystal microbalance with dissipation monitoring.," *Langmuir*, vol. 30, no. 30, pp. 9053–62, **2014**.
- [12] J. D. Kittle, X. Du, F. Jiang, C. Qian, T. Heinze, M. Roman, and A. R. Esker, "Equilibrium water contents of cellulose films determined via solvent exchange and quartz crystal microbalance with dissipation monitoring.," *Biomacromolecules*, vol. 12, no. 8, pp. 2881–7, **2011**.
- [13] T. H. Nguyen and M. Elimelech, "Adsorption of plasmid DNA to a natural organic matter-coated silica surface: kinetics, conformation, and reversibility.," *Langmuir*, vol. 23, no. 6, pp. 3273–9, **2007**.
- [14] M. B. Serrano-Santos, E. Llobet, V. C. Özalp, and T. Schäfer, "Characterization of structural changes in aptamer films for controlled release nanodevices.," *Chem. Commun. (Camb)*, vol. 48, no. 81, pp. 10087–9, **2012**.

- [15] C. Özal, M. B. Serrano-Santos, and T. Schäfer, "Responsive Membranes and Materials," *John Wiley Sons*, vol. 26, pp. 1–29, **2012**.
- [16] M. Rodahl and B. Kasemo, "Frequency and dissipation-factor responses to localized liquid deposits on a QCM electrode," *Sensors Actuators B Chem.*, vol. 37, no. 1–2, pp. 111–116, **1996**.
- [17] G. Sauerbrey, "Verwendung von Schwingquarzen zur Wägung dünner Schichten und zur Mikrowägung," *Zeitschrift für Phys.*, vol. 155, no. 2, pp. 206–222, **1959**.
- [18] N. Weber, H. P. Wendel, and J. Kohn, "Formation of viscoelastic protein layers on polymeric surfaces relevant to platelet adhesion.," *J. Biomed. Mater. Res. A*, vol. 72, no. 4, pp. 420–7, **2005**.
- [19] S. Ben Hamouda, Q. T. Nguyen, D. Langevin, C. Chappey, and S. Roudesli, "Polyamide 12-polytetramethyleneoxide block copolymer membranes with silver nanoparticles - Synthesis and water permeation properties," *React. Funct. Polym.*, vol. 67, no. 10, pp. 893–904, **2007**.
- [20] F. Höök, J. Vörös, M. Rodahl, R. Kurrat, P. Böni, J. . Ramsden, M. Textor, N. . Spencer, P. Tengvall, J. Gold, and B. Kasemo, "A comparative study of protein adsorption on titanium oxide surfaces using in situ ellipsometry, optical waveguide lightmode spectroscopy, and quartz crystal microbalance/dissipation," *Colloids Surfaces B Biointerfaces*, vol. 24, no. 2, pp. 155–170, **2002**.
- [21] M. B. Hovgaard, M. Dong, D. E. Otzen, and F. Besenbacher, "Quartz crystal microbalance studies of multilayer glucagon fibrillation at the solid-liquid interface.," *Biophys. J.*, vol. 93, no. 6, pp. 2162–9, **2007**.
- [22] S. X. Liu and J.-T. Kim, "Application of Kevine-Voigt Model in Quantifying Whey Protein Adsorption on Polyethersulfone Using QCM-D," *JALA J. Lab. Autom.*, vol. 14, no. 4, pp. 213–220, **2009**.

- [23] M. Tagaya, "In situ QCM-D study of nano-bio interfaces with enhanced biocompatibility," *Polym. J.*, vol. 47, no. 9, pp. 599–608, **2015**.
- [24] L. H. Sperling, "Introduction to Physical Polymer Science," *Wiley*, p. 880, **2006**.
- [25] M. V Voinova, M. Rodahl, M. Jonson, and B. Kasemo, "Viscoelastic Acoustic Response of Layered Polymer Films at Fluid-Solid Interfaces: Continuum Mechanics Approach," *Phys. Scr.*, vol. 59, no. 5, pp. 391–396, **1999**.
- [26] M. V Voinova, M. Jonson, and B. Kasemo, "Missing mass effect in biosensor's QCM applications.," *Biosens. Bioelectron.*, vol. 17, no. 10, pp. 835–41, **2002**.
- [27] M. A. Meyers and K. Chawla, "Mechanical Behavior of Materials," *Prentice Hall, Inc.*, pp. 570–580, **1999**.
- [28] F. Höök, M. Rodahl, P. Brzezinski, and B. Kasemo, "Energy Dissipation Kinetics for Protein and Antibody–Antigen Adsorption under Shear Oscillation on a Quartz Crystal Microbalance," *Langmuir*, vol. 14, no. 4, pp. 729–734, **1998**.
- [29] A. Kasturirangan, "Specific Interactions in Carbon Dioxide + Polymer Systems," *PhD Thesis*, no. December, pp. 1–185, **2007**.
- [30] J. Limson, O. Odunuge, H. Green, F. Höök, and G. Blatch, "The use of a quartz crystal microbalance with dissipation for the measurement of protein–protein interactions: a qualitative and quantitative analysis of the interactions between molecular chaperones," *Fac. Publ.*, **2004**.
- [31] G. Binnig and C. F. Quate, "Atomic Force Microscope," *Phys. Rev. Lett.*, vol. 56, no. 9, pp. 930–933, **1986**.
- [32] C. Frank, V. Rao, M. Despotopoulou, R. Pease, W. Hinsberg, R. Miller, and J. Rabolt, "Structure in Thin and Ultrathin Spin-Cast Polymer Films," *Science*, vol. 273, no. 5277, pp. 912–5, **1996**.

- [33] D. E. Bornside, C. W. Macosko, and L. E. Scriven, "On the modelling of spin coating," *J. Imaging Technol.*, vol. 13, no. 4, pp. 122–130, **1987**.
- [34] D. B. Hall, P. Underhill, and J. M. Torkelson, "Spin coating of thin and ultrathin polymer films," *Polym. Eng. Sci.*, vol. 38, no. 12, pp. 2039–2045, **1998**.

Chapter 7

Using QCM-D as a method for evaluating the effect of vapour sorption in thin polymer/IL blend membranes

7.1	Introduction	231
7.2	Pebax®2533 vapour sorption coefficient	232
7.3	Pebax2533-ILs sorption coefficients	242
7.3.1	Ethanol	242
7.3.2	Water	245
7.3.3	Hexane	250
7.3.4	Ethyl Acetate and toluene	253
7.4	Conclusions	260
7.5	References	261

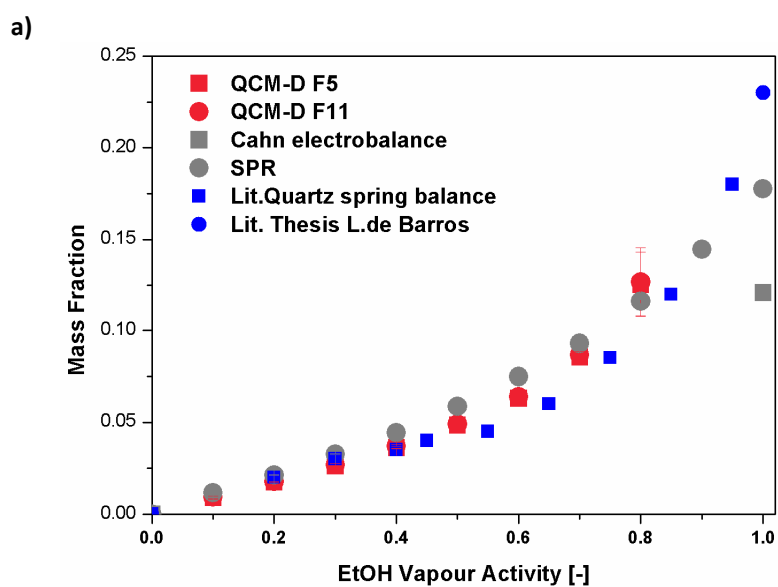
7.1 Introduction

Chapter 6 demonstrated that QCM-D is a promising and fast alternative to conventional gravimetric methods for determining the sorption of vapours in ultra-thin films as well as for studying their qualitative impact on the film morphology in terms of viscoelastic behaviour. Here, Pebax®2533 was submitted to step-wise increased vapor solvent activities with three different techniques: QCM-D, SPR and Cahn electrobalance. The activity of the vapours employed in QCM-D went from 0 up to 0.8. Higher activity values were not used in QCM-D since they produced an excessive and irreversible alteration in the polymer film which affected the QCM-D signal. For the case of SPR, activities used reached up to 1 and in Cahn electrobalance the tests carried out were performed only with saturated organic vapour (activity $a_i=1$).

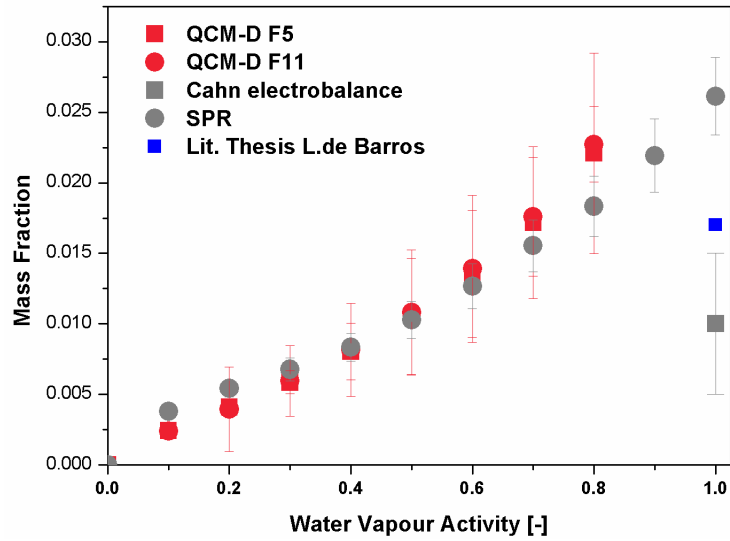
Figure 7. 1 depicts the experimental results obtained from QCM-D and SPR for an ultra-thin film of Pebax®2533 in comparison with results obtained for thick film in a Cahn electrobalance and when being submitted to vapours of water, ethanol, ethyl acetate, toluene, and hexane, respectively. For the QCM-D and Cahn electrobalance, each experiment was repeated three times with one and the same polymer deposition. Each sorption was followed by a desorption step with pure N₂ overnight to assure, under the respective conditions, a complete removal of any trace of solvent from the polymer. Measurement data therefore represent an average value with its respective standard deviation. In the case of SPR, the results consist of an average of the data provided from two measurement channels with their standard deviation.

7.2 Pebax®2533 vapour sorption coefficient

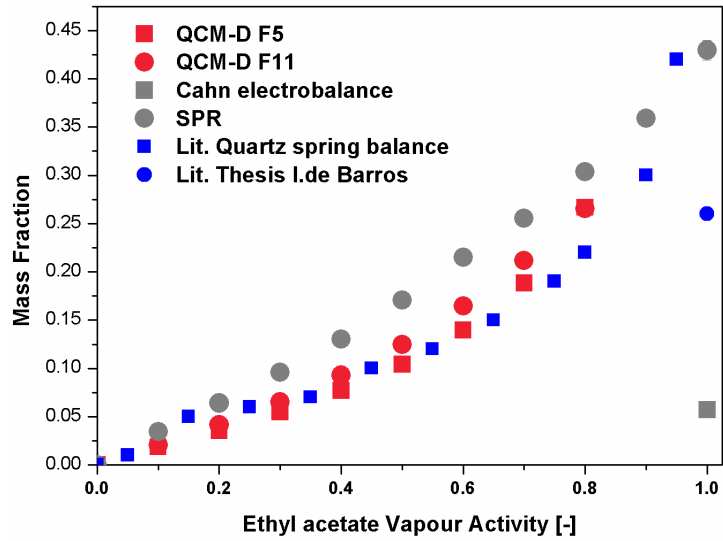
Raw data of the sorption of each solvent in pristine Pebax®2533 are listed in ANNEX 7.1. For the cases of ethanol, water and ethyl acetate, the results depicted in Figure 7. 1 allow a comparison of the three analytical techniques employed for vapour sorption, and, hence, an evaluation of the tendency and reproducibility of each method.



b)



c)



d)

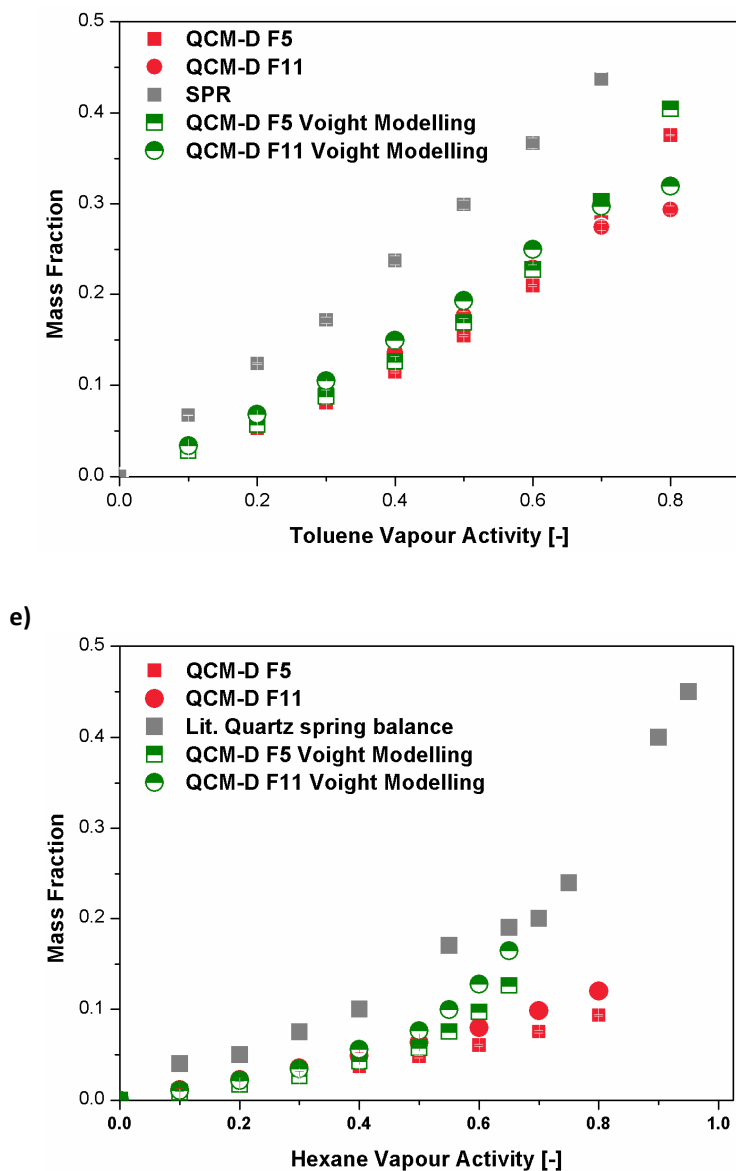


Figure 7. 1 Vapour sorption of Pebax®2533 determined by QCM-D, SPR and Cahn electrobalance. a) ethanol, b) water, c) ethyl acetate, d) toluene and e) hexane, respectively. Experimental data have also been compared with literature data where possible.

Our experimental results were additionally compared with those from literature, namely the work of Y. Cen et al. [1] as well as the PhD. Thesis of L. de Barros Ferreira [2] who have

studied the sorption of vapours in Pebax[®] using a quartz spring balance by step-wise increasing the vapour activity [1] and saturated vapour conditions in a home-made gravimetric method [2], respectively. For the cases of hexane and toluene sorptions, the Voigt viscoelastic model (Qtools -Biolin) was also employed.

It should be noted that in the work of Y. Cen et al. no information was provided about the particular PE and/or PA block content and properties which have been used for their study. However, in view of the similarity of their results with ours, we assume that the material employed by them has been Pebax[®]2533. In the work of L. de Barros et al. the material used was reported to be Pebax[®]4033 (~ 53% PE and 47% PA) whose composition is partially different to the one used in our work, Pebax[®]2533, as it possesses a higher semi-crystallinity. Both studies from literature repeated sorption experiments with one and the same polymer film followed by a desorption and observing that during repetitions the same sorption isotherms were obtained. This is noteworthy as it might be expected, as for example is the case during DSC experiments, that slight deviations in the sorption behaviour may be detected due to polymer chain rearrangement during sorption or desorption. However, for example L. de Barros quantified any variability observed between the first and second vapour sorption experiment to reach around 4% in the case of water, 1% for ethanol and around 5% for ethyl acetate. **Figure 7. 1** shows that in the case of ethanol sorption, it is remarkable how data from QCM-D, SPR as well as the data obtained from literature all follow the same sorption curve as a function of the vapour activity. The only two results that partially deviate belong to the measurement conducted in Cahn electrobalance and the literature value from Barros et al. Given that both values are single points, it is impossible to deduce whether this is a general trend or possibly only a deviation occurring at high vapour activities: after all, saturated vapour conditions are a delicate measurement condition owing to the high risk of localized partial condensation in the measurement system.

Also with regard to water and ethyl acetate, data from both QCM-D and SPR agree very well. Again, the tests done with Cahn electrobalance and the data obtained from the work

of L.de Barros, where saturated organic vapour have been employed, differ partially. Amongst the three vapours studied, the saturated vapour measurement of ethyl acetate shows the biggest difference in the case of Cahn electrobalance. Our main hypothesis for this deviation observed is that the thickness of the sample tested seems to be critical. QCM-D and SPR employed ultra thin films (tens of nanometers) cast onto a gold substrate, while the Cahn electrobalance as described in Chapter 2 (Materials and Methods) required samples of hundreds of microns with no substrate as support in order to quantify the mass gain with a certain confidence. Literature has already reported [3] that the polymer chain orientation, the state of organization layout [4] as well as other factors such as the use of a substrate support or the previous history of the material (i.e. thermal heatings) play an important role in their final mass transport properties; therefore a variation in the sorption mechanism on the nanoscale is probable to occur when compared to the same polymer in the bulk.

In the case of toluene, QCM-D yields lower sorption values than both SPR and Voigt model approximation. Experimental QCM-D data shows an evident difference between overtones 5 and 11. The difference between the data obtained between the three methods were quantified to be more than a 35% with SPR and around 7% with the Voigt model at an activity of 0.8. Unfortunately, no data from literature was found in order to compare and validate these results. However, it is known that QCM-D has the tendency to underestimate the mass sorbed in its surface layer when the latter undergoes a strong change in its viscoelasticity. Such change occurs, for example, in the case of swelling of the polymer. The underestimation of the sorbed mass is therefore an experimental artefact and is known as the "missing mass effect". Since SPR is not sensitive to such changes owing to its different measurement principle, the sorption of toluene might therefore be underestimated in the case of QCM-D.

In the case of hexane an even more noticeable observation was made, however, in this case between QCM-D and both literature data [1] and Voigt model approximation. Again, QCM-D apparently underestimates the sorption of hexane up to a 25% at an activity 0.8.

SPR measurements did not provide any conclusive result as after repeating the experiments for several times it was observed how the hexane molecules visibly damaged the Pebax®2533 film up to a total dissolution of the thin layer. Again, this indicates that a strong swelling of the ultra-thin film might have taken place which would explain why QCM-D strongly underestimated the hexane sorption.

Figure 7. 2 and Figure 7. 3 compile the sorption behavior of Pebax®2533 thin films when submitted to an increasing vapour activity, both in mass and molar fractions, respectively, of the sorbed solute. It can be seen how the sorption behavior of the different solvents can be lumped together in three different groups on the basis of their sorbed mass fraction: toluene and ethyl acetate sorb most in Pebax®2533, followed by an intermediate group of ethanol and hexane and finally the compound that least sorbed in Pebax®2533 ultra-thin films was shown to be water. This grouping of compounds becomes less evident when representing the molar fractions of sorbed compounds rather than mass fractions with the main difference being that hexane sorbs in Pebax®2533 at same molar fractions as toluene. Figure 7. 3 reflects the dual affinity of the polymer with a tendency to be hydrophilic as polar organic compounds such as ethyl acetate and ethanol sorb most, followed by water.

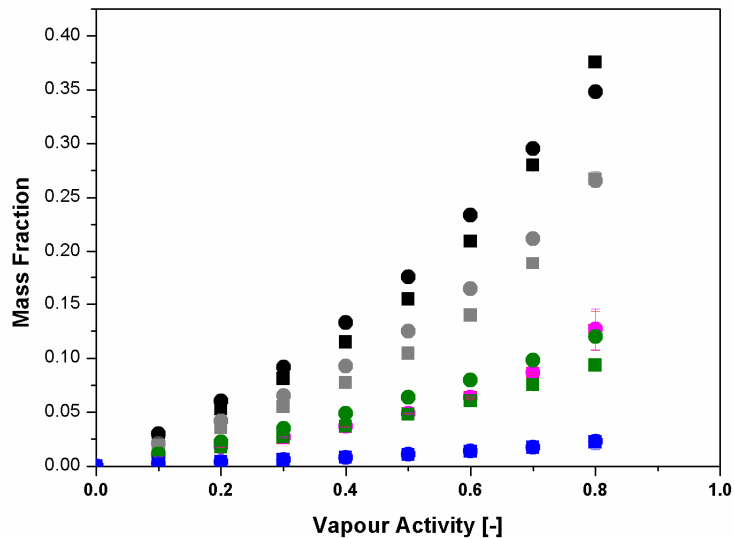


Figure 7. 2 Vapour sorption in mass fractions of Pebax®2533 when exposed to different activities of the vapours of: water (blue), ethanol (pink), ethyl acetate (grey), hexane (green), toluene (black). Squares for overtone 5 and circles for overtone 11.

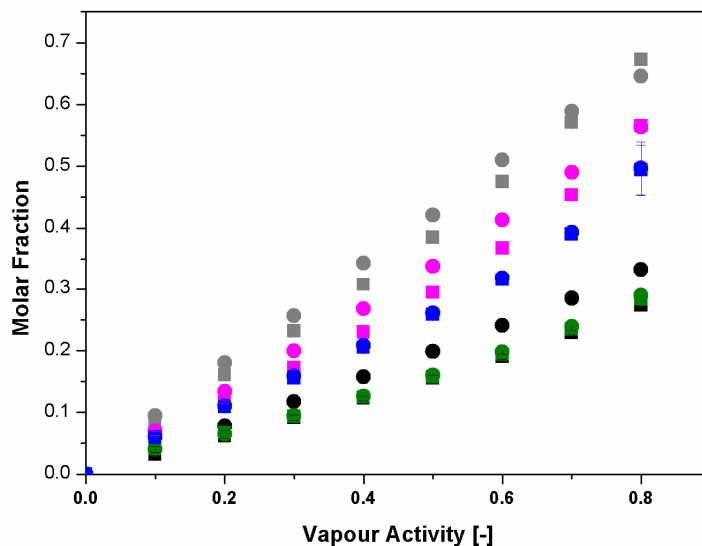


Figure 7. 3 Vapour sorption of Pebax®2533 in molar fractions when exposed to different activities of the vapours of: water (blue), ethanol (pink), ethyl acetate (grey), hexane (green), toluene (black). Squares for overtone 5 and circles for overtone 11.

In addition to yielding data on the sorption coefficients when a thin film is submitted to different gases or solvents, QCM-D can also provide information about how much this film can dissipate energy due to viscoelastic changes occurring during sorption. In this way, this complementary parameter provides information about any variation of the physical film bulk properties upon vapour sorption. It is important to note that the dissipation factor is not a quantitative value; however, it will be shown that it is a useful parameter to understand how the viscoelastic properties of a thin film vary depending on the solvents and materials being used.

Naturally, the dissipation factor ΔD increases with increasing mass sorbed. It is therefore important to normalize the dissipation factor by the mass absorbed. The latter is represented by the frequency change ΔF . Figure 7. 4 depicts $\Delta D/\Delta F$ values of pristine Pebax®2533 ultrathin films as a function of the vapour activity for different solvent vapours. It illustrates how the viscoelastic behaviour of one and the same polymer material can be altered by changing the solvent vapour to which it is exposed.

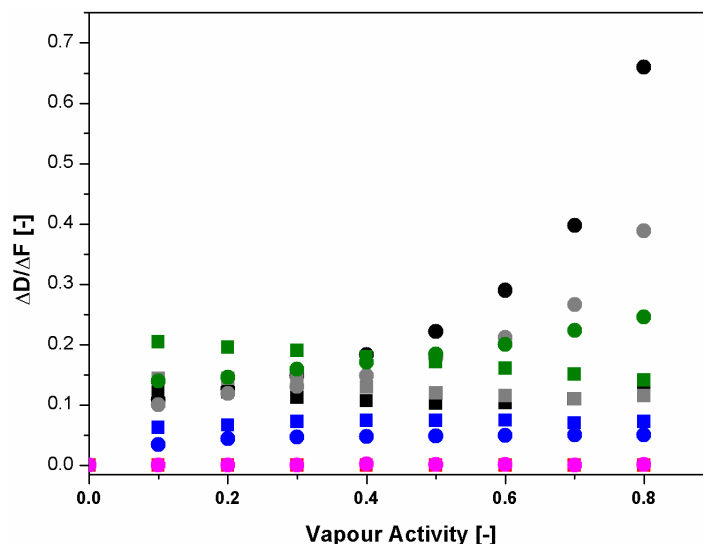


Figure 7. 4 Dissipation factor normalized by the respective frequency as a function of different vapour activities in Pebax®2533 thin films. Solvent vapours legend: Blue for water, pink for ethanol, grey for ethyl acetate, green for hexane, and black for toluene. Squares for overtone 5 and circles for overtone 11.

Apparently, ethanol exhibits a very low normalized dissipation no matter at which vapour activity. This implies that ethanol does not alter the viscoelastic properties of the film, at all, and it might be deduced that its sorption in the polymer occurs keeping the physical properties of the latter unchanged. In the case of water, from an activity of 0.1 onwards a slight increase in the normalized dissipation factor is observed, however, remaining at a constant value along the whole range of vapour activities studied and in the both overtones shown. This suggests that water produces a homogeneous softer material as compared to the pristine polymer, but without further changes of the polymer material once water has been introduced into the polymer network.

The most striking change in normalized dissipation upon vapour sorption is exhibited by the rest of solvents studied, namely ethyl acetate, hexane and toluene. These three solvents generate a bigger alteration of the viscoelastic properties of Pebax®2533. First, it can be seen in Figure 7. 4 how the tendency of both overtones varies for each vapour. It is recalled that lower overtones protrude more into the polymer layer and therefore are more sensitive to the bulk polymer or polymer layer surface while higher overtones are more sensitive to the layer close to the electrode surface where the polymer adheres to the sensor surface. A discrepancy in the behaviour of overtones indicates therefore a material anisotropy. It gets evident in Figure 7. 4 that upon sorption of these three vapours, the polymer material does indeed respond differently, and in particular from an activity of 0.5 onwards which seems to represent the inflection point at which viscoelastic variations can be easily seen.

In the case of toluene and ethyl acetate, overtone number 5 is increased upon vapour sorption from the lowest vapour activity onward but then remains constant just as was observed for water, although at a higher value. On the contrary, overtone 11 undergoes for both solvents an exponential increase more than triplicating values measured at low vapour activities. This indicates a strong anisotropy developing in the polymer material upon sorption of ethyl acetate and toluene with strong alterations occurring at the

polymer-sensor interface where the freedom of the polymer material to rearrange is particularly restricted. The case of hexane shows a completely opposite tendency in the viscoelastic properties depending on the overtone at which we focus. For overtone number 5, a decrease in the dissipation parameter is observed when increasing the vapour activity. This could be interpreted as a "hardening" of the polymer or indicate an anti-plasticization upon hexane molecules entering the polymer network. Indeed, due to the highly hydrophobic character of hexane, this might be plausible considering that Pebax®2533 is a block copolymer. On the other hand, overtone number 11 shows the opposite trend for the polymer-sensor interface.

Finally, it is interesting to note that these data on viscoelastic changes can be correlated with data from ¹³C NMR (Chapter 3, Table 3.6): water and ethanol show smaller viscoelastic changes than toluene, and the same was observed with regard to the respective upfield shifts.

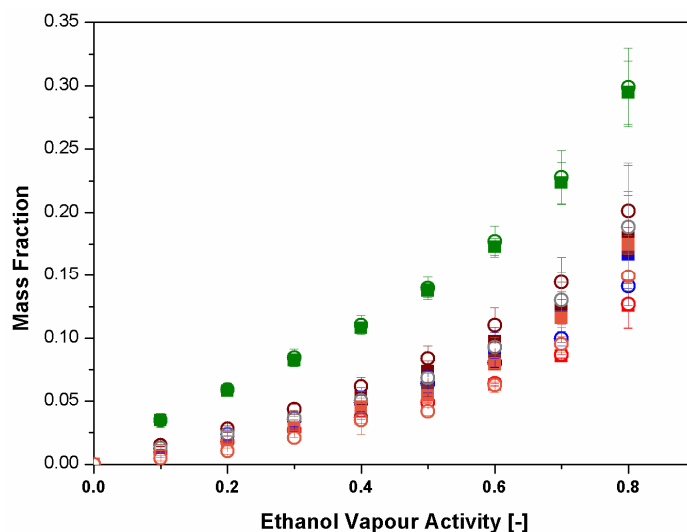
As a conclusion, we might state that QCM-D and SPR provide qualitatively reliable data on sorption coefficients, while QCM-D furthermore reveals interesting viscoelastic changes in the polymer. For example, ethyl acetate as the highest sorbing compounds and toluene as the lowest sorbing compounds in Pebax®2533 both produce the highest variation in the viscoelasticity of the polymer. On the other hand, although ethanol is significantly sorbed by Pebax®2533, it does not produce any alteration in the viscoelasticity of the material, at all.

Based on this analysis of the pristine membrane polymer as reference, in the following the same analysis will also be conducted for the composite thin films in order to evaluate the effect of each solvent once ILs are incorporated in the polymeric structure. However, due to the high number of experiments carried out (5 solvents and 5 ILs employed for composite membranes) and in order to avoid any repetitive explanation, we will only focus on those results that seem to be particularly noteworthy.

7.3 Pebax2533-ILs sorption coefficients

7.3.1 Ethanol

a)



b)

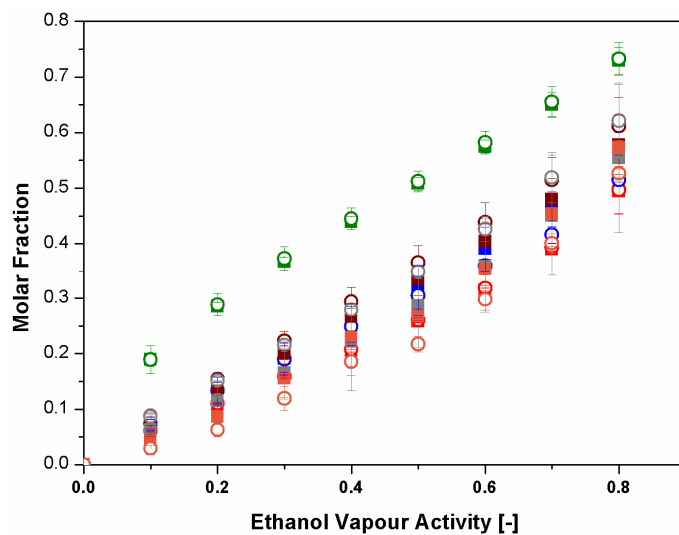


Figure 7. 5 Vapour sorption of pristine and Pebax2533-IL blend membranes expressed in **a)** as mass and **b)** molar fractions when exposed to a gradient of vapour activities of ethanol. Red for pristine Pebax®2533, green Pebax-[C₈MIM][Cl], blue Pebax- [BMIM][BF₄], brown Pebax-[BMIM][Ac], grey Pebax-[BMIM][Tf₂N] and orange Pebax- [TMG][BF₄]. Filled squares for overtone number 5 and open circles for overtone number 11.

Using QCM-D as a method for evaluating the effect of vapour sorption in thin polymer/IL blend membranes

In the case of ethanol sorption measurements (see Figure 7. 5), it is observed how most composite films describe the same sorption tendency indicating that the IL did not significantly affect the membrane affinity for ethanol. Only Pebax2533-[C₈MIM][Cl] showed a significant increase in the sorption capacity compared to the pristine polymer with increasing vapour activity. Values measured are around 0.15-0.25 units higher than those of other blend membranes and almost doubling the sorption of other blend membranes for certain vapour activities.

It should be remarked that for the experiments carried out in Cahn electrobalance, they were done with saturated vapour while those from QCM-D the vapour activity was of 0.8. Although the differences in the experimental conditions, we would like to compare, at least as a tendency, the results in Table 7. 1 obtained by the two experimental techniques.

In general, although slight differences, it could be said that the ethanol sorption results follow the same tendency no matter the experimental technique used.

Table 7. 1 Vapour sorption data for pristine Pebax®2533 and mixed membranes expressed in mass fraction and mole fraction determined by Cahn electrobalance (data taken from Chapter 4 in white) and QCM-D (data in red).

	ETHANOL			
	Mole Fraction (x_i)		Mass Fraction (w_i)	
Pebax®2533	0.48	0.49	0.12	0.13
Pebax2533-[C ₈ MIM][Cl]	0.65	0.73	0.22	0.29
Pebax2533-[BMIM][BF ₄]	0.49	0.52	0.13	0.15
Pebax2533-[BMIM][Ac]	0.73	0.60	0.30	0.18
Pebax2533-[BMIM][Tf ₂ N]	0.51	0.60	0.12	0.18
Pebax2533-[TMG][BF ₄]	0.80	0.55	0.39	0.16

In this case we have also plotted the normalized dissipation factor by the mass absorbed, as can be seen in Figure 7. 6.

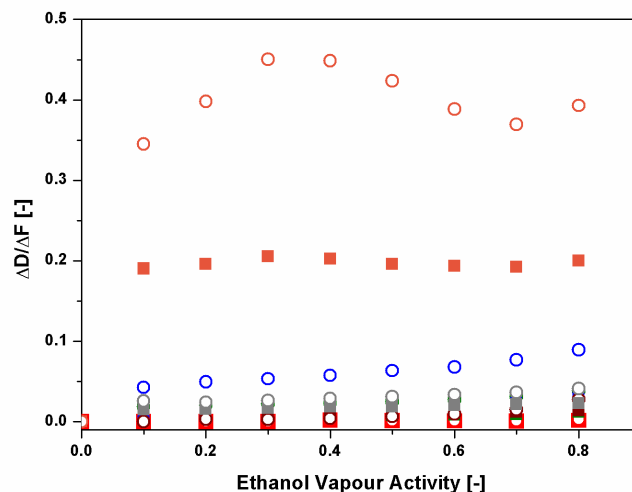


Figure 7. 6 Frequency-normalized dissipation as a function of the ethanol vapour activity for the different membranes. Red for pristine Pebax®2533, green Pebax-[C₈MIM][Cl], blue Pebax-[BMIM][BF₄], brown Pebax-[BMIM][Ac], grey Pebax-[BMIM][Tf₂N] and orange Pebax-[TMG][BF₄]. Filled squares for overtone number 5 and open circles for overtone number 11.

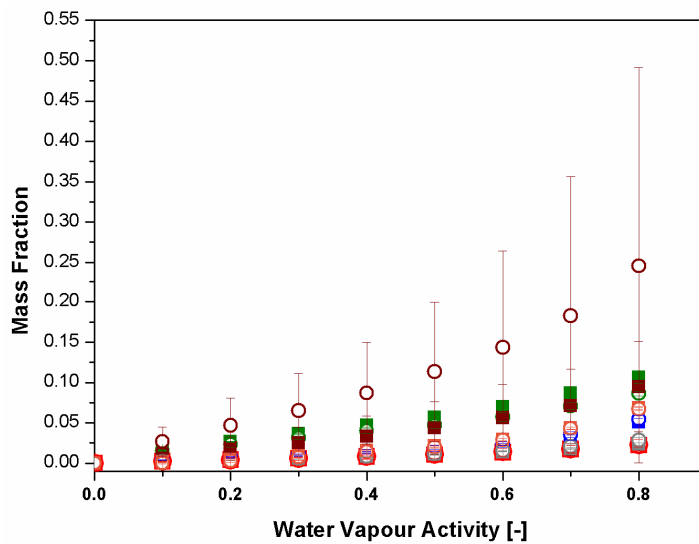
Interestingly, while the Pebax2533-[C₈MIM][Cl] blend membrane exhibited the biggest sorption, its frequency-normalized dissipated energy remained constant at very low values. On the contrary, it can be seen how Pebax2533-[TMG][BF₄] also yields a constant frequency-normalized dissipated energy but at much higher values, whatever the vapour activity. Figure 7. 4 already showed that small amounts of vapour sorbed cause a substantial rearrangement of the polymer mixture which then, however, does not further readjust upon further inclusion of vapour molecules. Figure 7. 6 illustrates the same holds for polymer/IL composites in the case of ethanol. This means that the IL does apparently not "plasticize" the polymer enough such that viscoelastic changes become less pronounced upon ethanol vapour sorption. It remained unclear whether the ondulation observed for Pebax2533-[TMG][BF₄] as a function of the vapour activity was significant. The polymer blend incorporating an IL with the same anion, Pebax-[BMIM][BF₄], also

Using QCM-D as a method for evaluating the effect of vapour sorption in thin polymer/IL blend membranes

reveals a significant increase in the $\Delta D/\Delta F$ -values upon vapour sorption however, at almost constant values over the whole range of vapour activities. This suggests that while it is widely assumed that interactions between IL and ethanol occur via the anion, the dissipation changes depended in their extent on the respective IL cation. [TMG] is a bulkier cation than [BMIM] which might explain the respective bigger changes in $\Delta D/\Delta F$ upon sorption of ethanol. It should also be noted that for the [BF₄] containing ILs there exists a strong dispersion between the two harmonics represented, indicating that the ethanol sorption induced a strong anisotropy in the polymer material. As a general observation, from Figure 7. 1 it can be seen that although ethanol vapour sorptions do not differ so much between Pebax®2533 and Pebax2533-IL blend membranes, Figure 7. 6 reveals that the presence of the IL in the polymer causes a significantly higher change in the overall viscoelastic properties upon ethanol sorption than observed for the pristine polymer.

7.3.2 Water

a)



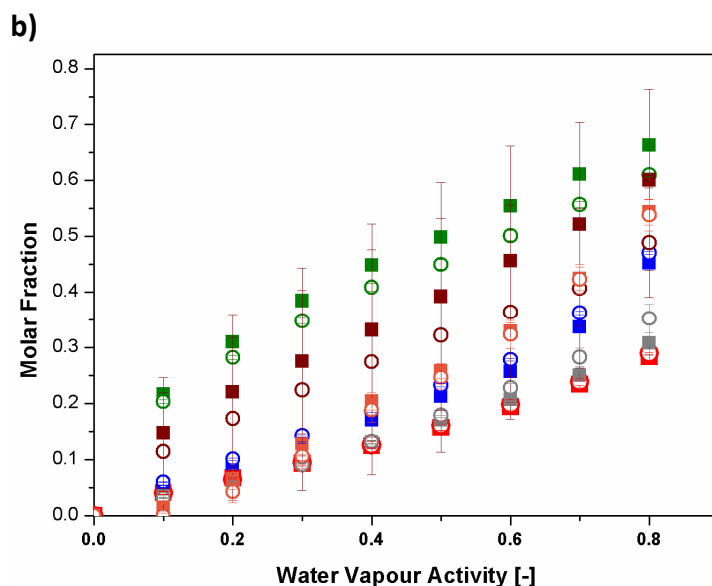


Figure 7. 7 Vapour sorption of pristine and Pebax2533-IL blend membranes expressed in **a)** as mass and **b)** molar fractions when exposed to a gradient of vapour activities of water. Red for pristine Pebax[®]2533, green Pebax-[C₈MIM][Cl], blue Pebax-[BMIM][BF₄], brown Pebax-[BMIM][Ac], grey Pebax-[BMIM][Tf₂N] and orange Pebax-[TMG][BF₄]. Filled squares for overtone number 5 and open circles for overtone number 11.

In the case of the tests carried out with water, it is observed how Pebax2533-[BMIM][Ac] film, with [BMIM][Ac] as being one of the most hydrophilic ILs, shows a dramatic sorption increase when compared with the other composite films (more easily to be observed in Figure 7. 7 a). This is in line with sorption data determined with the Cahn electrobalance (Table 4.2, Chapter 4). The dispersion of the harmonics in this particular case is noteworthy, revealing a dramatic anisotropy when Pebax2533-[BMIM][Ac] is submitted to water vapour. On the other hand, we would expect a very low sorption capacity in Pebax2533-[BMIM][Tf₂N] films since [BMIM][Tf₂N] is a hydrophobic IL and this is indeed what was observed. Pebax2533-[BMIM][Tf₂N] follows a behaviour apparently similar to pristine Pebax[®]2533 showing the smallest sorption data registered when compared to the other polymer/IL blends. In these cases, the overtones seem to be slightly more dispersed

Using QCM-D as a method for evaluating the effect of vapour sorption in thin polymer/IL blend membranes

than in the case of ethanol sorption. Again, here the data obtained are in very good agreement with those from the Cahn electrobalance.

A similar comparison with the data obtained from Cahn electrobalance is shown in **¡Error!**
No se encuentra el origen de la referencia.

Table 7. 2 Water vapour sorption data for pristine Pebax®2533 and mixed membranes expressed in mass fraction and mole fraction determined by Cahn electrobalance (data taken from Chapter 4 in white) and QCM-D (data in red).

	WATER			
	Mole Fraction (x_i)		Mass Fraction (w_i)	
Pebax®2533	0.15	0.28	0.01	0.02
Pebax2533-[C ₈ MIM][Cl]	0.24	0.62	0.02	0.09
Pebax2533-[BMIM][BF ₄]	0.20	0.46	0.02	0.05
Pebax2533-[BMIM][Ac]	0.42	0.50	0.04	0.10
Pebax2533-[BMIM][Tf ₂ N]	0.19	0.31	0.01	0.02
Pebax2533-[TMG][BF ₄]	0.21	0.53	0.02	0.07

In this case, although the values obtained by the two different experimental techniques follow a similar tendency, they do not show such similarity in the absolute data as occurred with ethanol. In this case, it is obvious how QCM-D overestimates the results obtained from Cahn electrobalance.

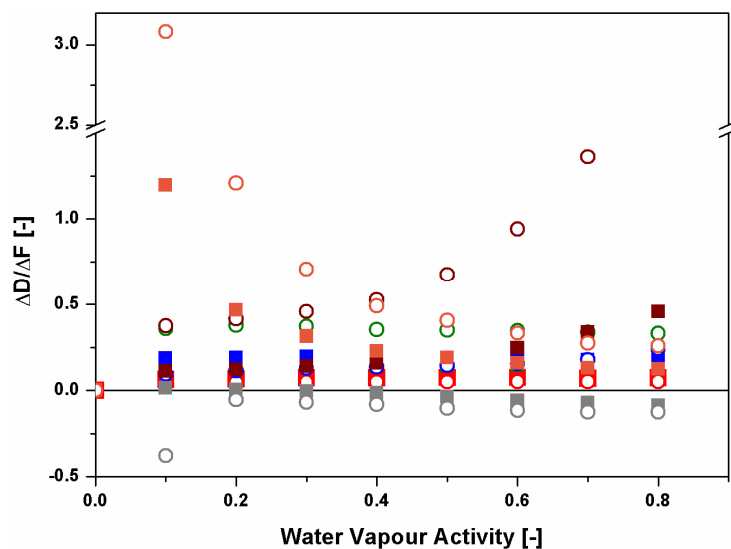


Figure 7. 8 Frequency-normalized dissipation as a function of the water vapour activity for the different membranes. Red for pristine Pebax®2533, green Pebax-[C₈MIM][Cl], blue Pebax-[BMIM][BF₄], brown Pebax-[BMIM][Ac], grey Pebax-[BMIM][Tf₂N] and orange Pebax-[TMG][BF₄]. Filled squares for overtone number 5 and open circles for overtone number 11.

The normalized dissipation reveals in the case of water for the a peculiar behaviour as negative values are observed for Pebax2533-[BMIM][Tf₂N] . This suggests that the material upon sorbing the vapour becomes more "rigid". One possible explanation would be that [BMIM][Tf₂N] acts as an antiplasticizer, tending to leave the block copolymer matrix upon water sorption and thus making the polymer film more rigid than before. This would in principle also indicate a tendency of this particular IL to migrate from the bulk polymer in presence of humidity, an observation which will be further checked in Chapter 8. Figure 7. 9 depicts a schematic illustration of how the increase of the rigidity in Pebax2533-[BMIM][Tf₂N] blend membranes could take place.

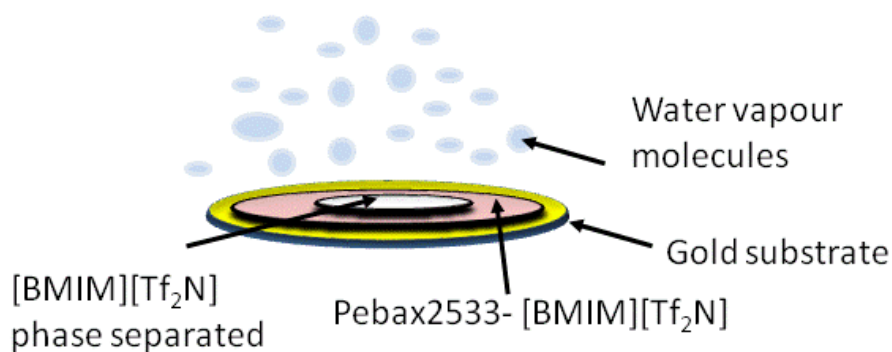


Figure 7. 9 Scheme of the phase separation produced in Pebax2533[BMIM][Tf₂N] blend membrane when exposed to water vapour.

The other blend membrane that experiments a non-expected behaviour corresponds to Pebax2533-[TMG][BF₄] as can be seen in Figure 7. 8. In this case, as increasing the water vapour activity, the normalized dissipation decreases considerably up to a value near to 0 for the highest activity studied.

It seems in this case that as incorporating more water molecules in the system, the material reorganizes becoming also less soft than before.

7.3.3 Hexane

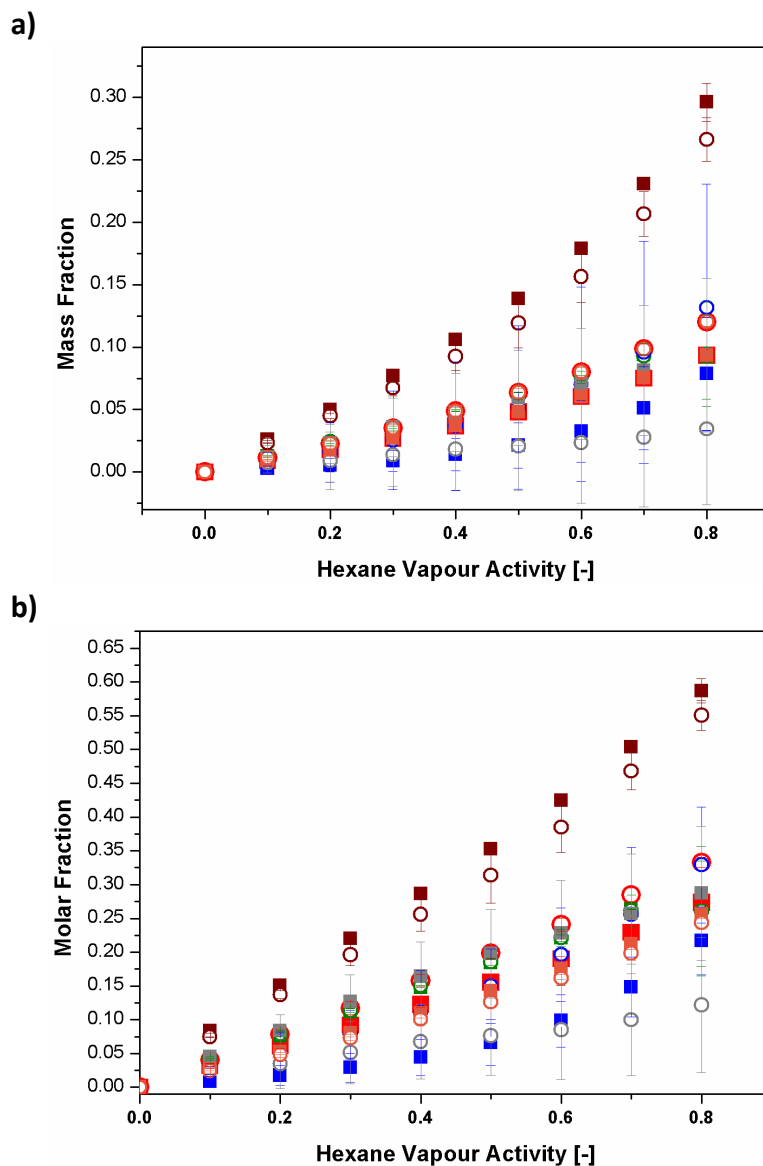


Figure 7. 10 Vapour sorption of pristine and Pebax2533-IL blend membranes expressed in **a)** as mass and **b)** molar fractions when exposed to a gradient of vapour activities of hexane. Red for pristine Pebax®2533, green Pebax-[C₈MIM][Cl], blue Pebax- [BMIM][BF₄], brown Pebax-[BMIM][Ac], grey Pebax-[BMIM][Tf₂N] and orange Pebax- [TMG][BF₄]. Filled squares for overtone number 5 and open circles for overtone number 11.

Using QCM-D as a method for evaluating the effect of vapour sorption in thin polymer/IL blend membranes

In the case of hexane, the sorption in Pebax2533-[BMIM][Ac] and Pebax2533-[BMIM][Tf₂N] thin films are of particular interest with the former having incorporated a strongly hydrophilic IL, and the latter the only hydrophobic one. Interestingly, it is the Pebax2533-[BMIM][Ac] thin film that exhibits by far the highest sorption as a function of the vapour activity, while Pebax2533-[BMIM][Tf₂N] remains at very low values. In pristine Pebax[®]2533, sorption of hexane might occur through interaction via the alkyl PE-chains of the polymer. With regard to these two ILs, any hydrophobic interactions would be expected to take place with the butyl chain of the cation. Hence, the reason for the higher sorption of hexane in Pebax2533-[BMIM][Ac] remains unclear and is neither revealed by the frequency-normalized dissipation: while Pebax2533-[BMIM][Ac] yields similar values to other blend membranes, it is precisely Pebax2533-[BMIM][Tf₂N] which exhibits a big difference between the two overtones studied and a high $\Delta D/\Delta F$ -value for the 11th overtone. In fact, the latter indicates that hexane strongly softens the polymer material causing a high dissipation of energy for all vapour activities. Indeed, after having repeated the hexane sorption measurement for three times, the QCM-D sensor was examined visually and we observed a drop in the center of the deposited material (see Figure 7. 12). Here, an obvious phase separation had occurred with hexane favouring the formation of a drop of [BMIM][Tf₂N]. This explains the high discrepancy between the $\Delta D/\Delta F$ -values observed for the 5th and the 11th overtone in **Figure 7. 11**.

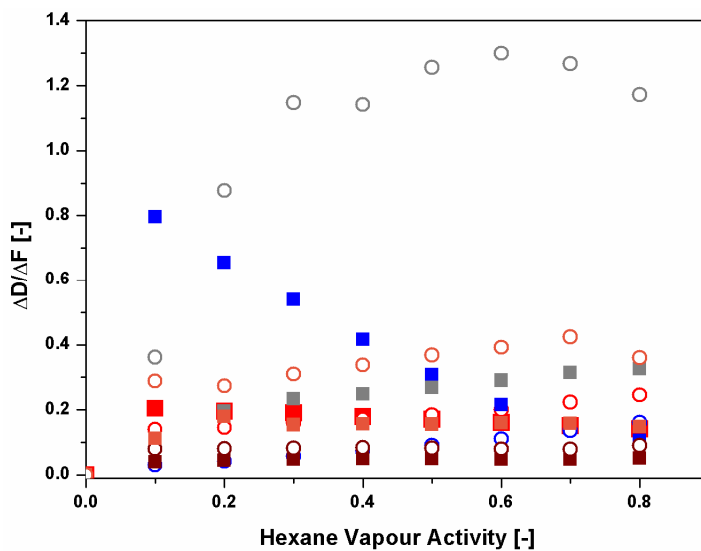


Figure 7. 11 Frequency-normalized dissipation as a function of the hexane vapour activity for the different membranes. Red for pristine Pebax[®]2533, green Pebax-[C₈MIM][Cl], blue Pebax-[BMIM][BF₄], brown Pebax-[BMIM][Ac], grey Pebax-[BMIM][Tf₂N] and orange Pebax-[TMG][BF₄]. Filled squares for overtone number 5 and open circles for overtone number 11.

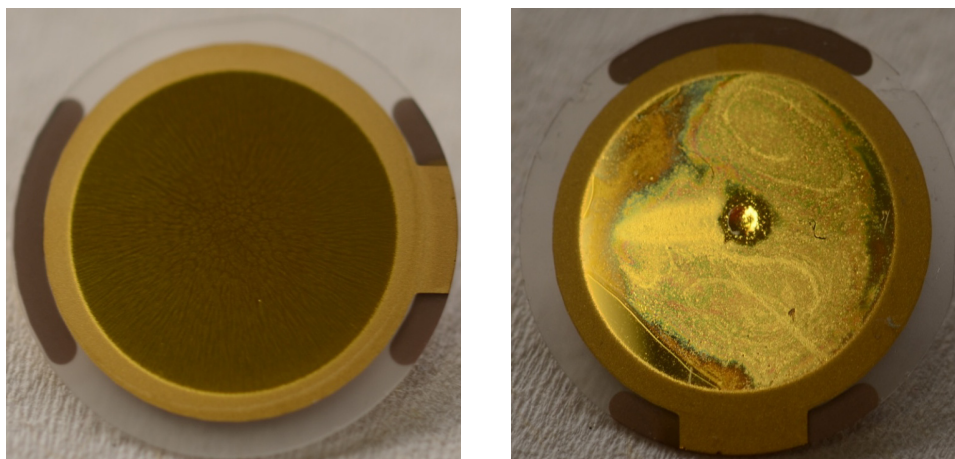
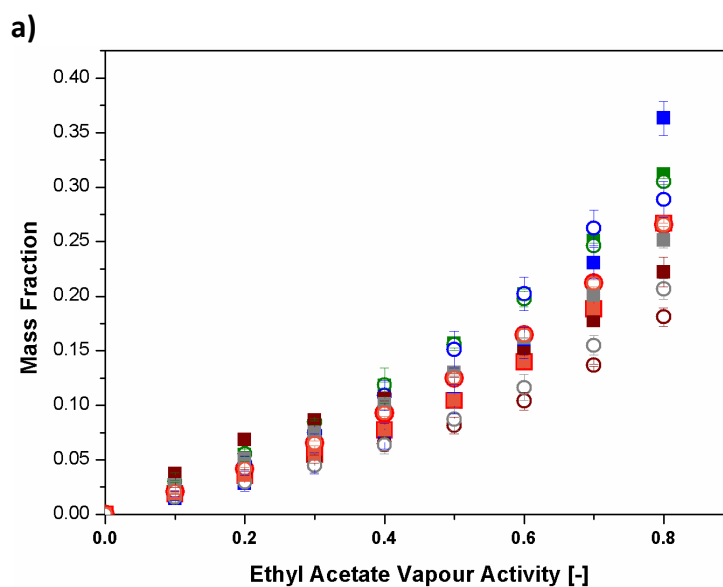


Figure 7. 12 Pebax2533-[BMIM][Tf₂N] ultra-thin film deposition before and after exposure to hexane vapour.

7.3.4 Ethyl Acetate and toluene

For the cases of ethyl acetate and toluene none of the composite materials experience any dramatic difference of sorption behaviour in comparison with the pristine polymer as can be observed in Figure 7. 13 and Figure 7. 14, respectively.



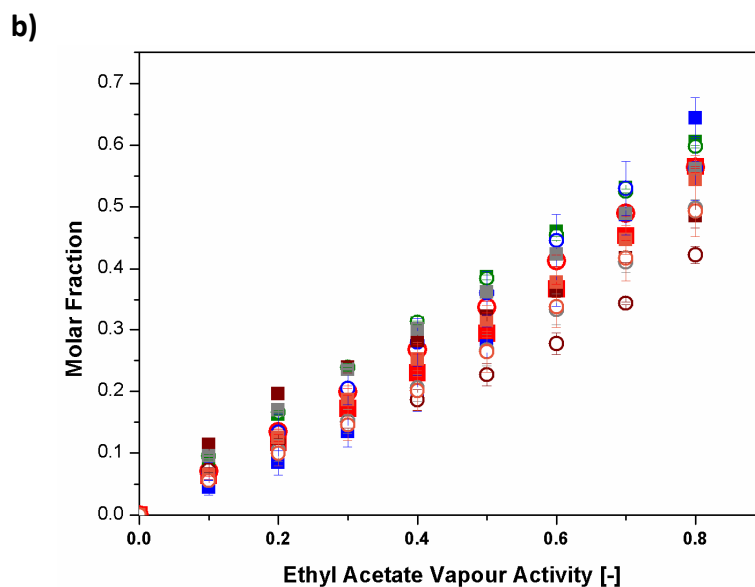


Figure 7. 13 Vapour sorption of pristine and Pebax2533-IL blend membranes expressed in **a)** as mass and **b)** molar fractions when exposed to a gradient of vapour activities of ethyl acetate. Red for pristine Pebax®2533, green Pebax-[C₈MIM][Cl], blue Pebax- [BMIM][BF₄], brown Pebax-[BMIM][Ac], grey Pebax-[BMIM][Tf₂N] and orange Pebax- [TMG][BF₄]. Filled squares for overtone number 5 and open circles for overtone number 11

Table 7. 3 show for ethyl acetate that the difference in the sorption values obtained by the two methods is even higher than in the case of water. Here again, QCM-D overestimates the results obtained. It is obvious then that the experimental conditions of the technique employed gain great importance in the final results due to the possible rearrangement or modifications in the material structure as a consequence of the vapour sorption.

Using QCM-D as a method for evaluating the effect of vapour sorption in thin polymer/IL blend membranes

Table 7. 3 Ethyl acetate vapour sorption data for pristine Pebax®2533 and mixed membranes expressed in mass fraction and mole fraction determined by Cahn electrobalance (data taken from Chapter 4 in white) and QCM-D (data in red).

	ETHYL ACETATE			
	Mole Fraction (x_i)		Mass Fraction (w_i)	
Pebax®2533	0.11	0.56	0.04	0.27
Pebax2533-[C ₈ MIM][Cl]	0.10	0.60	0.03	0.31
Pebax2533-[BMIM][BF ₄]	0.05	0.60	0.02	0.30
Pebax2533-[BMIM][Ac]	0.16	0.45	0.05	0.20
Pebax2533-[BMIM][Tf ₂ N]	0.23	0.51	0.07	0.23
Pebax2533-[TMG][BF ₄]	0.11	0.50	0.04	0.26

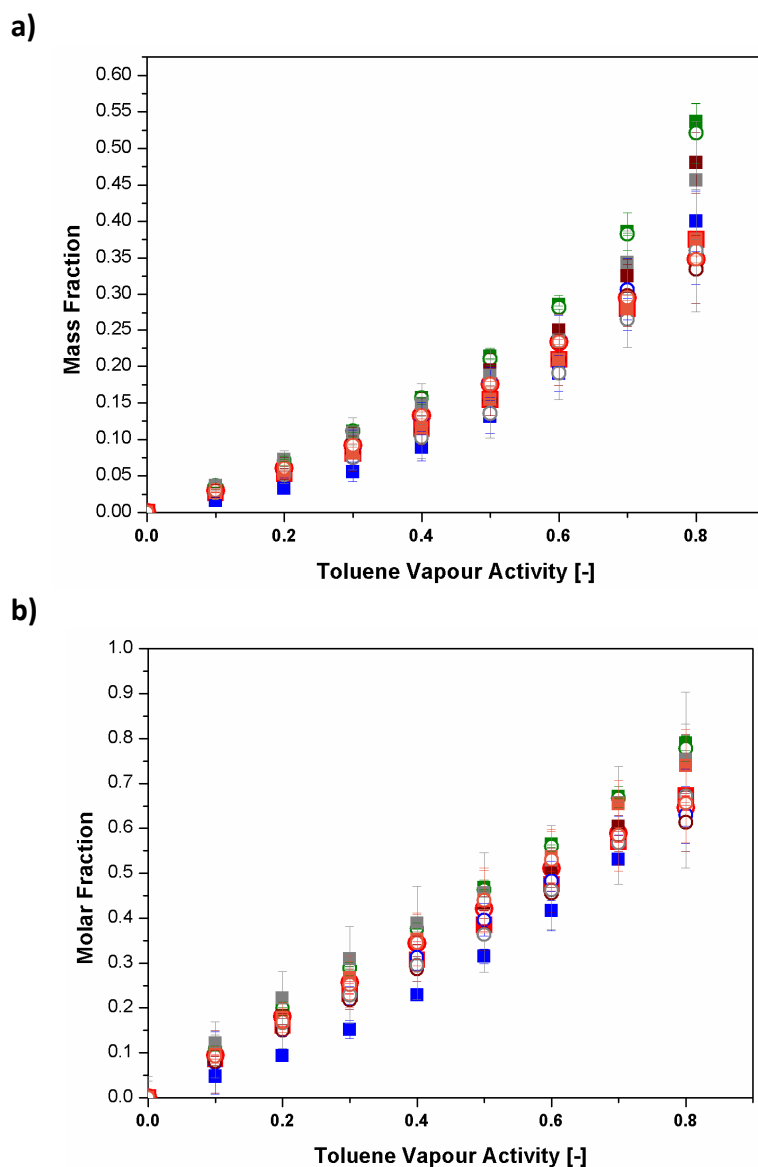


Figure 7. 14 Vapour sorption of pristine and Pebax2533-IL blend membranes expressed in **a)** as mass and **b)** molar fractions when exposed to a gradient of vapour activities of toluene. Red for pristine Pebax®2533, green Pebax-[C₈MIM][Cl], blue Pebax- [BMIM][BF₄], brown Pebax-[BMIM][Ac], grey Pebax-[BMIM][Tf₂N] and orange Pebax-[TMG][BF₄]. Filled squares for overtone number 5 and open circles for overtone number 11

It should be noted that Pebax2533-[BMIM][Ac] exhibits the lowest sorption in the case of ethyl acetate going along with a slight difference between its overtones. Hence, the concept of "like dissolves like" does not seem to apply in this case and confirms previous observations that the sorption of solutes in polymer-IL blends is a complex phenomenon.

In fact, Pebax2533-[BMIM][Ac] showed very high values for the frequency-normalized dissipation from low vapour activities on and indicating that the incorporation of ethyl acetate caused a certain rearrangement of the polymer chains and/or IL within the polymer/IL film. This is particularly notable in the 11th overtone depicting furthermore a tendency as a function of the vapour activity which is opposed to all others (see Figure 7. 15)

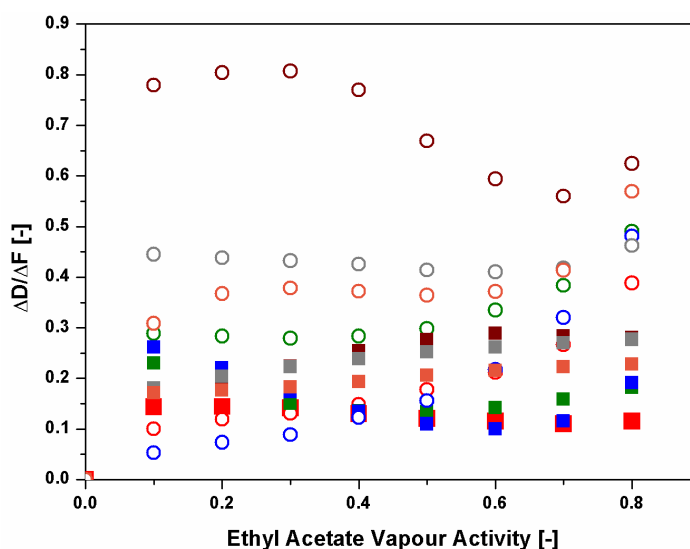


Figure 7. 15 Frequency-normalized dissipation as a function of the ethyl acetate vapour activity for the different membranes. Red for pristine Pebax®2533, green Pebax-[C₈MIM][Cl], blue Pebax-[BMIM][BF₄], brown Pebax-[BMIM][Ac], grey Pebax-[BMIM][Tf₂N] and orange Pebax-[TMG][BF₄]. Filled squares for overtone number 5 and open circles for overtone number 11.

In the case of toluene (Figure 7. 16), an increasing frequency-normalized dissipation is observed when increasing the toluene vapour activity while for lowest vapour activities

most polymer/IL blends show actually a lower frequency-normalized dissipation than the pristine polymer itself. This is interesting as apparently the polymer undergoes in some cases less swelling upon toluene sorption when containing IL.

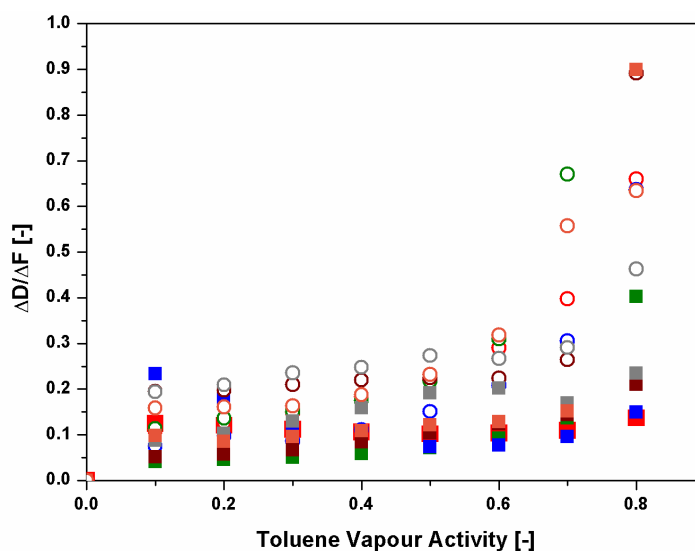


Figure 7. 16 Frequency-normalized dissipation as a function of the toluene vapour activity for the different membranes. Red for pristine Pebax®2533, green Pebax-[C₈MIM][Cl], blue Pebax-[BMIM][BF₄], brown Pebax-[BMIM][Ac], grey Pebax-[BMIM][Tf₂N] and orange Pebax-[TMG][BF₄]. Filled squares for overtone number 5 and open circles for overtone number 11.

As occurred in Chapter 3 (Figure 3.4), we observed how the incorporation of IL produced a variation in the permeability results upon different solvents. Here, from this chapter we can also get an idea of how the solubility to vapours gets also modified by ILs incorporation. In order to observe the evidence, a histogram of the blended membranes sorption is represented in Figure 7. 17 offset against the respective sorption of the pristine membrane (Pebax®2533) (hence, pristine membrane vapour sorptions become equal to zero).

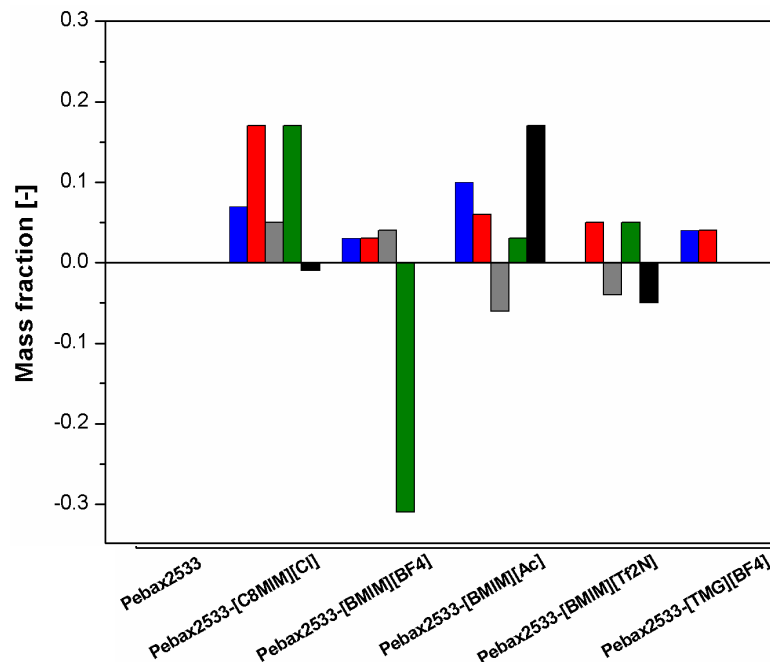


Figure 7. 17 Organic vapour QCM-D sorption experiments of the Pebax2533-IL membranes. Vapour sorptions in the Pebax2533 blends were offset against respective sorption of pristine Pebax®2533. Blue: water, red: ethanol, grey: ethyl acetate, black: toluene and green: hexane.

Here as well, it can be seen that the vapour sorption of the membranes varied depending on the nature of the IL incorporated in the block copolymer when being in contact with different vapours. Taking the values given by the pristine membrane as a reference, we observe how the membrane solubility is either increased or even decreased depending on the vapour studied. Most remarkable differences can be found between ethyl acetate and toluene; following to some extent some similarities with the permeability measurements studied in Chapter 3.

7.4 Conclusions

As commented before, D/F plots can provide complementary and in some cases non-expected and useful details concerning the vapour sorption in the different materials studied. By this technique we have been able to evaluate how the IL behave in such different way when being incorporated in the copolymer structure. Summarizing the data, we could say that for ethanol all the D/F data is relatively low in all cases; however when going on with water experiments, the results vary completely. The most outstanding results are noticed for Pebax2533-[BMIM][Tf₂N] and Pebax2533- [TMG][BF₄] where the first acquire negative D/F values as a consequence of the increase in the material rigidity and the latest experiments a decrease in the D/F values when increasing the vapour activity.

For the cases of ethyl acetate, hexane and toluene, the absolute data of D/F do not exceed a value of 1.0. Some of the IL blend membranes show specific high D/F results when being compared with the rest of the blends as it is the case of [BMIM][Tf₂N] for hexane and [BMIM][Ac] for ethyl acetate, however for the other cases the dispersion maintains into expected limits.

7.5 References

- [1] Y. Cen, C. Staudt-bickel, and R. N. Lichtenthaler, "Sorption properties of organic solvents in PEBA membranes," *J. Memb. Sci.*, vol. 206, pp. 341–349, **2002**.
- [2] L. de Barros Ferreira, "The feasibility of pervaporation in the purification of ethanol," *PhD Thesis*, pp. 1–328, **1998**.
- [3] J. I. Brauman and P. Szuromi, "Thin Films," *Science (80-.)*, vol. 273, no. 5277, p. 855, **1996**.
- [4] C. Frank, V. Rao, M. Despotopoulou, R. Pease, W. Hinsberg, R. Miller, and J. Rabolt, "Structure in Thin and Ultrathin Spin-Cast Polymer Films," *Science*, vol. 273, no. 5277, pp. 912–5, **1996**.

Chapter 8

Characterization of the free volume of block-copolymer/ionic liquid composite membranes by PALS and X-ray diffraction

8.1	Introduction	265
8.2	Results and discussion	267
8.3	X Ray Diffraction and DSC measurements	279
8.4	Conclusions	287
8.5	References	289

8.1 Introduction

As expected in our initial hypothesis, the addition of ILs as a liquid phase into a solid polymer would enhance the diffusivity of solutes permeating the polymer. This would be the reason for the physico-chemical interaction of ILs with either PA or PE segments, resulting in the case of PA in less semi-crystallinity, or due to an increase of the free volume in the polymer. On the contrary, Chapter 4 has revealed that the permeability to several organic vapours has been improved, but it should be highlighted that this variation arises mainly from the variation in the solubility of the blend membrane being the diffusivity almost unchanged when compared to pristine Pebax®2533.

Then, in order to study how the incorporation of several different ILs into Pebax®2533 affected its morphology, we have used different analytical techniques such as positron annihilation lifetime spectroscopy (PALS), which probes the electron density distribution in the blend membrane and hence will give us an idea of the free volume of the sample; X-ray diffraction where the crystalline volume fraction and particle size can be determined and finally by DSC measurements where the glass transition temperature (T_g) of each sample will be measured and compared if they are reasonable in accordance to the T_g determined by PALS.

Bear in mind that polymer/IL composites can also be prepared either through melt processing or solvent casting, we also will shortly focus on whether the preparation method affects the physico-chemical properties (mainly vapour transport properties) and performance of the final product.

From the results obtained along this work, and mainly what it has been observed in Chapter 3, it becomes apparent that the interactions of the ILs are expected to take place mainly with the PA segments, and only to a very minor extent with the PE-segments. As a consequence, the incorporation of these different ILs in the Pebax®2533 polymeric matrix would therefore be expected to alter mainly the degree of semi-crystallinity of the polymer. However, such a decrease in crystallinity of PA-segments could possibly affect the

adjacent PE-phase as an indirect result of the presence of the IL, which then should also be observed through changes in the glass transition temperature of the PE-phase.

Positron annihilation spectroscopy is a well established technique for free volume investigations in polymers [1]–[4] and polymer nanocomposites [5]–[8]. PALS probes the electron density distribution by measuring the lifetime of the so called orthopositronium (o-Ps). The lifetime of o-Ps is the time from emission of a positron from a positron source until the decay of the o-Ps. Once a positron is emitted by a positron source, it has three different decay possibilities: it can either decay as a free positron; it can recombine with the electrons from the polymer; or it can form para-positronium (p-Ps) with an electron with antiparallel spin (single state) or orthopositronium (o-Ps) with an electron with a parallel spin (triplet state). The p-Ps has a short lifetime in vacuum of 125 ps, in contrast to the long living o-Ps, which decays via so-called pick-off annihilation with an electron from the walls of the free volume holes. The pick-off annihilation of the o-Ps depends on the local electron density distribution, and thus the o-Ps lifetime can be used to determine the average free volume hole size radius by applying a standard quantum mechanical model originally developed in literature [9]–[11]. In this model, the o-Ps is assumed to be confined in a spherical potential well with an electron layer at its wall where it can decay by pick-off annihilation. The calculation of the overlap integral of the positronium probability density function and the electron layer leads to a direct relationship between the o-Ps lifetime (τ_3) and the average free volume hole radius (r) which is shown in Equation 8. 1, where it is assumed that o-Ps is confined in spherical holes (free volume cavities) with infinitely high walls:

Equation 8. 1
$$\tau_{o-Ps} = \lambda_0^{-1} \left(1 - \frac{R_h}{R_h + \delta R} + \frac{1}{2\pi} \sin \frac{2\pi R_h}{R_h + \delta R} \right)^{-1}$$

This equation includes the reciprocal o-Ps decay rate τ_3 , the spin averaged decay rate in the electron layer at the edge of the potential well, λ_0 , the thickness of the electron layer, which has been determined by using materials with a well known pore size [12] [$\delta R = 0.166$ nm] and the average free volume hole radius, R_h . Further information can be obtained from the intensities, which are the relative probabilities of the three decay possibilities. The positronium intensities (o-Ps and p-Ps) depend on the formation probability of positronium in the respective polymeric material, which are not known a priori and are often also related to the hole concentration [4]. The measured o-Ps intensity is proportional to the amount of polymer encountered by the positrons as well as to positronium formation probability.

8.2 Results and discussion

8.2.1 PALS measurements

The free volume in a polymeric membrane is generally considered as a determinant factor for the diffusion of molecules or their molecular mobility. Several studies have related the free volume with the transport mechanism of gas molecules through membranes [10], [13]–[15], demonstrating that an increase in free volume in general coincides with increased solute diffusivities. In order to measure the free volume in pristine Pebax®2533 and Pebax2533-IL composites, we carried out temperature dependent lifetime measurements with temperature ranging from -170°C to 20°C . All samples showed two clear transitions in Figure 8. 1, one at about -90°C , and the second one at about 0°C . Therefore three different regions can be distinguished: below -90°C , the material is in its glassy state; in the second, between -90 and 20°C , the polymer composite behaves as a

rubber; and in the last region, above 20°C, the “kink” temperature dependence of the o-Ps lifetime can be observed. Above this temperature, the vibration frequency of the polymer chains is in the same order of magnitude or even shorter than the reciprocal of the o-Ps lifetime (abbreviated with τ_3). As a consequence, the polymer cavities (free volume) are not stable on the time scale of the PALS measurement.

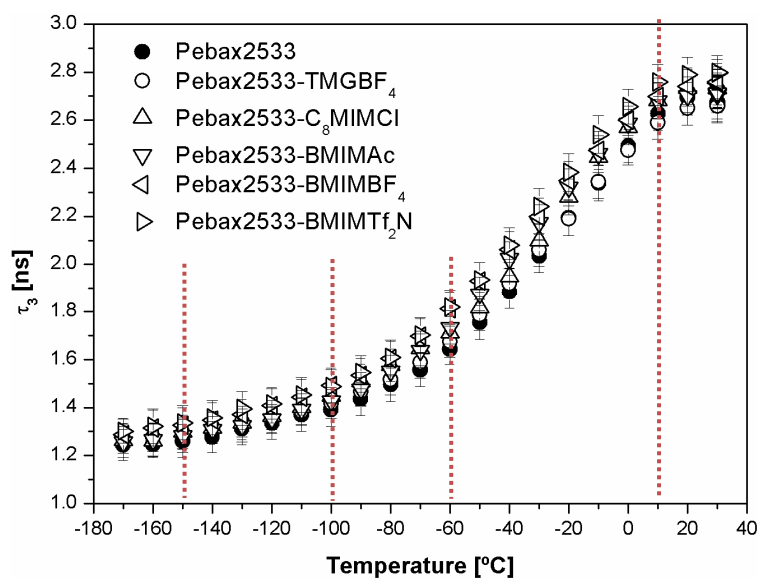


Figure 8. 1 o-Ps lifetime versus temperature for pure Pebax®2533 and Pebax2533/IL mixtures

Since there exist two main temperature ranges during these PALS experiments, the determination of the free volume cavities will accordingly yield distinct o-Ps lifetimes (τ_3) because the mobility of the polymer chains, and hence cavity stability, will differ. Thus, we denote with “ τ_3 (low T)” for the temperature range between -150 to 100°C, while “ τ_3 (high T)” denotes the o-Ps lifetime in the temperature range between -60 to 10°C. The absolute values of both lifetimes naturally differ; however, it could be observed that they qualitatively follow a similar tendency (Figure 8. 2), except for a minor deviation of Pebax2533-[BMIM][Ac]. Therefore, and since our interest was to characterize the free

volume at a temperature as close as possible to the operating temperature (RT) of the polymer and polymer blends without reaching the kink temperature, we focused in the following only on results from the high temperature range.

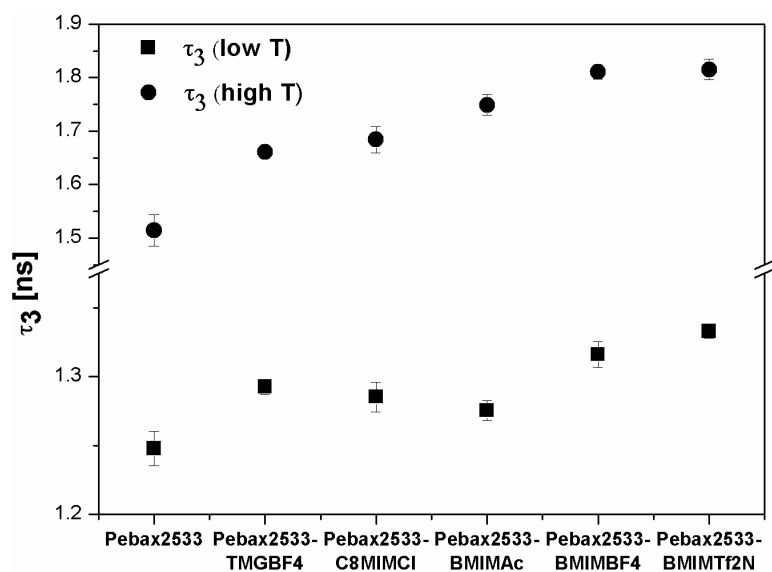


Figure 8. 2 o-Ps lifetime vs Polymer-IL composites in the range of low and high T

Figure 8. 2 furthermore evidences that irrespective of the IL incorporated, an increase of the o-Ps lifetime is observed as compared to the pristine polymer. When comparing the blend membranes' lifetime with that of the pristine Pebax[®]2533, it can be seen that data of τ_3 (low T) vary from 1.2490 ns to 1.3332 ns for the case of Pebax2533-[BMIM][Tf₂N] (a change of 6.7%), while the values of τ_3 (high T) undergo larger changes, from 1.5145ns for Pebax[®]2533 up to 1.8150 ns in Pebax2533-[BMIM][Tf₂N] blend membranes (a change of 19.8%).

For better visualization all the values have been compiled in Table 8. 1:

Table 8. 1 o-*Ps* lifetime [ns] in each IL blend membrane and their percentage [%] of variation with reference to Pebax®2533 membrane

	τ_3 [ns] (low T)	τ_3 [ns] (high T)	[%] variation (low T)	[%] variation (high T)
Pebax®2533	1.2490	1.5145	-----	-----
Pebax2533- [TMG][BF₄]	1.2928	1.6611	3.5	9.7
Pebax2533- [C₈MIM][Cl]	1.2850	1.6840	2.9	11.2
Pebax2533- [BMIM][Ac]	1.2759	1.7489	2.2	15.5
Pebax2533- [BMIM][BF₄]	1.3163	1.8105	5.4	19.5
Pebax2533- [BMIM][Tf₂N]	1.3332	1.8151	6.7	19.8

This is most probably due to the fact that at low temperature the IL is in a glassy rather than a liquid state, which as a consequence results in a smaller volume of blend polymer cavities. It is noteworthy to remark that [BMIM][Tf₂N], being the only IL with an hydrophobic nature causes the biggest increase in the free volume. But are these experimental values in agreement with the “mixing rule” by taking each percentage (80% for the case of Pebax®2533 and 20% for each IL)?

Characterization of the free volume of block-copolymer/ionic liquid composite membranes by PALS and X-ray diffraction

Table 8. 2 o-Ps lifetime [ns] experimentally measured and calculated based on the “mixing rule” of each component

	τ_3 [ns] (low T)- experimen tal	τ_3 [ns] (low T)- mixing rule: ($0.8 \cdot \tau_3$ Pebax [®] 2533) + ($0.2 \cdot \tau_3$ IL)	τ_3 [ns] (high T)- experim ental	τ_3 [ns] (high T)- mixing rule ($0.8 \cdot \tau_3$ Pebax [®] 2533) + ($0.2 \cdot \tau_3$ IL)
Pebax[®]2533	1.2490		1.5145	
Pebax2533- [TMG][BF₄]	1.2928	(not detected)	1.6611	(not detected)
Pebax2533- [C₈MIM][Cl]	1.2850	1.29382	1.6840	1.6941
Pebax2533- [BMIM][Ac]	1.2759	1.3066	1.7489	1.6552
Pebax2533- [BMIM][BF₄]	1.3163	1.3063	1.8105	1.6770
Pebax2533- [BMIM][Tf₂N]	1.3332	1.3885	1.8151	1.7919

It is observed how in Pebax2533-[BMIM][Ac] and Pebax2533-[BMIM][Tf₂N] blend membranes, the experimental results are considerably underestimating the “mixing rule” at low T; on the contrary, for the cases of Pebax2533-[BMIM][Ac] and Pebax2533-[BMIM][BF₄] at high T, they overestimate the already cited mixing rule.

Annihilation spectra yield two parameters, the lifetime of the positronium (τ_3) and its intensity (I_3), both of which are associated with certain properties of the free volume where the positron annihilates. The positron lifetime depends on the size of the free volume, whereas the intensity may reflect the positronium formation probability. The evaluation of the free volume of pristine Pebax®2533 and its blend membranes with respect to τ_3 (left axis) and intensity (right axis) determined at high temperature is depicted in Figure 8. 3. The error bars have been determined from statistics on the fit.

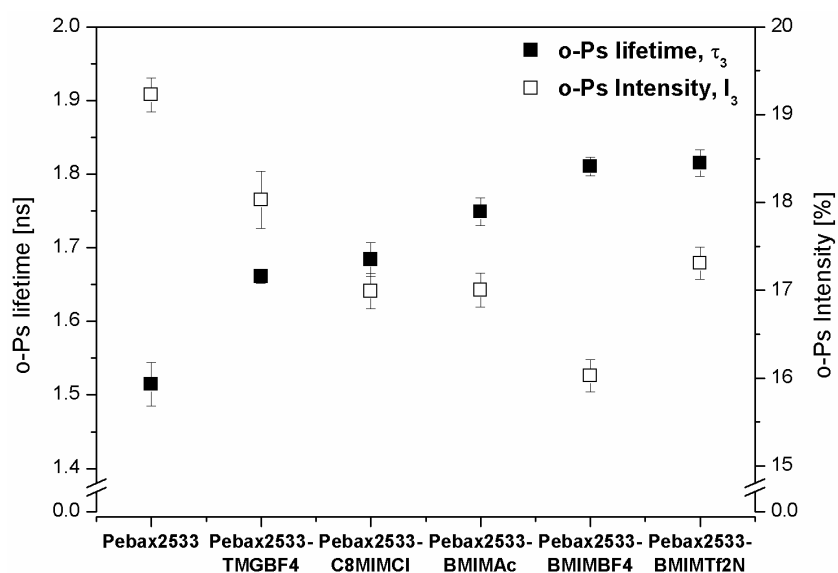


Figure 8. 3 o-Ps lifetime at high T (Y1 axis) and o-Ps intensity (Y2 axis) vs pristine Pebax®2533 and IL-blended membranes.

Interestingly, the increase in the lifetime when incorporating ILs goes anti-proportionally along with a decrease in intensities for all hydrophilic ILs. This could be interpreted as an increase in free volume cavities, however, on the cost of their number. Only the incorporation of the hydrophobic IL [BMIM][Tf₂N] results in a somewhat higher intensity than would be expected from the lifetime which hints at a possibly different actuation as a plasticizer than the hydrophilic ILs. Similar observations have been made previously [16] although to a much lesser extent, when PEG was added as plasticizer to a slightly

different kind of block-copolymer. In that case, the decrease in o-Ps intensity and increase in the lifetime were rather small while in our case the incorporation of ILs produces a bigger effect in both parameters.

According to Equation 8. 1, the lifetime of pristine Pebax[®]2533 of 1.51 ns corresponds to an average hole radius of 0.24 nm and an average hole volume of 0.06 nm³. In contrast, in the case of Pebax2533-[BMIM][Tf₂N] blend membranes for which the biggest increase in the free volume was observed, the respective o-Ps lifetime of 1.82 ns corresponds to an average hole radius of 0.27 nm and an average hole volume of 0.08 nm³. (See Table 8. 3)

Table 8. 3 Summary of the data obtained from PALS (high temperature interval): positron lifetime τ_3 , its error, the average radius, the resulting free volumen with its error and the increase of the free volume which is obtained by incorporating the respective IL into the polymer.

	τ_3 [ns]	τ_3 Error [ns]	Radius [nm]	Vol. [nm ³]	Increase Vol. [%]
Pebax[®]2533	1.5145	0.0295	0.2364	0.0554	
Pebax2533- [C₈MIM][Cl]	1.6840	0.0229	0.2544	0.0690	20
Pebax2533- [BMIM][Ac]	1.7490	0.0185	0.2613	0.0748	26
Pebax2533- [BMIM][BF₄]	1.8109	0.0128	0.2679	0.0805	31
Pebax2533- [BMIM][Tf₂N]	1.8157	0.0178	0.2684	0.0810	32
Pebax2533- [TMG][BF₄]	1.6611	0.0097	0.2520	0.0670	17

Figure 8. 3 corroborates that the ILs studied increase the average free volume of the block copolymer, with the error of the data being extremely low. Based on this observation, we speculated on how the IL accommodates within the polymer. Our hypothesis was that IL molecules would locate in the free space between polymer chains of the copolymer resulting in an increase of the free volume of the IL-blended membranes. On the other hand, it is known that ILs themselves possess a free volume as reported in literature [17]–[20]. We therefore determined first the total free volume in four of the five pristine ILs with the results depicted in Figure 8. 4:

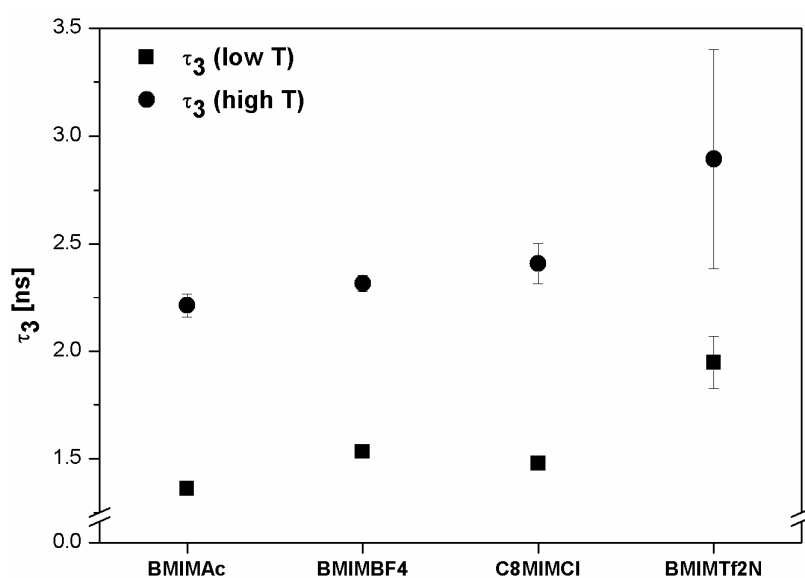


Figure 8. 4 τ_3 vs pure IL in the range of low and high T

Figure 8. 4 represents the lifetime of the pristine ILs tested in both temperature ranges. For the ILs [BMIM][BF₄] and [BMIM][Tf₂N] reference data can be found in literature showing that the values obtained at high T are slightly lower than the data from literature [20], while the ones obtained at lower T, fit better since the working temperature between both experiments are more approximated. It is observed that while τ_3 in polymer-IL blends did

Characterization of the free volume of block-copolymer/ionic liquid composite membranes by PALS and X-ray diffraction

not exceed 1.81 ns, in pure ILs it is about ~2.5 ns. According to Tao Eldrup model, the Pebax®2533 and Pebax-IL blend membrane's free volume is about to be between ~0.05 and 0.08nm³ while in the case of ILs, it is in the range of ~0.12 and 0.19 nm³ respectively. Hence, the free volume of the ILs is actually bigger than the free volume of Pebax®2533.

Table 8. 4 Summary of the data obtained from PALS (high temperature interval) for the ILs; for comparison reason, the free volume of the blend membrane, measured and calculated, is listed with data already shown in Table 1 except the respective data for Pebax®2533. The calculated volume of the blend membrane (second but last column) was determined by Vol=0.8*Vol(Pebax®2533)+0.2*Vol(IL). The theoretical volume fraction calculated of IL was determined using the SOLVER function of Excel and indicates the volume of IL theoretically to be expected if the free volume of both the polymer and IL were merely additive, i.e., both phases do not interact.

	τ_3 IL [ns]	τ_3 Error IL [ns]	Vol [nm ³]	Blend membrane volume, measured [nm ³] (from Figure 8. 3)	Blend membrane free volume theoretically calculated mixing rule [nm ³]	Free Volume measured/ calculated
[C₈MIM][Cl]	2.4097	0.0935	0.1378	0.0690	0.0719	0.96
[BMIM][Ac]	2.2133	0.0554	0.1193	0.0748	0.0682	1.10
[BMIM][BF₄]	2.3177	0.0380	0.1289	0.0805	0.0701	1.15
[BMIM][Tf₂N]	2.8943	0.5061	0.1914	0.0810	0.0826	0.98

This could hint to the intrinsic free volume of the IL itself contributing to an overall increased average free volume of the polymer/IL blend polymer, rather than an increase of the polymer free volume through interaction with the IL. Since PALS determines the

average free volume without providing direct information on how the IL accommodates within the polymer matrix, this could in an extreme case mean that both the IL and the polymer phase “co-exist” with their respective free volume but without interacting. In order to verify this hypothesis, we therefore calculated again the arithmetical average of the free volume based on the values measured for each phase, respectively, and assuming the blend polymer to consist of 80 wt% of Pebax®2533 and 20 wt% of IL. We hereby would consider both phases simply co-existing and not interacting, at all. Table 8. 4 lists the individual volumes for the free volume measured and calculated for the ILs, and for each blended membrane, respectively.

As can be seen in Table 8. 4, the arithmetically determined volume (“Blend membrane free volume theoretically calculated mixing rule.”) overestimates the experimental one (Blend membrane volume measured) for all ILs. The theoretically required volume fraction of IL was calculated in order to make the measured and calculated blend membrane values coincide on the basis of a mere arithmetic mean (=no interaction). As can be seen in the last column of Figure 8. 3, [BMIM][BF₄] was hereby within 10% of the expected volume fraction of 0.2, with the other ILs deviate increasingly in the order [BMIM][Ac], [BMIM][Tf₂N] and [C₈MIM][Cl]. [BMIM][BF₄] is hence the IL which interacts less with the polymer phases as is evidenced by an overall free volume close to a mere weighted addition of the respective free volumes. In contrast, [C₈MIM][Cl] is the IL that supposedly interacts most given that the overall free volume measured is 25% less than what would be expected from weighted addition of the respective free volumes. In other words, the presence of the IL in the polymer phase increases the average free volume, however, primarily owing to its own larger free volume and for most ILs studied even to less an extent than would be expected if both phases were co-existing. Hence, for all ILs studied (possibly except [BMIM][BF₄]), the IL interacts with the polymer such as to actually yield a smaller average free volume than could be expected if the IL acted indeed as a plasticizer.

*Characterization of the free volume of block-copolymer/ionic liquid composite membranes
by PALS and X-ray diffraction*

Based on this observation, and in order to better understand how the IL could possibly arrange within the polymer matrix, it is helpful to refer to the actual dimensions of the IL.

The molecular volume of each IL was calculated based on the equation $V = M_w \cdot N_A \cdot \rho$, and for comparison reasons listed them together with the free volume determined by PALS in (Table 8. 5, see also Figure 8. 5).

Table 8. 5 Molecular volume of ILs (theoretically calculated) compared with their free volume experimentally measured by PALS; for comparison reasons: the free volume of Pebax® 2533 was determined to be 201.7 Å³.

	Molec. Volume [Å³]	Free Volume determined by PALS [Å³]
[C₈MIM][Cl]	383	368.7
[BMIM][Tf₂N]	485	419.7
[BMIM][BF₄]	321	359.0
[BMIM][Ac]	312	348.0
[TMG][BF₄]	375	n.d.

The data listed in Table 8. 5 evidence that the molecular volume of each IL is significantly bigger than the free volume of Pebax®2533. This means that the IL may interact with the polymer, but certainly not accommodate within its free volume, as was our initial hypothesis. Again, this hints at the possibility of a co-existence of both phases. Figure 8. 5 demonstrates that in fact a linear tendency exists between individual data sets relating the molecular volume of the IL and its free volume. Data from our studies (blue line) as well as the data obtained by other researchers (red line) [18], reveal that the bigger the molecules

of the IL, the bigger is the free volume observed by PALS. This might be due to the difficulty in their molecular packing.

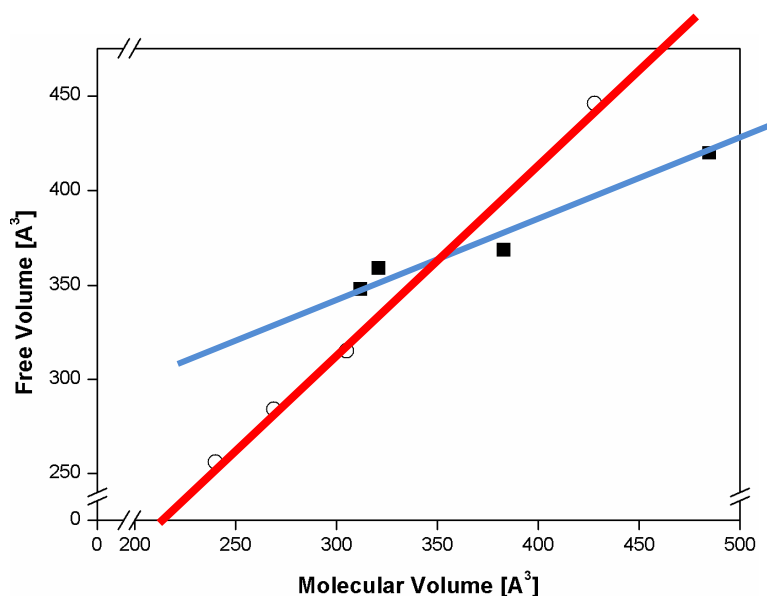


Figure 8. 5 Representation of free volume (\AA^3) determined by PALS as a function of the molecular volume (\AA^3) of each IL. (■ data obtained in this study; ○ data from W.Beichel).

Thus, in view of the results obtained where the free volume in polymer-IL blended membranes increased in comparison to pristine Pebax®2533 but less than would be expected from averaging the free volume of both, and accounting for the impossibility for any IL to settle within the cavities of the polymer matrix owing to their dimensions, we reach two main preliminary conclusions:

IL clusters may be coexisting with the polymer with which the degree of interaction depends on the individual IL. No “swelling” effect is exerted by the IL, on the contrary: for some ILs, the interactions with the polymer matrix apparently result in a smaller averaged free volume than would be expected theoretically.

This behavior depends on the physico-chemical properties of the IL added. According to PALS it was observed that both [C₈MIM][Cl] and [BMIM][Tf₂N] would be the ILs that most modify/interact with the co-polymer structure, while [BMIM][BF₄] and Pebax[®]2533 seem to behave as two fully independent phases.

It is noteworthy that the increase in the percentage of free volume average varying from 17% in the case of Pebax2533-[TMG][BF₄] to 32% in Pebax2533-[BMIM][Tf₂N] blended membranes (Table 8. 3) can be related with the permeability data obtained in gas permeation tests, where as an example, in the case of Pebax2533-[BMIM][BF₄] composites, the permeability increased in the specific case of toluene by around 7% which could be in the order of magnitude of the change in free volume.

In order to elucidate further to what degree the IL interacts with the base polymer, if at all, X-Ray diffraction and DSC measurements were carried out and the results presented in the following.

8.2.2 X Ray Diffraction and DSC measurements

Effect on crystallinity when adding different ILs to Pebax[®]2533 by casting method

8.2.2.1 PA phase

The interest of this work was in determining first to what extent interactions of IL with polymer segments might change the degree of semi-crystallinity of the PA phase. X-Ray measurements have been employed for this purpose and values measured were compared with those obtained from DSC measurements.

At room temperature, the PE-phase of Pebax[®]2533 is already in the amorphous state. Therefore, in the following we will only focus on the change of the semi-crystallinity of the

PA-phase owing to the presence of ILs which at this temperature were all in the liquid state.

The semi-crystallinity of Pebax®2533 copolymer was calculated by **Equation 8. 2** at room temperature accounting for the PA-12 crystallinity, only, because PTMO has a melting point below room temperature and assuming that the heat of fusion for pure PA-12 is 246 J/g.

$$\text{Equation 8. 2} \quad X_c = \frac{\Delta H_f}{w_{PA} \cdot \Delta H_{f0}}$$

Results observed are listed in Table 8. 6. It is emphasized that the data below refer predominantly to the PA-phase:

Table 8. 6 Summary of semi-crystallinity values obtained by X-ray diffraction and DSC.

	X-Ray X_c [%]	DSC X_c [%]
Pebax® 2533	21±2	12±2
Pebax2533-[BMIM][Tf₂N]	15±2	12±2
Pebax2533-[BMIM][BF₄]	13±2	10±2
Pebax2533-[C₈MIM][Cl]	11±2	11±2
Pebax2533-[BMIM][Ac]	11±2	10±2
Pebax2533-[TMG][BF₄]	11±2	8±2

Characterization of the free volume of block-copolymer/ionic liquid composite membranes by PALS and X-ray diffraction

Raw data from X-Ray diffractograms can be seen in Annex 8.2. The error of the crystallinity measured by DSC was considered to be of ± 2 , meaning that most of the DSC data (with exception of Pebax2533-[TMG][BF₄]) were around the same value of semi-crystallinity. This error was determined by selecting for three times the ΔH_f in each melting peak of the PA. As the baseline was not well defined, the values provided can consequently lead to different crystallinity values, which translates into a significant error. Clearer differences in crystallinity could be observed from X-ray diffraction data.

From Table 8. 4, it was observed/concluded that regardless the structure and physico-chemical properties of the IL incorporated in the polymer matrix, the semi-crystallinity of the polymer was reduced in all cases. The ILs studied acted, hence, as plasticizers when incorporated in the polymer matrix of Pebax[®]2533 [21]. A similar observation was made by C-W. Liew et al [22] where the addition of ILs induced a higher molecular motion of polymer chains reducing the degree of semi-crystallinity. This was corroborated by the melting and crystallization temperature of the PA segments as determined by DSC experiments in Chapter 3. T_m was determined as the maximum value of the PA melting peak and as such has a minimum error associated. As can be seen Table 8. 7, the T_m and T_c of all polymer-IL composites values suffer a shift to lower temperatures compared to the pristine polymer. This indicates a less perfect lamellar structure during melting, and a hindered formation of the crystals during the cooling step owing to the presence of the IL. Interestingly, the two ILs that lower T_m and T_c most are the ones that to some degree can undergo hydrophobic interactions: [BMIM][Tf₂N] and [C₈MIM][Cl]. These two ILs were also the ones that were identified during PALS experiments as the ILs that seemingly interacted most with the base polymer (Table 8. 7).

Table 8. 7: DSC experiments: Melting temperature and crystallization temperature of the PA-phase and the change in T_m and T_c owing to presence of IL when compared to the pristine polymer. Data obtained from DSC experiments in San Sebastián.

	T_m [°C]	ΔT_m [DSC]	T_{crist} [°C]	ΔT_{crist} [DSC]
Pebax®2533	141.3		45	
Pebax2533- [BMIM][Tf₂N]	122.4	-18.9	14.2	30.8
Pebax2533- [BMIM][BF₄]	136.1	-5.2	42.9	2.1
Pebax2533- [C₈MIM][Cl]	125.8	-15.5	25.3	19.7
Pebax2533- [BMIM][Ac]	131.5	-9.8	32.3	12.7
Pebax2533- [TMG][BF₄]	134.3	-7	39.3	5.7

Hence, we can postulate three options of how particularly [C₈MIM][Cl] and [BMIM][Tf₂N] can interfere with the semi-crystalline PA-phase: (1) through direct interaction which is more probable for [C₈MIM][Cl] given that it is hydrophilic while [BMIM][Tf₂N] is hydrophobic; (2) through steric hindrance with either IL constituting an “impurity” within the PA-phase that hinders crystallization, or (3) indirectly, through increasing the mobility of the PE-phase which in turn could then mix to a higher degree with the PA-phase. As regards option (1) and (2), previous ¹³C-NMR experiments have shown a downfield shift for the PA carbonyl group only in presence [BMIM][Tf₂N], which could result from the electronegativity of the nitrogen in [BMIM][Tf₂N]. No such shift was observed in the case of

[C₈MIM][Cl] despite its halide anion. However, from all ILs studied, only the latter caused a downfield shift in the methyl carbons of the polyether and possibly also in the methyl carbons of the PA-phase (in ¹³C-NMR, we cannot distinguish between both). This indicates that [BMIM][Tf₂N] is the only IL that acts directly on the PA-phase while [C₈MIM][Cl] acts only or also indirectly through interactions with the PE-phase. The latter is investigated in more detail in the following.

8.2.2.2 PE phase

The glass transition temperature (T_g) is related to the local segmental motion of polymer chains. When introducing plasticizing agents into a polymer, they may be conceived as intercalating with the polymer chains, in this way increasing the polymer chain mobility and consequently lower T_g . Scott et al. [21] demonstrated that [BMIM][PF₆] and [HMIM][PF₆] were excellent plasticizers for PMMA as they reduced the glass transition temperature while improving the thermal stability. On the contrary, anti-plasticizing agents reduce polymer chain mobility and thus increase T_g . As for the role of ILs in polymer/IL blends, we expect that ILs act as plasticizers [23].

However, depending on which technique selected for the determination of the glass transition temperature, big differences are observed. Such differences reside in the interval of temperature selected in PALS spectra. Varying this range (see data in Table 8. 8), the T_g can differ up to 11°C (Table 8. 8, column on PALS data).

Table 8. 8 Glass transition temperature T_g of the PE-phase determined by PALS (minimum and maximum temperature indicated as the values possess a big error) and by DSC. For DSC data, the increase/decrease with regard to the pristine polymer is listed (last column).

	T_g PALS [°C]		T_g DSC [°C]	ΔT_g DSC [°C]	T_m (IL) [°C]
Pebax®2533	-74	-70	-78		
Pebax2533- [BMIM][Tf₂N]	-81.3	-79	-75	3	-4
Pebax2533- [BMIM][BF₄]	-82.6	-76.3	-79	-1	-82
Pebax2533- [C₈MIM][Cl]	-75	-69.5	-81	-3	-82
Pebax2533- [BMIM][Ac]	-80.9	-75.3	-77	1	<-20
Pebax2533- [TMG][BF₄]	-85	-73.2	-77	1	----

Based on DSC data, the biggest increase of the T_g of the PE-phase was observed in the case of [BMIM][Tf₂N], but it still only reached a $\Delta T_g = 3^\circ\text{C}$. More significant variations of T_g have been observed in literature [24], where PEG has been used as plasticizer at 20 wt% resulting in a variation of T_g of $\sim 30^\circ\text{C}$. This leads to the conclusion that the previously decrease of semi-crystallinity is due to direct interference of the IL with the PA-phase rather than an indirect action. It should be noted that both phases of the block copolymer (PA and PE) are not totally independent. It is noteworthy that the T_g of the PTMO homopolymer (PE phase) is reported to amount to -82°C . Thus, with Pebax® 2533 exhibiting a T_g of -78°C and a reported microphase separation between both the PE and PA-segments, the IL could possibly act as a “linker” of both phases in presence of significant interactions.

*Characterization of the free volume of block-copolymer/ionic liquid composite membranes
by PALS and X-ray diffraction*

The data presented seem to suggest that interactions are not sufficiently strong such as the ILs chosen would act as what would intuitively be conceived as a “linker”.

This was confirmed by the melting and crystallinity temperature of the PE-phase in presence of ILs which did not suffer significant changes when adding ILs to the Pebax®2533 polymer matrix. Figures from DSC measurements in Chapter 3 depict the melting and crystallinity peaks respectively, with Table 8. 9 summarizing the data obtained for the PE phase. Minor variations were registered for T_m and T_c which could be considered in most cases being within the margin of error, except for the case of [BMIM][Tf₂N] which as the only hydrophobic IL proves to be the one that most modifies the structure of Pebax®2533.

Table 8. 9 Melting and crystallization temperature of the PE phase in the pristine polymer and the polymer/IL blends

	PE peak				
	ΔH_f [J/g]	T_m [°C]	ΔT_m [°C]	T_c [°C]	ΔT_c [°C]
Pebax®2533	25.1	10		-15	
Pebax2533-[BMIM][Tf₂N]	23.7	18.3	8.3	-13.0	2.0
Pebax2533-[BMIM][BF₄]	21.2	7.3	-3.7	-14.1	0.9
Pebax2533-[C₈MIM][Cl]	19.1	12.9	2.9	-14.7	0.3
Pebax2533-[BMIM][Ac]	18.4	13.2	3.2	-15.0	0.0
Pebax2533-[TMG][BF₄]	21.7	11.7	1.7	-14.5	0.5

8.2.2.3 Effect of membrane preparation method on crystallinity of the PA-phase

Polymer/IL composites may be prepared either by thermal compression (binary mixture) or through solvent casting (ternary mixture during casting). The presence of a solvent in the latter might affect how the IL distributes within the polymer matrix and as such might generate different degrees of crystallinity as compared to thermal compression where interactions take place solely between IL and the polymer. On the other hand, thermal compression might suffer from miscibility issues between both phases. Previous work has shown that thin films prepared by either route did not evidence any difference macroscopically, while vapour permeation studies showed higher permeabilities in compressed polymer films. Table 8. 10 summarizes the crystallinity values measured for both the pristine polymer and the polymer/IL blend (IL=[C₈MIM][Cl] as a case-study) obtained by solvent casting and thermal compression, respectively:

Table 8. 10 Summary of data on semi-crystallinity in solvent-cast membranes and compressed films, comparing both pristine Pebax®2533 and a Pebax2533-[C₈MIM][Cl] blend

	Xc Pebax®2533 cast [%]	Xc Pebax®2533 compressed [%]	Xc Pebax2533-[C ₈ MIM][Cl] cast [%]	Xc Pebax2533-[C ₈ MIM][Cl] compressed [%]
X-ray (Kiel)	21±2	17±2	11±2	14±2
DSC (San Seb.)	12±2	12±2	11±2	8±2
Literature	14% [25]	---	---	

From Table 8. 10 we observe that, within the analytical error, semi-crystallinity values obtained from X-ray diffraction are similarly independent of the preparation method for pristine polymer (21% and 17%) and the polymer/IL blend (11% and 14%), respectively. It can be observed from X-ray diffraction that the semi-crystallinity of the pristine polymer is somewhat lower in the compressed material (17%) than the one obtained by solvent casting (21%). This may be explained by the fact that thermal compressing is followed by a fast cooling step during which polymeric chains may not have enough time to re-orient and form the typical lamellae structure of the PA segments [26]. X-ray diffraction data for the Pebax2533-[C₈MIM][Cl] describe a reverse situation where the solvent cast material exhibits a slightly lower semi-crystallinity (11%) than the compressed one (14%) which might be the effect of a better mixing during casting, thus providing the opportunity for the IL to disperse more homogeneously within the polymer and thus more effectively interfere with the formation of the PA-lamellae. As regards DSC measurements, they yields again lower semi-crystallinity values than X-ray diffraction and for the Pebax2533-[C₈MIM][Cl] composite even an inverse result compared to X-ray diffraction (lower semi-crystallinity in the compressed than in the cast sample).

8.3 Conclusions

It has been shown that ILs can be incorporated as plasticizers in Pebax[®]2533 to form blend membranes. For all ILs studied, their addition to Pebax[®]2533 increased the overall free volume. However, this increase was found not to be a synergic effect but rather due to the intrinsically higher free volume of the IL itself. However, the average free volume as determined by PALS remained below the theoretically expected if averaging over both phases for the cases of Pebax2533-[C₈MIM][Cl] and Pebax2533-[BMIM][Tf₂N] while for Pebax2533-[BMIM][Ac] and Pebax2533-[BMIM][BF₄] an opposed behaviour was observed.

This suggests that the IL may interact with the base copolymer (bigger evidences for the cases of [C₈MIM][Cl] and [BMIM][Tf₂N]), but due to its volume it is not sterically possible to accommodate within its free volume.

The interpenetration between IL and the phases of the polymer is also evidenced in the decrease of the semi-crystallinity of the PA-phase (plasticization). While all ILs studied acted as plasticizers and followed within limits similar trends, differences could be detected depending on their physico-chemical properties. This draws the attention to the fact that as regards their interaction with polymers, ILs cannot be handled per se as a generalized group of compounds.

8.4 References

- [1] Mogensen O.E., "Positron Annihilation in Chemistry," *Springer*, **1995**.
- [2] C. Nagel, E. Schmidtke, K. Günther-Schade, D. Hofmann, §. D. Fritsch, A. T. Strunskus, and F. Faupel*, "Free Volume Distributions in Glassy Polymer Membranes: Comparison between Molecular Modeling and Experiments," **2000**.
- [3] C. Ohrt, K. Rätzke, N. Oshima, Y. Kobayashi, B. E. O'Rourke, R. Suzuki, A. Uedono, and F. Faupel, "Free Volume Profiles at Polymer–Solid Interfaces Probed by Focused Slow Positron Beam," *Macromolecules*, vol. 48, no. 5, pp. 1493–1498, **2015**.
- [4] Y. C. Jean, P. E. Mallon, and D. M. Schrader, "Principles and Applications of Positron and Positronium Chemistry," *WORLD Sci.*, **2003**.
- [5] G. Dlubek, U. De, J. Pionteck, N. Y. Arutyunov, M. Edelmann, and R. Krause-Rehberg, "Temperature Dependence of Free Volume in Pure and Silica-Filled Poly(dimethyl siloxane) from Positron Lifetime and PVT Experiments," *Macromol. Chem. Phys.*, vol. 206, no. 8, pp. 827–840, **2005**.
- [6] "Encyclopedia of Polymer Science and Technology," *John Wiley Sons, Inc.*, **2002**.
- [7] L. A. Utracki and A. M. Jamieson, "Polymer physics: from suspensions to nanocomposites and beyond," *Wiley*, p. 776, **2010**.
- [8] † Dana M. Sterescu, * Dimitrios F. Stamatialis, ‡ Eduardo Mendes, §. Jan Kruse, §. Klaus Rätzke, §. and Franz Faupel, and M. Wessling†, "Boltorn-Modified Poly(2,6-dimethyl-1,4-phenylene oxide) Gas Separation Membranes," **2007**.
- [9] S. J. Tao, "Positronium Annihilation in Molecular Substances," *J. Chem. Phys.*, vol.

- 56, no. 11, p. 5499, **1972**.
- [10] T. Koschine, K. Rätzke, F. Faupel, M. M. Khan, T. Emmler, V. Filiz, V. Abetz, L. Ravelli, and W. Egger, "Correlation of gas permeation and free volume in new and used high free volume thin film composite membranes," *J. Polym. Sci. Part B Polym. Phys.*, vol. 53, no. 3, pp. 213–217, **2015**.
- [11] C. Nagel, K. Günther-Schade, D. Fritsch, A. T. Strunskus, and F. Faupel*, "Free Volume and Transport Properties in Highly Selective Polymer Membranes," **2002**.
- [12] S. C. Sharma, *Positron annihilation: proceedings of the International Symposium on Positron Annihilation Studies of Fluids*. World Scientific, 1988.
- [13] Y. P. Yampolskii, I. Pinnau, and B. D. Freeman, "Materials science of membranes for gas and vapor separation," *Wiley*, p. 445, **2006**.
- [14] J. Kruse, K. Rätzke, F. Faupel, D. M. Sterescu, D. F. Stamatialis, and M. Wessling, "Free volume in C60 modified PPO polymer membranes by positron annihilation lifetime spectroscopy.," *J. Phys. Chem. B*, vol. 111, no. 50, pp. 13914–8, **2007**.
- [15] H. B. T. Jeazet, T. Koschine, C. Staudt, K. Raetzke, and C. Janiak, "Correlation of Gas Permeability in a Metal-Organic Framework MIL-101(Cr)-Polysulfone Mixed-Matrix Membrane with Free Volume Measurements by Positron Annihilation Lifetime Spectroscopy (PALS).," *Membranes (Basel)*, vol. 3, no. 4, pp. 331–53, **2013**.
- [16] W. Yave, A. Car, K.-V. Peinemann, M. Q. Shaikh, K. Rätzke, and F. Faupel, "Gas permeability and free volume in poly(amide-b-ethylene oxide)/polyethylene glycol blend membranes," *J. Memb. Sci.*, vol. 339, no. 1–2, pp. 177–183, **2009**.
- [17] M. S. Shannon, J. M. Tedstone, S. P. O. Danielsen, M. S. Hindman, A. C. Irvin, and J. E. Bara, "Free Volume as the Basis of Gas Solubility and Selectivity in Imidazolium-Based Ionic Liquids," *Ind. Eng. Chem. Res.*, vol. 51, no. 15, pp. 5565–5576, **2012**.

- [18] W. Beichel, Y. Yu, G. Dlubek, R. Krause-Rehberg, J. Pionteck, D. Pfefferkorn, S. Bulut, D. Bejan, C. Friedrich, and I. Krossing, "Free volume in ionic liquids: a connection of experimentally accessible observables from PALS and PVT experiments with the molecular structure from XRD data.," *Phys. Chem. Chem. Phys.*, vol. 15, no. 22, pp. 8821–30, **2013**.
- [19] Y. Yu, D. Bejan, and R. Krause-Rehberg, "Free volume investigation of imidazolium ionic liquids from positron lifetime spectroscopy," **2014**.
- [20] Y. Yu, W. Beichel, G. Dlubek, R. Krause-Rehberg, M. Paluch, J. Pionteck, D. Pfefferkorn, S. Bulut, C. Friedrich, N. Pogodina, I. Krossing, B. S. Lee, Y. S. Chi, J. K. Lee, I. S. Choi, C. E. Song, S. K. Namgoong, S. -g. Lee, R. D. Rogers, K. R. Seddon, K. R. Seddon, P. Wang, S. M. Zakeeruddin, R. Humphry-Baker, M. Grätzel, W. Xu, C. A. Angell, A. K. Doolittle, A. K. Doolittle, D. B. Doolittle, M. H. Cohen, D. Turnbull, D. Turnbull, M. H. Cohen, Y. P. Yampolskii, M. V. Motyakin, A. M. Wasserman, T. Masuda, M. Teraguchi, V. S. Khotimskii, B. D. Freeman, G. Golemme, J. B. Nagy, A. Fonseca, C. Algieri, Y. Yampolskii, R. J. Roe, J. J. Curro, P. M. Budd, N. B. McKeown, D. Fritsch, Y. P. Yampolskii, N. E. Kaliuzhnyi, S. G. Durgar'yan, Y. P. Yampolskii, G. Dlubek, J. Pionteck, Y. Yu, S. Thranert, M. Elsayed, E. Badawi, R. Krause-Rehberg, Y. Yu, G. Dlubek, R. Krause-Rehberg, M. Beiner, E. Hempel, G. Dlubek, M. Q. Shaikh, K. Ratzke, M. Paluch, F. Faupel, A. J. Hill, J. Huang, J. Efthimiadis, P. Meakin, M. Forsyth, D. R. MacFarlane, S. J. Pas, J. Huang, M. Forsyth, D. R. MacFarlane, A. J. Hill, J. H. Huang, A. Hill, M. Forsyth, D. MacFarlane, A. Hollenkamp, Y. Shekibi, A. Gray-Weale, D. R. MacFarlane, A. J. Hill, M. Forsyth, Y. Shekibi, S. J. Pas, N. M. Rocher, B. R. Clare, A. J. Hill, D. R. MacFarlane, M. Forsyth, T. Hirade, G. Dlubek, Y. Yu, R. Krause-Rehberg, W. Beichel, S. Bulut, N. Pogodina, I. Krossing, C. Friedrich, R. Fürth, D. Turnbull, M. H. Cohen, S. Bulut, P. Klose, I. Krossing, R. Simha, G. Carri, A. Bondi, C. Song, P. Wang, H. A. Makse, H. Tokuda, S. Tsuzuki, M. A. B. H. Susan, K. Hayamizu, M. Watanabe, R. G. Beaman, S. Sakka, J. D. Mackenzie, J. Kansy, S. J. Tao, M. Eldrup, D. Lightbody, J. N. Sherwood, G. Dlubek, J. Pionteck, K. Ratzke, J.

Kruse, F. Faupel, G. Dlubek, M. Q. Shaikh, K. Raetzke, F. Faupel, M. Paluch, C. P. Fredlake, J. M. Crosthwaite, D. G. Hert, S. N. V. K. Aki, J. F. Brennecke, H. Tokuda, K. Hayamizu, K. Ishii, M. A. B. H. Susan, M. Watanabe, H. Jin, B. O'Hare, J. Dong, S. Arzhantsev, G. A. Baker, J. F. Wishart, A. J. Benesi, M. Maroncelli, T. Nishida, Y. Tashiro, M. Yamamoto, A. Bondi, A. R. Choudhury, N. Winterton, A. Steiner, A. I. Cooper, K. A. Johnson, Y. U. Paulechka, G. J. Kabo, A. V. Blokhin, A. S. Shaplov, E. I. Lozinskaya, D. G. Golovanov, K. A. Lyssenko, A. A. Korlyukov, Y. S. Vygodskii, O. Yamamuro, Y. Minamimoto, Y. Inamura, S. Hayashi, H. -o. Hamaguchi, J. D. Holbrey, W. M. Reichert, M. Nieuwenhuyzen, S. Johnson, K. R. Seddon, R. D. Rogers, S. Saha, S. Hayashi, A. Kobayashi, H. -o. Hamaguchi, J. Karkkainen, J. Asikkala, R. S. Laitinen, M. K. Lajunen, S. M. Dibrov, J. K. Kochi, A. Triolo, A. Mandanici, O. Russina, V. Rodriguez-Mora, M. Cutroni, C. Hardacre, M. Nieuwenhuyzen, H.-J. Bleif, L. Keller, M. A. Ramos, G. J. Kabo, A. V. Blokhin, Y. U. Paulechka, A. G. Kabo, M. P. Shymanovich, J. W. Magee, R. Srithawatpong, Z. L. Peng, B. G. Olson, A. M. Jamieson, R. Simha, J. D. McGervey, T. R. Maier, A. F. Halasa, H. Ishida, M. Schmidt, M. Olsson, F. H. J. Maurer, D. Kilburn, G. Dlubek, J. Pionteck, D. Bamford, M. A. Alam, G. Dlubek, E. M. Hassan, R. Krause-Rehberg, J. Pionteck, G. Dlubek, J. Pionteck, M. Q. Shaikh, E. M. Hassan, R. Krause-Rehberg, G. Dlubek, M. Q. Shaikh, K. Raetzke, F. Faupel, J. Pionteck, M. Paluch, Schottky, G. Dlubek, A. Sen Gupta, J. Pionteck, R. Krause-Rehberg, H. Kaspar, K. H. Lochhaas, D. Kilburn, G. Dlubek, J. Pionteck, D. Bamford, M. A. Alam, H. Vogel, G. Tammann, W. Hesse, G. S. Fulcher, R. Fürth, R. Fürth, J. Klomfar, M. Soucková, J. Pátek, M. H. Ghatee, A. R. Zolghadr, D. Bamford, G. Dlubek, A. Reiche, M. A. Alam, W. Meyer, P. Galvosas, F. Rittig, D. Bamford, A. Reiche, G. Dlubek, F. Alloin, J. Y. Sanchez, M. A. Alam, J. T. Bendler, J. J. Fontanella, M. F. Shlesinger, J. T. Bendler, J. J. Fontanella, M. F. Shlesinger, M. C. Wintersgill, P. Eiden, S. Bulut, T. Kołchner, C. Friedrich, T. Schubert, I. Krossing, C. Schreiner, S. Zugmann, R. Hartl, H. J. Gores, A. Stoppa, O. Zech, W. Kunz, R. Buchner, A. B. Pereiro, J. L. Legido, A. Rodriguez, O. Zech, A. Stoppa, R. Buchner, W. Kunz, S. Bulut, P. Eiden, W. Beichel, J. M. Slattery, T. F. Beyersdorff, T. J. S. Schubert, I. Krossing, I. Krossing, J. M. Slattery, C. Daguinet, P. J. Dyson, A.

- Oleinikova, H. Weingärtner, H. D. B. Jenkins, H. K. Roobottom, J. Passmore, and L. Glasser, "Free volume and phase transitions of 1-butyl-3-methylimidazolium based ionic liquids from positron lifetime spectroscopy," *Phys. Chem. Chem. Phys.*, vol. 14, no. 19, p. 6856, **2012**.
- [21] M. P. Scott, C. S. Brazel, M. G. Benton, J. W. Mays, J. D. Holbrey, and R. D. Rogers, "Application of ionic liquids as plasticizers for poly(methyl methacrylate)," *Chem. Commun.*, no. 13, pp. 1370–1371, **2002**.
- [22] C. Ridings, V. Lockett, and G. Andersson, "Effect of the aliphatic chain length on electrical double layer formation at the liquid/vacuum interface in the [C(n)mim][BF₄] ionic liquid series.," *Phys. Chem. Chem. Phys.*, vol. 13, no. 38, pp. 17177–84, **2011**.
- [23] R. Casalini and C. M. Roland, "Alpha and beta relaxation and the excess wing in polychlorinated biphenyls," *Phys. Rev. B*, vol. 66, **2002**.
- [24] D. K. Pradhan, B. K. Samantaray, R. N. P. Choudhary, N. K. Karan, R. Thomas, and R. S. Katiyar, "Effect of plasticizer on structural and electrical properties of nanocomposite solid polymer electrolytes," *Ionics (Kiel)*, vol. 17, no. 2, pp. 127–134, **2011**.
- [25] V. I. Bondar, B. D. Freeman, and I. Pinnau, "Gas Sorption and Characterization of Poly (ether-b-amide)," *J. Polym. Sci. Part B Polym. Phys.*, vol. 37, pp. 2463–2475, **1999**.
- [26] S. Armstrong, B. Freeman, A. Hiltner, and E. Baer, "Gas permeability of melt-processed poly(ether block amide) copolymers and the effects of orientation," *Polymer (Guildf)*, vol. 53, no. 6, pp. 1383–1392, **2012**.

Chapter 9

Effect of aging in Pebax2533-LL blend membranes

9.1	Introduction	297
9.2	Results and Discussion.....	297
9.3	References	308

9.1 Introduction

Combining ILs and polymers has found manifold applications as referenced throughout this thesis. Although many works have characterized the performance of polymer composite materials under different conditions, it has not been reported to-date on how composite materials involving ILs undergo any morphological changes with time. Thus, the aim of this last chapter is to show whether any aging or migration effects occurred along time once ILs had been incorporated into a dense polymeric membrane. In particular, membranes that were prepared 5 years ago (at the beginning of this PhD) have been investigated in order to verify whether any significant variations had been taking place as regards their composition.

Aging of membranes is expected to result in a modification of their physico-chemical or mass transport properties. As an example, the aging of super glassy polymers such as poly(trimethylsilylpropyne) (PTMSP), poly(4-methyl-2-pentyne) (PMP), or polymers with intrinsic microporosity (PIM-1) have been reported [1] to show a reduction of their gas permeability, limiting therefore their application as gas separation membranes. With regard to polymer/IL composites, one of the main issues dealt with in literature is the migration or leakage of the IL phase from the polymeric base material under operating conditions [2], [3]. This became even more evident in blend membranes that had previously been in contact with vapours and due to which the IL underwent changes in its viscosity and surface tension [4]. Consequently, it appears relevant to investigate possible migration of ILs from such composites also over a prolonged time.

9.2 Results and Discussion

In Chapter 3, TGA and DSC provided experimental evidence on how the blend membranes had altered upon incorporation of ILs into the polymer matrix. While it is widely known that neither TGA nor DSC are quantitative techniques, they may nevertheless be employed

as a qualitative measure in order to elucidate possible alteration the polymer/IL membranes may have undergone with time. We therefore characterized Pebax2533-IL blended membranes that had been stored for more than five years by TGA and DSC in order to observe any possible modifications with time. For all cases, these membranes had been stored over the years under identical conditions on a glass petri dish in a vacuum oven at 60°C.

As can be seen from Figure 8.1, a pristine, recently cast Pebax®2533 membrane and a five-year old one did not undergo any alteration that could be detected thermogravimetrically. This means that the thermal stability of the pristine Pebax®2533 membrane did not change with time.

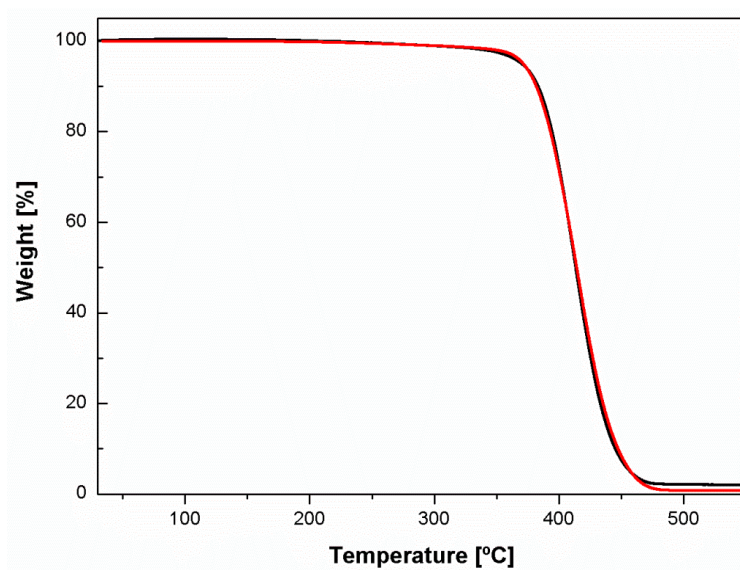


Figure 9. 1 TGA thermogram of Pebax®2533 (red: recently cast membrane; black: 5-year old membrane)

On the contrary, Pebax®2533 membranes containing ILs suffered in part significant alterations over the years (see Figure 9. 2) although strongly depending on the physico-chemical properties of the respective IL.

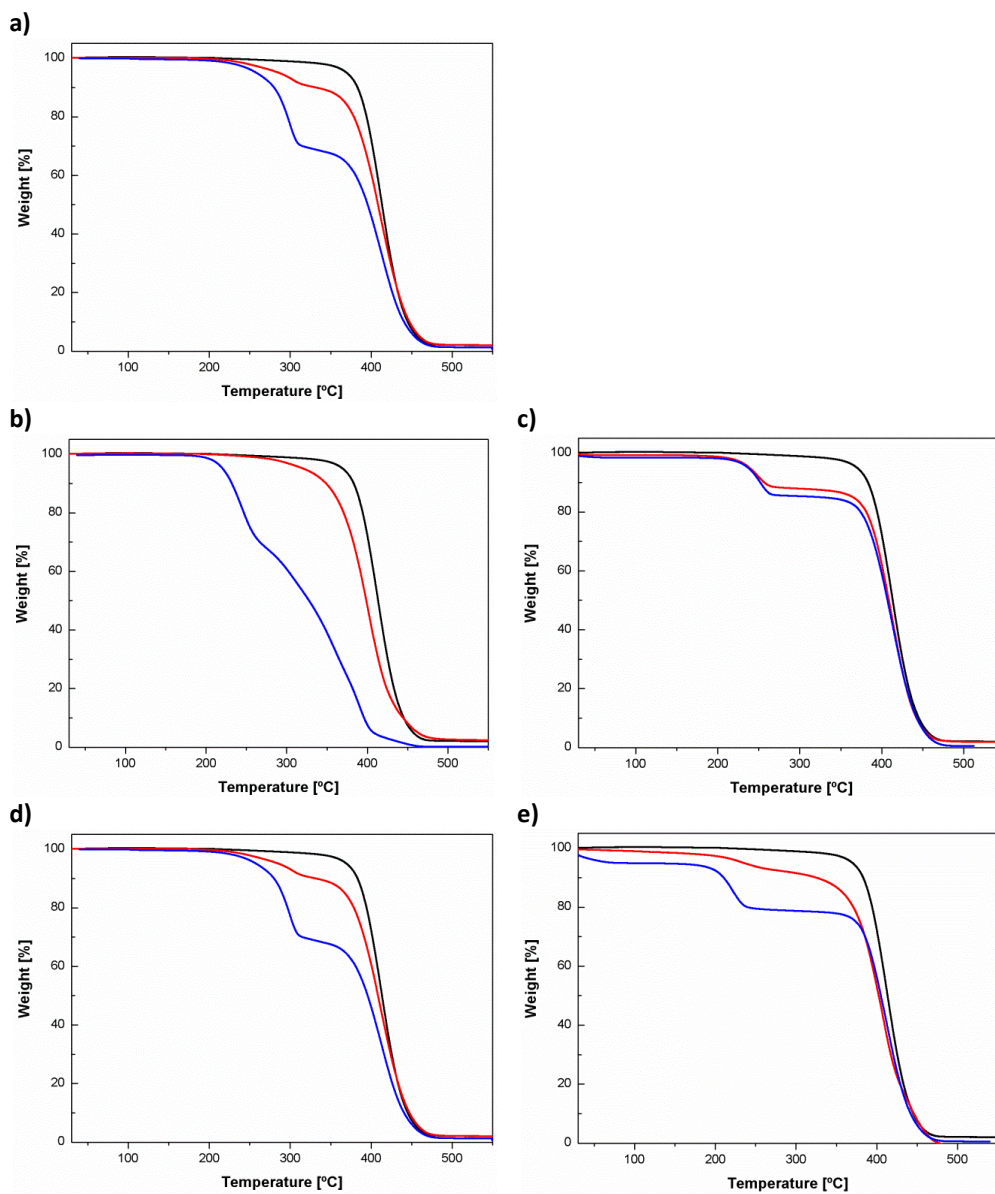


Figure 9. 2 TGA thermogram of Pebax2533-IL blend membranes (black: 5-year-old Pebax[®]2533 membrane, blue: recently cast Pebax-IL blended membranes and red: 5-year-old Pebax-IL blended membranes); a) Pebax2533-[BMIM][BF₄], b), Pebax2533-[BMIM][Tf₂N], c) Pebax2533-[C₈MIM][Cl], d) Pebax2533--[TMG][BF₄], e) Pebax2533-[BMIM][Ac]

In Chapter 3, it was concluded that the ILs resulted in thermally most and least stable blend membranes was [BMIM][BF₄] and [BMIM][Tf₂N], respectively, while the other ILs yielded blend membranes with an intermediate thermal stability. Indeed, a similar tendency could be observed for the migration of ILs from these membranes.

As opposed to other blend membranes, Pebax2533-[BMIM][BF₄] degrades in only one step (Figure 9.2a). The curves between the fresh membrane and the 5-year-old one do not differ significantly. However, it can be observed that in the case of the 5-year-old membrane (red curve), the temperature at which the membrane starts to degrade (starts to lose weight) takes place at about 290°C, around 30°C earlier than the "fresh" Pebax2533-[BMIM][BF₄] blend membrane. Still, apparently no IL has migrated from the block copolymer structure. In stark contrast, Figure 9.2b depicts an entirely different case: as detailed in depth in Chapter 3, [BMIM][Tf₂N] is a hydrophobic IL with possibly low affinity for Pebax[®]2533. In this case, the "fresh" Pebax2533-[BMIM][Tf₂N] blend membrane shows a two-step degradation while the 5-year-old exhibits only one step and a TGA-curve close to the one of pristine Pebax[®]2533. Hence, as could be expected, the low affinity of the IL resulted in a practically complete migration. This extreme case of [BMIM][Tf₂N] blend membranes highlights the importance of the affinity of an IL for the functional groups of the base polymer in order to yield stable blend membranes over time.

In the case of the membranes containing [C₈MIM][Cl], [TMG][BF₄], and [BMIM][Ac], respectively, both in the "fresh" and the 5-year-old membranes, the degradation takes place in two steps: as commented in Chapter 3, this happens due to the first degradation of the IL and secondly that of the block copolymer. The temperature onset of both the fresh and the aged membranes is identical but apparently for all three ILs investigated the 5-year-old membrane has lost some quantity of the IL which consequently has migrated from the block copolymer. It should be stressed, however, that particularly Pebax2533-[C₈MIM][Cl] has only lost a minor amount of IL over the years, indicating a still relatively stable blend membrane as opposed to Pebax2533-[BMIM][Ac] and Pebax2533-[TMG][BF₄].

Quantifying IL migration from the base copolymer by this technique may be risky. Anyhow, and just for providing an approximate value, it has been employed the TA Universal Analysis to determine the limits at which the degradation starts and quantify the degree of migration of IL from the copolymer structure. Figure 8.3 shows schematically how the respective values were determined and then calculated according to Equation 9. 1

Equation 9. 1
$$\text{Weight \% of IL} = \frac{\text{Weight IL migrated}}{\text{Weight IL initial}} \cdot 100$$

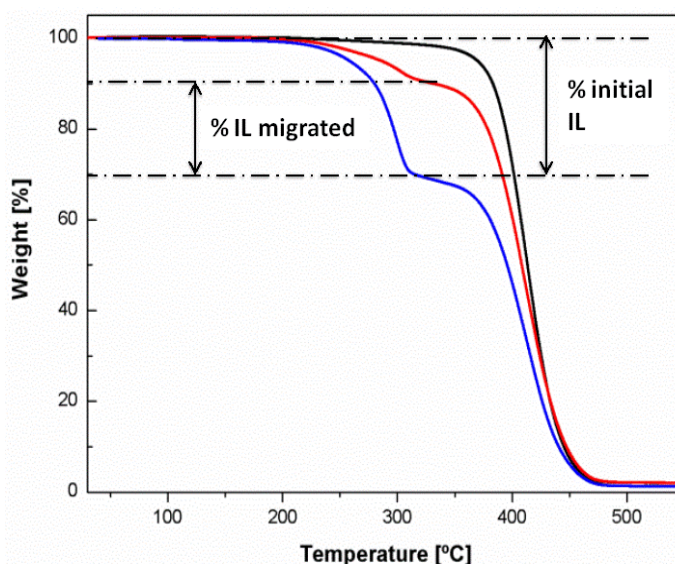


Figure 9. 3 Scheme of how to quantify the mass of IL migrated from the blend membrane

Table 9. 1 summarizes the degree of leakage of the ILs from the 5-year-old membranes when compared to those recently prepared.

Table 9. 1 Summary of the leakage of each IL in weight % in each blend membrane after five years of storage:

	weight % of IL leakage
Pebax2533-[C₈MIM][Cl]	35
Pebax2533-[BMIM][BF₄]	below detection limit
Pebax2533-[TMG][BF₄]	45
Pebax2533-[BMIM][Tf₂N]	100
Pebax2533-[BMIM][Ac]	50

Thus, although the accuracy is difficult to assure by this technique, we can observe that the least stable blend membrane is Pebax2533-[BMIM][Tf₂N] followed by Pebax2533-[BMIM][Ac] and Pebax2533-[TMG][BF₄], while on the opposite we find Pebax2533-[C₈MIM][Cl] and Pebax2533-[BMIM][BF₄] being the most stable ones in terms of IL migration.

Following TGA analysis, DSC measurements were carried out in order to observe any displacement of the melting peaks as a consequence of the migration of the ILs.

First of all, pristine Pebax[®]2533 thermograms of the fresh membrane and the 5-year-old one are plotted in Figure 9. 4.

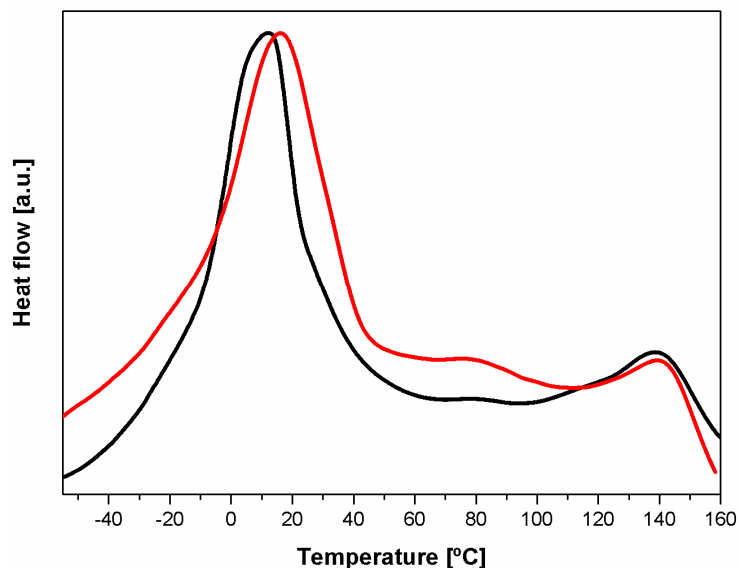


Figure 9. 4 DSC thermogram of Pebax[®]2533 (black: recently cast membrane; red: 5-year old membrane)

It can be seen that the PE peak of the 5-year-old sample is partially shifted to a higher temperature; however, we do not consider this change as relevant since it could be within the error stemming from the sample handling and the measurement. Since otherwise both DSC curves are widely similar, we concluded that Pebax[®]2533 did not suffer any relevant alteration or restructuring during five years. A different observation was made for the polymer/IL blend membranes.

Figure 9. 5 depicts the DSC thermograms of all Pebax2533-IL blend membranes studied in this work.

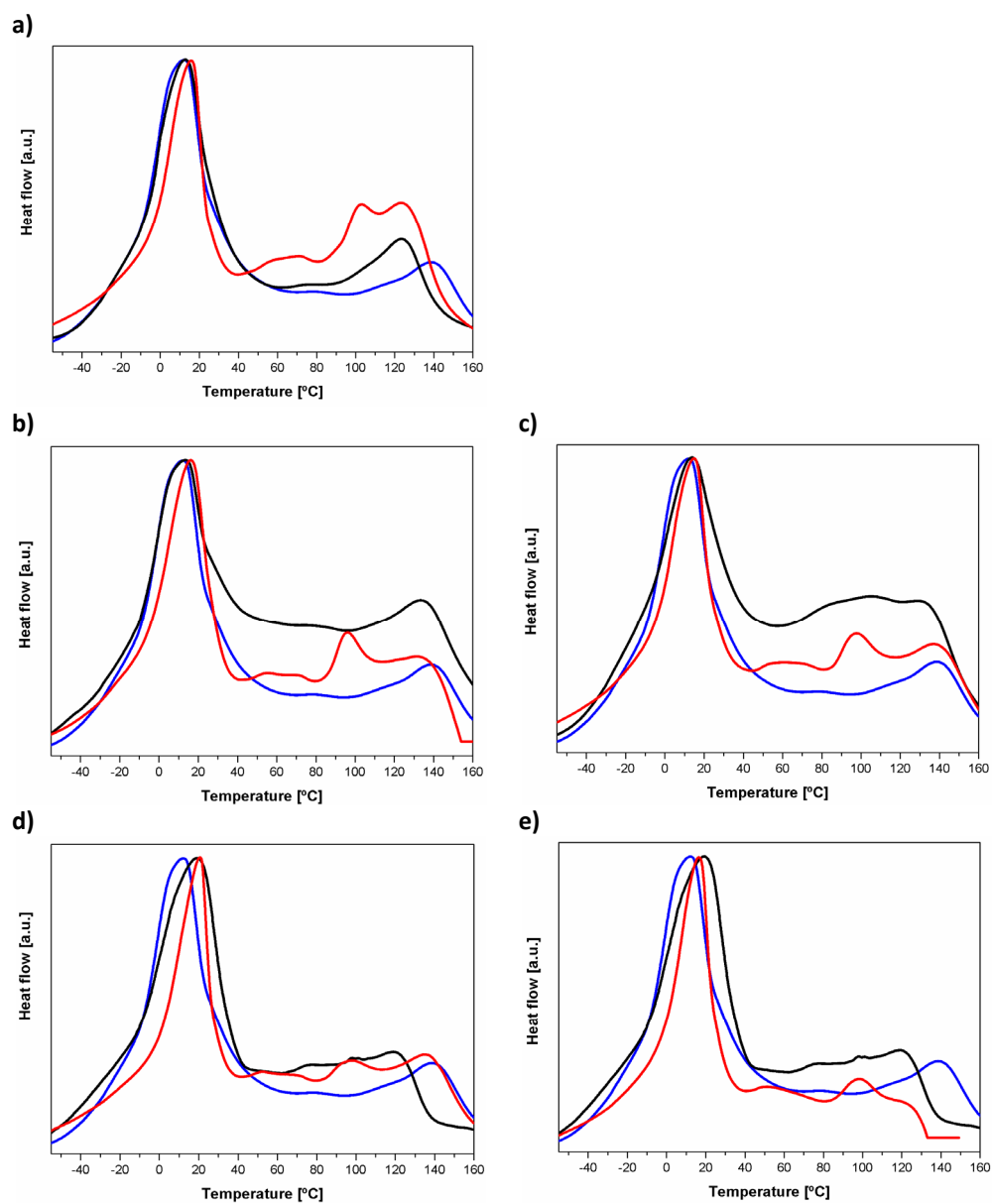


Figure 9. 5 DSC thermogram of Pebax2533-IL blend membranes (blue: recently cast pristine Pebax®2533, red: 5-year-old Pebax-IL blend membrane and black: recently cast Pebax-IL blend membrane) for the following composites: a) Pebax2533-[C₈MIM][Cl], b) Pebax2533-[BMIM][BF₄], c) Pebax2533--[TMG][BF₄], d) Pebax2533-[BMIM][Tf₂N], e) Pebax2533-[BMIM][Ac]

As was also discussed in Chapter 3, Figure 9. 5 shows how the PE peak that initially was the less affected peak as a consequence of the addition of the IL also remains rather unchanged over time. In contrast, the PA peak shows a dramatic change. PA was previously determined to be particularly sensitive to IL addition as the latter would interfere with the formation of the PA lamellae and, hence, lower the crystallinity. As can be seen, the PA peak that in fresh membranes is only one, is found divided into two small and not well defined peaks ("shoulders") in the five-year old membranes. In all cases the first "shoulder" appears at a lower temperature than the single PA peak of the fresh membrane. Thus, it can be assumed that this is the experimental evidence for the IL leaving the PA domain of the polymer resulting in a first melting peak at a lower temperature, subsequently producing a reorganization of the PA segments.

It has been shown in literature [5], [6] that in other systems involving poly(lactic acid) (PLA) when being copolymerized with thermoplastics such as poly(ethylene oxide), poly(ϵ -caprolactone), or poly(vinyl acetate), as well as when blended with plasticizers as poly(ethylene glycol, oligomeric lactic acid, glycerol or low-molar-mass citrates in a 15 wt% the migration is facilitated under ambient conditions due to a phase separation. The removal/migration of the cited additives leads then to a partial degradation of the poly(lactic acid) (PLA). As concerns this system, Table 9. 2 summarizes the variation of crystallinity in percentage determined in both fresh and aged membranes for PE and PA peaks, respectively. The description of how this calculation is carried out was described in Chapter 3 where it also was pointed out that the determination of an accurate value of ΔH_{PA} is not easy due to the width of the peaks, which is why the error made is high.

It can be seen how the semi-crystallinity of the PA phase of the aged blend membranes has increased considerably as a consequence of the increase of ΔH_{PA} . This increase in semi-crystallinity of the aged blend membranes would be expected due to the migration of the IL and also because the material has become more brittle. For the PE phase, a similar tendency is observed but to a much lesser extent. This increase in semi-crystallinity of the

PA phase is observed for all blend membranes revealing that, whatever the physico-chemical property of the IL, significant aging of the membranes occurs over the years.

Table 9. 2 Semi-crystallinity of each copolymer phase in % for pristine Pebax®2533 and IL blend membranes, both fresh and aged.

MATERIALS	PE fresh membrane	PA fresh membrane	PE aged membrane	PA aged membrane
	X _c [%]	X _c [%]	X _c [%]	X _c [%]
Pebax®2533	19	12	20	11
Pebax2533-[C ₈ MIM][Cl]	14	11	18	41
Pebax533-[BMIM][BF ₄]	16	10	18	32
Pebax2533-[BMIM][Ac]	14	10	19	29
Pebax2533-[BMIM][Tf ₂ N]	18	12	21	29
Pebax2533-[TMG][BF ₄]	16	8	22	30

In general, it has been seen over this work both in chapter 3 (with FTIR, NMR, etc. experimental measurements) as well as in chapter 8 (PALS technique) that the interactions occurring between the ILs and the chemical groups of Pebax®2533 are weak. Moreover, as described in depth in Chapter 8, the free volume of the polymer is not big enough for the IL molecules to get retained within this space. Hence, the IL is expected to migrate relatively freely with time.

Only the blend membrane containing [BMIM][BF₄], shows an apparently negligible IL leakage, although the final semi-crystallinity in the PA phase was found increased when

compared to the fresh membrane indicating migration of the liquid phase within the block copolymer but not outside its structure. This was in line with findings in Chapter 3, where Pebax2533-[BMIM][BF₄] blend membrane degrades in only one step being the most thermally stable when compared with the other Pebax2533-IL composites and demonstrating no significant changes between the fresh and the 5-year-old blend membrane. This behaviour also confirms what is observed in Chapter 8 where for the case of [BMIM][BF₄] the IL doesn't seem to interact with the block copolymer; but it could happen that the IL could get retained or more protected in between the copolymer chains difficulting its migration as occurs in the other IL blend membranes.

As a conclusion, this preliminary study proves the importance of selecting the most appropriate ILs not only for the applications they should fulfill but also for their interaction with the base polymer as there is experimental evidence that ILs tend to leave the base copolymer structure with time. Therefore, when using such blend membranes it should be taken into consideration how long the membranes are expected to last in their future applications.

9.3 References

- [1] C. H. Lau, P. T. Nguyen, M. R. Hill, A. W. Thornton, K. Konstas, C. M. Doherty, R. J. Mulder, L. Bourgeois, A. C. Y. Liu, D. J. Sprouster, J. P. Sullivan, T. J. Bastow, A. J. Hill, D. L. Gin, and R. D. Noble, "Ending Aging in Super Glassy Polymer Membranes," *Angew. Chemie Int. Ed.*, vol. 53, no. 21, pp. 5322–5326, **2014**.
- [2] M. Matsumoto, A. Panigrahi, Y. Murakami, and K. Kondo, "Effect of ammonium- and phosphonium-based ionic liquids on the separation of lactic acid by supported ionic liquid membranes (SILMs)," *Membranes (Basel)*, vol. 1, no. 2, pp. 98–108, **2011**.
- [3] M. Paven, P. Papadopoulos, S. Schöttler, X. Deng, V. Mailänder, D. Vollmer, and H.-J. Butt, "Super liquid-repellent gas membranes for carbon dioxide capture and heart–lung machines," *Nat. Commun.*, vol. 4, **2013**.
- [4] S. Herminghaus, "Roughness-induced non-wetting," *Eur. Lett.*, vol. 52, no. 2, pp. 165–170, **2000**.
- [5] N. Ljungberg and B. Wesslén, "Thermomechanical film properties and aging of blends of poly(lactic acid) and malonate oligomers," *J. Appl. Polym. Sci.*, vol. 94, no. 5, pp. 2140–2149, **2004**.
- [6] S. P. Appu, S. K. De, M. J. Khan, and M. A. Al-Harhi, "Natural weather ageing of starch/polyvinyl alcohol blend: effect of glycerol content," *J. Polym. Eng.*, vol. 0, no. 0, pp. 1–7, **2013**.

Chapter 10

General Conclusions

The general objective of this thesis consisted on the development of stable non-porous Pebax2533-IL composite membranes. Once observed their modularity, different characterization techniques have been carried out in order to determine their behaviour, effects and evolution of the blended materials as a consequence of the addition of the ILs.

From the results obtained in this study and taking into consideration the general objectives proposed for this work, the following conclusions can be extracted:

- The methodology for incorporating ILs in a polymer matrix such as Pebax®2533 in a 20% wt could be considered to be a new alternative to the development of SILMs. It has been demonstrated that they provide thermal as well as mechanical stability.
- In general, the analytical techniques employed (AFM, DSC, TGA, FTIR or ¹³C NMR), for material characterization have shown very limited sensitivity for the detection of the low interactions taking place between Pebax®2533 and the ILs.
- Vapour and gas permeation tests revealed that the addition of ILs indeed modified the transport properties of the blended membrane, being the solubility the parameter that governs this variation in permeability. However, in both gas and vapour permeation tests, the permeability increase as a consequence of the IL addition cannot be considered to be high; showing also no difference whether the membranes were obtained by a casting technique or thermal compression.

- According to literature data, the use of ILs with the aim of improving the selectivity to CO₂ seems not to be high enough to be economically profitable, in comparison with the wide range of commercially available polymers such as PIMS, MOFs or MMMs that provide rather promising results.
- For the particular case of the CO₂ sorption in [C₈MIM][Cl] it has been demonstrated the importance of the exposure time in the experiment. It has also been revealed the differences of the CO₂ interaction preference between the gas phase and the bulk of the IL. In addition, the “associated-water” inside the IL plays an important role in the final result showing surprisingly high sorption values for carbon dioxide.
- QCM-D has been confirmed to be a fast and reliable technique for vapour sorption tests, showing the results obtained to be in good agreement with the data determined by other analytical techniques such as Cahn electrobalance, SPR and data from literature.
- D/F plots obtained from QCM-D represent an added value in order to evaluate the behaviour of the material being studied. As an example, it should be remarked the performance of Pebax2533-[BMIM][Tf₂N] blend membrane, where the material gets more rigid as a consequence of the water sorption.
- PALS and X-Ray experiments have shown that the addition of ILs increases the average free volume of the blend membranes. However, as opposed to what expected, the increase was found not to be a synergic effect but rather due to the intrinsically higher free volume of the IL itself. It was also demonstrated the impossibility for ILs to get into the free space between the polymer chains.

- The aging effect of Pebax2533-IL blend membranes showed in most cases a migration effect of the liquid phase from the base material owing to the low interaction between the two systems.
- These findings suggest that the addition of ILs to form blend membranes will be useful just for those cases where ILs possess a particular and significant selectivity for a determined solute.

Appendix

ABBREVIATIONS

¹³C NMR: Solid-State Carbon-13 Nuclear Magnetic Resonance

CO₂: Carbon dioxide

DSC: Differential Scanning Calorimetry

EtOH: Ethanol

EtAc: Ethyl Acetate

e⁻: electron

e⁺: positron

FTIR: Fourier Transform Infrared Spectroscopy

H₂O: Water

Hz: Hertz

Hex: Hexane

ΔH_m: Melting enthalpy

I₃: o-Ps Intensity

IL: Ionic Liquid

Mw: Molecular Weight (weight average)

N₂: Nitrogen

PALS: Positron annihilation lifetime spectroscopy

PE: Polyether phase

PTMO: Poly(tetra methylene) oxide

PA: Polyamide phase

Abbreviations

PA12: Polyamide 12

PEO: Poly(ethylene oxide)

QCM-D: Quartz Crystal Microbalance with Dissipation

RT: Room Temperature

SPR: Surface Plasmon Resonance

σ_3 : hole size distribution

SI: Supporting Information

t: time

τ_3 : o-PS Lifetime

T: Temperature

T_d: Temperature for maximum decomposition rate

T_m: Melting Temperature

T_g: Glass transition temperature

T_c: Crystallization Temperature

TGA: Thermal Gravimetric Analysis

Tol: Toluene

X-Ray: X-ray diffraction

